

Optimization of primary endothelial culture methods and assessment of cell signaling pathways in the context of inflammation

by

Ta-Chun Hang

B.Bm.E., Biomedical Engineering
B.A., Human Physiology
University of Minnesota, 2005

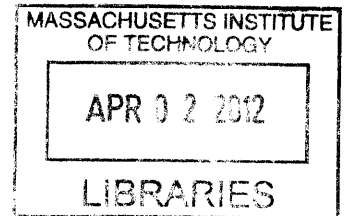
Submitted to the Department of Biological Engineering
in Partial Fulfillment of the Requirements for the Degree of

Doctor of Philosophy

at the

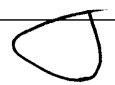
Massachusetts Institute of Technology

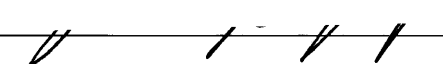
February 2012

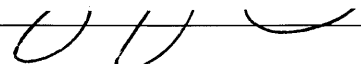


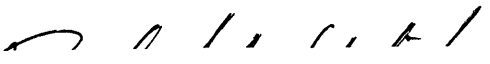
ARCHIVES

© 2012 Massachusetts Institute of Technology. All rights reserved.

Signature of Author: _____
 Department of Biological Engineering
December 29, 2011

Certified by: _____
 Douglas A. Lauffenburger
Professor of Biological Engineering, Biology, and Chemical Engineering
Thesis Supervisor

Certified by: _____
 Linda G. Griffith
Professor of Biological and Mechanical Engineering
Thesis Supervisor

Accepted by: _____
 Forest White
Associate Professor of Biological Engineering
Course XX Graduate Program Committee Chairperson

THESIS COMMITTEE

Roger D. Kamm
Professor, Departments of Biological and Mechanical Engineering
Massachusetts Institute of Technology
Thesis Committee Chair

Douglas A. Lauffenburger
Professor, Departments of Biological Engineering, Biology, and Chemical Engineering
Thesis Supervisor

Linda G. Griffith
Professor, Departments of Biological and Mechanical Engineering
Thesis Supervisor

Donna B. Stolz
Associate Professor, Department of Cell Biology and Physiology
University of Pittsburgh School of Medicine

Optimization of primary endothelial culture methods and assessment of cell signaling pathways in the context of inflammation

by

Ta-Chun Hang

Submitted to the Department of Biological Engineering on December 29, 2011 in Partial Fulfillment of the Requirements for the Degree of Doctor of Philosophy in Biological Engineering

ABSTRACT

Tissue engineering is a potentially valuable tool for clinical treatment of diseases where host tissues or organs need to be replaced. Progression of engineering metabolically complex organs and tissues has been severely limited by the lack of established, functional vasculature. The thesis work described herein focused on methods of establishing and studying specific endothelial cell types *in vitro* for potential applications in establishing functional microvascular architecture.

To achieve these objectives, a model system of primary liver sinusoidal endothelial cells (LSEC) was initially studied due to the high metabolic requirements of the liver, as well as the unique phenotype that they possess. We were able to demonstrate that free fatty acids were able to rescue LSEC in culture, promote proliferation, and maintain their differentiated phenotype. Our work with lipid supplementation in serum-free conditions provides flexibility in engineering liver tissue with a functional vasculature comprised with relevant endothelial types encountered *in vivo*.

Following up our work with LSEC, we explored the human dermal microvascular endothelial cell (HDMVEC) system to understand the signaling mechanisms involved in sprouting angiogenesis. Engineered tissues that are implanted will require integration with host vasculature. We established a method to collect large signaling data sets from a physiologically relevant *in vitro* culture system of HDMVEC that permitted angiogenic sprouting. We were able to find statistically significant data regarding how angiostatic cues like Platelet Factor 4 can modulate angiogenesis signaling pathways.

Our results from working with both types of endothelial cell systems provide insight into potential methods for establishing specialized microvasculature for engineered tissues, both in propagation of differentiated endothelial cells *in vitro* and promotion of tissue/organ survival following their implantation.

Thesis Supervisor: Douglas A. Lauffenburger

Title: Whitaker Professor of Biological Engineering, Biology, and Chemical Engineering

Thesis Supervisor: Linda G. Griffith

Title: School of Engineering Professor of Biological and Mechanical Engineering

Acknowledgements

First and foremost, I would like to thank my advisors Doug Lauffenburger and Linda Griffith for providing me with the opportunities to work in their labs. It has been one rollercoaster of a ride, and I've learned a great deal from the projects that I have been able to work on, as well as observe from afar. I also appreciate the great endeavors that they have gone to in helping me develop through my graduate career. Second, I would like to thank my committee (Donna Stolz and Roger Kamm) for being supportive and understanding of my work, especially how frustrating working with primary liver sinusoidal endothelial cells were.

Of course, a great deal of this work could not have been possible without a multitude of people who were so willing to help me during the time that I have been here. These include a long list of people who have contributed in some way or another in advice, suggestions, or teaching me protocols/way of life, or merely just being there for conversation: Andres Abin-Fuentes, Luis Alvarez, Abhinav Arneja, Neda Bagheri, Michelle Berry, Michael Beste, Lorenna Buck, Dave Clarke, Ben Cosgrove, Dan Darling, Ajit Dash, Dalia Fares, Arthur Goldsipe, Cathy Greene, Nancy Guillen, Shannon Hughes-Alford, Walker Inman, Brian Joughin, HD Kim, Sarah Kolitz, Tushar Kulkarni, Hsinhwa Lee, Nina Lee, Matthew Lim, Ryan Littrell, Aaron Meyer, Miles Miller, Emily Miraldi, Joe Moritz, Melody Morris, Kristen Naegle, Bryan Owens, Megan Palmer, Aran Parillo, Nicole Pfaeffle-Doyle, Manu Platt, Rachel Pothier, Justin Pritchard, Joy Rimchala, JoAnn Sorrento, Yasuko Toshimitsu, Jorge Valdez, Laura Vineyard, Joel Wagner, Shan Wu. A particular thanks and gratitude goes to Nate Tedford, who has been a great mentor, collaborator, mentor, and friend that without his presence, the last two thirds of this thesis would never have been. Additionally, I would like to thank our UROP, Raven Reddy, whose curiosity and dedication for science contributed to the angiogenesis project.

Although a late introduction into my life here at MIT, the community of Muddy Charles Pub has a fond place in my memories now, especially with all the interesting times (and life lessons I've gained there). Thanks in particular to Mike Grenier- the Muddy was a great place to be when I needed to take a break from my work and it wouldn't have been the same without having you as a manager and friend.

I also would like to thank my parents and my sister Julie (and eventually my brother-in-law Mike) for being always supportive (from a distance) and letting me begin this scientific journey relatively on my own. Finally, the number of friends and classmates who made life a little easier by being my second family that weren't listed above (or were doubly important to be here too): Abhinav Arneja, Justin and Lorenna Buck, Kristin Bernick, Scott Carlson, Sara Darcy-Belcher, Jennifer Fang, Bonnie Huang, Sonya Huang, Dave Kubiak, Brandon Kwong, Rachel Miller, James Mutamba (and Sharon Jin), Amy Nichols, Alex (and Karen) Sheh, Nidhi Shrivastav (and Saurabh Awasthi). And my lifting buddies (past and present), who became like brothers I never had and put up with my crazy workouts and antics: Philip Bransford, Luke Robinson, and Benjamin Wunsch.

This list could go on, but I am running out of space here in my acknowledgements. If I missed anyone, I apologize, there are so many people that made such a profound difference in my life! Thank you all for being there with me on this journey, and hopefully more in the future.

Table of Contents

Abstract	4
Acknowledgements	5
List of Tables and Figures	12
Chapter 1	15
Introduction and Background	
1.1. State of <i>ex vivo</i> tissue and organ engineering	15
1.2. Overview of vasculature and endothelial cells	18
1.3. Overview of the liver and its microvasculature	20
1.4. Overview of inflammation and wound healing	26
1.5. Physiologically relevant intracellular models of angiogenesis for vascular regulation	31
1.6. Thesis overview	33
1.7. References	36
Chapter 2	49
Lipids promote survival, proliferation, and maintenance of differentiation of rat liver sinusoidal endothelial cells <i>in vitro</i>	
2.1. Introduction	49
2.1.1. Role of fatty acids and lipids in liver function and metabolism	49
2.1.2. Lipids signal through a variety of pathways	50
2.1.3. Chapter overview	51
2.2. Experimental Procedures	53
2.2.1. Chemically defined culture media	53
2.2.2. Primary LSEC isolation and culture	54

2.2.3. Live/Dead assay	54
2.2.4. Alamar Blue metabolic assay	55
2.2.5. Acetylated-LDL uptake assay	55
2.2.6. Immunofluorescence microscopy	55
2.2.7. Scanning electron microscopy	56
2.2.8. Flow cytometry analysis of phenotype and proliferation	56
2.2.9. Phenotype and phospho-protein Western blotting	57
2.2.10. Image and statistical data analysis	57
2.3. Results	58
2.3.1. FFA lipids support cell survival past the first 48 hours in serum free media	58
2.3.2. FFAs support metabolic and endocytic functionality in LSEC past day 3	61
2.3.3. LSEC phenotype and proliferation are maintained with lipids in growth factor-reduced, serum-free media	61
2.3.4. Temporal dependence of LSEC on PI3K and MAPK pathways observed at Days 3 and 5 in FFA-treated cultures	66
2.4. Discussion	71
2.4.1. Lipids and FFA support LSEC function and survival	71
2.4.2 FFA influence on phosphoprotein signaling pathways	72
2.4.3. Diametric effects emphasize need of lipid balance for optimal function	72
2.4.4. Consideration of lipids in liver and LSEC biology	74
2.5. References	75

Chapter 3	84
Development of cell signaling protocols for human dermal microvascular endothelial cells cultured on 3D collagen gels	
3.1. Introduction	84
3.1.1. Background and motivation for the study of angiogenesis	84
3.1.2. Inflammatory chemokines can influence outcomes of angiogenesis	86
3.1.3. Chapter overview	87
3.2. Experimental procedures	88
3.2.1. Cell culture	88
3.2.2. Three-dimensional collagen gel sprouting system	89
3.2.3. Cell lysis protocols established for mass spectrometry preparation	90
3.2.3.1. Direct Urea Lysis	90
3.2.3.2. Urea Surface Lysis	90
3.2.3.3. Sample harvesting with collagenase cocktails followed by urea lysis	90
3.2.3.4. Detergent surface lysis with subsequent urea lysis	91
3.2.4. Total protein determination assay	92
3.2.5. Western blotting	92
3.2.6. Phosphotyrosine mass spectrometry	93
3.2.7. Luminex xMAP bead based signaling assays	94
3.3. Results	94
3.3.1. Protein signaling dynamics from HDMVEC on collagen gels are observably different using Western blotting	94
3.3.2. Collagen contribution is reduced when using surface detergent lysis method	96
3.3.3. Mass spectrometry detection of phosphorylation sites increases following reduction of collagen contribution to cell lysates	98
3.3.4. Luminex normalization and subsequent time course analysis reveal difficulty in phosphoproteomic data from typical analytic procedures	100

3.4. Discussion	104
3.4.1. PF-4 influences endothelial signaling pathways	104
3.4.2. Lysate collection from 3D collagen gels is nontrivial	104
3.4.3. Summary	106
3.5. References	107
Chapter 4	112
Angiostatic Platelet Factor 4 cues modulate distinct phosphoprotein signaling pathways involved with migration and sprouting in endothelial cells	
4.1. Introduction	112
4.1.1. Inflammation and angiogenesis in tissue engineering	112
4.1.2. Chemokines induce inflammatory, angiogenic, and angiostatic responses	113
4.1.3. Chapter overview	113
4.2. Experimental Procedures	114
4.2.1. Cell culture	114
4.2.2. Three-dimensional collagen gel cultures	115
4.2.3. Confocal microscopy	115
4.2.4. Detergent surface lysis with subsequent urea lysis	116
4.2.5. Phosphotyrosine mass spectrometry	116
4.2.6. Manual validation of mass spectra fragments	117
4.2.7. Data processing and statistical analysis	117
4.2.8. Correlation network modeling	118
4.3. Results	118
4.3.1. Optimization of collagen gel culture system for collection of cue, signal, and response data	118
4.3.2. PTMScout Outputs and Predictions	120
4.3.3. Time-resolved tyrosine phosphorylation measure by quantitative mass spectrometry indicate statistically significant differences over the course of stimulation	122

4.3.4. Correlation network modeling reveals significant changes in protein interactions involved in cell migration mechanisms	125
4.4. Discussion	129
4.4.1. Increased P38 α MAPK activity agrees with previously reported results	130
4.4.2. PF-4 modulates phosphorylation of proteins involved with cell migration	130
4.4.3. Other observed protein phosphorylation are delayed or attenuated	131
4.4.4. Implications from late time point data and integration with full time course signaling dynamics	131
4.4.5. Correlation network models predict positive role of Annexin I but potentially negative regulatory role of EphA2 in angiogenesis	132
4.4.6. Caveats to signaling data	135
4.4.7. Summary	137
4.5. References	138
Chapter 5	146
Concluding remarks	
5.1. Concluding remarks	146
5.1.1. Microvascular physiology and the future of tissue engineering	146
5.1.2. Applications, limitations, and future work with primary differentiated LSEC cultures <i>in vitro</i>	146
5.1.3. Applications, limitations, and future work of molecular pathways for inflammatory angiogenesis	147
5.1.4. Conclusion	148
5.2. References	149
Appendices	
Appendix A: Abbreviations	150

Appendix B: Modified HGM recipe and primary LSEC isolation protocol	153
B.1. Preparation of Hepatocyte Growth Medium (HGM) for primary rat sinusoidal endothelial cultures	153
B.2. Primary liver Sinusoidal endothelial cell isolation	157
Appendix C: Phosphotyrosine enriched mass spectrometry protocol	161
C.1. Buffer solutions	161
C.2. Chemical modification and digestion	161
C.3. Sep-Pak, Speed-Vac, and lyophilization	162
C.4. 8-plex iTRAQ labeling	163
C.5. Phosphotyrosine peptide IP	163
C.6. IMAC enrichment of phosphotyrosine peptides using Ni-NTA agarose conjugates	164
Appendix D: LTQ Orbitrap MS spectra validation protocol	166
D.1. Spectra validation set-up	166
D.2. Rules for assigning peaks	168
D.3. Brief outline of steps	172
Appendix E: Platelet Factor 4 Time Course Data	173
Appendix F: Correlation network model code and script	174
Appendix G: pVEGFR2 Luminex data	180

List of Tables and Figures

Chapter 1

Figure 1-1. Rising discrepancy between transplants, donors, and waiting lists for organs in the US.

Figure 1-2. Diagrammatic representation of important liver cell types and structure.

Figure 1-3. Schematic of wound repair process

Figure 1-4. Microfluidic device incorporating fluid flow for studying angiogenesis

Chapter 2

Figure 2-1. Lipids in FFA form sustain long-term culture.

Figure 2-2. LSEC death at 48 hours is abrogated following treatment with FFA.

Figure 2-3. OA and lipid supplement support phenotype and function in LSEC cultures.

Figure 2-4. LSEC differentiation marker CD32b, proliferation marker PCNA, and nuclear Hoechst co-localize to same cells in FFA cultures.

Figure 2-5. OA and lipid supplement help promote proliferation and maintain differentiation in long term LSEC culture.

Figure 2-6. Lipid and oleic acid treated LSEC had higher phospho-ERK and phospho-Akt activity.

Figure 2-7. OA and lipid supplement support cultures through early maintenance of low threshold of phospho-Akt followed by late phospho-ERK signaling.

Chapter 3

Figure 3-1. Angiogenesis during wound healing process and vessel sprouting to support metabolic demands of tissues.

Figure 3-2. Microfluidic device and collagen gel setup.

Figure 3-3. Initial Western blots on signaling activity in HDMVEC at early time points.

Table 3-1. Percentage of collagen contribution to cell lysates collected using different methods (select methods and representative values shown).

Figure 3-4. Liberase TM harvesting and cell detachment protocol to reduce collagen contamination.

Figure 3-5. Surface lysis of HDMVEC seeded on collagen gels.

Table 3-2. Significant targets identified by phospho-tyrosine enriched mass spectrometry increases with surface lysis technique.

Figure 3-6. Luminex xMAP bead kit optimization curves.

Figure 3-7. GAPDH curves for loading surface lysed samples.

Figure 3-8. Phospho-protein signal is mainly captured at early time points for Luminex xMAP bead kits.

Chapter 4

Figure 4-1. 3D collagen gel culture enables endothelial sprout initiation.

Figure 4-2. PTMScout gene ontology outputs of processes, functions, and compartmentalization of phosphoprotein signal measurements.

Table 4-1. Predicted binding sites and kinase activity.

Table 4-2. Full time course phosphoproteomic coverage and their respective phosphosite.

Figure 4-3. Graphs of statistically significant time course data from time resolved tyrosine phosphorylation measurements by quantitative mass spectrometry.

Figure 4-4. Heatmaps of statistically significant pairwise correlation in both VEGF with and without PF-4 treatments.

Figure 4-5. Diagrams of signaling pathways involved and changes in crosstalk when PF-4 is introduced.

Figure 4-6. Multiple hypothesis testing correction of statistically significant correlations returns a smaller subset with some overlap.

Appendices

Figure D-1. Sample spectra of GSK3 β .

Figure E-1. Time course of PF-4 dosing.

Figure G-1. pVEGFR2 activation levels do not change significantly when stimulated in presence of PF-4.

Chapter 1

Introduction and Background

This thesis is focused on establishing an understanding of cellular signaling mechanisms involved in the function of liver sinusoidal and dermal microvascular endothelial cells. The following chapter contains both background and rationale for the endothelial cell types and their biological systems used in this thesis that will be helpful in understanding later chapters.

1.1. State of *ex vivo* tissue and organ engineering

In addition to blunt body trauma, there are a myriad of diseases that terminally end in organ failures. For many patients, the only hope for survival lies with replacement of the lost organ(s). Organ transplant methods have come a far ways from meager beginnings with poor survival and host rejection. Rejection rates were significantly decreased after the 1980s, when immunosuppressant drug cyclosporine was approved by the FDA for use following transplants (129). These drugs were able to reduce rejection rates (e.g. cyclosporine inhibits calcineurin and activation of T cells) and as a consequence increased survival rates of patients.

As the modern world has developed and improved methods to treat medical problems with replacement organs and tissues, demand on these life-saving procedures have far outpaced the supply. In the United States alone, there are currently over 100,000 people are on the waiting list for organ transplants, with only a tenth of that number of donors (Based on OPTN/SRTR Data as of May 2009). The number of people requiring transplants will continue to increase at a rate much higher than the availability of organs (Figure 1-1), leading to higher number of patient deaths that can be prevented if there were sufficient supply. Technological progress has increased preservation and transport quality of organs, along with enabling multiple tissue and organ harvests from a single donor. Despite these advancements, organ and tissue availability are still limited by the number of donors.

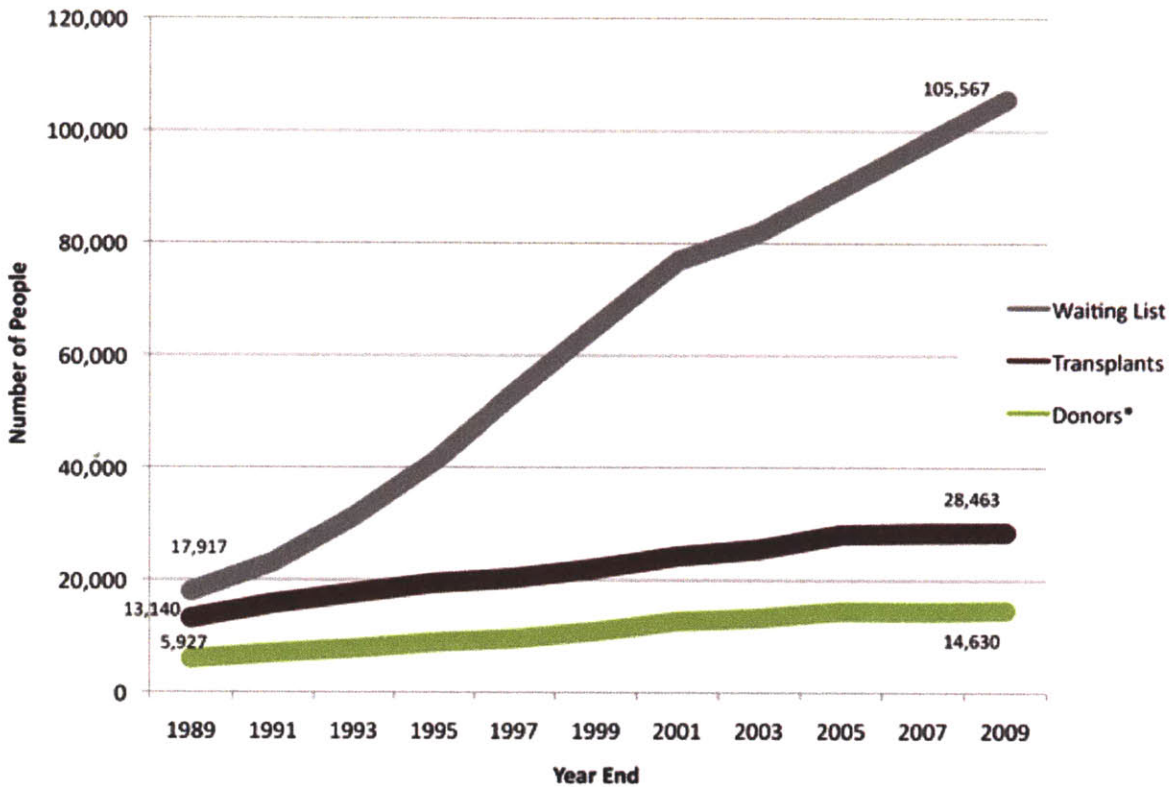


Figure 1-1. Rising discrepancy between transplants, donors, and waiting lists for organs in the US (62). The need for organ transplants far exceeds the availability of viable organs. Approximately 7,000 of those patients on waiting lists die before they receive a transplant (Based on OPTN/SRTR Data as of May 4 2009). Of those who survive who stay on the waiting list, receiving a transplant or tissue graft can extend survival rates or significantly increasing quality of life. Tissue engineering can conceivably be used to target the gap in supply for patients whom require replacement tissue and organs. From <http://www.organdonor.gov/aboutStatsFacts.asp>. Data from <http://optn.transplant.hrsa.gov> and OPTN/SRTR Annual Report.

In efforts to combat the scarcity and reduce mortality rates of those on organ waiting lists, tissue engineering has attempted to try to satisfy some of the needs with *in vitro* and even synthetic tissue constructs for non-organ replacements. Currently, innovative discoveries in tissue engineering have enabled the successful construction of viable organs and tissues such as dermal grafts (58, 104, 119, 143), bladders, urethras, kidney nephron units, and blood vessel valves (9,

43). Some of these tissue constructs are generated by using cell transplants from organs or use of stem cells rather than whole organ transplants (143).

However, due to the difficulty of recapitulating and supporting organ structure *ex vivo*, current tissue engineering faces severe limitations to helping cover the gap in supply to those who need organs. It is acknowledged in regenerative medicine that pitfalls and limitations for many of these organs are a result of the lack of a defined, stable vasculature (43, 69, 119, 127). Many tissue grafts or synthetic tissues created with cellular seeding do not survive past the first stages of integration into a host due to lack of proper vascularization. Furthermore, artificial tissues cannot fully recapitulate functions of their *in vivo* equivalent. Thus, the limited success of tissue engineered grafts hinder progress in covering this observed gap in demand.

Current technological developments for tissue engineering have simultaneously focused on elucidating cellular interactions and mechanisms and establishing suitable environments for developing vascularization. Microfabrication tools such as photolithography, soft lithography, and substrate tuning have been used to understand how to construct tissues *ex vivo* by elucidating cell-cell interactions (12, 44, 72). These methods can help ascertain scaffold structures and specific combinations of extracellular matrix proteins that are necessary to help maintain cell differentiation and survival for respective organ milieus.

In tandem with microfabrication techniques, creating scaffolds with proper three-dimensional microarchitecture is also an important approach that has been taken to help improve tissue engineering. Biodegradable scaffolds made from extracellular matrix (ECM) proteins collagen, fibrin or degradable polymers have been utilized for creating *ex vivo* tissues that can be relatively easily grafted and integrated into host tissues (80, 151). In addition to the use of ECM scaffolds, other inorganic polymers such as chitosan, alginate, polyethylene glycol/ethylene oxide, and polylactic-co-glycolic acid can be used to generate synthetic biodegradable scaffolds and hydrogels that can be populated with cells and matrix proteins to generate *de novo* tissue (9, 71, 72, 90, 146). The versatility of these biomaterials and polymers has lent themselves to be applied to various tissue engineering prospects, including cardiac, dermal, bone, and cartilage tissue engineering.

Self-contained bioreactors that simulate flow and shear stress experienced in the *in vivo* fluidic environment have been explored as an additional alternative for artificial organs. Microfluidic bioreactors have been designed to mimic similar shear stress and oxygenation environments that are observed *in vivo* either as a result of interstitial or blood flow, particularly with metabolically active organs such as the liver (4, 5, 33). These bioreactors are designed to simulate cell and tissue behavior response in the format of a “organ-on-a-chip” on a small scale for functional and pharmaceutical evaluations (126). Bioreactors have also been used as a temporary replacement for organ function, such as non-implanted bioartificial liver and kidney devices (9). The rates at which these technologies are developed are promising for the progress in developing tissue and organ replacements.

1.2. Overview of vasculature and endothelial cells

For multicellular aerobic organisms that achieve a certain mass, simple diffusion-based transport of nutrients and wastes to and from cells are insufficient (3, 153). Evolutionary demands required many of these organisms to adopt methods of transporting efficiently to and from each cell. In vertebrates, a closed circulatory system provides both diffusion and convective based transport to tissues (23).

Circulatory systems in humans essentially define the entire framework for nutrient and waste exchange. In each of the specialized tissues in the body, the vascular network has differentiated to cater to their specific metabolic needs. In general, blood vessels present in the adult human body are segregated into three different types: arteries, veins, and capillaries (153). Although only 5% of the total amount of blood within the circulatory system is found in capillaries at any given time, they are the most crucial blood vessels that perform the nutrient and waste transport function of the vascular system (153).

A specific type of cell (sometimes mistaken as epithelial in origin) lines the interior of all these types of blood vessels. These cells are known as endothelial cells and serve as a barrier between blood cells and the tissues. Since endothelial cells regulate transport of nutrients and waste

between the blood and tissue, regulation of their phenotype and function is crucial for homeostasis to occur. Endothelial cells and the vasculature are supported by mesenchymal cells known as pericytes within microvascular beds. They are a heterogeneous population of cells that differ dependent on the type of blood vessel that they support and as such serve distinct functions for each type (47). Some speculation on the stabilization of mature vessels occurs as a result of the presence of pericytes through paracrine signaling mechanisms (21, 114). Additionally, the phenotype and function of capillary endothelial cells in various tissues and organs will be catered to each of their specific functions.

Mechanisms to propagate blood vessel generation should be considered when observing the development of a mature circulatory system. Vessel formation can occur via several different methods; vasculogenesis, sprouting angiogenesis, and intussusception. Tumor vasculature can be formed by additional methods of vessel co-option, vascular mimicry, or generation of their own endothelium (21). Vasculogenesis is the process of blood vessel formation *de novo*, occurring during embryonic development. Mesodermally derived angioblasts, vascular endothelial cells which have not yet formed lumens, form a primitive vascular network (known commonly as a vascular plexus) which serves as the basis for the circulatory system (113, 116). Angiogenesis differs from vasculogenesis and defined as the formation of blood vessels from pre-existing vasculature (1, 45). Intussusception is the generation of smaller vessels from the branching of a precursor larger vessel (32). Following the construction of the vessel framework, most blood vessel maturation occurs via sprouting angiogenesis or intussusception (116). A final mechanism of angiogenesis can occur through the recruitment of endothelial progenitor cells. Endothelial progenitor cells can differentiate into vascular endothelium and lead mobilization of the different methods described above (61, 115).

The most physiologically relevant form of angiogenesis that occurs in the adult vascular system is sprouting angiogenesis within the context of inflammation (8). *In vivo*, most angiogenesis or formation of vasculature occurs either during the menstrual cycle (47, 116), wound healing (11, 13, 87), or rises out of pathological disease states such as rheumatoid arthritis, diabetic retinopathy, endometriosis, and cancer (30, 47, 77, 116). Extensive work has been performed on understanding inflammatory angiogenesis and how it is regulated. What is currently known is

that vessel structures are formed similar to processes observed in neuronal axon guidance (21, 109, 110, 120, 133, 150). Sprouting angiogenesis is a multistep process; breakdown of ECM and basal lamina surrounding a leading cell (tip cell), migration and extension of a sprout into the medium towards an angiogenic cue, encountering and connecting with other blood vessels, followed by stabilization of the neovasculature (21, 109, 110, 120, 133, 150).

In a sprouting vessel, the cell types typically consist of a tip cell followed by stalk (or trunk) cells. These endothelial cells undergo distinct morphology changes that are easily classified by the behaviors that they undertake (150). The tip cell leads the migration of endothelial cells into the extracellular matrix and does not undergo proliferation, serving as an analogous growth cone in neural development by extending numerous filopodia that sense and respond to its local environment (22, 48, 59). Furthermore, these sprout cells have a decreased sensitivity to anti-angiogenic factors, such as the low expression of the thrombospondin-1 receptor CD36 (6). Stalk and trunk cells follow the tip cell and proliferate while migrating to permit extension of the blood vessel. These new blood vessels eventually encounter one another and create a closed circulatory system in a process known as anastomosis (150). Interestingly, a previous study has found that signaling by the main isoform of VEGF (VEGF-A) acts differentially on the sprout, where VEGF distribution determines tip cell directionality and VEGF concentration influences stalk and trunk cell proliferation (48).

1.3. Overview of the liver and its microvasculature

One of the central metabolic organs of the body, the liver is responsible for multiple functions including but not limited to: lipid, protein, and carbohydrate metabolism, bile secretion, detoxification, immune response, ECM protein synthesis, albumin secretion, lymph generation, and erythrocyte production (fetal liver) (39, 54, 80, 82, 111, 122, 139). In fact, there are so many functions the liver provides that no single technology currently exists that can reproduce all of its functions. Despite the availability and use of liver dialysis, long-term survival without the liver is thus implausible since it can only replace some function. A host of different diseases and afflictions can affect the function of the liver, including steatosis/hepatosteatosis, drug induced liver injury, fatty liver disease, nonalcoholic fatty liver disease, hepatitis, or cancer, all of which

can lead to fibrosis, cirrhosis and ultimately liver failure (7, 28, 29, 41, 67, 89, 91, 93, 97, 138, 154, 155). Absence of the liver or its functions will eventually lead to death of the host (98).

The liver is situated in the upper abdomen underneath the diaphragm. While the general architecture of the liver can differ among mammalian species, a majority of the structure is either conserved or highly analogous (75, 122). For the purposes of this introduction, the human liver anatomy will be of primary discussion. In humans, the nomenclature of the liver is split into 4 lobes; two main anatomical lobes known as the right and left, and two smaller lobes referred to as the quadrate and caudate lobes. The right and left lobes are separated by the falciform ligament, with the right lobe being six times the volume of the left lobe. The quadrate and caudate lobes are much smaller than the left lobe. The quadrate lobe is located behind the right and next to the gall bladder while the caudate lobe is situated behind and underneath the right lobe and quadrate lobe respectively (82). The lobes of the liver can be further divided into 8 segments (I-VIII; 9 segments if IVa and IVb are considered separately) based on the main vasculature using the Couinaud nomenclature (75, 82). Hepatic arteries and the portal vein supply 25% and 75% of the blood respectively to the liver (54, 82), while blood leaves from the liver into the vena cava via multiple hepatic veins. Although the rat liver differs in the macroscopic appearance of the liver, its lobes and segments correspond to segments that are found in the human liver (75).

The segments that are described in gross anatomy can be broken down and classified into smaller functional units known as lobules (Figure 1-2) (54, 82, 98). The hepatic arteries, lymph vessels, and portal vein are collectively known as the portal triad. The hepatic artery and portal vein serve as the input source of blood into the lobule, which percolates through the sinusoidal capillaries before being collected and transported away through the central vein (82). Since the liver is highly metabolic and supplied with a mixed pool of low oxygenated blood, the amount of oxygen decreases dramatically traveling from the portal triad to the central vein. This gradation in oxygenation influences the type of metabolic functions that occur within the lobule (4, 5, 98). Gluconeogenesis, hormone secretion, urea oxidation, and lipid breakdown occur in the periportal regions of the liver (60-70 mm Hg O₂), while glycolysis, detoxification and lipid synthesis occur in the perivenous regions of the liver (25-35 mm Hg O₂) (4).

Numbering around 50,000 to 100,000 in the adult liver, the liver lobules are composed of multiple cell types divided between the parenchymal cells and nonparenchymal cells.

Hepatocytes are the parenchymal cells that reside in the liver and compose about 60% of the total cell population. Nonparenchymal cell types include large vessel and sinusoidal endothelial cells, resident macrophages called Kupffer cells, and resident fibroblast-like cells known as stellate (or Ito) cells. Of the remaining 40% known as the nonparenchymal cell population, sinusoidal endothelial cells are the most numerous and comprise about half of the number cells. They are followed in number by the Kupffer cells, which consist of roughly 15% of the nonparenchymal population (131).

The functional structure and nomenclature associated with the liver lobule and sinusoid are still greatly debated, particularly in regards to the microcirculation architecture (122). In general, hepatocytes are organized into discrete sheets (plates) of cells which are separated by sinusoidal capillaries that deliver nutrients and wastes between the parenchyma and the blood (54, 82, 98). Sinusoidal capillaries are lined with discontinuous, fenestrated endothelial cells that serve to filter macromolecule and particulate exchange between the hepatocytes and blood (40).

The space of Disse separates hepatocytes from the endothelial cells that line the sinusoidal capillaries. Roughly about 1-1.5 μm in thickness (95), the Space of Disse is generally considered to lack a true basement membrane despite the presence of many ECM proteins. It is lined mostly with fibronectin and collagen IV. Collagens I and III, and laminin appear sparsely in normal liver, but increase in abundance in fibrotic livers, along with the other ECM proteins (27, 52, 96). While being the volume that physically separates liver sinusoidal endothelial cells (LSEC) and hepatocytes, the Space of Disse also serves a crucial role in the lymphatic system. Lymph secreted by hepatocytes and leaked from the sinusoids are collected in the Space of Disse. The lymph then travels to the space of Mall, located between the stroma and outermost hepatocytes. From here the lymph that was secreted is transferred into the lymphatic system through the portal hepatis and the limiting plate surrounding the portal triad (54).

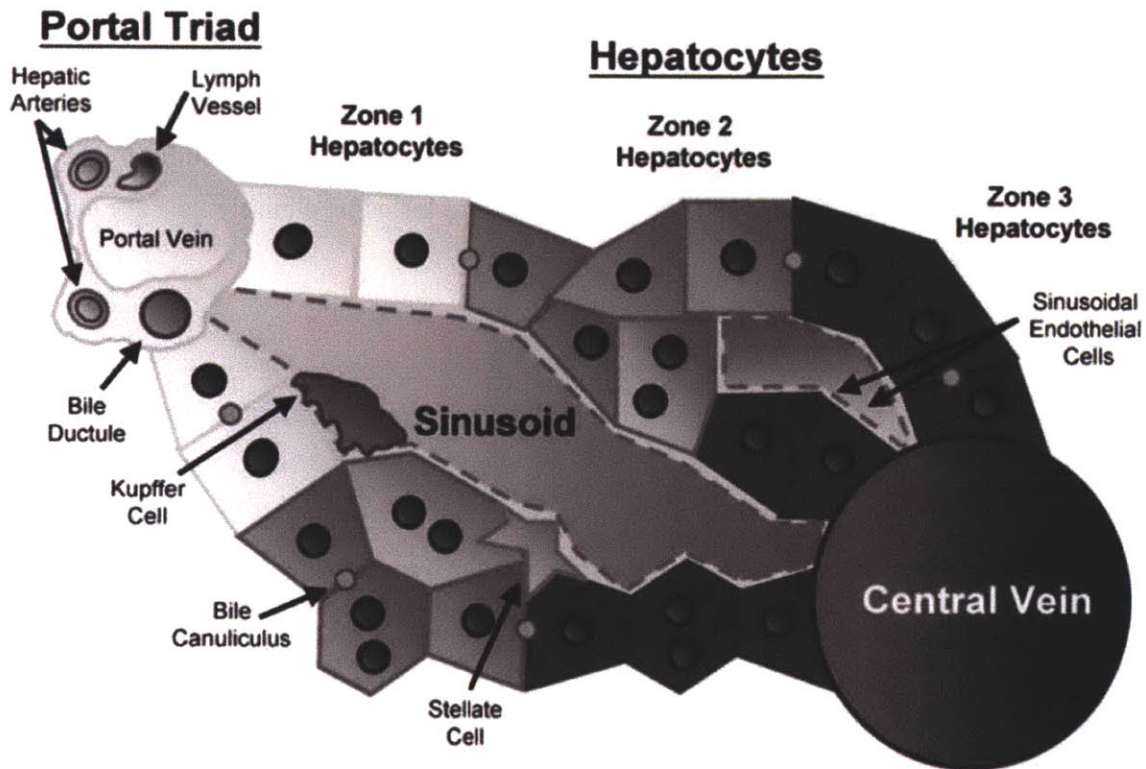


Figure 1-2. Diagrammatic representation of important liver cell types and structure (98). Reproduced with kind permission from Springer Science+Business Media: Michalopoulos GK, DeFrances M. "Liver Regeneration." *Adv Biochem Eng Biotechnol* (2005). 93:101-34. Figure 1. © Springer-Verlag Berlin Heidelberg 2005.

The parenchymal cells are primarily responsible for the metabolic and secretory functions provided by the liver (54). The liver secretes bile to facilitate lipid digestion in the gastrointestinal tract. Bile is secreted from hepatocytes into bile canaliculi and drained into the interlobular bile duct. Two main bile ducts from the right and left lobes comprise the main biliary system and collect bile from the ducts of the liver lobules before converging into the common bile duct. The gall bladder serves as part of the auxiliary biliary system and concentrates and stores bile delivered via the common duct (54, 82, 122).

Many types of model and culture systems have been employed to study and understand liver physiology. A model of liver physiology that has been extensively studied is that of liver regeneration after a partial hepatectomy (PHx) in rodents. Partial hepatectomies involve the

removal of approximately 70% of the liver mass (3 of 5 lobes) and observing the compensation of liver mass by the remaining lobes over a span of a week (20, 42, 70, 98, 139). This physiological model has elucidated a great detail of information on the cellular and molecular processes involved in simultaneous proliferation and provision of metabolic functions by the liver. Data from these models have had various applications, including clinical relevance and treatment in understanding liver cirrhosis and failure (42, 57).

Another clinical model that is intensely studied involved the process of ischemia reperfusion liver injury. During resection or transplantation, livers experience a reduction in blood flow (ischemia) followed by restoration of blood flow (reperfusion) (53). Ischemia reperfusion can elicit inflammatory responses in the liver and thereby damage it, reducing its functionality and viability. Studies using this model have been performed and have helped garner an understanding of methods to reduce the deleterious effects of this process (68, 134, 157, 159).

In vitro cultures have been utilized in addition to PHx and ischemia/reperfusion models to understand the various metabolic functions that the liver carries out. The simplest culturing method for hepatocytes has been to seed hepatocytes on ECM-coated tissue culture polystyrene or glass following mechanical disruption and purification of hepatocytes isolated from the liver. Unfortunately, 2D monolayer hepatocyte cultures lose their differentiated phenotype relatively quickly (83). Methods to improve hepatocyte differentiation maintenance for longer time intervals *in vitro* incorporate biological hydrogels made from ECM proteins such as collagen or Matrigel®, and additional steps of pre-assembling hepatocytes into cell clustered spheroids (83, 101, 126).

Biomaterials have also been used to maintain hepatocyte differentiation and function in cell cultures. Use of biopolymers like polyethylene glycol with photopatterning technology can generate three-dimensional scaffolds that can be created to the almost any specification (72, 86). Polyelectrolyte scaffolds have been produced to create stratified three-dimensional architecture to simulate *in vivo* conditions (112).

Previous work in the Griffith lab developed a perfused bioreactor system for three-dimensional liver tissue culture (34). The bioreactor system was modified and updated to a 24-multiwell plate system that allowed for cocultures of cells (hepatocytes, LSEC, and Kupffer cells) to be sustained for 7 days in the fluidic system (33, 63). Other microfluidic bioreactors have been constructed to study liver physiology *in vitro*, including those that can generate oxygen gradients (4), highly controlled micropatterned architecture (72), or high throughput to study pharmacological drug responses in the liver (46).

Majority of cellular studies in the liver have focused on the parenchymal population due to the myriad of roles hepatocytes assume. Recently, the important role that nonparenchymal cells play maintaining survival and differentiation of hepatocytes *in vitro* have come into the spotlight. Furthermore, the inclusion of nonparenchymal cells provide a more accurate representation of liver function. As the largest population of nonparenchymal cells, LSEC have been brought forward as an additional focus in their roles and interactions with hepatocytes (73, 76, 92, 94, 101, 102, 121).

LSEC are different from the traditional definition of vascular endothelial cells in multiple ways. First, they possess pores that span across the cell called fenestrae. These pores are 100-200 nm in diameter and permit the transport and exchange of certain macromolecules and nutrients between the blood and hepatocytes (19). Fenestrae are clustered on the surface of cells referred to as sieve plates. Although most span across the cell to permit transport, about one third of the fenestrae are terminal and prevent movement past the sinusoid (18). Second, LSEC do not typically express the pan endothelial marker CD31/PECAM-1 on their surfaces. Rather, the antigen is expressed only in the endosomes of the cell; CD31 is only expressed on LSEC surfaces once they dedifferentiate and lose their unique phenotype. Third, these cells possess a surface antigen that is known as SE-1 in rats (142). This surface antigen is only expressed on LSEC and are not found in any other tissue (40). A recent study found that the identity of SE-1 in humans and mice was known as CD32b and was found to be associated with endocytosis of immune complexes (94).

Supplementary to their role as the arbiters between blood and parenchyma, LSEC have high scavenger activity for multiple macromolecules. These include fatty acids (105, 142), lipoproteins (64, 85, 100), proteoglycans such as hyaluronan (55), and immune/inflammatory markers such as LPS (66, 78). Additionally, they serve as a major component along with macrophages of the reticuloendothelial system for clearing waste from the liver (39). Finally, unlike typical vascular endothelial cells, LSEC do not possess a basal lamina; LSEC attach to ECM proteins that sparsely populate the space of Disse.

Current *in vitro* culturing methods have been developed that allow LSEC survival from 6 up to 30 days. These methods employ the use of hepatocyte conditioned medium or presence of multiple growth factors (76), or utilize a “synthetic serum” that is made from non-animal sources (15, 38).

1.4. Overview of inflammation and wound healing

Wound healing is a physiological process that occurs in the adult body in response to trauma or injury to a localized area. Trauma and injury can be inflicted externally, through the introduction of a foreign agent into the localized region (immune response), or be an absence of self-recognition (autoimmune). Although quite complex in nature, steps in wound healing can be categorized into five general steps following tissue damage (Figure 1-3): 1) blood clotting and hemostasis; 2) inflammation and acute immune response; 3) granulation tissue formation; 4) reepithelialization; 5) matrix formation and remodeling (152). Wound repair is orchestrated by a multitude of cytokines, growth factors, and chemokines that are released simultaneously during these stages (13). As a broad outline of a bodily response, these steps may include different permutations resulting in how inflammation and immune response (step 2) are locally induced. In conjunction with these molecules, ECM proteins play an important role in binding cytokines and presenting cell adhesion sites, thereby facilitating cell-cell, cell-matrix, and cell-cytokine interactions. Different ECM proteins are important for particular interactions to take place at certain stages, and abnormalities in ECM proteins can prevent proper progression in wound repair (24, 124). Thus, ECM proteins help facilitate paracrine and autocrine signaling of cells within localized wound regions. Aberrations and disruptions in the healing process via changes

in ECM protein or cytokine expression can create sub-optimal, altered tissues such as scarring, fibrosis, or metaplasia (128). The balance of these cytokines and cues are crucial to completing the wound repair process.

Following stabilization and clotting of a wound directly after injury, the process of wound healing continues, mainly directed by inflammatory response. Inflammation induces the release of multiple cytokines from resident cells in damaged tissue (e.g. platelets in circulation, keratinocytes in skin) that elicit immune responses and the rest of wound repair (13). Some of the important immune response cues released during wound healing are members of chemokines. Chemokines are a subset of cytokines that were first discovered and categorized as biomolecules that induced chemotaxis of immune cells and initiate localized inflammation (49, 50). With highly conserved amino structures, chemokines can be divided into two general sub-groups: one group that has two cysteine residues (CC chemokines) and another group that has a non cysteine residue that separates the two (CXC chemokines) (10). Within these two subgroups, chemokines can potentially possess a N-terminal motif of Glutamate-Leucine-Arginine (ELR), which can confer differential recruitment of cell types (88). Chemokines share a high degree of homology among the different types and can exert their effects by binding to multiple ligands or receptors. They can also bind to distinct chemokine receptors which are classified as canonical seven transmembrane G-coupled protein receptors (88, 140).

Chemokines such as CXCR2, along with potent cytokines VEGF, PDGF, FGF, and many others, elicit endothelial migration/recruitment and angiogenesis to restore homeostasis to the tissue. Of particular note is that most of pro-angiogenic signaling is generated while many angiostatic signals are simultaneously being elicited via inflammatory pathways. Interestingly, a majority of the chemokines that have been reported to have a role in affecting angiogenesis are members of the CXC chemokine family. Pro-angiogenic effects are conferred through the presence of the ELR sequence while it is absent in angiostatic chemokines (ELR- chemokines) (117).

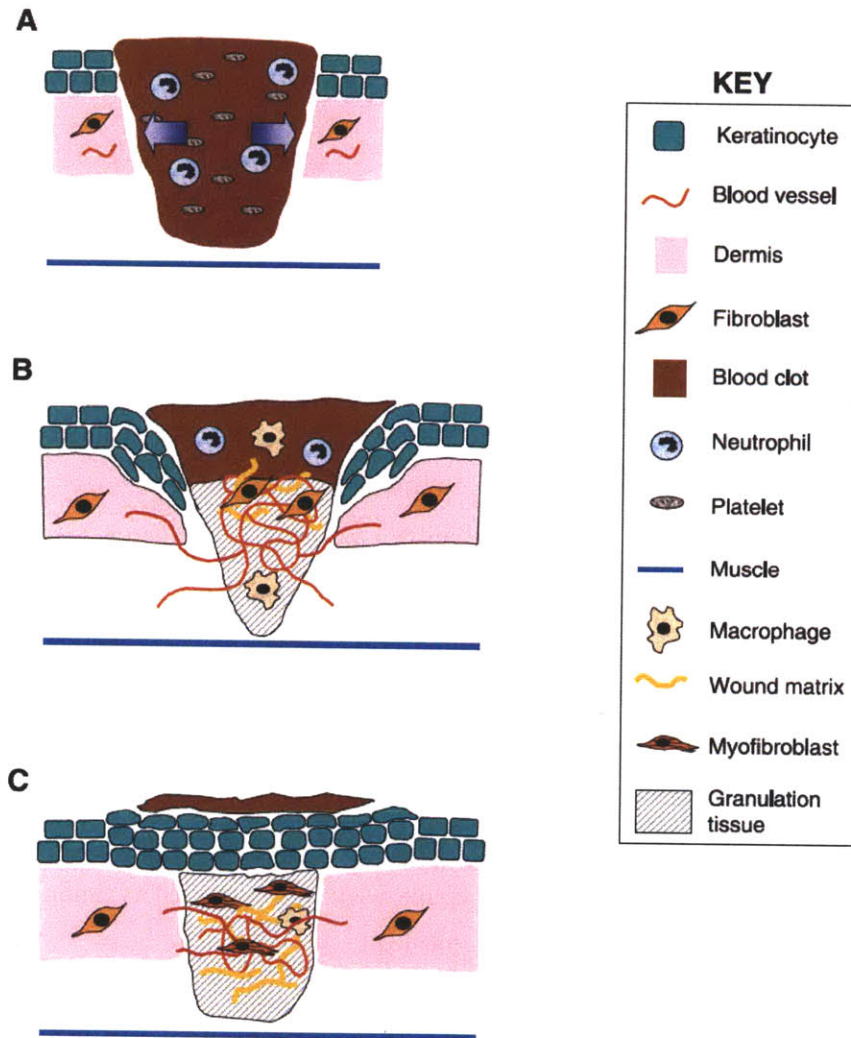


Figure 1-3. Schematic of wound repair process adapted from (152). Following wounding to tissue (e.g. skin), a blood clot is formed by the aggregation of platelets creating a hemostatic plug (A). Shortly after this, inflammation ensues and induces an immune response along with granulation tissue formation (B). During this time, angiogenesis and recruitment of endothelial cells occur, facilitating re-epithelialization, matrix formation, and remodeling by resident cell populations (e.g. keratinocytes) and immune cells (C) until the original tissue status is re-established.

Following the introduction of trauma or injury to a site, platelet factor 4 (PF-4) is released in large quantities from platelets into the damaged area of the tissue, where levels can reach up to 25 μM (2). In wound healing, platelets will release certain ECM proteins (e.g. fibrinogen, fibronectin) that will generate a hemostatic plug to fill in the wounded tissue area. This process is

immediately followed by inflammatory responses, where immune cells are recruited to the localized area by resident cells (e.g. keratinocytes in dermal wounds). During inflammation, several growth factors (e.g., FGF-2, TGF- β , PDGF, and VEGF) are released by various cells participating in the response process (e.g., macrophages, neutrophils, platelets, smooth muscle cells, mast cells, endothelial cells, fibroblasts, keratinocytes) that also affect the vascularization of the wounded area to allow for granulation and re-epithelialization steps to occur (13).

Chronically elevated expression and levels of chemokines can prevent the progression of wound healing (via chronic inflammation or incomplete recruitment of angiogenesis); expression of these chemokines in circulating blood plasma can also serve as predictive indicators of diseases such as atherosclerosis and lesion formation (135). Decreased or absence of chemokines during wound healing can also prevent reformation of the tissue, creating a chronic inflammatory or wound state, such as that observed in rheumatoid arthritis or ulcers (123, 136).

Much data have been revealed on chemokines and their angiostatic effect on endothelial cells, particularly PF-4 (2, 117, 125, 137, 149). There are several mechanisms that PF-4 is speculated to act on endothelial cells. PF-4 can either affect endothelial cells by interfering with the VEGFR2 pathway by sequestering VEGF or heparan sulfate proteoglycans on the cell surface used to assist in binding to VEGFR2. PF-4 can also bind to integrins and outcompete ECM proteins that are used for cell migration (e.g., fibronectin). Finally, PF-4 can bind to and signal through its own receptor, known as CXCR3/CXCR3B (2).

While the responses PF-4 elicits are well established, not much is known about the molecular mechanisms employed to accomplish this. Currently, the only published literature on PF-4 induced signal pathways in endothelial cells indicate an increase in phospho-P38 MAPK levels following activation of its receptor CXCR3 (106). Other literature indicate that PF-4 can affect many multiple pathways including Akt, ERK, PKA, p21waf, and others, although the caveat being in other cell types. A spliced variant of PF-4, CXCL4L1, is also secreted by platelets. It is more potent in its angiostatic activity, although does not seem to be directly involved in inflammatory responses since it does not induce chemotactic responses by monocytes or lymphocytes (36, 132, 147).

Although chemokines play a key role in facilitating the wound healing process, their role is more expansive for inflammation and are involved with other physiological processes. Chemokines are present in the liver normally as hepatocytes are the primary agents that remove chemokines from the bloodstream (118). Furthermore, CXC chemokines (including PF-4) have been implicated in promoting liver regeneration and inducing dysfunction (35, 56, 145, 158). PF-4 may not only have angiostatic effects on endothelial cells, but also promote angiogenesis through other mechanisms, such as its pleiotropic effects on pericytes, which are known to assist in neovascular capillary stabilization (79, 81, 106).

Thus, endothelial cells induce the process of angiogenesis following the inflammation stage in wound healing. However, they also perform other important duties such as the recruitment of key immune cell populations to inflamed tissue. As such, endothelial cells are important for most inflammatory events that occur as a response mechanism to prevent further injury or infection (74, 107). Evidence supports that angiogenesis and inflammation are closely intertwined; angiogenesis in the adult body may not occur without the presence of inflammation, such as the recruitment of immune cells and the secretion of chemokines (51, 107). For complete restoration of wounded or inflamed tissue, endothelial cells play critical roles by generating functional vasculature, participating in wound closure, generating granulation tissue immediately after inflammatory immune responses, and even secreting inflammatory cytokines of their own to recruit additional immune cells (11, 16, 49, 107, 152). Angiogenesis therefore is a particularly important area of focus and study to understand wound healing and its potential applications, including the role it plays in cancer (30, 103, 148).

Many links are being established between cancer development, inflammation, and angiogenesis. Prolonged inflammation has been associated with approximately 25% of the types of known cancers (77). Angiogenesis has even been considered one of the critical links between inflammation and the development of cancer due to a positive feedback role it takes on; inflammation induces angiogenesis, and angiogenesis induces migration of immune cells that secrete inflammatory cytokines and growth factors further exacerbating inflammation (8, 74). This can prime the environment for tumor initiation due to high levels of inflammatory

byproducts such as reactive oxygen species and DNA damage promoting agents (30, 77). Furthermore, tumor growth has been found to be dependent on angiogenesis. Tumors can hijack the angiogenic vessel formation processes in order to propagate its growth, whether it arises from avascular origin or is a metastatic offshoot of a malignant tumor (14, 21, 45, 156). It is evident that inflammation has many implications in both normal and pathological angiogenesis.

1.5. Physiologically relevant models of angiogenesis for vascular regulation

There is currently no gold standard for angiogenesis assays. Many different types of assays are utilized to quantify and study the various aspects of endothelial behavior. Commonly used *in vivo* angiogenesis assays exist, including sponge implantation, chick chorioallantoic membrane assay, corneal micropocket assay, dorsal air sac model, and rabbit ear chamber model (26, 108, 130).

Classical *in vitro* assays are more varied and focus on different facets of endothelial cell phenotype and behavior. MTT, BrdU, cell cycle analysis, and tritiated thymidine assays are used to assess proliferation, while phagokinetic track, wound healing models, and Boyden chambers are used to measure migratory behavior of endothelial cells (130, 144). The process of angiogenesis and differentiation in endothelial cells can be measured using various matrix-coated assays (e.g. collagen, Matrigel®) or 3D gels (using the same matrix or synthetic polymers such as peptide gels) (32, 71, 130).

Modern *in vitro* assays incorporate engineering aspects into the classical culturing assays to provide model systems where all different endothelial phenotypes can be potentially measured. These include the use of microfluidic systems that can simulate fluid flow that endothelial cells experience *in vivo*. Microfluidic bioreactors were used to simulate interstitial flow experienced by endothelial cells *in vivo*. Previous work demonstrated that sprouting angiogenesis was induced in the direction of fluid flow (although the number of sprouts were independent of flow velocity) (60). A follow-up with more elaborate work in the Kamm Laboratory at MIT has gone into designing a high throughput microfluidic device to be used to study proliferation, migration, and angiogenic sprouting (Figure 1-4) (25, 65).

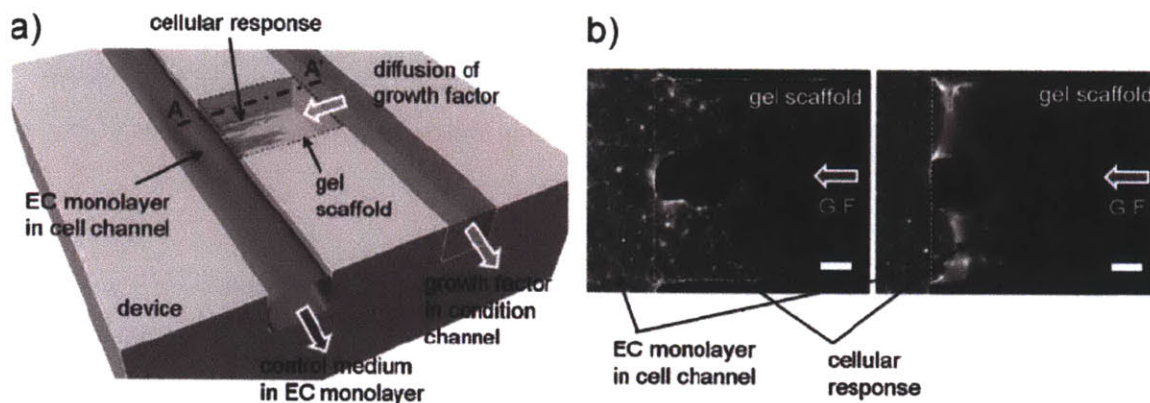


Figure 1-4. Microfluidic device incorporating fluid flow for studying angiogenesis (25). Reproduced with kind permission from John Wiley & Sons: Chung S., Sudo R., Zervantonakis K, Rimchala T, Kamm RD. "Surface-Treatment-Induced Three-Dimensional Capillary Morphogenesis in a Microfluidic Platform." *Adv Mater* (2009). 21(47): 4863-4867, © WILEY-VCH Verlag GmbH & Co. KGaA, Weinheim 2009.

Computational techniques can be applied to the angiogenic process to simulate and predict their behavior in these *in vitro* model systems. However, angiogenesis is complex and difficult to model *in silico*. Computational work has been completed on transport mechanisms that are associated with capillary morphogenesis and vasculature, such as oxygen transport (37). Multiple methods, including the use of ordinary and partial differential equations, have been used to model the process of angiogenic sprouting although may not be completely accurate due to the deterministic nature of those equations (84). More recently, approaches have focused on hybrid modeling techniques in order to capture as much of the biological phenomena reflected in experimental observations *in vitro* and *in vivo* (31, 99, 109, 110, 141). The hybrid techniques utilize an agent-based model approach to simulate sprouting angiogenesis, where each cell or cell population (serving as the "agent") behaves following a described set of rules. The rule sets can describe how these cells act in paracrine or autocrine fashion, and in the case of angiogenesis, the decision for sprouting to occur (17, 31, 141). As such, a combination of these computational techniques with experimental models can provide a wealth of data and insight into potential clinical therapies involving angiogenesis or anti-angiogenic treatments.

1.6. Thesis overview

Tissue engineering has made giant advances towards synthesizing organs and tissues in efforts to combat the rapidly rising needs and medical shortages that currently exist. However, it is very clear that current limitations seen by the field of tissue engineering prevent maximization of its potential and progress in applications towards treatments. Thus this work focuses on studying methods that can potentially advance the field forward by providing a platform and mechanistic insight into providing and sustaining a functional vasculature for *ex vivo* tissue constructs.

In rationalizing our work, we focused on the liver due to its complex metabolic functions and demands, making it ideal for consideration as an *ex vivo* engineered tissue. This led to our work on culturing LSEC *in vitro*; our work focused on extending their survival in culture (beyond current means) and understanding their physiology and role in maintaining their own and parenchymal function. If LSEC die *ex vivo*, the microvasculature dies with them, essentially killing off the tissue.

Once engineered tissue is successfully generated with functional microvasculature, there is a need to ensure that the tissue integrates with the host following implantation. In order for this to occur, angiogenesis must happen between the host's pre-existing circulatory system and the new tissue surrogate. Thus the second component of this work entails studies on how the integrative angiogenesis will happen, as the implantation process of the tissue will induce inflammation (similar to that observed with wound healing). The work is then focused on understanding the signaling pathways/cues involved in inducing angiogenesis to occur and permit successful fusion of the tissue into the host body's vasculature. Unfortunately, since this is difficult to do with LSEC in *ex vivo* constructs, a commercially available, robust model of adult human dermal microvascular endothelial cells (HDMVEC) was used as a replacement.

Obtaining large collections of data is a nontrivial obstacle when working with primary cells, especially LSEC as they are not as abundant, cannot be expanded, and require very high seeding densities for survival due to their reliance on cell-cell contacts. As such, the secondary, more amenable HDMVEC system was introduced to help generate and optimize protocols for exploring signaling pathways. In addition to the development of signaling assay applications for

LSEC, the HDMVEC system could be used to directly address questions about physiological phenomena that occur during inflammation that is conducive to angiogenesis, which can be applicable to the liver system as well. Signaling data sets from HDMVEC culture system and their conclusions may also allow us to infer behavior of LSEC.

Thus, the overall objective of this work is to generate *in vitro* frameworks to understand microvascular endothelial cells in response to inflammatory signaling cues, thereby providing insight on host responses to implanted tissues or physiological surrogates. The underlying hypothesis is that a balance of both positive and negative cues simultaneously regulates microvascular endothelial cell function by providing differential spatial and temporal signaling activation. Although microvessel endothelial cells possess unique characteristics, traits, and responses dependent on their localized milieu, cue-signal relationships are still highly conserved among cell types. Thereby it is possible to infer signaling pathways crucial for specialized behaviors across different endothelial archetypes.

Chapter 2 covers the development of *in vitro* culture techniques for sustaining LSEC phenotype, function, and proliferation via lipid supplementation. Chapter 3 covers protocol development for collecting signaling data in the HDMVEC system from angiostatic and angiogenic conditions streamlined with the microfluidic system developed in the Kamm lab (Figure 1-4). Chapter 4 presents the data sets collected on signaling pathways involved with angiogenic signaling.

There are multiple implications in findings of this thesis work as a result. Lipids are seemingly required for LSEC survival and phenotype maintenance; they may play an important role during this process as hepatocytes release a large concentration of lipids during liver tissue injury. This can thus provide insight both into inflammatory injury responses, as well as fatty liver disease physiological responses (along with cirrhosis/fibrosis and other liver dysfunctions). Second, the liver is one of the central regulators for clearance of inflammatory factors within the bloodstream. As sinusoidal endothelial cells are the filters between hepatocytes and the blood, they will be the first to see these molecules (such as PF-4, which is primarily cleared in the liver) before they are processed and removed by hepatocytes. Third, the study of angiogenesis in context of inflammation is very important, as most adult angiogenesis occurs in this

environment, pathological and physiological. This study can elucidate how angiogenesis is induced during this process, and perhaps how to manipulate it on a cellular basis via signaling cues in cases where angiogenesis is needed. Finally, this can provide insight into how certain vascular diseases occur as a result of inflammation – such as rheumatoid arthritis or the formation of myeloid bodies due to under and over vascularization (and chronic wounds), also the formation and onset of cancer.

1.7. REFERENCES

1. **Adair TH, Montani J-P.** Angiogenesis [Online]. Morgan & Claypool Life Sciences. <http://www.ncbi.nlm.nih.gov/books/NBK53242/>.
2. **Aidoudi S, Bikfalvi A.** Interaction of PF4 (CXCL4) with the vasculature: a role in atherosclerosis and angiogenesis. *Thromb. Haemost.* 104: 941–948, 2010.
3. **Alberts B, Johnson A, Lewis J, Raff M, Roberts K, Walter P.** Molecular Biology of the Cell [Online]. 4th ed. Garland Science. <http://www.ncbi.nlm.nih.gov/books/NBK21054/>.
4. **Allen JW, Bhatia SN.** Formation of steady-state oxygen gradients in vitro: application to liver zonation. *Biotechnol. Bioeng.* 82: 253–262, 2003.
5. **Allen JW, Khetani SR, Bhatia SN.** In vitro zonation and toxicity in a hepatocyte bioreactor. *Toxicol. Sci.* 84: 110–119, 2005.
6. **Anderson CR, Hastings NE, Blackman BR, Price RJ.** Capillary sprout endothelial cells exhibit a CD36 low phenotype: regulation by shear stress and vascular endothelial growth factor-induced mechanism for attenuating anti-proliferative thrombospondin-1 signaling. *The American Journal of Pathology* 173: 1220–1228, 2008.
7. **Angulo P.** Nonalcoholic fatty liver disease. *N Engl J Med* 346: 1221–1231, 2002.
8. **Arroyo AG, Iruela-Arispe ML.** Extracellular matrix, inflammation, and the angiogenic response. *Cardiovascular Research* 86: 226–235, 2010.
9. **Atala A.** Engineering organs. *Current Opinion in Biotechnology* 20: 575–592, 2009.
10. **Balestrieri ML, Balestrieri A, Mancini FP, Napoli C.** Understanding the immunoangiostatic CXC chemokine network. *Cardiovascular Research* 78: 250–256, 2008.
11. **Bao P, Kodra A, Tomic-Canic M, Golinko MS, Ehrlich HP, Brem H.** The role of vascular endothelial growth factor in wound healing. *J. Surg. Res.* 153: 347–358, 2009.
12. **Barber RW, Emerson DR.** Biomimetic design of artificial micro-vasculatures for tissue engineering. *Altern Lab Anim* 38 Suppl 1: 67–79, 2010.
13. **Barrientos S, Stojadinovic O, Golinko MS, Brem H, Tomic-Canic M.** Growth factors and cytokines in wound healing. *Wound Repair Regen* 16: 585–601, 2008.
14. **Bergers G, Benjamin LE.** Tumorigenesis and the angiogenic switch. *Nat Rev Cancer* 3: 401–410, 2003.

15. **Bertheussen K.** Growth of cells in a new defined protein-free medium. *Cytotechnology* 11: 219–231, 1993.
16. **Blum A, Miller HI.** The role of inflammation in atherosclerosis. *Isr. J. Med. Sci.* 32: 1059–1065, 1996.
17. **Bonabeau E.** Agent-based modeling: methods and techniques for simulating human systems. *Proc. Natl. Acad. Sci. U.S.A.* 99 Suppl 3: 7280–7287, 2002.
18. **Braet F, Riches J, Geerts W, Jahn KA, Wisse E, Frederik P.** Three-dimensional organization of fenestrae labyrinths in liver sinusoidal endothelial cells. *Liver Int* 29: 603–613, 2009.
19. **Braet F, Wisse E.** Structural and functional aspects of liver sinusoidal endothelial cell fenestrae: a review. *Comp Hepatol* 1: 1, 2002.
20. **Brasaemle DL.** Cell biology. A metabolic push to proliferate. *Science* 313: 1581–1582, 2006.
21. **Carmeliet P, Jain RK.** Molecular mechanisms and clinical applications of angiogenesis. *Nature* 473: 298–307, 2011.
22. **Carmeliet P, Tessier-Lavigne M.** Common mechanisms of nerve and blood vessel wiring. *Nature* 436: 193–200, 2005.
23. **Carmeliet P.** Angiogenesis in life, disease and medicine. *Nature* 438: 932–936, 2005.
24. **Chaudhuri V, Karasek MA.** Mechanisms of microvascular wound repair II. Injury induces transformation of endothelial cells into myofibroblasts and the synthesis of matrix proteins. *In Vitro Cell. Dev. Biol. Anim.* 42: 314–319, 2006.
25. **Chung S, Sudo R, Zervantonakis IK, Rimchala T, Kamm RD.** Surface-treatment-induced three-dimensional capillary morphogenesis in a microfluidic platform. *Adv. Mater. Weinheim* 21: 4863–4867, 2009.
26. **Cimpean A-M, Ribatti D, Raica M.** A brief history of angiogenesis assays. *Int. J. Dev. Biol.* 55: 377–382, 2011.
27. **Clement B, Grimaud JA, Campion JP, Deugnier Y, Guillouzo A.** Cell types involved in collagen and fibronectin production in normal and fibrotic human liver. *Hepatology* 6: 225–234, 1986.
28. **Cosgrove BD, Alexopoulos LG, Hang T-C, Hendriks BS, Sorger PK, Griffith LG, Lauffenburger DA.** Cytokine-associated drug toxicity in human hepatocytes is

- associated with signaling network dysregulation. *Mol Biosyst* 6: 1195–1206, 2010.
29. **Coulon S, Heindryckx F, Geerts A, Van Steenkiste C, Colle I, Van Vlierberghe H.** Angiogenesis in chronic liver disease and its complications. *Liver Int* 31: 146–162, 2011.
 30. **Coussens LM, Werb Z.** Inflammation and cancer. *Nature* 420: 860–867, 2002.
 31. **Das A, Lauffenburger D, Asada H, Kamm RD.** A hybrid continuum-discrete modelling approach to predict and control angiogenesis: analysis of combinatorial growth factor and matrix effects on vessel-sprouting morphology. *Philos Transact A Math Phys Eng Sci* 368: 2937–2960, 2010.
 32. **Davis GE, Bayless KJ, Mavila A.** Molecular basis of endothelial cell morphogenesis in three-dimensional extracellular matrices. *Anat. Rec.* 268: 252–275, 2002.
 33. **Domansky K, Inman W, Serdy J, Dash A, Lim MH, Griffith LG.** Perfused multiwell plate for 3D liver tissue engineering. *Lab Chip* 10: 51–58, 2010.
 34. **Domansky K, Sivaraman A.** Micromachined bioreactor for in vitro cell self-assembly and 3D tissue formation. In: *Lab-on-Chips for Cellomics: Micro and Nanotechnologies for Life Science*, edited by Andersson H, van den Berg A. Norwell, MA: Kluwer Academic Publishers, 2004.
 35. **Dominguez M, Miquel R, Colmenero J, Moreno M, García-Pagán J-C, Bosch J, Arroyo V, Ginès P, Caballería J, Bataller R.** Hepatic expression of CXC chemokines predicts portal hypertension and survival in patients with alcoholic hepatitis. *Gastroenterology* 136: 1639–1650, 2009.
 36. **Dubrac A, Quemener C, Lacazette E, Lopez F, Zanibellato C, Wu W-G, Bikfalvi A, Prats H.** Functional divergence between 2 chemokines is conferred by single amino acid change. *Blood* 116: 4703–4711, 2010.
 37. **Egginton S, Gaffney E.** Tissue capillary supply--it's quality not quantity that counts! *Exp. Physiol.* 95: 971–979, 2010.
 38. **Elvevold K, Nedredal GI, Revhaug A, Bertheussen K, Smedsrød B.** Long-term preservation of high endocytic activity in primary cultures of pig liver sinusoidal endothelial cells. *Eur. J. Cell Biol.* 84: 749–764, 2005.
 39. **Elvevold K, Smedsrød B, Martinez I.** The liver sinusoidal endothelial cell: a cell type of controversial and confusing identity. *Am. J. Physiol. Gastrointest. Liver Physiol.* 294:

- G391–400, 2008.
40. **Enomoto K, Nishikawa Y, Omori Y, Tokairin T, Yoshida M, Ohi N, Nishimura T, Yamamoto Y, Li Q.** Cell biology and pathology of liver sinusoidal endothelial cells. *Med Electron Microsc* 37: 208–215, 2004.
 41. **Fainboim L, Cheriñavsky A, Paladino N, Flores AC, Arruvito L.** Cytokines and chronic liver disease. *Cytokine Growth Factor Rev.* 18: 143–157, 2007.
 42. **Fausto N, Campbell JS, Riehle KJ.** Liver regeneration. *Hepatology* 43: S45–53, 2006.
 43. **Feil G, Daum L, Amend B, Maurer S, Renninger M, Vaegler M, Seibold J, Stenzl A, Sievert K-D.** From tissue engineering to regenerative medicine in urology--the potential and the pitfalls. *Adv. Drug Deliv. Rev.* 63: 375–378, 2011.
 44. **Flaim CJ, Chien S, Bhatia SN.** An extracellular matrix microarray for probing cellular differentiation. *Nat. Methods* 2: 119–125, 2005.
 45. **Folkman J.** Angiogenesis. *Annu. Rev. Med.* 57: 1–18, 2006.
 46. **Gebhardt R, Hengstler JG, Müller D, Glöckner R, Buening P, Laube B, Schmelzer E, Ullrich M, Utesch D, Hewitt N, Ringel M, Hilz BR, Bader A, Langsch A, Koose T, Burger H-J, Maas J, Oesch F.** New hepatocyte in vitro systems for drug metabolism: metabolic capacity and recommendations for application in basic research and drug development, standard operation procedures. *Drug Metab. Rev.* 35: 145–213, 2003.
 47. **Gerhardt H, Betsholtz C.** Endothelial-pericyte interactions in angiogenesis. *Cell Tissue Res.* 314: 15–23, 2003.
 48. **Gerhardt H, Golding M, Fruttiger M, Ruhrberg C, Lundkvist A, Abramsson A, Jeltsch M, Mitchell C, Alitalo K, Shima D, Betsholtz C.** VEGF guides angiogenic sprouting utilizing endothelial tip cell filopodia. *The Journal of Cell Biology* 161: 1163–1177, 2003.
 49. **Gillitzer R, Goebeler M.** Chemokines in cutaneous wound healing. *J. Leukoc. Biol.* 69: 513–521, 2001.
 50. **Gomperts B, PER T, KM I.** Signal Transduction [Online]. 2nd ed. Academic Press. <http://www.elsevierdirect.com/ISBN/9780123694416/Signal-Transduction>.
 51. **Griffioen AW, Molema G.** Angiogenesis: potentials for pharmacologic intervention in the treatment of cancer, cardiovascular diseases, and chronic inflammation. *Pharmacol.*

- Rev.* 52: 237–268, 2000.
52. **Griffiths MR, Keir S, Burt AD.** Basement membrane proteins in the space of Disse: a reappraisal. *Journal of Clinical Pathology* 44: 646–648, 1991.
 53. **Gurusamy KS, Gonzalez HD, Davidson BR.** Current protective strategies in liver surgery. *WJG* 16: 6098–6103, 2010.
 54. **Guyton AC.** *Textbok of Medical Physiology*. 8th ed. Philadelphia, PA: W.B. Saunders Company, 1991.
 55. **Hansen B, Longati P, Elvevold K, Nedredal GI, Schledzewski K, Olsen R, Falkowski M, Kzhyshkowska J, Carlsson F, Johansson S, Smedsrød B, Goerdts S, Johansson S, McCourt P.** Stabilin-1 and stabilin-2 are both directed into the early endocytic pathway in hepatic sinusoidal endothelium via interactions with clathrin/AP-2, independent of ligand binding. *Experimental Cell Research* 303: 160–173, 2005.
 56. **Harvey CE, Post JJ, Palladinetti P, Freeman AJ, Ffrench RA, Kumar RK, Marinos G, Lloyd AR.** Expression of the chemokine IP-10 (CXCL10) by hepatocytes in chronic hepatitis C virus infection correlates with histological severity and lobular inflammation. *J. Leukoc. Biol.* 74: 360–369, 2003.
 57. **Hata S, Namae M, Nishina H.** Liver development and regeneration: from laboratory study to clinical therapy. *Dev. Growth Differ.* 49: 163–170, 2007.
 58. **Hendrickx B, Vranckx JJ, Lutun A.** Cell-based vascularization strategies for skin tissue engineering. *Tissue Eng Part B Rev* 17: 13–24, 2011.
 59. **Herbert SP, Stainier DYR.** Molecular control of endothelial cell behaviour during blood vessel morphogenesis. *Nat Rev Mol Cell Biol* 12: 551–564, 2011.
 60. **Hernández Vera R, Genové E, Alvarez L, Borrós S, Kamm R, Lauffenburger D, Semino CE.** Interstitial fluid flow intensity modulates endothelial sprouting in restricted Src-activated cell clusters during capillary morphogenesis. *Tissue Eng Part A* 15: 175–185, 2009.
 61. **Hillen F, Griffioen AW.** Tumour vascularization: sprouting angiogenesis and beyond. *Cancer Metastasis Rev* 26: 489–502, 2007.
 62. **HRSA.** gapgraph [Online]. OPTN. <http://www.organdonor.gov/aboutStatsFacts.asp>.
 63. **Hwa AJ, Fry RC, Sivaraman A, So PT, Samson LD, Stolz DB, Griffith LG.** Rat liver sinusoidal endothelial cells survive without exogenous VEGF in 3D perfused co-

- cultures with hepatocytes. *FASEB J.* 21: 2564–2579, 2007.
64. **Irving MG, Roll FJ, Huang S, Bissell DM.** Characterization and culture of sinusoidal endothelium from normal rat liver: lipoprotein uptake and collagen phenotype. *Gastroenterology* 87: 1233–1247, 1984.
 65. **Jeong GS, Han S, Shin Y, Kwon GH, Kamm RD, Lee S-H, Chung S.** Sprouting angiogenesis under a chemical gradient regulated by interaction with endothelial monolayer in microfluidic platform. *Anal. Chem.* (October 10, 2011). doi: 10.1021/ac202170e.
 66. **Kamimoto M, Rung-Ruangkijkrui T, Iwanaga T.** Uptake ability of hepatic sinusoidal endothelial cells and enhancement by lipopolysaccharide. *Biomed. Res.* 26: 99–107, 2005.
 67. **Kaplowitz N.** Liver biology and pathobiology. *Hepatology* 43: S235–8, 2006.
 68. **Karaa A, Kamoun WS, Clemens MG.** Oxidative stress disrupts nitric oxide synthase activation in liver endothelial cells. *Free Radic. Biol. Med.* 39: 1320–1331, 2005.
 69. **Kauly T, Kaufman-Francis K, Lesman A, Levenberg S.** Vascularization--the conduit to viable engineered tissues. *Tissue Eng Part B Rev* 15: 159–169, 2009.
 70. **Khan AZ, Mudan SS.** Liver regeneration: mechanisms, mysteries and more. *ANZ J Surg* 77: 9–14, 2007.
 71. **Khan OF, Sefton MV.** Endothelialized biomaterials for tissue engineering applications in vivo. *Trends Biotechnol.* 29: 379–387, 2011.
 72. **Khetani SR, Bhatia SN.** Engineering tissues for in vitro applications. *Current Opinion in Biotechnology* 17: 524–531, 2006.
 73. **Khetani SR, Szulgit G, Del Rio JA, Barlow C, Bhatia SN.** Exploring interactions between rat hepatocytes and nonparenchymal cells using gene expression profiling. *Hepatology* 40: 545–554, 2004.
 74. **Kobayashi H, Lin PC.** Angiogenesis links chronic inflammation with cancer. *Methods Mol. Biol.* 511: 185–191, 2009.
 75. **Kogure K, Ishizaki M, Nemoto M, Kuwano H, Makuuchi M.** A comparative study of the anatomy of rat and human livers. *J Hepatobiliary Pancreat Surg* 6: 171–175, 1999.
 76. **Krause P, Markus PM, Schwartz P, Unthan-Fechner K, Pestel S, Fandrey J, Probst I.** Hepatocyte-supported serum-free culture of rat liver sinusoidal endothelial cells.

- Journal of Hepatology* 32: 718–726, 2000.
77. **Kundu JK, Surh Y-J.** Inflammation: gearing the journey to cancer. *Mutat. Res.* 659: 15–30, 2008.
 78. **Lai WK, Sun PJ, Zhang J, Jennings A, Lalor PF, Hubscher S, McKeating JA, Adams DH.** Expression of DC-SIGN and DC-SIGNR on human sinusoidal endothelium: a role for capturing hepatitis C virus particles. *The American Journal of Pathology* 169: 200–208, 2006.
 79. **Lasagni L, Francalanci M, Annunziato F, Lazzeri E, Giannini S, Cosmi L, Sagrinati C, Mazzinghi B, Orlando C, Maggi E, Marra F, Romagnani S, Serio M, Romagnani P.** An alternatively spliced variant of CXCR3 mediates the inhibition of endothelial cell growth induced by IP-10, Mig, and I-TAC, and acts as functional receptor for platelet factor 4. *J. Exp. Med.* 197: 1537–1549, 2003.
 80. **Laurens N, Koolwijk P, de Maat MPM.** Fibrin structure and wound healing. *J. Thromb. Haemost.* 4: 932–939, 2006.
 81. **Lazzeri E, Romagnani P.** CXCR3-binding chemokines: novel multifunctional therapeutic targets. *Curr Drug Targets Immune Endocr Metabol Disord* 5: 109–118, 2005.
 82. **Le Bail B, Balabaud C.** Anatomy and Structure of the Liver and Biliary Tree. In: *Hepatobiliary Diseases*, edited by Prieto J, Rodes J, DA S. Berlin: Springer-Verlag, 1992, p. 1–38.
 83. **LeCluyse EL, Bullock PL, Parkinson A.** Strategies for restoration and maintenance of normal hepatic structure and function in long-term cultures of rat hepatocytes. *Adv. Drug Deliv. Rev.* 22: 133–186, 1996.
 84. **Levine HA, Sleeman BD, Nilsen-Hamilton M.** Mathematical modeling of the onset of capillary formation initiating angiogenesis. *J Math Biol* 42: 195–238, 2001.
 85. **Li R, Oteiza A, Sørensen KK, McCourt P, Olsen R, Smedsrød B, Svistounov D.** Role of liver sinusoidal endothelial cells and stabilins in elimination of oxidized low-density lipoproteins. *AJP: Gastrointestinal and Liver Physiology* 300: G71–81, 2011.
 86. **Liu Tsang V, Chen AA, Cho LM, Jadin KD, Sah RL, DeLong S, West JL, Bhatia SN.** Fabrication of 3D hepatic tissues by additive photopatterning of cellular hydrogels. *FASEB J.* 21: 790–801, 2007.

87. **Lockhart AC, Braun RD, Yu D, Ross JR, Dewhirst MW, Klitzman B, Yuan F, Grichnik JM, Proia AD, Conway DA, Mann G, Hurwitz HI.** A clinical model of dermal wound angiogenesis. *Wound Repair Regen* 11: 306–313, 2003.
88. **Loetscher M, Gerber B, Loetscher P, Jones SA, Piali L, Clark-Lewis I, Baggiolini M, Moser B.** Chemokine receptor specific for IP10 and mig: structure, function, and expression in activated T-lymphocytes. *J. Exp. Med.* 184: 963–969, 1996.
89. **Luedde T, Trautwein C.** Intracellular survival pathways in the liver. *Liver Int* 26: 1163–1174, 2006.
90. **Malchesky PS.** Artificial organs 2010: a year in review. *Artif Organs* 35: 316–350, 2011.
91. **Malhi H, Gores GJ.** Cellular and molecular mechanisms of liver injury. *Gastroenterology* 134: 1641–1654, 2008.
92. **Malik R, Selden C.** The role of non-parenchymal cells in liver growth. *Seminars in Cell and Developmental Biology.*
93. **Mandrekar P.** Signaling mechanisms in alcoholic liver injury: role of transcription factors, kinases and heat shock proteins. *WJG* 13: 4979–4985, 2007.
94. **March S, Hui EE, Underhill GH, Khetani S, Bhatia SN.** Microenvironmental regulation of the sinusoidal endothelial cell phenotype in vitro. *Hepatology* 50: 920–928, 2009.
95. **Martinez-Hernandez A, Amenta PS.** The extracellular matrix in hepatic regeneration. *FASEB J.* 9: 1401–1410, 1995.
96. **Martinez-Hernandez A.** The hepatic extracellular matrix. I. Electron immunohistochemical studies in normal rat liver. *Lab. Invest.* 51: 57–74, 1984.
97. **Merion RM.** Current status and future of liver transplantation. *Semin. Liver Dis.* 30: 411–421, 2010.
98. **Michalopoulos GK, DeFrances M.** Liver regeneration. *Adv. Biochem. Eng. Biotechnol.* 93: 101–134, 2005.
99. **Milde F, Bergdorf M, Koumoutsakos P.** A hybrid model for three-dimensional simulations of sprouting angiogenesis. *Biophys. J.* 95: 3146–3160, 2008.
100. **Nagelkerke JF, Barto KP, van Berkel TJ.** In vivo and in vitro uptake and degradation of acetylated low density lipoprotein by rat liver endothelial, Kupffer, and parenchymal

- cells. *J. Biol. Chem.* 258: 12221–12227, 1983.
101. **Nahmias Y, Berthiaume F, Yarmush ML.** Integration of technologies for hepatic tissue engineering. *Adv. Biochem. Eng. Biotechnol.* 103: 309–329, 2007.
 102. **Nahmias Y, Schwartz RE, Hu W-S, Verfaillie CM, Odde DJ.** Endothelium-mediated hepatocyte recruitment in the establishment of liver-like tissue in vitro. *Tissue Eng.* 12: 1627–1638, 2006.
 103. **Noonan DM, De Lerma Barbaro A, Vannini N, Mortara L, Albini A.** Inflammation, inflammatory cells and angiogenesis: decisions and indecisions. *Cancer Metastasis Rev* 27: 31–40, 2008.
 104. **Orlando G, Baptista P, Birchall M, De Coppi P, Farney A, Guimaraes-Souza NK, Opara E, Rogers J, Seliktar D, Shapira-Schweitzer K, Stratta RJ, Atala A, Wood KJ, Soker S.** Regenerative medicine as applied to solid organ transplantation: current status and future challenges. *Transpl. Int.* 24: 223–232, 2011.
 105. **Palombo JD, Bistrrian BR, Fechner KD, Blackburn GL, Forse RA.** Rapid incorporation of fish or olive oil fatty acids into rat hepatic sinusoidal cell phospholipids after continuous enteral feeding during endotoxemia. *Am. J. Clin. Nutr.* 57: 643–649, 1993.
 106. **Petrai I, Rombouts K, Lasagni L, Annunziato F, Cosmi L, Romanelli RG, Sagrinati C, Mazzinghi B, Pinzani M, Romagnani S, Romagnani P, Marra F.** Activation of p38(MAPK) mediates the angiostatic effect of the chemokine receptor CXCR3-B. *The International Journal of Biochemistry & Cell Biology* 40: 1764–1774, 2008.
 107. **Pober JS, Sessa WC.** Evolving functions of endothelial cells in inflammation. *Nat. Rev. Immunol.* 7: 803–815, 2007.
 108. **Poulaki V.** Angiogenesis assays. *Methods Mol. Biol.* 731: 345–358, 2011.
 109. **Qutub AA, Mac Gabhann F, Karagiannis ED, Vempati P, Popel AS.** Multiscale models of angiogenesis. *IEEE Eng Med Biol Mag* 28: 14–31, 2009.
 110. **Qutub AA, Popel AS.** Elongation, proliferation & migration differentiate endothelial cell phenotypes and determine capillary sprouting. *BMC Syst Biol* 3: 13, 2009.
 111. **Racanelli V, Rehmann B.** The liver as an immunological organ. *Hepatology* 43: S54–62, 2006.
 112. **Rajagopalan P, Shen CJ, Berthiaume F, Tilles AW, Toner M, Yarmush ML.**

- Polyelectrolyte nano-scaffolds for the design of layered cellular architectures. *Tissue Eng.* 12: 1553–1563, 2006.
113. **Red-Horse K, Crawford Y, Shojaei F, Ferrara N.** Endothelium-microenvironment interactions in the developing embryo and in the adult. *Dev. Cell* 12: 181–194, 2007.
 114. **Ribatti D, Nico B, Crivellato E.** The role of pericytes in angiogenesis. *Int. J. Dev. Biol.* 55: 261–268, 2011.
 115. **Ribatti D.** The discovery of endothelial progenitor cells. An historical review. *Leuk. Res.* 31: 439–444, 2007.
 116. **Risau W.** Mechanisms of angiogenesis. *Nature* 386: 671–674, 1997.
 117. **Rosenkilde MM, Schwartz TW.** The chemokine system -- a major regulator of angiogenesis in health and disease. *APMIS* 112: 481–495, 2004.
 118. **Rucinski B, Knight LC, Niewiarowski S.** Clearance of human platelet factor 4 by liver and kidney: its alteration by heparin. *Am. J. Physiol.* 251: H800–7, 1986.
 119. **Sahota PS, Burn JL, Brown NJ, MacNeil S.** Approaches to improve angiogenesis in tissue-engineered skin. *Wound Repair Regen* 12: 635–642, 2004.
 120. **Sainson RCA, Johnston DA, Chu HC, Holderfield MT, Nakatsu MN, Crampton SP, Davis J, Conn E, Hughes CCW.** TNF primes endothelial cells for angiogenic sprouting by inducing a tip cell phenotype. *Blood* 111: 4997–5007, 2008.
 121. **Saito M, Matsuura T, Masaki T, Maehashi H, Shimizu K, Hataba Y, Iwahori T, Suzuki T, Braet F.** Reconstruction of liver organoid using a bioreactor. *WJG* 12: 1881–1888, 2006.
 122. **Saxena R, Theise ND, Crawford JM.** Microanatomy of the human liver-exploring the hidden interfaces. *Hepatology* 30: 1339–1346, 1999.
 123. **Schultz GS, Davidson JM, Kirsner RS, Bornstein P, Herman IM.** Dynamic reciprocity in the wound microenvironment. *Wound Repair Regen* 19: 134–148, 2011.
 124. **Schultz GS, Wysocki A.** Interactions between extracellular matrix and growth factors in wound healing. *Wound Repair Regen* 17: 153–162, 2009.
 125. **Shao XJ, Xie FM.** Influence of angiogenesis inhibitors, endostatin and PF-4, on lymphangiogenesis. *Lymphology* 38: 1–8, 2005.
 126. **Sivaraman A, Leach JK, Townsend S, IIDA T, Hogan BJ, Stolz DB, Fry R, Samson LD, Tannenbaum SR, Griffith LG.** A microscale in vitro physiological model of the

- liver: predictive screens for drug metabolism and enzyme induction. *Curr Drug Metab* 6: 569–591, 2005.
127. **Soker S, Machado M, Atala A.** Systems for therapeutic angiogenesis in tissue engineering. *World J Urol* 18: 10–18, 2000.
128. **Stappenbeck TS, Miyoshi H.** The role of stromal stem cells in tissue regeneration and wound repair. *Science* 324: 1666–1669, 2009.
129. **Statistics NCFH.** *Health, United States, 2009.* Hyattsville, MD: National Center for Health Statistics, 2010.
130. **Staton CA, Stribbling SM, Tazzyman S, Hughes R, Brown NJ, Lewis CE.** Current methods for assaying angiogenesis in vitro and in vivo. *Int J Exp Pathol* 85: 233–248, 2004.
131. **Stolz DB.** Chapter 7: Sinusoidal Endothelial Cells. In: *Molecular Pathology of Liver Diseases*, edited by Monga SPS. Boston, MA: Springer US, 2010, p. 97–107.
132. **Struyf S, Salogni L, Burdick MD, Vandercappellen J, Gouwy M, Noppen S, Proost P, Opdenakker G, Parmentier M, Gerard C, Sozzani S, Strieter RM, Van Damme J.** Angiostatic and chemotactic activities of the CXC chemokine CXCL4L1 (platelet factor-4 variant) are mediated by CXCR3. *Blood* 117: 480–488, 2011.
133. **Su S-C, Maxwell SA, Bayless KJ.** Annexin 2 regulates endothelial morphogenesis by controlling AKT activation and junctional integrity. *Journal of Biological Chemistry* 285: 40624–40634, 2010.
134. **Sun H-W, Shen F, Zhou Y-M.** Influence of perfusion by gaseous oxygen persufflation on rat donor liver. *HBPD INT* 5: 195–198, 2006.
135. **Surmi BK, Hasty AH.** The role of chemokines in recruitment of immune cells to the artery wall and adipose tissue. *Vascul. Pharmacol.* 52: 27–36, 2010.
136. **Szekanecz Z, Pakozdi A, Szentpetery A, Besenyei T, Koch AE.** Chemokines and angiogenesis in rheumatoid arthritis. *Front Biosci (Elite Ed)* 1: 44–51, 2009.
137. **Tabruyn SP, Griffioen AW.** Molecular pathways of angiogenesis inhibition. *Biochemical and Biophysical Research Communications* 355: 1–5, 2007.
138. **Tanaka Y, Sohda T, Matsuo K, Anan A, Irie M, Takeyama Y, Iwata K, Shakado S, Sakisaka S.** Vascular endothelial growth factor reduces Fas-mediated acute liver injury in mice. *J Gastroenterol Hepatol* 23: e207–11, 2008.

139. **Taub R.** Liver regeneration: from myth to mechanism. *Nat Rev Mol Cell Biol* 5: 836–847, 2004.
140. **Thelen M.** Dancing to the tune of chemokines. *Nat. Immunol.* 2: 129–134, 2001.
141. **Thorne BC, Hayenga HN, Humphrey JD, Peirce SM.** Toward a multi-scale computational model of arterial adaptation in hypertension: verification of a multi-cell agent based model. *Front Physiol* 2: 20, 2011.
142. **Tokairin T, Nishikawa Y, Doi Y, Watanabe H, Yoshioka T, Su M, Omori Y, Enomoto K.** A highly specific isolation of rat sinusoidal endothelial cells by the immunomagnetic bead method using SE-1 monoclonal antibody. *Journal of Hepatology* 36: 725–733, 2002.
143. **Turner R, Gerber D, Reid L.** The future of cell transplant therapies: a need for tissue grafting. *Transplantation* 90: 807–810, 2010.
144. **van Moorst M, Dass CR.** Methods for co-culturing tumour and endothelial cells: systems and their applications. *J. Pharm. Pharmacol.* 63: 1513–1521, 2011.
145. **Van Sweringen HL, Sakai N, Tevar AD, Burns JM, Edwards MJ, Lentsch AB.** CXC chemokine signaling in the liver: impact on repair and regeneration. *Hepatology* 54: 1445–1453, 2011.
146. **Van Vlierberghe S, Dubruel P, Schacht E.** Biopolymer-based hydrogels as scaffolds for tissue engineering applications: a review. *Biomacromolecules* 12: 1387–1408, 2011.
147. **Vandercappellen J, Liekens S, Bronckaers A, Noppen S, Ronsse I, Dillen C, Belleri M, Mitola S, Proost P, Presta M, Struyf S, Van Damme J.** The COOH-terminal peptide of platelet factor-4 variant (CXCL4L1/PF-4var47-70) strongly inhibits angiogenesis and suppresses B16 melanoma growth in vivo. *Mol. Cancer Res.* 8: 322–334, 2010.
148. **Vandercappellen J, Van Damme J, Struyf S.** The role of CXC chemokines and their receptors in cancer. *Cancer Letters* 267: 226–244, 2008.
149. **Vandercappellen J, Van Damme J, Struyf S.** The role of the CXC chemokines platelet factor-4 (CXCL4/PF-4) and its variant (CXCL4L1/PF-4var) in inflammation, angiogenesis and cancer. *Cytokine Growth Factor Rev.* 22: 1–18, 2011.
150. **Wacker A, Gerhardt H.** Endothelial development taking shape. *Curr. Opin. Cell Biol.* (November 1, 2011). doi: 10.1016/j.ceb.2011.10.002.

151. **Wallace DG, Rosenblatt J.** Collagen gel systems for sustained delivery and tissue engineering. *Adv. Drug Deliv. Rev.* 55: 1631–1649, 2003.
152. **Werner S, Grose R.** Regulation of wound healing by growth factors and cytokines. *Physiol. Rev.* 83: 835–870, 2003.
153. **Widmaier EP, Raff H, Strang KT.** Vander, Sherman, Luciano's Human Physiology [Online]. 9th ed. McGraw-Hill. <http://www.mhhe.com/widmaier9>.
154. **Xu B, Broome U, Uzunel M, Nava S, Ge X, Kumagai-Braesch M, Hultenby K, Christensson B, Ericzon B-G, Holgersson J, Sumitran-Holgersson S.** Capillarization of hepatic sinusoid by liver endothelial cell-reactive autoantibodies in patients with cirrhosis and chronic hepatitis. *The American Journal of Pathology* 163: 1275–1289, 2003.
155. **Yamashina S, Ikejima K, Enomoto N, Takei Y, Sato N.** Glycine as a therapeutic immuno-nutrient for alcoholic liver disease. *Alcohol. Clin. Exp. Res.* 29: 162S–5S, 2005.
156. **Yancopoulos GD, Davis S, Gale NW, Rudge JS, Wiegand SJ, Holash J.** Vascular-specific growth factors and blood vessel formation. *Nature* 407: 242–248, 2000.
157. **Yokoyama Y, Nimura Y, Nagino M, Bland KI, Chaudry IH.** Role of thromboxane in producing hepatic injury during hepatic stress. *Arch Surg* 140: 801–807, 2005.
158. **Zaldivar MM, Pauels K, Hundelshausen von P, Berres M-L, Schmitz P, Bornemann J, Kowalska MA, Gassler N, Streetz KL, Weiskirchen R, Trautwein C, Weber C, Wasmuth HE.** CXC chemokine ligand 4 (Cxcl4) is a platelet-derived mediator of experimental liver fibrosis. *Hepatology* 51: 1345–1353, 2010.
159. **Zhang Y, Ikejima K, Honda H, Kitamura T, Takei Y, Sato N.** Glycine prevents apoptosis of rat sinusoidal endothelial cells caused by deprivation of vascular endothelial growth factor. *Hepatology* 32: 542–546, 2000.

Chapter 2

Lipids promote survival, proliferation, and maintenance of differentiation of rat liver sinusoidal endothelial cells *in vitro*

NOTE: The content of this chapter is based on published article: Hang TC, Lauffenburger DA, Griffith LG, Stolz DB. *Am J Physiol* (2011 Nov 10). The article is © 2011

2.1. INTRODUCTION

2.1.1. Role of fatty acids and lipids in liver function and metabolism

Cells are composed of biomolecules that can be classified into four fundamental categories of building blocks: sugars, amino acids, nucleotides, and fatty acids (1). Of these, fatty acids play important roles in various aspects of cell function, ranging from energy storage as fat to membrane structure as phospholipids (9, 69).

As basic building blocks, fatty acids can exist in multiple forms and require processing and metabolizing to be properly generated. The liver serves as a nexus for lipid metabolism (Figure 2-1), and transforming fatty acids between storage, functional, and energy forms (91).

Furthermore, lipid metabolism in the liver is deeply intertwined with other processes for maintaining glucose homeostasis (14, 82, 91). This is especially evident in liver injury, where fatty acids released into the circulation by adipocytes and taken up by the liver parenchyma (9, 36). Gluconeogenesis is upregulated in regenerating cells, which can be brought upon by free fatty acid stimulation (14, 67, 82).

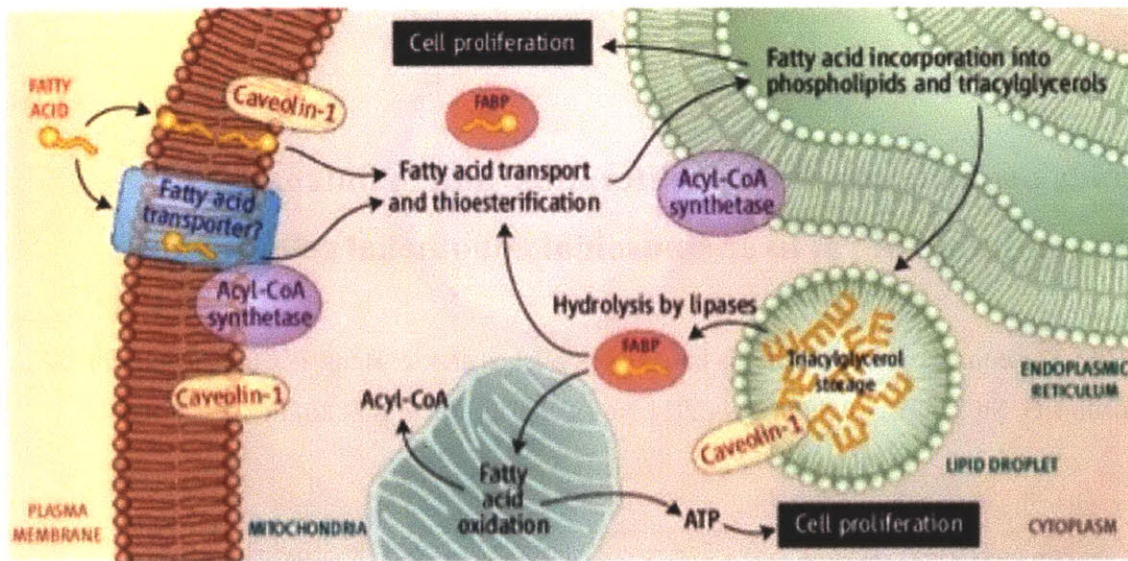


Figure 2-1. Lipid metabolism during liver regeneration (9). Fatty acids and lipids play multiple different roles in cell by providing energy basis for proliferation, lipids as structural components, and storage of fat in triglyceride form for later use. Destabilization of these processes can be symptomatic or the result of diseases that cause hepatocytes to behave abnormally (e.g. steatosis, fatty liver disease).

When hepatocytes lose their function, problematic symptoms arise which include the accumulation of fat in the liver in the form of triglyceride droplets known as steatosis (11, 84, 90). Further increase in steatosis can eventually lead to irreversible fat deposition and liver disease. The imbalance of lipids in the liver can also be indicative of other diseases; a prevalent example is the causative link found between obesity/fatty acid increase and diabetes (46, 66).

2.1.2. Lipids signal through a variety of pathways

The vast library of literature on lipids and their ability to affect cellular mechanisms is a testament to their prominence in signaling. Lipids in their different moieties can influence signaling by participating in crosstalk, as well as being in diametric opposition due to the many forms in which lipids can exist.

One of the main questions posed on how lipids and fatty acids can affect signaling depends on how it is taken into the cell. Although lipid transport can be facilitated by binding proteins and receptors such as fatty acid G-protein coupled receptors (GPCR), CD36 and fatty acid binding

protein (FABP) (3, 22, 28, 29, 32, 55, 65, 72, 84, 86, 87, 89), lipids can easily move across cell membranes directly into the cytosol and nucleus (39, 76)(72). Lipid uptake has also been reported to be taken in by endocytosis, by the process of utilizing caveolae on cell surfaces (62) as well as through the cotransport of albumin (5, 34, 64, 74, 75).

As such, signaling activation of cells in response to fatty acids can occur at the receptor level, through binding with fatty acid receptors (55) or crosstalk with other phospho-signaling receptors such as EGFR (23, 81, 83). Bio-active phospholipids such as lysophosphatidylcholine or lysophosphatidic acid have been shown to directly activate Src and protein kinase C (PKC) downstream of EGFR or selective activation of Akt respectively (4, 42). Fatty acids and lipids can activate Akt, ERK1/2, P38 MAP kinase, PKC, JNK, and many others along with lipid metabolism cycle stages (14, 31, 40, 50, 92). Additionally, free fatty acids have been found to influence phosphatase activity, such as downregulation of PTEN, a phosphatase that inhibits the PI3K/Akt signaling pathway (84). As they can freely pass through lipid membranes of the cell, fatty acids and lipids can also move directly into the nucleus and bind to nuclear receptors to induce signaling pathways (15, 47, 56, 76, 79, 90).

It is unknown whether fatty acids directly act upon cytosolic proteins to induce their activation, or whether adaptor or binding proteins are required in order to facilitate this process (63, 86, 89). Despite the data that already exist on lipids and their mechanisms of actions, there is still a great deal of mystery involved in the processes in which they influence cellular behavior.

2.1.3. Chapter overview

Liver sinusoidal endothelial cells (LSEC) play important roles in regulating liver function. LSEC line capillaries of the microvasculature and possess fenestrae to facilitate filtration between the liver parenchyma and sinusoid by serving as a selectively permeable barrier (8, 27). This role is augmented by high endocytic uptake rates, making LSEC effective scavengers for molecules such as albumin, acetylated low density lipoproteins, hyaluronan and antigens in the bloodstream (26, 27, 35, 48, 57, 61). Furthermore, LSEC have a phenotype unique from traditional vascular endothelial cells, such as pan-endothelial marker CD31 localized only to endosomes in differentiated, unstimulated LSEC (19). Differentiated LSEC are capable of

affecting resident liver cell proliferation, survival, or maintaining their quiescence. As such, loss of function may underlie various hepatic pathologies (8, 20, 30, 46, 77, 93).

LSEC are also targets or facilitators of infection and toxicological damage to liver (7). In addition to intrinsically vital contributions they make to proper liver tissue function *in vivo*, cultured LSEC are important to consider as essential non-parenchymal components of *ex vivo* tissue engineered models of liver physiology, which are of emerging importance in drug discovery and development (21, 41, 70, 80).

Despite this importance, much of LSEC biology remains unknown because they are difficult to maintain in a differentiated state for prolonged periods *in vitro*. Conventional endothelial culturing techniques are not as successful with LSEC; low serum concentrations (5%) can be toxic and cells die within 48 to 72 hours in serum-free monocultures even in the presence of VEGF (25, 44)(24)(24). Previously, attempts at serum-free LSEC culture resulted in cell viability maintenance from 6 up to 30 days with surviving cells maintaining endocytic uptake (24, 25, 44). Receptor mediated endocytic uptake is a characteristic feature of endothelial phenotype, but is insufficient for specific characterization of LSEC differentiation as large venule endothelial cells in the liver, as well as several vascular endothelial cells also exhibit this function (25, 38, 57, 59, 85). Another rat study was also able to prolong cell survival *in vitro* with use of multiple growth factors such as FGF, hepatocyte growth factor, and PMA within the context of hepatocyte-conditioned medium (44). Human LSEC cultures have been reported to be sustained for long periods, however, these LSEC were positively selected for, or had a higher expression of CD31, a marker of LSEC dedifferentiation (16, 45). There are also controversies regarding phenotyping human LSEC, as there are reports of heterogeneous expression of surface markers used to characterize LSEC, such as von Willebrand Factor and immunological markers (25).

This study tested the hypothesis that an alternative approach emphasizing non-protein components could be beneficial in maintaining LSEC function in culture. Due to the location of the liver downstream of the intestinal tract and a center for lipid metabolism (10), we hypothesized that LSEC require lipids to maintain cell viability. We found that even in serum-

free, minimal growth factor (*i.e.*, solely VEGF) media, free fatty acids (FFAs) were able to sustain LSEC culture. The addition of lipid supplements to serum-free media with 50 ng/mL VEGF allowed us to bypass the critical time point between 48 and 72 hours when most differentiated LSEC die *in vitro*. We identified oleic acid (OA) as a major contributing agent responsible for enhancing this survival. OA and lipids in culture could also eventually induce proliferation of cells with LSEC phenotype to confluency, although OA alone was insufficient for maintaining long-term confluent cultures. Furthermore, our results indicate that OA and lipids can maintain multiple LSEC phenotype markers simultaneously for at least 5 days in culture. Our findings indicate that OA and lipids influence early Akt/PKB signaling to mediate cell survival, while late ERK signaling is necessary in culture for viability and proliferation to persist.

2.2. EXPERIMENTAL PROCEDURES

For more details on culture media composition and primary LSEC isolation protocols please refer to Appendix B.

2.2.1. Chemically Defined Culture Media

Serum/growth factor-free base medium was made as described with modifications (37, 44). Low glucose DMEM (Invitrogen, Carlsbad, CA) was supplemented with 0.03g/L L-proline, 0.10g/L L-ornithine, 0.305 g/L niacinamide, 1 g/L glucose, 2 g/L galactose, 2 g/L BSA, 50 µg/mL gentamicin (Sigma-Aldrich, St. Louis, MO), 1 mM L-glutamine (Invitrogen), 5 µg/mL insulin-5 µg/mL transferrin-5 ng/mL sodium selenite (Roche Applied Science, Mannheim, Germany). “Modified hepatocyte growth medium” (HGM) included 200 µM ethanolamine and phosphoethanolamine, 100 nM ascorbic acid, 110 nM hydrocortisone (Sigma-Aldrich), 20 µg/mL heparin (Celsus Laboratories, Cincinnati, OH) and 50 ng/mL VEGF (R&D Systems, Minneapolis, MN). Additional treatments included 1% Chemically Defined Lipid Concentrate (~8µM final concentration) (Invitrogen 11905031) or 50 µM OA, FFA-free BSA, phosphatidylcholine (PC, 50 µM), and lysophosphatidylcholine (LPC 50 µM) (Sigma-Aldrich). For signaling studies, PI3K inhibitor LY294002 and MEK1/2 inhibitor PD0325901 (EMD Calbiochem, Gibbstown, NJ) were added to LSEC cultures 4 hours following seeding and maintained throughout the experiment. Inhibitors were reconstituted in DMSO (Sigma-Aldrich)

to 20 mM. LY294002 was dosed at concentrations of 10 μ M and 3 μ M, while PD0325901 was used at 1 μ M and 0.3 μ M. Inhibitors were replenished once a day with fresh medium changes.

2.2.2. Primary LSEC Isolation and Culture

Livers from approximately 180 to 250 gram male Fisher rats (Taconic, Hudson, NY) were used under the guidelines set forth by Massachusetts Institute of Technology's Committee on Animal Care. Cells were isolated using a two-step collagenase perfusion (37, 70) using Liberase Blendzyme (Roche Applied Science) in place of collagenase. The liver was perfused initially at 25 mL/min and reduced down to 15 mL/min flow rates in calcium free 10 mM HEPES (Sigma-Aldrich) buffer followed by 10 mM HEPES buffer with Blendzyme for cell isolation. The supernatant cell suspension from the perfusion was used to isolate LSEC at room temperature (6, 27). Very briefly, supernatant suspensions were spun down at 50 x g for 3 minutes. Supernatants were spun at 100 x g for 4 minutes. Supernatants following the spin were pelleted at 350 x g for 10 minutes and resuspended in 20 mL modified HGM without VEGF. The suspension was loaded over 25%/50% Percoll (Sigma-Aldrich)/PBS layers and centrifuged at 900 x g for 20 minutes. The interface between the Percoll layers were taken and resuspended with 1:1 modified HGM without VEGF before being spun down at 950 x g for 12 minutes. This LSEC enriched pellet was then resuspended into modified HGM with 25 ng/mL VEGF and 2% FBS (Hyclone/Thermo Fisher Scientific, South Logan, UT). Cells were counted using Sytox Orange exclusion and Hoechst 33342 (Invitrogen) staining on disposable hemacytometers (inCyto, Seoul, Korea). LSEC were then seeded onto 10 μ g/mL fibronectin (Sigma-Aldrich) coated tissue culture plates at 400,000 cells/cm². Four to six hours following seeding, culture media were changed with serum-free modified HGM supplemented with VEGF. Additional conditions included supplementing 50 μ M OA, 50 μ M LPC, 50 μ M PC, and 1% lipid concentrate to the culture over the course of 5 days at 37 °C and 5% CO₂. Media for all cultures were changed on a daily basis for all experiments.

2.2.3. Live/Dead Assay

LSEC viability was assessed using the Live/Dead Assay kit (Invitrogen L3224). LSEC were incubated for 1 hour with 2 μ M Calcein AM and 4 μ M Ethidium Bromide Homodimer in modified HGM. Cultures were washed with warm media prior to imaging.

2.2.4. Alamar Blue Metabolic Assay

Metabolic activity of LSEC was assessed over the time period of 5 days using Alamar Blue (Invitrogen) reduction assays. Positive reference standards were first made by heating base modified HGM at 125 °C with 10% Alamar Blue until the entire reagent was oxidized and converted to a bright shade of red. On the days of analysis, 10% Alamar Blue reagent was introduced to each well and allowed to incubate at 37 °C, 5% CO₂ for 6 hours prior to screening in a SpectraMax E2 (MDS Analytical Technologies, Sunnyvale, CA) fluorescent plate reader. Reference standards were included on each plate as positive controls and served as a point of reference in interpreting results. Fluorescent measurements were read by exciting the samples at 530 nm and reading the emission wavelengths at 590 nm. Samples were pooled across 3 biological replicates (5 technical replicates) for a total of 15 data points. All data points were normalized to blank readings prior to relative comparison to control samples.

2.2.5. Acetylated-LDL Uptake Assay

LSEC were grown on Thermanox coverslips (Nalgene Nunc, Rochester, NY) coated with 10 µg/mL fibronectin. On day 5, SECs were incubated for four hours with 10 µg/mL 1,1'-dioctadecyl 3,3,3',3' tetramethylindo carbocyanine perchlorate labeled acetylated LDL (Di-I-Ac-LDL) (Biomedical Technologies, Inc., Stoughton, MA). Cells were washed several times with probe free modified HGM then rinsed with PBS. LSEC were fixed for 30 minutes in 3% paraformaldehyde (Electron Microscopy Sciences, Hatfield, PA), rinsed with PBS, mounted on glass slides with Fluormount (Sigma-Aldrich), and sealed with nail polish. Samples were compared with positive controls using human dermal microvascular endothelial cells (HDMVEC) (Lonza Inc., Allendale, NJ).

2.2.6. Immunofluorescence Microscopy

LSEC were cultured for up to 5 days on Thermanox coverslips coated with 10 µg/mL fibronectin. Samples were rinsed with PBS and fixed in 3% paraformaldehyde in PBS for 30 minutes. Following fixation, samples were rinsed three times with PBS and permeabilized with 0.1% Triton X-100 (Sigma-Aldrich) for one hour, excluding samples immunostained for CD31 which were not permeabilized so as to evaluate only surface expression. Following

permeabilization, samples were rinsed three times with 2% BSA in 0.1% Tween-20 in PBS (PBS-T). Samples were blocked with 5% goat or donkey serum (Jackson ImmunoResearch, West Grove, PA) in 2% BSA PBS-T for 1 hour before overnight incubation at 4 °C with primary antibodies for anti-rat CD32b/SE-1 (IBL America, Inc., Minneapolis, MN) at 1:100, CD31/PECAM-1 (Chemicon/Millipore, Temecula, CA) at 1:100, and PCNA (Abcam, Cambridge, MA) at 1:600. The following day, samples were rinsed 3 times in 2% BSA PBS-T before a 1 hour incubation step with secondary AlexaFluor 488/555 (Invitrogen) antibodies at 1:250. Coverslips were then rinsed in 2% BSA PBS-T and stained with 1:500 Hoechst. Following incubation with secondary antibodies, samples were rinsed once in 2% BSA PBS-T prior to being treated briefly with nuclear Hoechst staining for 1 minute. Following Hoechst staining, samples were rinsed twice in normal PBS before being mounted onto glass slides with Fluormount and sealed with nail polish.

2.2.7. Scanning Electron Microscopy (SEM)

LSEC were grown on fibronectin-coated Thermanox coverslips. On days 3-5, LSEC were rinsed with PBS and fixed in 2.5% glutaraldehyde (Electron Microscopy Sciences) for 30 minutes. Samples were prepared following previously established protocols (37).

2.2.8. Flow Cytometry Analysis of Phenotype and Proliferation

Twenty-four hours before harvesting, 10 μ M of 5-ethynyl-2'-deoxyuridine (EdU) (Invitrogen) was added to all conditions. Samples were detached with 0.025% Trypsin (Invitrogen) the following day, quenched with media containing 10% FBS, and immediately spun down at 1,600 rpm for 5 minutes. Cells were washed in PBS before being fixed in 2% paraformaldehyde in PBS for 15-30 minutes at room temperature. LSEC were centrifuged and resuspended in 1% BSA in PBS and incubated with primary CD32b antibody (1:100) prior to use of the Click-iT EdU kit, following manufacturer's instructions. Samples were analyzed on an Accuri-C6 (Accuri Cytometers, Inc., Ann Arbor, MI) flow cytometer and processed using FlowJo software (FlowJo, Ashland, OR). HDMVEC were used as a negative control population. Total and cellular events were captured with gates created using forward and side scatter data from HDMVEC populations. Following this, CD32b and EdU gates were designated using the double negative HDMVEC population.

2.2.9. Phenotype and Phospho-protein Western Blotting

LSEC were harvested on day 5 of culture by incubating with cell lysis buffer (68) for 30 minutes. Cell lysis buffer consisted of 1% Triton X-100, 50mM β -glycerophosphate, 10 mM sodium pyrophosphate, 30 mM sodium fluoride (Sigma-Aldrich), 50 mM Tris (Roche Applied Science), 150 mM sodium chloride, 2 mM EGTA, 1 mM DTT, 1 mM PMSF, 1% Protease Inhibitor Cocktail and 1% Phosphatase Inhibitor Cocktails (Sigma-Aldrich). Samples were spun down at 12,000 rpm for 12 minutes at 4 °C and supernatants were reserved. Total protein content of sample lysates was determined using micro bicinchoninic acid kits (Thermo Fisher Scientific, Rockford, IL) before being loaded onto the NuPage Novex system (Invitrogen). Lysates were loaded with 6X reducing buffer (Boston BioProducts, Worcester, MA) in 4%-12% Bis-Tris gels (Invitrogen) and transferred to polyvinylidene fluoride membranes (Bio-Rad, Hercules, CA). Membranes were blocked with 5% BSA in PBS-T and incubated with antibodies for β -actin (1:5000), phosphoERK1/2 (1:5000), ERK1/2 (1:5000), phosphoAkt (1:1000), and Akt (1:5000) (Cell Signaling Technology, Beverly, MA) overnight at 4 °C. Membranes washed and then incubated for 1 hour with horseradish peroxidase conjugated anti-mouse and anti-rabbit antibodies (Amersham/GE Healthcare Biosciences, Pittsburgh, PA) at 1:10,000 dilution in PBS-T with 5% blotting grade nonfat dry milk (Bio-Rad). Membranes were subsequently visualized using chemiluminescent ECL kits (Amersham/GE Healthcare Biosciences) on a Kodak Image Station (Perkin Elmer, Waltham, MA).

2.2.10. Image and Statistical Data Analysis

All experiments were repeated a minimum of three times with duplicate or triplicate samples. Fluorescent images were analyzed using Cell Profiler (Broad Institute, Cambridge, MA) and ImageJ (NIH, Bethesda, MD). Intact cell body counts from phase contrast were assessed at 100X magnification. Cells from a camera area of 1360 by 900 μ m were counted from three biological replicates across seven days. Statistical significance was determined using ANOVA and Student's t-test (Microsoft Excel).

2.3. RESULTS

2.3.1. FFA lipids support cell survival past the first 48 hours in serum free media

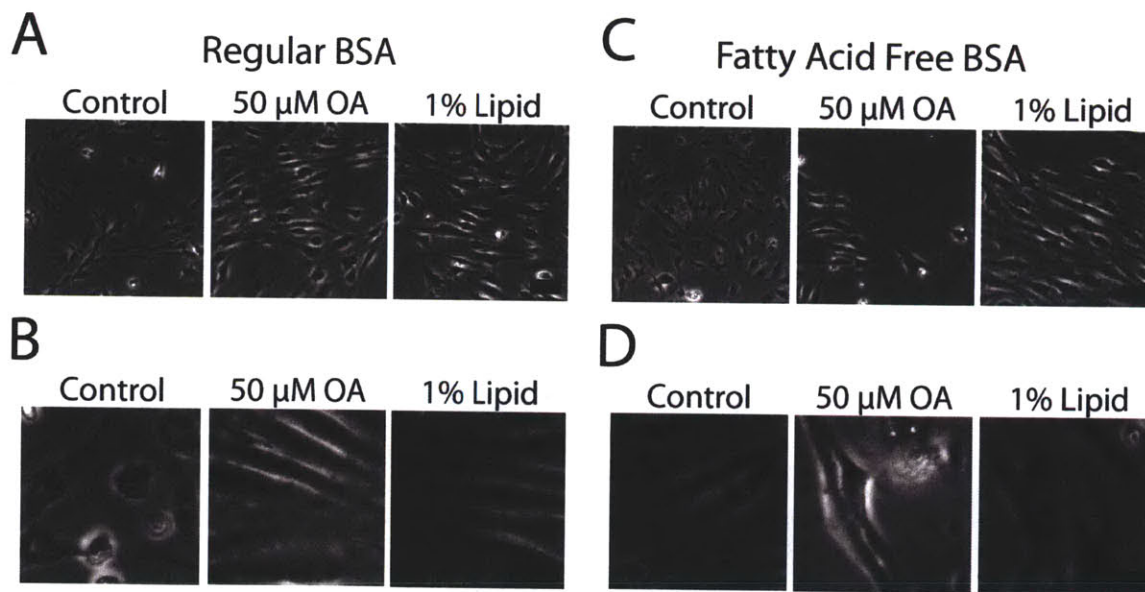


Figure 2-2. Lipids in FFA form sustain long-term culture. Phase contrast images of LSEC were taken at day 5 of culture in serum-free medium (modified HGM) with regular BSA (**A,B**) or fatty acid (FFA)-free BSA (**C,D**). LSEC were cultured with 50 ng/mL VEGF (control), plus 50 μ M oleic acid (50 μ M OA), or 1% chemically defined lipid concentrate (1% lipid). Only conditions with OA or lipid appeared favorable for persistence of cell culture. Higher magnification images indicate a pronounced change in morphology in lipid treated conditions compared to untreated control cells which appeared more granular (**B,D**). Scale bars = 50 μ m (**A,C**), 20 μ m (**B,D**).

Isolated LSEC were plated and cultured using different lipid supplements of 50 μ M OA or 1% lipid (a cocktail of saturated and unsaturated fatty acids) (Figure 2-2). Immunofluorescence staining of LSEC 24 hours after isolation indicated high purity of LSEC (Figure 2-6C). Distinct morphological changes were observed starting on day 3 in cultures with 50 μ M OA or 1% lipid supplement, compared to control cultures (Figure 2-2A,B). Notably, LSEC cultured with 1% lipid underwent proliferation, and by day 5, the culture was at or near confluency. Both regular and FFA-free BSA were evaluated to account for potential variability of BSA-bound lipids. Medium supplemented with 50 μ M OA yielded similar results as 1% lipid at day 5 in regular

BSA. When FFA-free BSA was used, cells treated with 50 μ M OA died after day 4 of culture (Figure 2-2C,D), although this was not observed with regular BSA. Untreated cells took on a granular appearance indicating that lipid moiety is a critical component for LSEC viability (Figure 2-2B,D). Granular morphology was also observed in LSEC cultured with PC and LPC (data not shown).

Live/Dead images of LSEC across conditions in both regular and FFA-free BSA were taken during five days of culture (Figure 2-3A, B). Massive cell death observed in the control concur with previously reported observations of LSEC demise beyond 48 hours in culture. While all conditions experienced cell number decline between days 2 and 3, lipid and OA cultures recovered and proliferated in both types of BSA, with statistically significant differences in population after day 3 compared to control ($p < 5E-4$). (Figure 2-3C, D). Phase and live/dead staining indicate pronounced and distinct morphological changes for surviving LSEC. Lipid supplementation maintained LSEC to day 5. Cells grown with OA in normal BSA were viable after 4 days after isolation; however, FFA-free BSA did not synergize with OA to maintain cell viability. Lipid and OA conditions had persistently higher total live cell percentages compared to control, PC, and LPC conditions; PC and LPC did not offer any growth advantage for LSEC relative to control ($p > 0.24$) (Figure 2-3). Live/Dead assay confirmed that LSEC with unhealthy granular appearance were dead and positive for ethidium bromide. PC and LPC cell cultures did not survive past day 2 in regular BSA (data not shown).

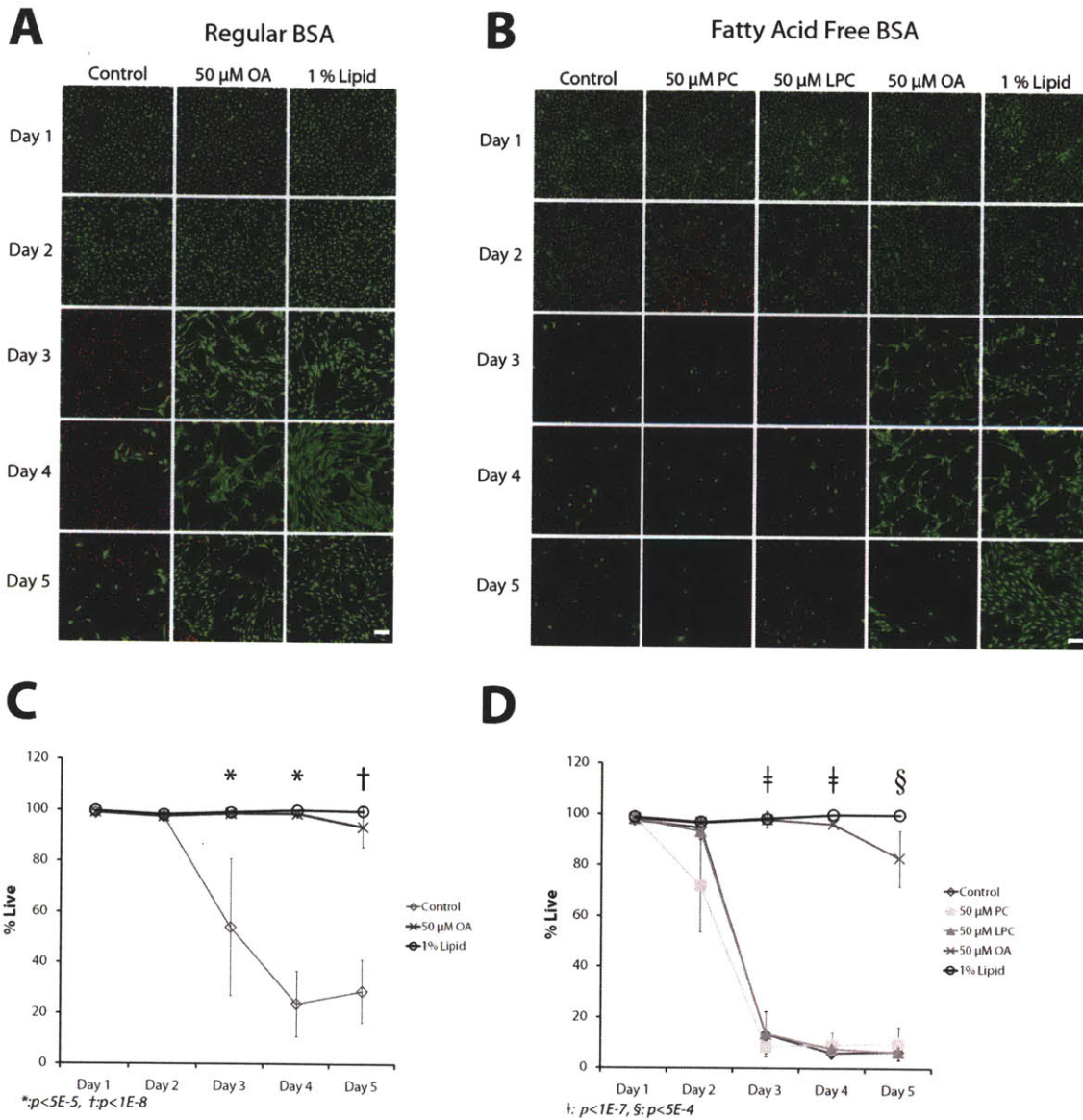


Figure 2-3. LSEC death at 48 hours is abrogated following treatment with FFA. Live/Dead assays were performed on LSEC culture across several conditions (A,B), with cell number quantification by Cell Profiler (C,D). Samples were treated with calcein AM (green) for live cells and ethidium bromide homodimer (red) for dead cells. While all conditions experienced steep drops in total population by day 3, only OA or lipid treatments had significant live cell numbers ($p < 5E-4$ compared to control), indicating lipid type importance. Abbreviations: PC = phosphatidylcholine, LPC = lysophosphatidylcholine, OA = oleic acid. Scale bar = 100 μ m.

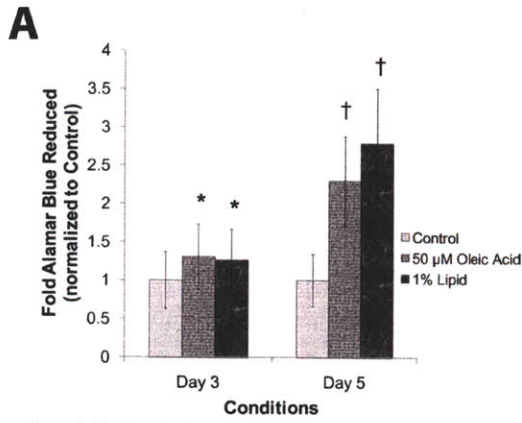
2.3.2. FFAs support metabolic and endocytic functionality in LSEC past day 3

OA and lipid supplement supported significantly higher Alamar Blue reduction relative to control, in agreement with live/dead stain results (Figure 2-4A). These trends were also observed in FFA-free BSA cultures (Figure 2-4B). Endocytic capacity was measured using Di-I-Ac-LDL uptake as a functional assay for endothelial phenotype (Figure 2-4C). OA and lipid treatments sustained high endocytic uptake at day 5; cells positive for nuclear Hoechst were also strongly positive for Di-I-Ac-LDL. Many cells in the control did not remain after fixation; those that did remain stained positive for Hoechst but were negative for Di-I-Ac-LDL.

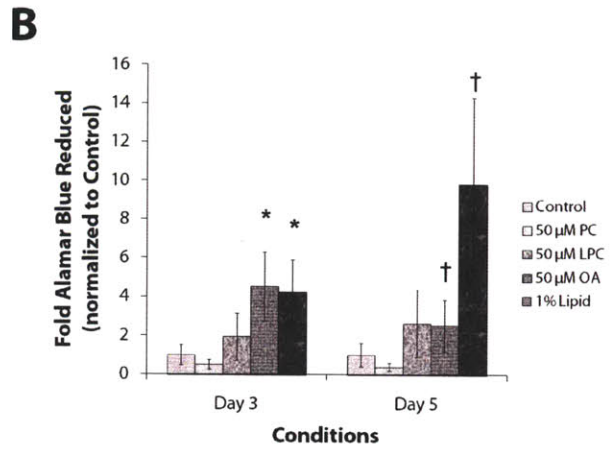
2.3.3. LSEC phenotype and proliferation are maintained with lipids in growth factor-reduced, serum-free media

Following cell number reduction at day 3, LSEC phenotype was assessed. A crucial LSEC marker is the presence of fenestrae on cell surfaces. Using scanning electron microscopy, we found both 50 μ M OA and 1% lipid treated LSEC expressed numerous fenestrae at day 5 of culture (Figure 2-5), while control cells did not maintain fenestrae. Only about 5% of all FFA-treated cells expressed fenestrations in sieve plates. A larger percentage (10-15%) expressed large holes (Figure 2-5H, I) that are suspected to be sieve plate remnants. When the population was taken as a whole, porosity was well below the 10% observed for healthy LSEC *in vivo* (8), indicating that FFA alone does not maintain fenestrations at normal levels.

Figure 2-4. OA and lipid supplement support phenotype and function in LSEC cultures. Alamar Blue measurements were statistically higher at days 3 ($p < 0.05$) and 5 ($p < 0.005$) in 50 μ M OA and 1% lipid supplement treatments over control for LSEC in regular BSA (A). Similar trends were also observed in FFA free BSA cultures (B). Alamar Blue reduction was statistically higher at day 3 for 50 μ M OA and 1% lipid supplement treatments over control, PC, and LPC. At day 5, only 1% lipid supplement treatment was statistically significant over control, PC, and LPC, indicating that the 50 μ M OA condition was insufficient to sustain long term cultures without the presence of other fatty acids. Most cells in the control condition did not survive past day 3; remaining cells did not co-stain for Hoechst (blue) and Di-I-Ac-LDL (red), while OA and lipid conditions consistently co-stained for both on day 5 (C). Contrast and brightness were adjusted for the entire image for Hoechst staining due to background fluorescence arising from the Thermanox coverslips. Abbreviations: PC = phosphatidylcholine, LPC = lysophosphatidylcholine, OA = oleic acid. Scale bars = 100 μ m (C), 2.5 μ m (D).

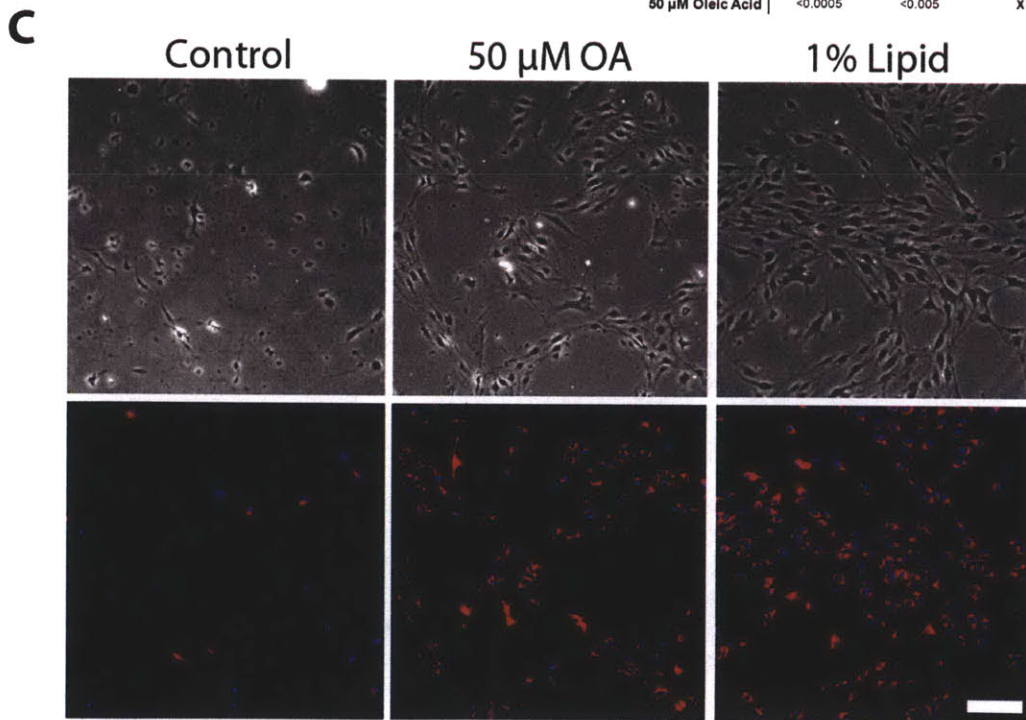


*: $p < 0.05$; †: $p < 0.005$ from Control on Days 3 and 5



* (Day 3)			
p-value	Control	50 μM PC	50 μM LPC
Lipid	<1E-7	<0.005	X
50 μM Oleic Acid	<1E-7	<0.005	<0.05

† (Day 5)			
p-value	Control	50 μM PC	50 μM LPC
Lipid	<1E-7	<0.001	<0.01
50 μM Oleic Acid	<0.0005	<0.005	X



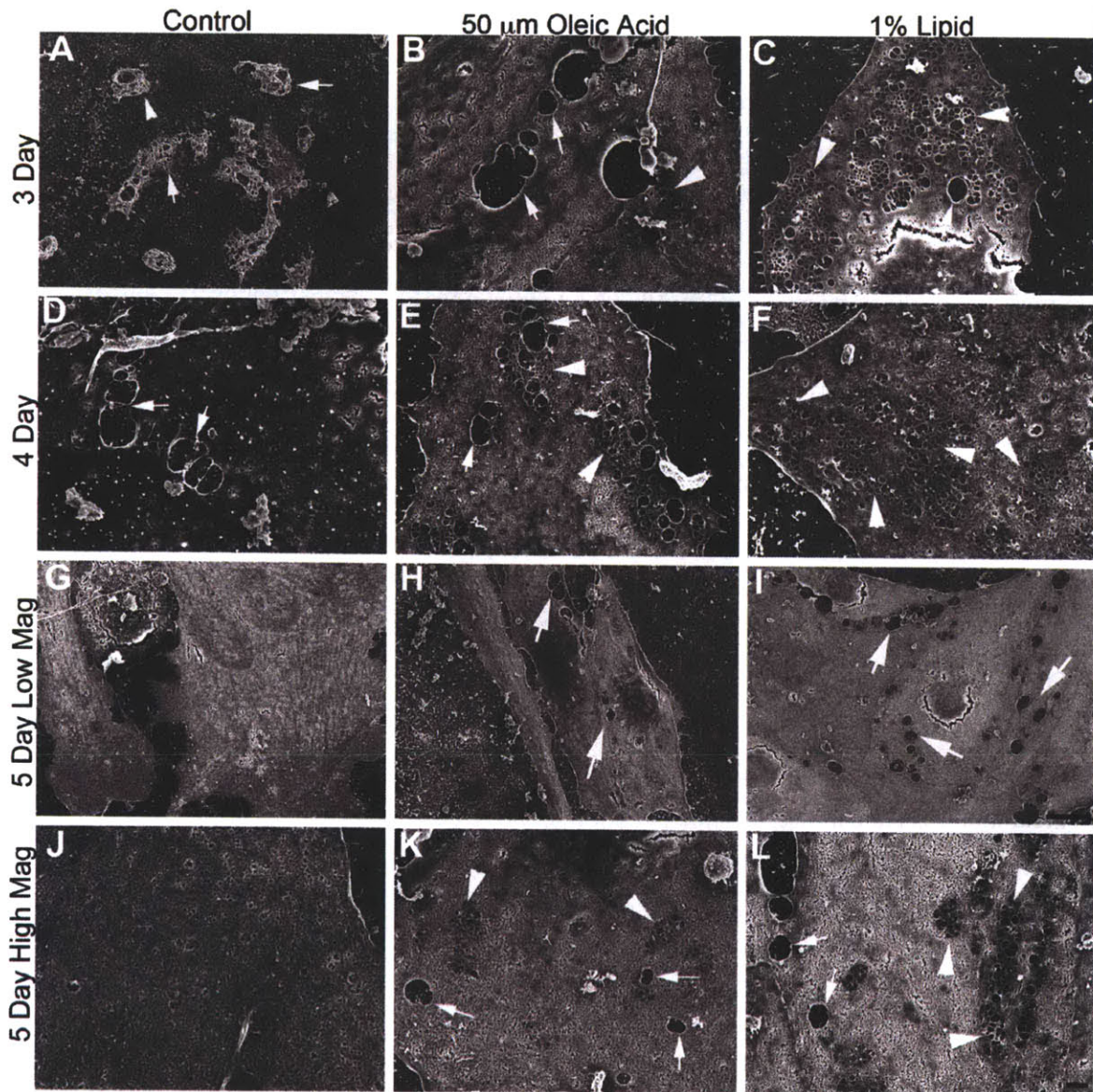


Figure 2-5. Maintenance of fenestrations in FFA cultures. LSEC cultures were evaluated for fenestrations at 3, 4, and 5 days following isolation in the presence or absence of lipid supplementation. At day 3 most cells in the control condition were dead (arrows) or had no visible fenestrations (A, D, G, J) while OA (B, E, H, K) and lipid (C, F, I, L) treated cultures displayed some cells with fenestrations arranged in sieve plates (arrowheads). Some cells displayed very large transcytotic pores (arrows). These fenestrations (arrowhead) and large pores (arrows) were maintained in a fraction of the treated cells until day 5. Magnifications: Scale bar in L represents 1 μm for panels B-F and J-L. Scale bar in I represents 10 μm panels A, G-I.

Another characteristic LSEC marker, CD32b, was used to corroborate phenotype. Immunostained coverslips revealed that cells treated with FFAs maintained CD32b expression at day 5 (Figure 2-6A). Control cells remaining in culture did not have colocalization of CD32b surface expression with nuclei; CD32b appeared as punctate staining which were most likely dead cell remnants. Non-viable adherent cells appeared less frequently in protocols with multiple rinse steps (e.g., Di-I-Ac-LDL uptake, Figure 2-4C; co-immunostaining, Figure 2-6; flow cytometry, Figure 2-7B). Although we stained for CD31, we did not observe CD31 expression on the cell surfaces of LSEC in FFA-treated conditions or remaining adherent cells in the control unless samples were permeabilized prior to staining (Figure 5B). CD32b⁺ cells comprised a greater proportion of total cell populations in lipid treated LSEC in flow cytometry compared to controls (Figure 2-7C). The enhanced presence of CD32b⁺ cells in OA and lipid is consistent with immunostaining results. CD32b staining was still present on day 5 cultures treated with lipid (Figure 2-6C) and OA (not shown), but signal intensity was diminished compared to LSEC evaluation on day 1 following isolation.

Proliferative capabilities were measured using PCNA and EdU (a BrdU analog) incorporation. OA and lipid treated cells stained positive for both PCNA and CD32b expression at day 5 while untreated cells did not (Figure 5A). Most cells were PCNA⁻ in the control; those that were PCNA⁺ were CD32b⁻. Day 5 cells had higher proportions CD32b⁺/EdU⁺ cells in OA compared to control (Figure 2-7A, C). 1% lipid treated LSEC did not have statistically significant CD32b⁺/EdU⁺ populations over the control. However, this is likely attributed to the culture achieving confluency by days 4 and 5 relative to the OA condition; we were able to obtain a greater number of overall and CD32b⁺ events for 1% lipid samples than with any other condition. Even when debris is included we have statistically significant larger populations of distinct double positive cells following treatment. Combined with immunostaining observations, we can state that PCNA observed in untreated conditions most likely stems from contaminating cell types and/or dedifferentiated LSEC.

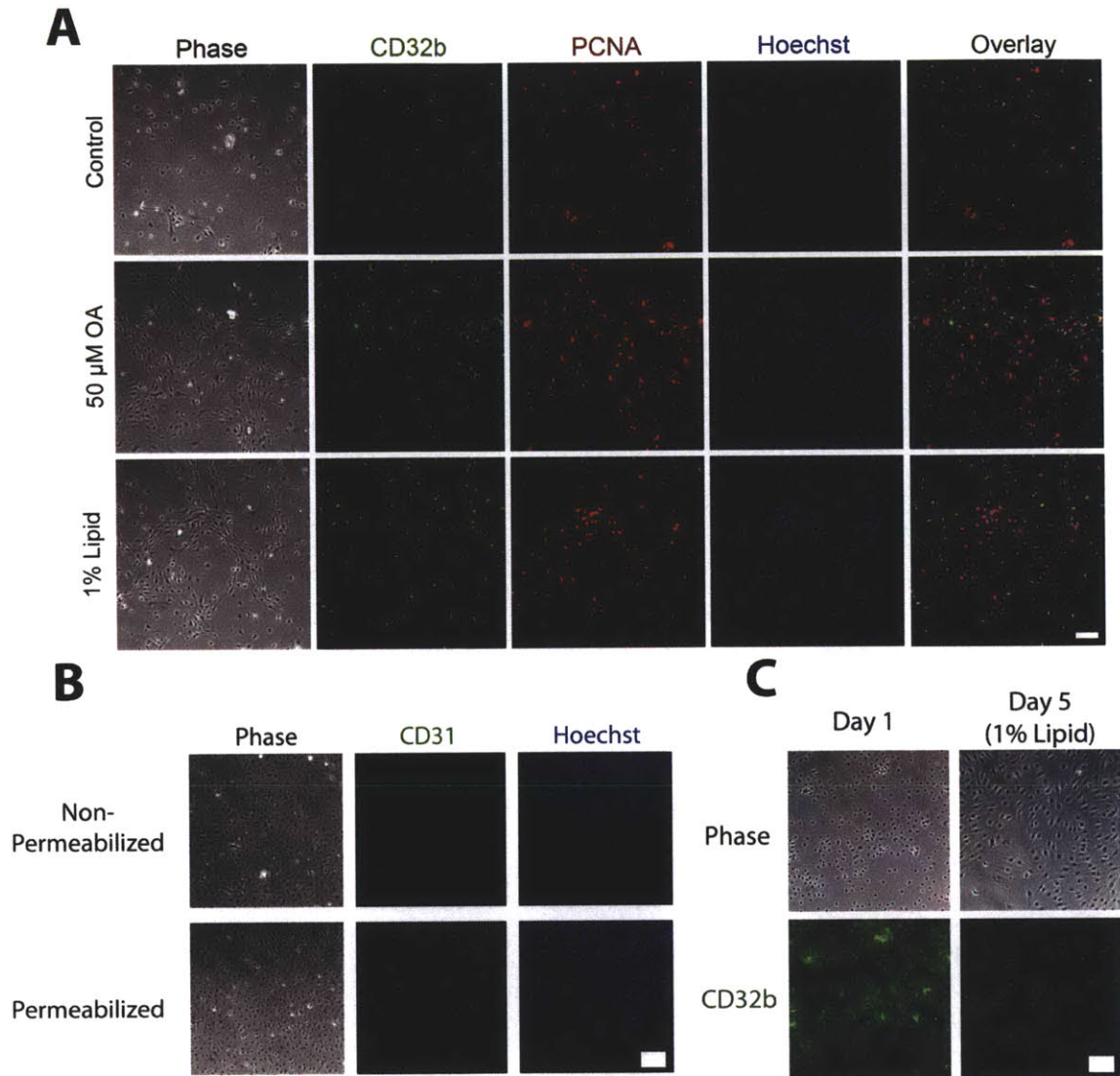


Figure 2-6. LSEC differentiation marker CD32b, proliferation marker PCNA, and nuclear Hoechst co-localize to same cells in FFA cultures. 5-day-old LSEC cultures were imaged for CD32b (green), nuclear PCNA antigen (red), and nuclear Hoechst dye (blue) (A). Punctate CD32b staining was observed in the control and did not co-localize with Hoechst. Broad, diffuse CD32b staining was observed in OA and lipid cultures on cells positive for PCNA and Hoechst, demonstrating that differentiated LSEC undergo proliferation at day 5 *in vitro*. Immunostaining controls for absence of CD31 (B) and CD32b (C) signal degradation were performed. LSEC were cultured for 24 hours prior to being stained with CD31 and Hoechst (B). Samples that were permeabilized were positive for CD31 while non-permeabilized LSEC did not stain positive for CD31. LSEC culture were highly pure in LSEC population after 24 hours using CD32b staining (C). After several days in culture, LSEC increase in surface area while CD32b staining appears to have decreased in overall intensity as compared to freshly isolated cells. This may indicate that LSEC no longer are actively synthesizing new CD32b antigen. Contrast and brightness were adjusted for the entire image due to background fluorescence arising from the Thermanox coverslips. Scale bar = 100 μm .

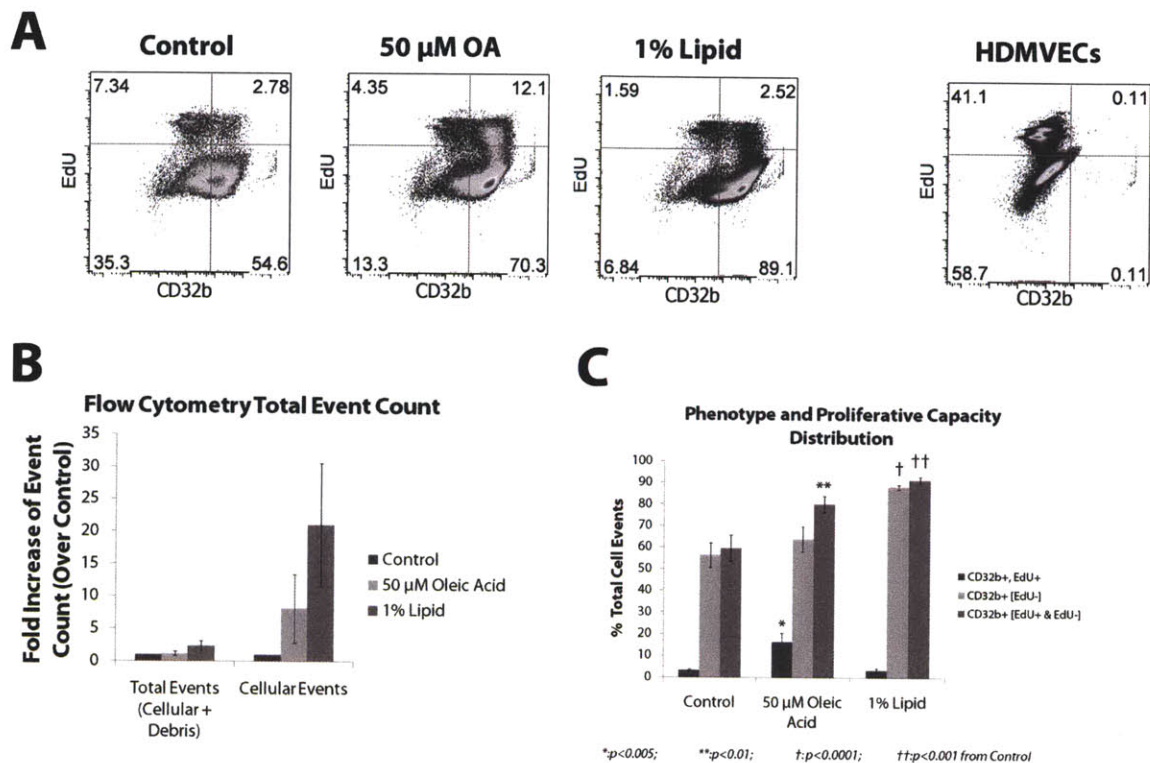


Figure 2-7. OA and lipid supplement help promote proliferation and maintain differentiation in long term LSEC culture. Day 5 total events were captured by flow cytometry and gated for CD32b and EdU using a double negative HDMVEC (A). Total event (cellular + debris) and cellular event counts were tallied and presented as fold number over control, showing consistently 5-20 fold greater number of cellular events in OA and lipid conditions (B). OA and lipid conditions maintained CD32b and were also EdU⁺. LSEC with OA or lipid had statistically significant larger percentages of total events for CD32b⁺, EdU⁺, and dual CD32b⁺/EdU⁺ populations compared to control (C). Overall CD32b expression in OA and lipid conditions were statistically significant from untreated cells (p<0.01, p<0.001).

2.3.4. Temporal dependence of LSEC on PI3K and MAPK pathways observed at Days 3 and 5 in FFA-treated cultures

Akt and ERK1/2 proteins were probed on days 3 and 5 by Western blotting, as significant phenotypic changes occurred at these times (Figure 2-8A, B). Signaling trends observed for Akt and ERK1/2 were consistent across biological replicates. Phospho-Akt/Akt ratios decreased dramatically by day 5 in OA and lipid treated LSEC. Day 3 total and phospho-ERK1/2 levels were similar for all conditions but increased by day 5 in OA and lipid treated LSEC. Phospho-ERK/ERK ratios remained relatively unchanged for ERK2 but increased by day 5 for ERK1,

indicating ERK1 as the primary contributor to overall phospho-ERK/ERK in OA and lipid cultures. Despite no observable statistical significance for phospho-protein signals in Western blots, we found a temporal significance with regard to total signaling proteins present at days 3 and 5 compared to control conditions. Total Akt was statistically significant at days 3 ($p < 0.05$) and 5 for OA ($p < 0.05$) and day 5 lipid ($p < 0.05$) conditions, while total ERK1 (p44) was statistically significant at day 5 ($p < 0.05$) compared to control. Phospho-Akt levels remained relatively constant across all conditions and times, while total Akt increased in treated conditions compared to control through day 5.

Inhibition studies were performed using PI3K inhibitor LY294002 and MEK1/2 inhibitor PD0325901. Inhibitors did not affect LSEC for the first 24 hours of incubation (Figure 2-9A, 2-10A) despite lower concentrations effectively reducing downstream Akt and ERK1/2 phosphorylation (Figure 2-10D). By day 2, 10 μM PI3K inhibitor had adverse effects despite addition of OA or lipid (Figure 2-9B, 2-10A-C). Lower PI3K inhibitor concentrations (3 μM) showed similar effects in unsupplemented medium, but cultures with OA or lipid survived while only the lipid condition continued to proliferate (Figure 2-9B, 2-10B, C). High MEK1/2 inhibitor concentrations only slightly affected OA conditions at day 2 by reducing attached cell number, although culture quality appeared similar to treatments without inhibitor. Lipid cultures did not appear to be perturbed by 1 μM MEK1/2 inhibitor by day 2. MEK1/2 inhibition prevented culture survival after day 4 (Figure 2-9C,D, 2-10C). Lower MEK1/2 inhibitor concentration (0.3 μM) did not vary from the high dose used ($p \gg 0.05$ between all MEK1/2 inhibitor conditions at every time point), indicating LSEC may be more sensitive to changes downstream of MEK1/2 versus PI3K later in culture.

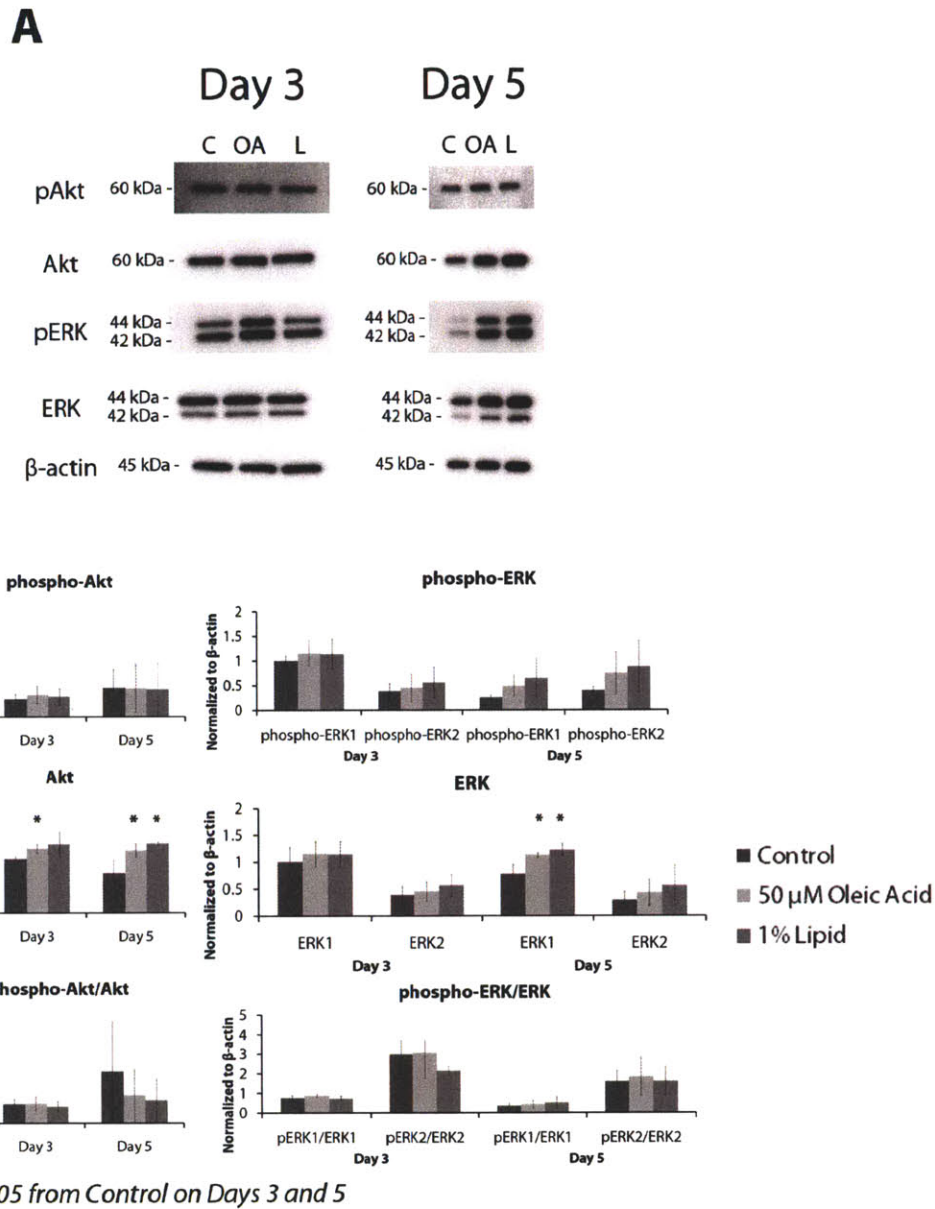


Figure 2-8. Lipid and oleic acid treated LSEC had higher phospho-ERK and phospho-Akt activity. Phospho- and total protein blots were performed for Akt and ERK at days 3 and 5 (representative shown (A)). Signaling trends observed for Akt and ERK1/2 were consistent across biological replicates. Replicates and pixel intensity data were analyzed using ImageJ and plotted against control after normalizing to β-actin values (B). OA and lipid conditions had higher phospho-ERK1/total phospho-ERK1 ratios than in control. Phospho-Akt/total Akt ratios were lower in OA and lipid conditions than in control. Total Akt increased in OA and lipid conditions ($p < 0.05$ from control at days 3 and 5), while total ERK1 increased at day 5 ($p < 0.05$ from control).

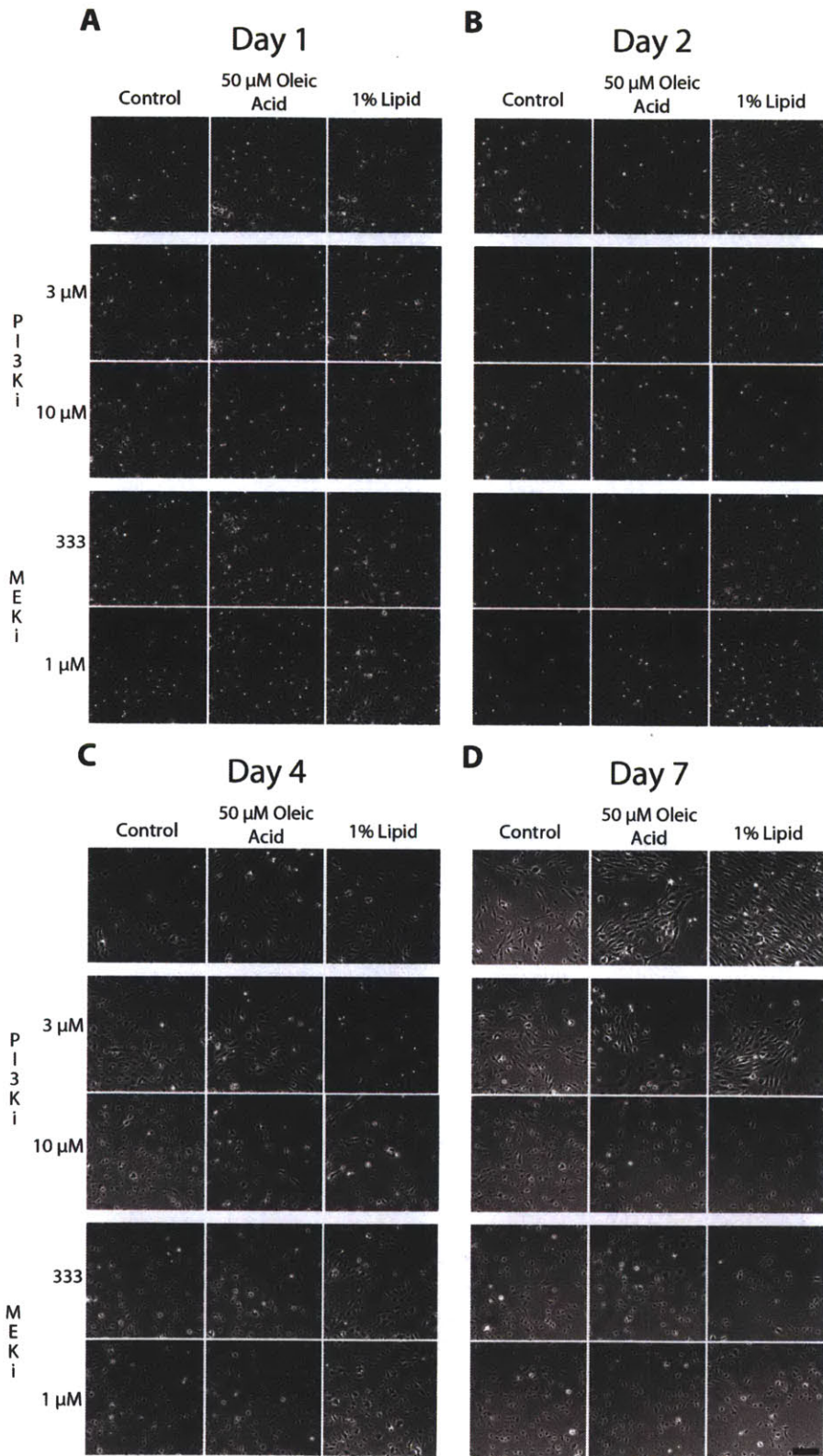


Figure 2-9. Oleic acid and lipid supplement support cultures through early maintenance of low threshold of phospho-Akt followed by late phospho-ERK signaling. Cells were cultured in identical conditions with PI3K inhibitor (LY294002 1 or 10 μM) or MEK1/2 inhibitor (PD0325901 0.3 or 1 μM) for 7 days. Drug inhibitors had no significant effects on cell cultures following the first day of drug inhibitor treatment (A). Significant cell integrity loss was observed in LSECs with 10 μM PI3K inhibitor, with less pronounced effects in 1 μM PI3K inhibitor by day 2, while MEK1/2 inhibitor started to affect oleic acid cultures but not 1% lipid treated SECs (B). SECs in oleic acid or 1% lipid were able to maintain culture viability by days 4 and beyond in culture despite low PI3K inhibitor concentrations (C,D). MEK1/2 inhibitor did eventually affect lipid treated SECs by day 4 (C), although many cells managed to survive in low MEK1/2 inhibitor concentrations. No SECs remained by day 7 of culture with MEK1/2 inhibitor, while low PI3K inhibited SECs treated with either oleic acid or 1% lipid recovered (D). Scale bar = 100 μm .

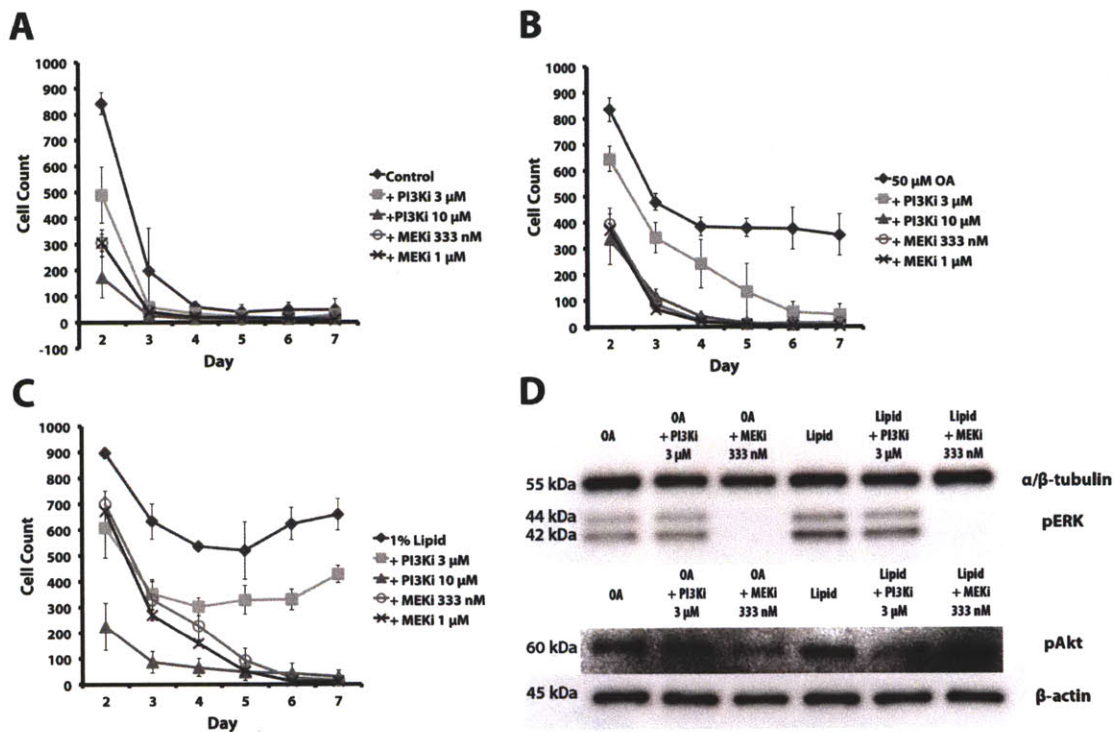


Figure 2-10. OA and lipid supplement support cultures through early maintenance of low threshold of phospho-Akt followed by late phospho-ERK signaling. Intact cell body counts show temporal difference in Akt and ERK signaling (A-C). Low PI3K inhibitor delayed LSEC recovery in OA and lipid conditions while high concentrations prevented culture recovery as early as day 2. Following PI3K inhibition, OA condition was eventually unable to rescue the culture entirely, as the culture decline after day 5. Delays in intact cell loss were observed for low and high MEK inhibition until day 3 in lipid conditions, and LSEC did not recover at later times following MEK inhibition. Although control conditions contained many intact cell bodies, cells had granular morphology of dead cells observed in Figure 2. Western blots show PI3K and MEK1/2 inhibitors effectively reduce phosphoprotein signals within the first 24 hours of treatment (D). Abbreviations: C = Control, OA = 50 μM oleic acid, L = 1% lipid, MEKi = MEK1/2 inhibitor PD0325901, PI3Ki = PI3K inhibitor LY294002.

2.4. DISCUSSION

2.4.1. Lipids and FFA support LSEC survival and function

To test our hypothesis on the requirement of lipids to maintain LSEC viability, we evaluated several different types of lipids in both regular and FFA-free BSA. FFA-free BSA permitted individual testing of lipids for effects on LSEC culture, since native albumin exists bound to a variety of FFAs (5, 6). By day 5, we observed that LSEC cultured with FFAs maintained metabolic and endocytic activity, and proliferated to confluency. The particular form of lipids delivered to LSEC was important, since membrane lipids PC and LPC did not maintain viability. PC and LPC can facilitate cell signaling and stimulate proliferation in many cell types (4, 60), but did not maintain LSEC in culture. We observed that OA alone was insufficient for supporting long-term culture in FFA-free BSA, although OA could recapitulate the lipid supplement effects in regular BSA. In comparison, the 1% lipid supplement, a cocktail of saturated and unsaturated FFAs, was able to support LSEC viability regardless of the BSA used, affirming the necessity for a variety of FFAs to sustain survival and proliferation.

A hallmark of LSEC is the presence of fenestrae, which were maintained in both OA and lipid samples on day 5. Of the few living cells remaining in the control, none were found to possess fenestrae, consistent with previous findings that fenestrae disappear within the first 48 hours of culture (8). Additional evaluation with CD32b phenotype marker validated findings that surviving LSEC in lipid or OA maintained differentiation, by expressing this marker, one specific to liver sinusoidal endothelium (52). Along with CD32b expression, we also looked at the proliferative capacity of LSEC, since no previous studies have explicitly reported that differentiated rat LSEC can simultaneously undergo proliferation. We successfully demonstrated that differentiated LSEC undergo proliferation, via nuclear PCNA expression and EdU incorporation, when treated with FFAs, which to our knowledge is the first explicit evidence reported (58). Despite maintenance of several phenotypic characteristics in prolonged cultures, we did observe slight degradation of some markers. Although fenestrae arranged in sieve plates were observed, they were not abundant in OA and lipid treated cultures, and a large percentage of these LSEC no longer exhibited fenestrae by day 5. Many cells in the FFA-treated conditions possessed large transcytotic pores greater than 1 μm in diameter. These may be the remnants of sieve plates that have degraded or fenestrae that have fused. We noticed that

although LSEC still expressed CD32b, the presence was diffuse and overall fluorescent intensity was lower than for freshly isolated LSEC (Figure 2-6C). Other studies have reported sharper declines in specific LSEC phenotype markers during culture, mostly associated with the dedifferentiation process, recently reported to involve Leda-1 (30, 52). We suspect that lipid-treated LSEC maintain a state of differentiation that allows them to persist and proliferate *in vitro*, but do not maintain physiological levels of CD32b antigen.

2.4.2. FFA influence on phosphoprotein signaling pathways

In LSEC we observed phospho-Akt/Akt levels decreased in FFA conditions as time progressed, while the inverse occurred with phospho-ERK/ERK, primarily by ERK1. From these observations and inhibitor studies, we believe low threshold levels of phospho-Akt are required for cell survival between days 2 and 3. At this point, high concentrations of PI3K inhibitor LY294002 abolished the beneficial effects that OA and 1% lipid have on LSECs, while lower concentrations did not affect cultures. Beyond 3 days, cells in low PI3K inhibitor could proliferate and recover albeit not to the level seen in uninhibited samples. Granular morphology appeared earlier at day 2 (as opposed to day 3 in control samples without inhibitor) in untreated samples with PI3K inhibitor. This may indicate that downstream signals of PI3K are closely associated with cell survival during this time. Past day 3, MEK1/2 inhibition was fatal to cultures, as LSEC did not survive or proliferate regardless of the concentration of MEK1/2 inhibitor PD0325901 added to cultures. Interestingly, OA and lipid-treated cultured LSEC did not have a significant dependence on MAPK before this time, as 10 μ M inhibitor only slightly affected the number of cells in culture. At early time points, MEK1/2 inhibition also prevented LSECs from undergoing increased spreading seen with FFA treatments. As such, MAPK signaling may be partially responsible for the morphology change induced by FFAs before day 3, but required afterward for survival and proliferation.

2.4.3. Diametric effects emphasize need of lipid balance for optimal function

While it is understood that ECM, cell-cell contacts (52), and paracrine/autocrine signaling (18) are absolutely vital to achieve functional LSEC, consideration of the role of lipids is important given the results of this study. Effects of FFAs on LSEC can have several implications on liver pathophysiology. In general, lipids are crucial for survival for all mammalian cells as energy

substrates, membrane lipid bases, and influencing cell signal processes (9). Concentrations of FFAs in circulation can vary dramatically depending on the metabolic state, but have been reported to be anywhere between 10 μM to 1 mM in human plasma, though generally within the range of 200 to 600 μM (33, 64, 66). Approximately 150 μM total plasma FFA is taken up in the liver, of which about 50 μM is comprised of OA (and is recapitulated in our experimental conditions) (33, 43). The liver is the primary organ responsible for lipid metabolism as 75% of the blood that enters into the liver arrives from the intestine which absorbs lipids from the gut or lipolysis from adipose tissue (11). Thus, FFAs are likely to have a profound influence on LSEC. Past studies have shown that polyunsaturated FFAs can protect hepatocytes from superoxide radicals (73), while bioactive lipids like sphingosine 1-phosphate provide oxidative protection to LSEC following liver injury (93). In contrast, studies also argue for the presence of lipids as precursors to chronic disease, apoptosis, steatosis, and insulin resistance/diabetes (2, 46, 49, 51). For example, caveolin-1 is important to lipid metabolism during liver regeneration, but may also implicate a role of pathogenesis in LSEC since it is upregulated in dedifferentiating cells (9, 11, 78). Moreover, we observed that cocultures of hepatocytes and LSEC induce hepatic cell death in lipid conditions, suggesting concentrations beneficial to LSECs can be lipotoxic for hepatocytes (data not shown).

OA and other unsaturated FFAs have been reported to have numerous effects on metabolically active cells although the main mechanisms of OA and other FFA incorporation are still not fully understood. OA has been found to participate in crosstalk with EGFR and other pathways by affecting MAPK and PI3K (13, 14, 83, 84, 88, 92). However, much of the data from previous studies are contradictory in either stimulating or inhibiting these pathways dependent on the system being studied.

Unsaturated FFAs have been found to be able to protect against oxidative stress by reducing lipid peroxidation and inhibiting the inflammatory pathway NF- κ B which can lead to endothelial cell activation (10, 12, 17, 54). Thus, OA may prevent oxidative stress in LSEC that decreases ERK1/2 activity (53, 71), thereby allowing cells to resume cell survival and proliferation after day 3. This would be in agreement with the results we observed in increased phospho-ERK1/2 activity. Furthermore, increased saturated to unsaturated fatty acid levels are strongly correlated

with insulin resistance and decreased glucose production in the liver (46, 51). The introduction of more unsaturated FA into the system may facilitate insulin signaling and activation of phospho-Akt for cell survival in our early time points. While it is most likely that FFAs indirectly modulate proteomic responses via metabolic pathways, we observed distinct changes in phospho-protein signaling pathways. We could directly influence viability in OA and lipid treated LSEC by inhibiting PI3K and MAPK pathways, showing a temporal shift in phospho-protein signaling dependence from PI3K to MAPK.

2.4.4. Consideration of lipids in liver and LSEC biology

Our results implicate the underlying importance of FFAs in the basic function of LSEC, as FFA modulate LSEC phenotype, survival, and proliferation in the absence of serum. Changes in the FFA profile due to shifts in systemic or dietary delivery to the liver can potentially result in LSEC dysfunction, leading to oxidative stress and activation of inflammatory pathways. Additionally, decreases in unsaturated FFA (and increase in saturated FFA) could lead to steatosis and insulin resistance. As such, lipid balance in the liver is required to prevent onset of disease. We demonstrated that LSEC monocultures can maintain their unique phenotype in culture through at least 5 days of culture and were concomitantly proliferating. Our chemically defined media system provides an *in vitro* platform to effectively move forward in understanding the phenomena involved in LSEC biology.

2.5. REFERENCES

1. **Alberts B, Johnson A, Lewis J, Raff M, Roberts K, Walter P.** Molecular Biology of the Cell [Online]. 4th ed. Garland Science.
<http://www.ncbi.nlm.nih.gov/books/NBK21054/>.
2. **Angulo P.** Nonalcoholic fatty liver disease. *N Engl J Med* 346: 1221–1231, 2002.
3. **Augé N, Santanam N, Mori N, Keshava C, Parthasarathy S.** Uptake of 13-hydroperoxylinoleic acid by cultured cells. *Arteriosclerosis, Thrombosis, and Vascular Biology* 19: 925–931, 1999.
4. **Bassa BV, Noh JW, Ganji SH, Shin M-K, Roh DD, Kamanna VS.** Lysophosphatidylcholine stimulates EGF receptor activation and mesangial cell proliferation: regulatory role of Src and PKC. *Biochim. Biophys. Acta* 1771: 1364–1371, 2007.
5. **Berk PD, Stump DD.** Mechanisms of cellular uptake of long chain free fatty acids. *Mol. Cell. Biochem.* 192: 17–31, 1999.
6. **Bojesen IN, Bojesen E.** Binding of arachidonate and oleate to bovine serum albumin. *The Journal of Lipid Research* 35: 770–778, 1994.
7. **Bolt HM.** Vinyl chloride—a classical industrial toxicant of new interest. *Crit Rev Toxicol* 35: 307–323, 2005.
8. **Braet F, Wisse E.** Structural and functional aspects of liver sinusoidal endothelial cell fenestrae: a review. *Comp Hepatol* 1: 1, 2002.
9. **Brasaemle DL.** Cell biology. A metabolic push to proliferate. *Science* 313: 1581–1582, 2006.
10. **Brooks JD, Musiek ES, Koestner TR, Stankowski JN, Howard JR, Brunoldi EM, Porta A, Zanoni G, Vidari G, Morrow JD, Milne GL, McLaughlin B.** The fatty acid oxidation product 15-A(3t)-Isoprostane is a potent inhibitor of NFκB transcription and macrophage transformation. *J Neurochem* (August 12, 2011). doi: 10.1111/j.1471-4159.2011.07422.x.
11. **Canbay A, Bechmann L, Gerken G.** Lipid metabolism in the liver. *Z Gastroenterol* 45: 35–41, 2007.

12. **Carluccio MA, Massaro M, Bonfrate C, Siculella L, Maffia M, Nicolardi G, Distante A, Storelli C, De Caterina R.** Oleic acid inhibits endothelial activation : A direct vascular antiatherogenic mechanism of a nutritional component in the mediterranean diet. *Arteriosclerosis, Thrombosis, and Vascular Biology* 19: 220–228, 1999.
13. **Casabiell X, Zugaza JL, Pombo CM, Pandiella A, Casanueva FF.** Oleic acid blocks epidermal growth factor-activated early intracellular signals without altering the ensuing mitogenic response. *Experimental Cell Research* 205: 365–373, 1993.
14. **Collins QF, Xiong Y, Lupo EG, Liu H-Y, Cao W.** p38 Mitogen-activated protein kinase mediates free fatty acid-induced gluconeogenesis in hepatocytes. *J. Biol. Chem.* 281: 24336–24344, 2006.
15. **Conzen SD.** Minireview: nuclear receptors and breast cancer. *Mol. Endocrinol.* 22: 2215–2228, 2008.
16. **Daneker GW, Lund SA, Caughman SW, Swerlick RA, Fischer AH, Staley CA, Ades EW.** Culture and characterization of sinusoidal endothelial cells isolated from human liver. *In Vitro Cell. Dev. Biol. Anim.* 34: 370–377, 1998.
17. **De Caterina R, Spiecker M, Solaini G, Basta G, Bosetti F, Libby P, Liao J.** The inhibition of endothelial activation by unsaturated fatty acids. *Lipids* 34 Suppl: S191–4, 1999.
18. **DeLeve LD, Wang X, Hu L, McCuskey MK, McCuskey RS.** Rat liver sinusoidal endothelial cell phenotype is maintained by paracrine and autocrine regulation. *Am. J. Physiol. Gastrointest. Liver Physiol.* 287: G757–63, 2004.
19. **DeLeve LD, Wang X, McCuskey MK, McCuskey RS.** Rat liver endothelial cells isolated by anti-CD31 immunomagnetic separation lack fenestrae and sieve plates. *Am. J. Physiol. Gastrointest. Liver Physiol.* 291: G1187–9, 2006.
20. **DeLeve LD.** Hepatic microvasculature in liver injury. *Semin. Liver Dis.* 27: 390–400, 2007.
21. **Domansky K, Inman W, Serdy J, Dash A, Lim MH, Griffith LG.** Perfused multiwell plate for 3D liver tissue engineering. *Lab Chip* 10: 51–58, 2010.
22. **Drover VA, Nguyen DV, Bastie CC, Darlington YF, Abumrad NA, Pessin JE, London E, Sahoo D, Phillips MC.** CD36 mediates both cellular uptake of very long chain fatty acids and their intestinal absorption in mice. *J. Biol. Chem.* 283: 13108–13115,

- 2008.
23. **Duval C, Augé N, Frisach M-F, Casteilla L, Salvayre R, Nègre-Salvayre A.** Mitochondrial oxidative stress is modulated by oleic acid via an epidermal growth factor receptor-dependent activation of glutathione peroxidase. *Biochem. J.* 367: 889–894, 2002.
 24. **ELVEVOLD K, Nedredal GI, REVHAUG A, BERTHEUSSEN K, SMEDSRØD B.** Long-term preservation of high endocytic activity in primary cultures of pig liver sinusoidal endothelial cells. *Eur. J. Cell Biol.* 84: 749–764, 2005.
 25. **Elvevold K, Smedsrød B, Martinez I.** The liver sinusoidal endothelial cell: a cell type of controversial and confusing identity. *Am. J. Physiol. Gastrointest. Liver Physiol.* 294: G391–400, 2008.
 26. **Elvevold KH, Nedredal GI, Revhaug A, Smedsrød B.** Scavenger properties of cultivated pig liver endothelial cells. *Comp Hepatol* 3: 4, 2004.
 27. **Enomoto K, Nishikawa Y, Omori Y, Tokairin T, Yoshida M, Ohi N, Nishimura T, Yamamoto Y, Li Q.** Cell biology and pathology of liver sinusoidal endothelial cells. *Med Electron Microsc* 37: 208–215, 2004.
 28. **Eyre NS, Cleland LG, Mayrhofer G.** FAT/CD36 expression alone is insufficient to enhance cellular uptake of oleate. *Biochemical and Biophysical Research Communications* 370: 404–409, 2008.
 29. **Eyre NS, Cleland LG, Tandon NN, Mayrhofer G.** Importance of the carboxyl terminus of FAT/CD36 for plasma membrane localization and function in long-chain fatty acid uptake. *The Journal of Lipid Research* 48: 528–542, 2007.
 30. **Géraud C, Schledzewski K, Demory A, Klein D, Kaus M, Peyre F, Sticht C, Evdokimov K, Lu S, Schmieder A, Goerdts S.** Liver sinusoidal endothelium: a microenvironment-dependent differentiation program in rat including the novel junctional protein liver endothelial differentiation-associated protein-1. *Hepatology* 52: 313–326, 2010.
 31. **Grammatikos SI, Subbaiah PV, Victor TA, Miller WM.** Diverse effects of essential (n-6 and n-3) fatty acids on cultured cells. *Cytotechnology* 15: 31–50, 1994.
 32. **Guo W, Huang N, Cai J, Xie W, Hamilton JA.** Fatty acid transport and metabolism in HepG2 cells. *Am. J. Physiol. Gastrointest. Liver Physiol.* 290: G528–34, 2006.
 33. **Hagenfeldt L, Wahren J, Pernow B, Räf L.** Uptake of individual free fatty acids by

- skeletal muscle and liver in man. *J. Clin. Invest.* 51: 2324–2330, 1972.
34. **Hamilton JA, Era S, Bhamidipati SP, Reed RG.** Locations of the three primary binding sites for long-chain fatty acids on bovine serum albumin. *Proc. Natl. Acad. Sci. U.S.A.* 88: 2051–2054, 1991.
 35. **Hansen B, Longati P, Elvevold K, Nedredal GI, Schledzewski K, Olsen R, Falkowski M, Kzhyskowska J, Carlsson F, Johansson S, Smedsrød B, Goerdt S, Johansson S, McCourt P.** Stabilin-1 and stabilin-2 are both directed into the early endocytic pathway in hepatic sinusoidal endothelium via interactions with clathrin/AP-2, independent of ligand binding. *Experimental Cell Research* 303: 160–173, 2005.
 36. **Hata S, Namae M, Nishina H.** Liver development and regeneration: from laboratory study to clinical therapy. *Dev. Growth Differ.* 49: 163–170, 2007.
 37. **Hwa AJ, Fry RC, Sivaraman A, So PT, Samson LD, Stolz DB, Griffith LG.** Rat liver sinusoidal endothelial cells survive without exogenous VEGF in 3D perfused co-cultures with hepatocytes. *FASEB J.* 21: 2564–2579, 2007.
 38. **Irving MG, Roll FJ, Huang S, Bissell DM.** Characterization and culture of sinusoidal endothelium from normal rat liver: lipoprotein uptake and collagen phenotype. *Gastroenterology* 87: 1233–1247, 1984.
 39. **Kamp F, Guo W, Souto R, Pilch PF, Corkey BE, Hamilton JA.** Rapid flip-flop of oleic acid across the plasma membrane of adipocytes. *J. Biol. Chem.* 278: 7988–7995, 2003.
 40. **Khan WA, Blobe GC, Hannun YA.** Arachidonic acid and free fatty acids as second messengers and the role of protein kinase C. *Cellular Signalling* 7: 171–184, 1995.
 41. **Khetani SR, Bhatia SN.** Microscale culture of human liver cells for drug development. *Nat Biotechnol* 26: 120–126, 2008.
 42. **Kim EK, Yun SJ, Do KH, Kim MS, Cho M, Suh D-S, Kim CD, Kim JH, Birnbaum MJ, Bae SS.** Lysophosphatidic acid induces cell migration through the selective activation of Akt1. *Exp. Mol. Med.* 40: 445–452, 2008.
 43. **Kokatnur MG, Oalman MC, Johnson WD, Malcom GT, Strong JP.** Fatty acid composition of human adipose tissue from two anatomical sites in a biracial community. *Am. J. Clin. Nutr.* 32: 2198–2205, 1979.
 44. **Krause P, Markus PM, Schwartz P, Unthan-Fechner K, Pestel S, Fandrey J, Probst I.** Hepatocyte-supported serum-free culture of rat liver sinusoidal endothelial cells.

- Journal of Hepatology* 32: 718–726, 2000.
45. **Lalor PF, Lai WK, Curbishley SM, Shetty S, Adams DH.** Human hepatic sinusoidal endothelial cells can be distinguished by expression of phenotypic markers related to their specialised functions in vivo. *WJG* 12: 5429–5439, 2006.
 46. **Leclercq IA, Da Silva Morais A, Schroyen B, Van Hul N, Geerts A.** Insulin resistance in hepatocytes and sinusoidal liver cells: mechanisms and consequences. *Journal of Hepatology* 47: 142–156, 2007.
 47. **Li J, Wilson A, Kuruba R, Zhang Q, Gao X, He F, Zhang L-M, Pitt BR, Xie W, Li S.** FXR-mediated regulation of eNOS expression in vascular endothelial cells. *Cardiovascular Research* 77: 169–177, 2008.
 48. **Li R, Oteiza A, Sørensen KK, McCourt P, Olsen R, Smedsrød B, Svistounov D.** Role of liver sinusoidal endothelial cells and stabilins in elimination of oxidized low-density lipoproteins. *AJP: Gastrointestinal and Liver Physiology* 300: G71–81, 2011.
 49. **Malhi H, Barreyro FJ, Isomoto H, Bronk SF, Gores GJ.** Free fatty acids sensitise hepatocytes to TRAIL mediated cytotoxicity. *Gut* 56: 1124–1131, 2007.
 50. **Malhi H, Bronk SF, Werneburg NW, Gores GJ.** Free fatty acids induce JNK-dependent hepatocyte lipoapoptosis. *J. Biol. Chem.* 281: 12093–12101, 2006.
 51. **Manco M, Mingrone G, Greco AV, Capristo E, Gniuli D, De Gaetano A, Gasbarrini G.** Insulin resistance directly correlates with increased saturated fatty acids in skeletal muscle triglycerides. *Metab. Clin. Exp.* 49: 220–224, 2000.
 52. **March S, Hui EE, Underhill GH, Khetani S, Bhatia SN.** Microenvironmental regulation of the sinusoidal endothelial cell phenotype in vitro. *Hepatology* 50: 920–928, 2009.
 53. **Martinez I, Nedredal GI, Øie CI, Warren A, Johansen O, Le Couteur DG, Smedsrød B.** The influence of oxygen tension on the structure and function of isolated liver sinusoidal endothelial cells. *Comp Hepatol* 7: 4, 2008.
 54. **Massaro M, De Caterina R.** Vasculoprotective effects of oleic acid: epidemiological background and direct vascular antiatherogenic properties. *Nutr Metab Cardiovasc Dis* 12: 42–51, 2002.
 55. **Milligan G, Stoddart LA, Brown AJ.** G protein-coupled receptors for free fatty acids. *Cellular Signalling* 18: 1360–1365, 2006.

56. **Muzio G, Maggiora M, Oraldi M, Trombetta A, Canuto RA.** PPAR α and PP2A are involved in the proapoptotic effect of conjugated linoleic acid on human hepatoma cell line SK-HEP-1. *Int. J. Cancer* 121: 2395–2401, 2007.
57. **Nagelkerke JF, Barto KP, van Berkel TJ.** In vivo and in vitro uptake and degradation of acetylated low density lipoprotein by rat liver endothelial, Kupffer, and parenchymal cells. *J. Biol. Chem.* 258: 12221–12227, 1983.
58. **Nahmias Y, Berthiaume F, Yarmush ML.** Integration of technologies for hepatic tissue engineering. *Adv. Biochem. Eng. Biotechnol.* 103: 309–329, 2007.
59. **Netland PA, Zetter BR, Via DP, Voyta JC.** In situ labelling of vascular endothelium with fluorescent acetylated low density lipoprotein. *Histochem. J.* 17: 1309–1320, 1985.
60. **Nolan CJ, Madiraju MSR, Delghingaro-Augusto V, Peyot M-L, Prentki M.** Fatty acid signaling in the beta-cell and insulin secretion. *Diabetes* 55 Suppl 2: S16–23, 2006.
61. **Nonaka H, Tanaka M, Suzuki K, Miyajima A.** Development of murine hepatic sinusoidal endothelial cells characterized by the expression of hyaluronan receptors. *Dev. Dyn.* 236: 2258–2267, 2007.
62. **Pilch PF, Souto RP, Liu L, Jedrychowski MP, Berg EA, Costello CE, Gygi SP.** Cellular spelunking: exploring adipocyte caveolae. *The Journal of Lipid Research* 48: 2103–2111, 2007.
63. **Raza H, Chung WL, Mukhtar H.** Specific high-affinity binding of fatty acids to epidermal cytosolic proteins. *J. Invest. Dermatol.* 97: 323–326, 1991.
64. **Richieri GV, Kleinfeld AM.** Unbound free fatty acid levels in human serum. *The Journal of Lipid Research* 36: 229–240, 1995.
65. **Ring A, Le Lay S, Pohl J, Verkade P, Stremmel W.** Caveolin-1 is required for fatty acid translocase (FAT/CD36) localization and function at the plasma membrane of mouse embryonic fibroblasts. *Biochim. Biophys. Acta* 1761: 416–423, 2006.
66. **Seppälä-Lindroos A, Vehkavaara S, Häkkinen A-M, Goto T, Westerbacka J, Sovijärvi A, Halavaara J, Yki-Järvinen H.** Fat accumulation in the liver is associated with defects in insulin suppression of glucose production and serum free fatty acids independent of obesity in normal men. *J. Clin. Endocrinol. Metab.* 87: 3023–3028, 2002.
67. **Shah P, Vella A, Basu A, Basu R, Adkins A, Schwenk WF, Johnson CM, Nair KS, Jensen MD, Rizza RA.** Effects of free fatty acids and glycerol on splanchnic glucose

- metabolism and insulin extraction in nondiabetic humans. *Diabetes* 51: 301–310, 2002.
68. **Shults MD, Janes KA, Lauffenburger DA, Imperiali B.** A multiplexed homogeneous fluorescence-based assay for protein kinase activity in cell lysates. *Nat Methods* 2: 277–283, 2005.
 69. **Singh R, Kaushik S, Wang Y, Xiang Y, Novak I, Komatsu M, Tanaka K, Cuervo AM, Czaja MJ.** Autophagy regulates lipid metabolism. *Nature* 458: 1131–1135, 2009.
 70. **Sivaraman A, Leach JK, Townsend S, IIDA T, Hogan BJ, Stolz DB, Fry R, Samson LD, Tannenbaum SR, Griffith LG.** A microscale in vitro physiological model of the liver: predictive screens for drug metabolism and enzyme induction. *Curr Drug Metab* 6: 569–591, 2005.
 71. **Smathers RL, Galligan JJ, Stewart BJ, Petersen DR.** Overview of lipid peroxidation products and hepatic protein modification in alcoholic liver disease. *Chem. Biol. Interact.* 192: 107–112, 2011.
 72. **Smith J, Su X, El-Maghrabi R, Stahl PD, Abumrad NA.** Opposite regulation of CD36 ubiquitination by fatty acids and insulin: effects on fatty acid uptake. *J. Biol. Chem.* 283: 13578–13585, 2008.
 73. **Sohma R, Takahashi M, Takada H, Takada H, Kuwayama H.** Protective effect of n-3 polyunsaturated fatty acid on primary culture of rat hepatocytes. *J Gastroenterol Hepatol* 22: 1965–1970, 2007.
 74. **Sorrentino D, Stump DD, Van Ness K, Simard A, Schwab AJ, Zhou SL, Goresky CA, Berk PD.** Oleate uptake by isolated hepatocytes and the perfused rat liver is competitively inhibited by palmitate. *Am. J. Physiol.* 270: G385–92, 1996.
 75. **Spector AA, John K, Fletcher JE.** Binding of long-chain fatty acids to bovine serum albumin. *The Journal of Lipid Research* 10: 56–67, 1969.
 76. **Staudinger JL, Lichti K.** Cell signaling and nuclear receptors: new opportunities for molecular pharmaceuticals in liver disease. *Mol. Pharm.* 5: 17–34, 2008.
 77. **Straub AC, Clark KA, Ross MA, Chandra AG, Li S, Gao X, Pagano PJ, Stolz DB, Barchowsky A.** Arsenic-stimulated liver sinusoidal capillarization in mice requires NADPH oxidase-generated superoxide. *J. Clin. Invest.* 118: 3980–3989, 2008.
 78. **Straub AC, Stolz DB, Ross MA, Hernandez-Zavala A, Soucy NV, Klei LR, Barchowsky A.** Arsenic stimulates sinusoidal endothelial cell capillarization and vessel

- remodeling in mouse liver. *Hepatology* 45: 205–212, 2007.
79. **SUN K, WANG Q, HUANG X-H.** PPAR gamma inhibits growth of rat hepatic stellate cells and TGF beta-induced connective tissue growth factor expression. *Acta Pharmacol. Sin.* 27: 715–723, 2006.
 80. **Sung JH, Esch MB, Shuler ML.** Integration of in silico and in vitro platforms for pharmacokinetic-pharmacodynamic modeling. *Expert Opin Drug Metab Toxicol* 6: 1063–1081, 2010.
 81. **Sylvester PW, Birkenfeld HP, Hosick HL, Briski KP.** Fatty acid modulation of epidermal growth factor-induced mouse mammary epithelial cell proliferation in vitro. *Experimental Cell Research* 214: 145–153, 1994.
 82. **Taub R.** Liver regeneration: from myth to mechanism. *Nat Rev Mol Cell Biol* 5: 836–847, 2004.
 83. **Vacaresse N, Lajoie-Mazenc I, Augé N, Suc I, Frisach MF, Salvayre R, Nègre-Salvayre A.** Activation of epithelial growth factor receptor pathway by unsaturated fatty acids. *Circulation Research* 85: 892–899, 1999.
 84. **Vinciguerra M, Veyrat Durebex C, Moukil MA, Rubbia Brandt L, Rohner Jeanrenaud F, Foti M.** PTEN down-regulation by unsaturated fatty acids triggers hepatic steatosis via an NF-kappaBp65/mTOR-dependent mechanism. *Gastroenterology* 134: 268–280, 2008.
 85. **Voyta JC, Via DP, Butterfield CE, Zetter BR.** Identification and isolation of endothelial cells based on their increased uptake of acetylated-low density lipoprotein. *The Journal of Cell Biology* 99: 2034–2040, 1984.
 86. **Wang G, Chen QM, Minuk GY, Gong Y, Burczynski FJ.** Enhanced expression of cytosolic fatty acid binding protein and fatty acid uptake during liver regeneration in rats. *Mol. Cell. Biochem.* 262: 41–49, 2004.
 87. **Wang J, Wu X, Simonavicius N, Tian H, Ling L.** Medium-chain fatty acids as ligands for orphan G protein-coupled receptor GPR84. *J. Biol. Chem.* 281: 34457–34464, 2006.
 88. **Wang XL, Zhang L, Youker K, Zhang M-X, Wang J, LeMaire SA, Coselli JS, Shen YH.** Free fatty acids inhibit insulin signaling-stimulated endothelial nitric oxide synthase activation through upregulating PTEN or inhibiting Akt kinase. *Diabetes* 55: 2301–2310, 2006.

89. **Wolfrum C.** Cytoplasmic fatty acid binding protein sensing fatty acids for peroxisome proliferator activated receptor activation. *Cell. Mol. Life Sci.* 64: 2465–2476, 2007.
90. **Wu X, Tong Y, Shankar K, Baumgardner JN, Kang J, Badeaux J, Badger TM, Ronis MJJ.** Lipid fatty acid profile analyses in liver and serum in rats with nonalcoholic steatohepatitis using improved gas chromatography-mass spectrometry methodology. *J. Agric. Food Chem.* 59: 747–754, 2011.
91. **Xu C, Lin F, Qin S.** Relevance between lipid metabolism-associated genes and rat liver regeneration. *Hepatol. Res.* 38: 825–837, 2008.
92. **Yonezawa T, Haga S, Kobayashi Y, Katoh K, Obara Y.** Unsaturated fatty acids promote proliferation via ERK1/2 and Akt pathway in bovine mammary epithelial cells. *Biochemical and Biophysical Research Communications* 367: 729–735, 2008.
93. **Zheng D-M, Kitamura T, Ikejima K, Enomoto N, Yamashina S, Suzuki S, Takei Y, Sato N.** Sphingosine 1-phosphate protects rat liver sinusoidal endothelial cells from ethanol-induced apoptosis: Role of intracellular calcium and nitric oxide. *Hepatology* 44: 1278–1287, 2006.

Chapter 3

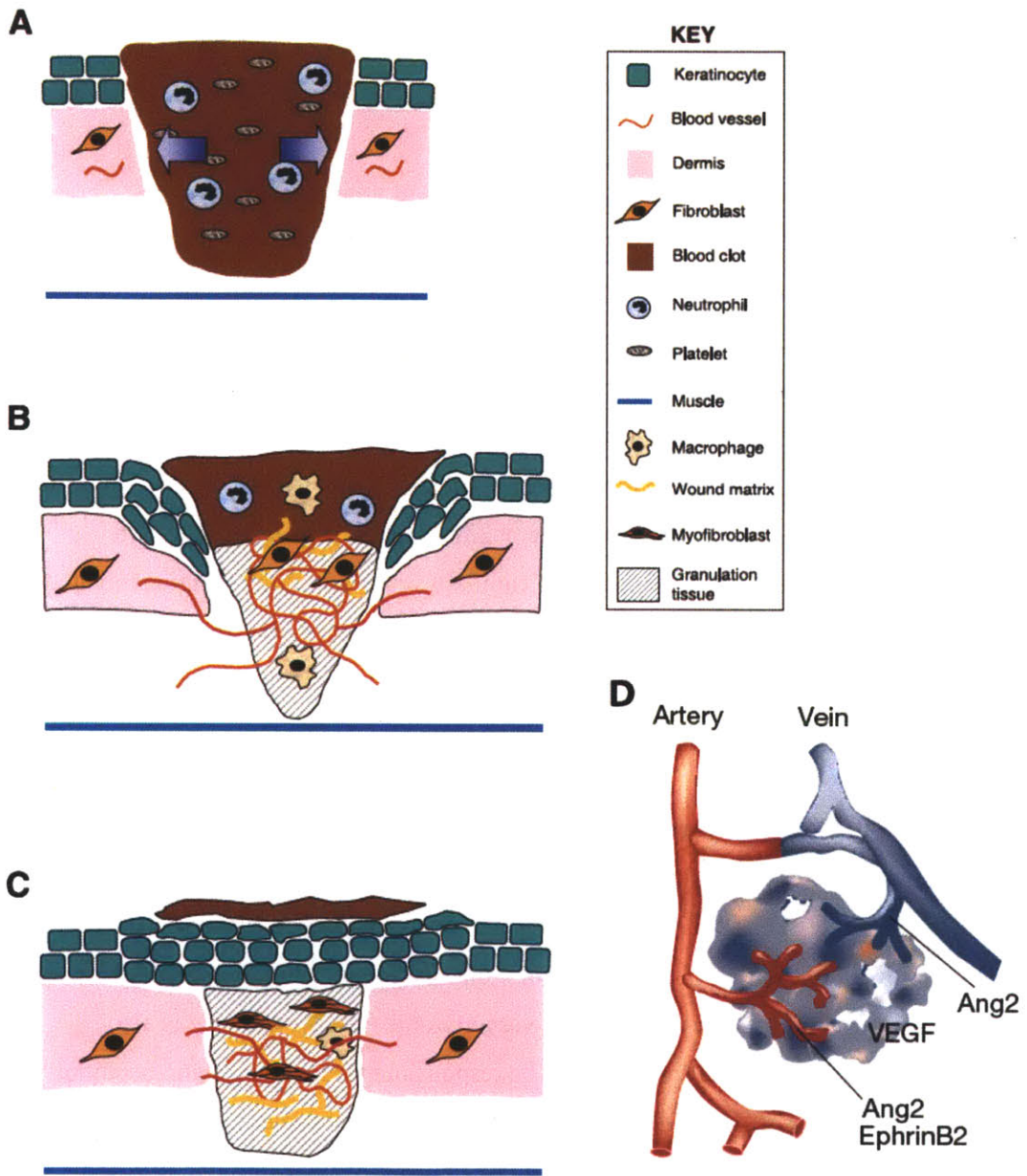
Development of cell signaling protocols for human dermal microvascular endothelial cells cultured on 3D collagen gels

3.1 INTRODUCTION

3.1.1. Background and motivation for the study of angiogenesis

Angiogenesis is an important foundation to functions of organ and tissue regeneration to re-establish homeostasis. A great deal of work has been done in focus on understanding this phenomenon as it occurs *in vivo*. Angiogenesis, the formation of blood vessels from pre-existing blood vessels, is absolutely essential for regenerating tissue that has been injured or growing tissue mass by providing a system for nutrient and waste transport (Figure 3-1A) (1). The process is also critical in creating specialized vascular structures, such as veins, arteries, or capillaries, for supporting metabolic processes that may be unique to the tissue (12). Furthermore, pro-angiogenic proteins such as VEGF could not sustain stable structures by itself and required other proteins such as angiopoietins 1 and 2 to assist in vessel pruning and stabilization in embryonic angiogenesis (31, 34, 46), demonstrating the need for both positive and negative regulating signals for vessel stabilization and maturation.

Figure 3-1. Angiogenesis during wound healing process and vessel sprouting to support metabolic demands of tissues (44, 46). Following a wound, platelets release coagulation and growth factors to form a hemostatic clot plug (A). Following the hemostatic plug, inflammation occurs and signals for restoration of injured tissue area. Granulation tissue is formed and blood vessel structures begin to innervate healing wound (B). Following vascularization, re-epithelialization, matrix formation, and remodeling of the tissue occur as the milieu is returned to homeostatic conditions (C). Angiogenesis is a complicated process of vessel sprouting from pre-existing blood vessels to help support metabolic needs of complex tissue. Vessel sprouting into a tumor is shown as a model of angiogenesis in adult vascular system (D). (A,B,C) Adapted with permission from The American Physiological Society: *Physiological Reviews*. Werner S, Grose R. "Regulation of wound healing by growth factors and cytokines." *Physiol Rev* (2003). 83(3):835-870. © 2003. (D) Adapted with permission from MacMillan Publishers Ltd: *Nature*. Yancopoulos GD, Davis S, Gale NW, Rudge JS, Wiegand SJ, Holash J. "Vascular-specific growth factors blood vessel formation." *Nature* (2000). 407(6801):242-248. © 2000.



On the opposite spectrum to embryonic development, adult angiogenesis and inflammation are closely related processes that occur in the body. Following the hemostatic response to tissue injury or trauma, inflammation signals for the initiation of processes to return tissues to their

original state (Figure 3-1A). In order to facilitate this, microarchitecture must be restored by the vasculature (4, 14, 15). As major players in wound healing and inflammation (in the recruitment of immune cells), recent studies have shed light on the role that chemokines can also take on in angiogenesis (5, 19, 22, 30).

3.1.2. Inflammatory chemokines can influence outcomes of angiogenesis

Chemokine molecular weight can range between approximately 8 to 12 kDa (22, 26). There is a large amount of conserved structure between the different chemokines, where charge, or a very few number of key amino acid placement confer their different behavior. Chemokine receptors have a conserved structure among the different classes with their specificity localized to the extracellular carboxyl terminus (30, 39, 41). There are 4 classes of chemokines; the two largest are CC which possess a double cysteine motif, and the other is CXC, which have two cysteines separated by an amino acid (30)., CXC family chemokines tend to have a larger role in angiogenesis, in both promotion and inhibition of capillary vessel sprouting. Angiogenic and angiostatic abilities of CXC chemokines are conferred by the presence or absence of a three sequence peptide motif of Glu-Leu-Arg (ELR) preceding the first cysteine residue respectively (3, 5, 30, 39).

The majority of the ELR- chemokines with angiostatic activity bind the GPCR CXCR3. The chemokines include platelet factor-4 (PF-4/CXCL4), Mig (CXCL9), interferon- γ inducible protein 10 (IP-10/CXCL10), and I-TAC (CXCL11). These chemokines, such as IP-10, have been shown to have strong angiostatic effects, to the point of preventing endothelial cord assembly of HDMVEC cultured on Matrigel (6, 7). A spliced variant of the CXCR3 receptor is also expressed on endothelial cells. It is speculated to be responsible for the angiostatic behavior and signaling facilitated by PF-4 (21). PF-4 is one of the first chemokines released in response to tissue injury, and can be found in concentrations up to 25 μ M in wound sites (2). Primarily synthesized by megakaryocytes and platelets, PF-4 can be found in plasma levels at roughly 2-10 ng/mL and is ubiquitous in the body (35). Imbalances in PF-4 concentrations can be correlated with many disorders and diseases not just limited to chronic wound and inflammation (43). A spliced variant of PF-4, CXCL4L1, is a more potent angiostatic factor, although does not play a role in inflammation as it does not recruit monocyte or lymphocytes. CXCL4L1 can also

influence similar angiogenesis pathways as it has a near identical structure as PF-4 (19, 37, 42, 43).

Data are scarce for signaling dynamics of PF-4 in endothelial cells; a great deal exist for the immune cell counterparts, but only a few studies have published on PF-4 signaling mechanisms. One of the few studies have found that PF-4 inhibits angiogenesis by activation of P38 MAPK through CXCR3-B/CXCR3 (28) . PF-4 can also inhibit angiogenic signaling cascades by directly interfering with the VEGF signaling pathway rather than through its own receptor CXCR3/CXCR3B, either through antagonistic binding of VEGFR2, sequestration of heparan sulfate, or binding to the heparin-binding domains of VEGF ligands (2, 38, 40).

3.1.3. Chapter overview

A great deal of research involved in understanding angiogenesis for tissue regeneration or engineering tissues have focused primarily on positive, pro-angiogenic growth factor rich environments such as VEGF, angiopoietins, ephrins, and FGFs (8). However, physiologically this never exists without the presence angiostatic molecules. In the adult vascular system, we hypothesize that both pro-angiogenic (e.g. VEGF) and anti-angiogenic (e.g. PF-4) cues are required in concert to help coordinate stable blood vessel growth in an inflammatory environment.

Our hypothesis would be evaluated in a more physiologically relevant microfluidic system (Figure 3-2). Although there are clear benefits to the high throughput microfluidic device, obstacles were encountered in attempts to further assess intracellular mechanisms. Due to the size of the microfluidic device, it is quite difficult to obtain large samples of cellular lysate for use in phosphoproteomic analyses (9, 18). There is a need to step down some of the need for complete physiological relevance and use methods that can provide vital information about the system, such as the use of collagen gels instead of tissue culture polystyrene. Despite a lack of shear stress and other signals, cell cultures on and in collagen gels are considered more physiologically relevant than cultures on tissue culture plastic (1). However, the extraction of cells from these systems for high throughput intracellular measurements is more difficult to

execute (20, 45). The focus of this work will be to collect signaling data that can be streamlined with experimental work performed in parallel with the angiogenesis microfluidic system.

The following protocols described were developed in an effort to reduce extracellular matrix contamination and consequent overestimation of total protein in samples. We were successfully able to use a surface lysis technique using detergent based lysis buffer to obtain samples in a manner compatible with mass spectrometry (MS) specifications. We are able to show that phospho-protein signaling data can be collected within a system that utilizes monolayer seeding on a 3D gel with Western blotting, Luminex bead kits, and MS. Our work provides a step forward in applying high throughput phosphoproteomics data collection to more physiologically relevant experimental conditions.

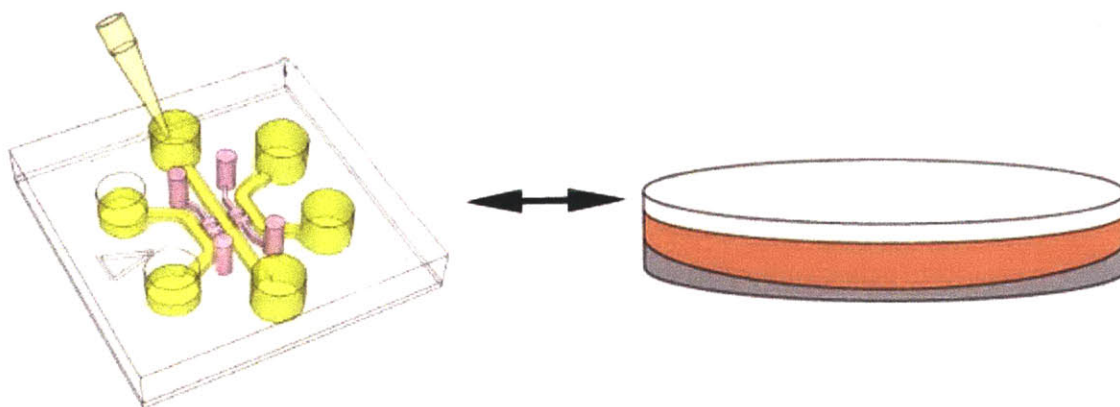


Figure 3-2. Microfluidic device and collagen gel setup (18). Cells were cultured on collagen gels to obtain phosphoprotein signaling data to inform microfluidic device. Protocols were streamlined between the two collaborating labs in order to minimize differences in experimental setup. Computational models would use input from collagen gel lysates to infer intracellular behavior of HDMVEC within the microfluidic device. Adapted with permission from Jeong GS, Han S, Shin Y, Kwon GH, Kamm RD, Lee SH, Chung S. “Sprouting angiogenesis under a chemical gradient regulated by interaction with endothelial monolayer in microfluidic platform.” *Anal Chem* (2011). *In press*. © 2011 American Chemical Society.

3.2 EXPERIMENTAL PROCEDURES

3.2.1. Cell culture

Adult human dermal microvascular endothelial cells (HDMVEC) were commercially purchased at passage 4 (Lonza, Allendale, NJ). Cells were cultured in EGM-2MV (Lonza) media until near

confluency. Once near confluency, cells were rinsed with 1X PBS (Invitrogen, Carlsbad, CA) and detached by incubating with 0.05% Trypsin-EDTA (Invitrogen) for 3-5 minutes at 37°C and 5% CO₂. Once cells were detached, they were neutralized with EBM-2 (Lonza) with 5% FBS (Thermo Fisher Scientific/Hyclone, Logan, UT) and 50 µg/mL gentamicin (Sigma-Aldrich, St. Louis, MO) and spun down at 1600 rpm (~450 g) for 5 minutes. Cells were resuspended in EGM-2MV and seeded on 50 µg/mL rat tail collagen I (BD Biosciences, Bedford, MA) coated tissue culture flasks at a minimum of 5,000 cells/cm². Medium was changed 24 hours following seeding. After initial media change, EGM-2MV was replaced for cells once every 48 hours until nearing confluency. Cells were expanded to passages 6 and 7 and frozen for cryogenic storage at -196°C in 80% EGM-2MV, 10% FBS, and 10% DMSO (Sigma-Aldrich). Ligands used on HDMVEC included VEGF, I-TAC (CXCL11), monokine induced by interferon-γ (Mig/CXCL9), interferon-γ inducible protein 10 (IP-10/CXCL10), and platelet factor 4 (PF-4/CXCL4) (Peprotech, Rocky Hill, NJ).

3.2.2. Three-dimensional collagen gel sprouting system

Collagen gels were used as part of the system to study capillary sprouting. Collagen gel solutions were made using 10X PBS (10%), rat tail collagen I solution stock, and 1N NaOH (Sigma-Aldrich) added at 2.3% of the collagen stock solution volume used. 1 mL of collagen gel solution (pH 7.4) was added to each well in 6 well plates (9.6 cm² per well). MilliQ purified water was added to reach the desired total volume / dilution and kept on ice until use. Gels were formed at a density of 2.0 mg/mL, and allowed to set at 37 °C for 2 hours before being rinsed with 1X PBS. Gels were then preconditioned with EBM-2 + 5% FBS over the course of two days to minimize background changes and nonspecific ligand binding when dosing conditions were introduced to cells seeded on the gels.

HDMVEC were thawed and grown on 50 µg/mL collagen I coated tissue culture flasks up to passage 9. Cells were trypsinized with 0.05% Trypsin-EDTA for 5 minutes before being neutralized with EBM-2 + 5% FBS and gentamicin. Cells were spun down at 1600 rpm for 5 minutes before being resuspended in EGM-2MV. Cells were counted using Neubauer-improved disposable C-Chip hemocytometers (INCYTO, Seoul, Korea) and subsequently seeded onto collagen gels at 50,000 cells/cm². Cells were allowed to adhere for 4-6 hours at 37°C in 5% CO₂

prior to rinsing with PBS and replacing the media with EBM-02 + 5% FBS. HDMVEC were allowed to incubate overnight. Following 24 hours after seeding, plates of HDMVEC were dosed with or without 500 ng/mL PF-4 and/or 20 ng/mL VEGF across for designated time intervals. For optimization protocols, 15 and 30 min dosing time points with treatments of 20 ng/mL VEGF and 20 ng/mL VEGF with PF-4 were used for collecting lysates for MS and Luminex xMAP bead kits.

3.2.3. Cell Lysis Protocols Established for Mass Spectrometry Preparation

3.2.3.1. Direct Urea Lysis

Plates were placed on ice and rinsed with chilled PBS. 3 mL of 8M urea buffer with 1 mM activated sodium orthovanadate (Sigma-Aldrich) were added to each well to achieve a minimum concentration of 6M. The solutions were mixed vigorously with cell scrapers in order to ensure complete denaturation of HDMVEC and collagen. Samples from each plate were consolidated and spun down using a high speed centrifuge at 25,000 g for 3 minutes. Centrifugation generated a faint line towards the bottom of the tubes; supernatant from above the line was collected and snap frozen in liquid nitrogen before placing into storage at -80°C.

3.2.3.2. Urea Surface Lysis

Following rinsing with chilled PBS, sample plates were immediate snap frozen by pouring liquid nitrogen directly onto the gels. Once the collagen gels had solidified, 1 mL of 8M urea buffer were added to each well. Cell scrapers were used to remove the top layer of HDMVEC on the frozen collagen gel before the lysate was pooled and collected.

3.2.3.3. Sample harvesting with collagenase cocktails followed by urea lysis

HDMVEC were detached from collagen gels using a slightly modified version of previously established protocols (11). Prior to Liberase TM harvesting, gels were rinsed with 1X PBS to wash off potentially dead, floating cells. 500 μ L of Liberase TM (at 100 μ g/mL) were added to each well of samples in a 6 well plate before returning to the incubator. Samples were incubated for 3-5 minutes at 37°C before the gel and cells were gently broken and mixed using a cell scraper. The suspension was consolidated from all the wells into a pre-chilled 15 mL Falcon tube

and spun at 1600 rpm (~450 g) at 4°C for 5 minutes. Once the spin was completed, samples were placed back on ice. The supernatant was then aspirated, making sure the pellet remained undisturbed. 8M urea was added to the pellet. To help facilitate lysis, the tube was vortexed to help dissipate the pellet. Once samples were completely processed, the lysates were stored at -80°C prior to chemical modification and digestion.

A second protocol involving Liberase TM treatment uses modified steps in the protocol to obtain cells without harvesting the collagen gel. Following the PBS rinse, 500 µL of Liberase TM (at 100 µg/mL) were added to each well using wide orifice micropipette tips to reduce disruption of the collagen gel. The solution was gently pipetted across the surface of the gel before being placed into the incubator for 3 minutes at 37°C. Following 3 minutes of incubation, the Liberase solution in each well was gently pipetted across the surface of the gel with wide orifice tips to help facilitate detachment without compromising collagen gel integrity. The plate is tapped against the hand to help facilitate additional detachment before returned to the incubator for another minute. The liquid from the top of the gels are collected from the six well plate and consolidated into a 15 mL Falcon tube and spun at 1600 rpm at 4°C for 5 minutes. The supernatant was aspirated and the pellet was resuspended in 8M urea. Again, the pellets were vortexed until they were completely dissolved into the buffer prior to storage at -80°C.

3.2.3.4. Detergent Surface Lysis with Subsequent Urea Lysis

Detergent based lysis buffer was made following previously established protocols(33). Slight modifications were made to the base protocol in order to maintain compatibility with MS lysate preparation protocols. Cell lysis buffer consisted of 1% Triton X-100, 50mM β-glycerophosphate, 10 mM sodium pyrophosphate, 30 mM sodium fluoride (Sigma-Aldrich), 50 mM Tris (Roche Applied Science), 150 mM sodium chloride, 2 mM EGTA, 1% Protease Inhibitor Cocktail (Sigma-Aldrich) and 1% Phosphatase Inhibitor Cocktail Sets I and II (EMD Calbiochem, Gibbstown, NJ).

Following rinse with PBS on ice, 200 µL of cold lysis buffer was gently added to the top of each gel. Plates were then quickly transferred to a Model 1000 standard orbital shaker (VWR International) set at approximately 185 rpm for 15 minutes at 4°C. Following lysis, lysate from

the 6 well plate was consolidated into one biological sample replicate at approximately 1.2 mL volume and mixed with 3.6 mL of 8M urea to achieve a final concentration of 6M urea. Samples were then immediately snap frozen in liquid nitrogen before placing into storage at -80°C. To reduce potential detergent concentration and prevent iTRAQ ligand depletion, detergent absorbent microsphere Bio-Beads (Bio-Rad, Hercules, CA) could be used following 8M urea addition. Pooled samples were combined with absorbent beads (minimum 50 mg/mL final concentration) were returned to the shaker and vigorously nutated for about 5 minutes (up to 2 hours) to allow detergent penetration into the microspheres. Samples were then passed through 0.2 µm pore-sized syringe filters (Pall, Ann Arbor, MI) and subsequently flash frozen and stored at -80°C.

3.2.4. Total protein determination assay

Total protein assay was executed several times during different stages of sample preparation. The bicinchoninic acid (BCA) kits (Thermo Fisher Scientific/Pierce, Rockford, IL) were used following manufacturer's instructions. Samples directly following detergent lysis and/or urea lysis were collected at approximately 50-75 µL aliquots and frozen at -20°C until running the assay. Aliquots were also collected after chemical processing for MS. Sample dilutions for the kit were run at 1:5, 1:10, 1:20 and 1:50, well below maximum compatibility concentrations described per manufacturer instructions. Absorbance measurements were read using Spectramax M2e plate reader (MDS Analytical Technologies, Sunnyvale, CA) set at 562 nm.

3.2.5. Western Blotting

Signaling in HDMVEC seeded on collagen gels were assessed by dosing with around 1-10 µM doses, concentrations at least 2 orders of magnitude above those used in previously reported literature (29), and comparable to experiments performed to assess endothelial cord disassembly (6, 7). Samples were lysed using the detergent-based lysis buffer described above for MS sample preparation. In addition to the components listed above, 1 mM DTT and 1 mM PMSF were included to prevent phosphatase activity and protein degradation (33). 6 well plates were placed on ice and rinsed with cold PBS prior to the addition of 200 µL of lysis buffer to each well. Cell scrapers were used to break up the collagen gel and facilitate lysis of cells. Samples were collected and spun down in an ultracentrifuge at 14,000 rpm (~16,000 g) for 12-15 minutes until

debris was pelleted from the supernatant. The supernatant was collected into eppendorf tubes at approximately 1.2 mL each and stored at -80°C while the pellet was discarded. The NuPage Novex System (Invitrogen) was used to run the gel electrophoresis. Lysates were loaded with 6X reducing buffer (Boston BioProducts, Worcester, MA) in 4%-12% Bis-Tris gels (Invitrogen) and transferred to polyvinylidene fluoride membranes (Bio-Rad, Hercules, CA). Membranes were blocked with 5% BSA in PBS-T and incubated with antibodies for β -actin (1:5000), α/β tubulin (1:5000), phospho-ERK1/2 (1:5000), ERK1/2 (1:5000), phospho-Akt (1:1000), Akt (1:5000), phospho-P38 (1:1000), P38 (1:1000), catalytic phospho-PKA-C α , and catalytic PKA-C α (Cell Signaling Technology, Beverly, MA) overnight at 4 °C. Membranes washed and then incubated for 1 hour with horseradish peroxidase conjugated anti-mouse and/or anti-rabbit antibodies (Amersham/GE Healthcare Biosciences, Pittsburgh, PA) at 1:10,000 dilution in PBS-T with 5% blotting grade nonfat dry milk (Bio-Rad). Membranes were subsequently visualized using chemiluminescent ECL kits (Amersham/GE Healthcare Biosciences) on a Kodak Image Station (Perkin Elmer, Waltham, MA).

3.2.6. Phosphotyrosine mass spectrometry

After frozen lysates were thawed, sample processing followed protocols for chemical reduction, alkylation, trypsin digestion, and fractionation as previously described (36, 47). Samples were labeled with either four or eight isotopic iTRAQ reagents (Applied Biosystems, Carlsbad, CA) for 1 or 2 hours at room temperature respectively. Samples were then combined and concentrated before immunoprecipitated with a mixture of anti-phosphotyrosine antibodies (4G10 (Millipore, Billerica, MA), pTyr100 (Cell Signaling), and PT-66 (Sigma)) immobilized onto protein G agarose beads (Calbiochem) in iTRAQ IP buffer (100 mM Tris, 100 mM NaCl, 1% NP-40, pH 7.4) overnight at 4°C. Enrichment of phosphotyrosine peptides, analysis, and quantification were conducted on an LTQ-Orbitrap vs ESI LC/MS/MS (Thermo Fisher Scientific/Scherf Praezision Europa GmbH, Meiningen-Dreissigacker, Germany). Raw files were processed with MSQuant software and DTASupercharge (23) before phosphopeptides were identified using Mascot analysis software (Matrix Science, Boston, MA). Spectra were manually validated(24). Phosphopeptide scores and signals were thresholded for significant hits and values were normalized to a master lysate or control before normalized to total protein values obtained from the supernatant. See Appendix C for more details on MS protocol.

3.2.7. Luminex xMAP bead based signaling assays

Various xMAP bead kits were used to assess phospho-protein signaling pathways, following previously established protocols (10). Pan phospho-VEGFR2, total VEGFR2 (Novagen/EMD Calbiochem), phospho-ERK1/2 (Thr²⁰²/Tyr²⁰⁴, Thr¹⁸⁵/Tyr¹⁸⁷), phospho-Akt (Ser⁴⁷³), phospho-P38 (Thr¹⁸⁰/Tyr¹⁸²), phospho-JNK (Thr¹⁸³/Tyr¹⁸⁵), phospho-Hsp27 (Ser⁷⁸), phospho-Src (Tyr⁴¹⁶), phospho-GSK3 α/β (Ser²¹/Ser⁹), phospho-P70S6K (Thr⁴²¹/Ser⁴²⁴) (Bio-Rad), β -actin (Procarta/Affymetrix, Santa Clara, CA), GAPDH, phospho-ERK1/2 (Thr¹⁸⁵/Tyr¹⁸⁷), phospho-Akt (Ser⁴⁷³), phospho-Hsp27 (Ser⁷⁸), and phospho-P70S6K (Thr⁴¹²) (Millipore) were assessed and optimized for characterization of the HDMVEC sprout system. HDMVEC lysis was performed using respective lysis buffer kits from each of the vendors using complete gel harvesting or surface lysis protocols outlined above. For phospho-VEGFR2 and total VEGFR2, the Novagen widescreen reagent kit was used for quantifying protein abundance (Appendix G). Millipore kits were developed using the Millipore detection reagent kit, while all Bio-plex kits obtained from Bio-Rad were quantified using the phospho-protein detection reagent kit. The β -actin kit from Procarta/Affymetrix provided the lysis and detection reagents with the beads. Following quantification with kits, all samples were analyzed on the Bio-plex 200 platform (Bio-Rad). For optimization of loading curves, 50 ng/mL VEGF and 20 ng/mL VEGF + 500 ng/mL PF-4 were used along with the control (no treatment) conditions to test the potential signaling landscape used by HDMVEC within the system. For a broad coverage of potentially interesting signaling pathways, 1 μ M NaCl was added as a condition to induce stress response pathways P38 and JNK in the case where PF-4 did not (27). HDMVEC were dosed with respective conditions for 15 minutes prior to their lysis using the detergent surface lysis technique. Samples were then immediately frozen in liquid nitrogen and placed into -80°C storage until Luminex assays were performed.

3.3 RESULTS

3.3.1. Protein signaling dynamics from HDMVEC on collagen gels are observably different using Western blotting

The system was first initially surveyed to determine whether HDMVECs would truly respond to angiostatic cues. Of particular interest were the CXCR3 family ligands, as they were chemokines

with angiostatic properties. All CXCR3 family ligands that were examined demonstrated a decrease in phospho-ERK activity following dosing with 50 nM of chemokine for 30 minutes (Figure 3-3A), including I-TAC/CXCL11 (data not shown). We observed the sharpest decrease in phospho-ERK intensity from PF-4 treatment and went forward to evaluate the system for phosphorylation data collection. The angiostatic properties of CXCR3 ligand IP-10 has been previously reported to be mediated by μ -calpain (6). We examined Protein Kinase A (PKA) catalytic subunit phosphorylation as a negative regulator of calpain (Figure 3-3B) and did not see any noticeable differences, which agree with previous research on PKA and IP-10 signaling (32). However, we did not notice a change in PKA catalytic subunit phosphorylation in the presence of VEGF, nor with the presence of heparin, a proteoglycan known for facilitating binding kinetics of VEGF and PF-4 with cell surface receptors (2, 13, 25).

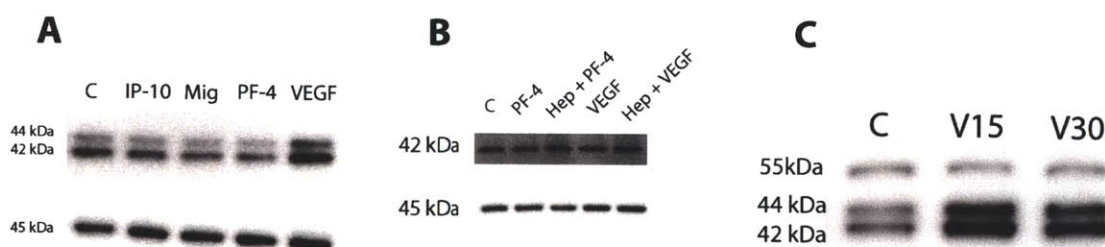


Figure 3-3. Initial Western blots on signaling activity in HDMVEC at early time points. 12 hour serum starved HDMVEC on tissue culture plastic were evaluated for phospho-ERK1/2 signaling with different CXCR3 ligands at 50 nM (435 ng/mL IP-10, 585 ng/mL Mig, 390 ng/mL PF-4 respectively) or VEGF at 50 ng/mL for 30 minutes (A). Phospho-ERK1/2 activity decreases more with PF-4 compared to other CXCR3 family ligands on tissue culture plastic. The phosphorylation of Protein Kinase A catalytic subunits do not significantly change when 500 ng/mL PF-4 or 50 ng/mL VEGF are added to cultures with complete medium for 30 minutes on tissue culture plastic (B). The presence of heparin (Hep), which has been reported to help facilitate PF-4 and VEGF binding to the cells, did not significantly alter PKA catalytic activity either. Examination of surface lysing technique upon phospho-ERK1/2 detection via Western blot (C). Surface lysed HDMVEC on collagen gels were tested for phospho-ERK detection via Western blotting in EBM + 5% FBS. Samples were dosed with 20 ng/mL VEGF for 15 (V15) or 30 (V30) minutes before undergoing lysing protocol. Western results indicate that surface lysis can successfully obtain cellular protein while reducing collagen contribution. β -actin (45 kDa) and α / β -tubulin were (55 kDa) were run as standards for A,B and C respectively.

Western blots were also used as an initial assay to confirm that signaling dynamics could still be captured when the cell culture was moved onto collagen gels, particularly the detergent surface

lysis technique, as the majority of MS sample processing would use these lysates (Figure 3-3C). We were able to still detect the presence of phospho-ERK1/2 after HDMVEC stimulation on collagen gels for 15 and 30 minutes in base medium with 5% FBS. Furthermore, we were still able to discern a noticeable difference in band intensity between VEGF stimulation and control, where no additional factors were added on top of the FBS.

3.3.2. Collagen contribution is reduced when using surface detergent lysis method

Method (<i>n</i> samples)	% Collagen Contribution
Urea Lysis (<i>n</i> =6)	124.1* ± 29.1%
Urea Lysis + Spin (<i>n</i> =6)	95.4 ± 7.3%
Urea Lysis + Freeze/Thaw + Spin (<i>n</i> =6)	100.4* ± 10.6%
Liberase Detachment + Urea Lysis (<i>n</i> =4)	88.8 ± 19.7%
Detergent Surface Lysis + Urea Lysis (<i>n</i> =4)	74.9 ± 4.0%

Table 3-1. Percentage of collagen contribution to cell lysates collected using different methods (select methods and representative values shown). Total BCA values were calculated for samples collected using each method and compared between two conditions – empty collagen gels or collagen gels with cells seeded (50,000 cells/cm²). Methods represented above for sample processing were either: 1) directly lysed with urea; 2) lysed with urea followed by an ultracentrifuge spin (25,000 g for 3 minutes); 3) Snap frozen and thawed prior to ultracentrifuge spin; 4) cells detached with liberase and lysed with urea; or 5) detergent surface lysis on an orbital shaker before lysing with urea. Percentages show the amount of collagen present in the lysate when normalized to the empty collagen gel from that comparison. * Indicates that empty gel lysates had higher total protein reading output from the BCA than lysis performed on gels with cells, which would account for a >100% output.

Direct urea lysis with inclusion of collagen gels ran consistently high in BCA assays for total protein (Table 3-1). Following normalization of samples with respect to blank collagen gels, cellular contribution to protein values were negligible or not significantly different, and in some cases were higher due to variability of collagen contribution to samples. To reduce collagen gel protein values, samples were spun down using an ultracentrifuge at a high speed of 25,000 g. A decrease in the amount of collagen contribution was observed, although significant amounts of collagen still persisted in the samples. Other attempts to help assist breakdown and removal of collagen gel from urea-lysed samples included a snap freeze and immediate thaw prior to ultracentrifuge spin. The thaw step did not provide a decrease in collagen contribution in BCA readings. To optimize lysate to collagen contribution in the lysates, Liberase TM collagenase cocktail was effective for detaching cells in the first set of samples run (Figure 3-4). However,

after time being kept at 37°C, Liberase became progressively less effective at detaching HDMVEC from the collagen gel (Figure 3-4C). Despite vigorous pipetting and tapping force applied to the plate, cells would not detach to the same extent within 5 minutes of Liberase treatment. Collagen contribution to total protein was decreased by roughly 10% further with Liberase detachment compared to strict urea lysis (Table 3-1). Use of detergent adsorbent beads was deemed an unnecessary step and discontinued (data not shown).

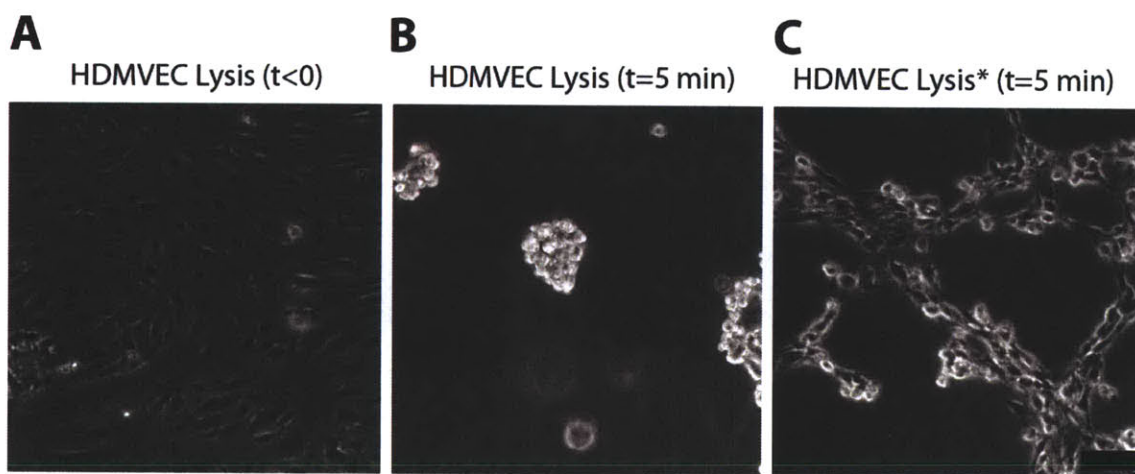


Figure 3-4. Liberase TM harvesting and cell detachment protocol to reduce collagen contamination. HDMVEC cultured on collagen gels (A) were treated with 500 μ L of 100 μ g/mL Liberase TM in order to detach the cells. With freshly prepared Liberase TM solution, HDMVEC were easily detached from the collagen gel within 5 minutes of treatment (B). Liberase needed to be used as soon as possible, as the solution lost efficacy about 15 minutes after being initially prepared (C) and cells were not efficiently detached from the collagen gel surface. Scale bar = 100 μ m.

Detergent lysis of HDMVEC gels on their surface gave a reduced collagen contribution to the lysates (Table 3-1), the lowest amount of contamination achieved with the different protocols that were applied. We were able to consistently have a yield of approximately 25-30% cellular protein contribution to the lysate collected. Surface lysing technique left what appeared to be small, dark nuclear bodies on the surface of the gels after lysate was collected (Figure 3-5). We speculate that these nuclear bodies are remnants of nuclei or potentially structural proteins that were left due to the high salt concentration in the lysis buffer. HDMVEC samples used for phosphoproteomic data analysis from here on were generated using the surface lysis technique.

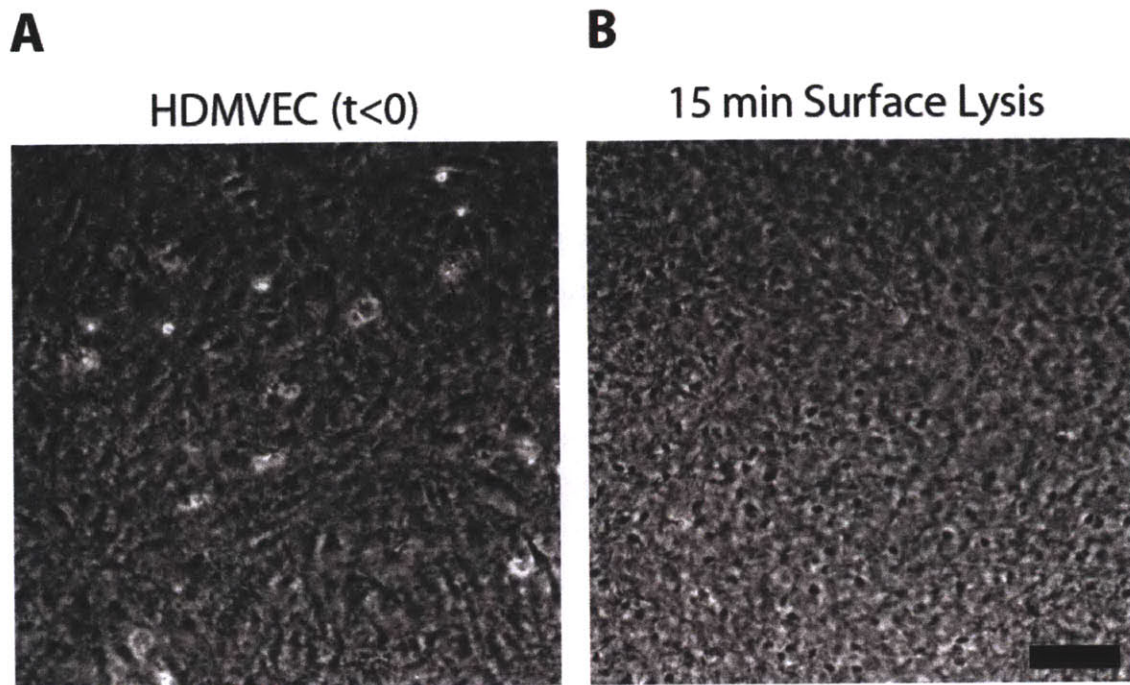


Figure 3-5. Surface lysis of HDMVEC seeded on collagen gels. Following 24 hours after seeding, confluent monolayers of HDMVEC (A) underwent 15 minute incubation with detergent based lysis buffer (B). Imaging of post surface lysis protocol indicate that the majority of cells were successfully lysed, with remnants of cell bodies and nuclei as dark bodies. Scale bar = 100 μ m.

3.3.3. Mass spectrometry detection of phosphorylation sites increases following reduction of collagen contribution to cell lysates

Initial MS attempts on samples dosed with VEGF and PF-4 yielded low phosphoproteomic data when collected with direct urea lysis protocols due to the high abundance of collagen in the samples (Table 3-2). Following surface lysis protocol, we observed a significant increase in number of phosphosites identified through MASCOT. Using very stringent threshold parameters, we were able to find enough phosphosites that covered 36 different proteins with quantifiable values across different dosing conditions. There appeared to only be a partial overlap of proteins between the two protocols; the loss of proteins observed by surface lysis samples may be inherent in error and variation from day to day use of the LTQ-Orbitrap, as well as the abundance of other proteins saturating out signals from those originally observed now that collagen gel contribution is reduced.

Protein	Direct Urea Lysis*	Surface Lysis*
Albumin precursor	-	pY162
ATPase, class I, type 8B, member 1	-	pY1217
BMP-2 inducible kinase isoform b	pS649	-
BCAR1	pY410	pY249; pY410
Caveolin 1	-	pY14
Coiled-coil domain containing 123	-	pY157
Collagen, type XX, α 1	pT398	
Connexin 43 (Gap Junction α 1)	-	pY313
Cortactin isoform a	pS447	pS380
Dachsous 1 precursor	pS2884	-
DYRK1B isoform a	-	pY273
EphA2 receptor	-	pY575; pY772
EphB1 receptor precursor	-	pT429/pS435
ErbB2 interacting protein isoform 2	-	pY1107
EBP41L2	-	pY263
FGD5	-	pY563; pY820
GSK3 β	pS215; pY216	pS215; pY216
Microtubule-associated protein 1B	-	pY1062
ERK2 (MAPK1)	-	pT185; pY187; pT185/pY187
P38 α (MAPK14 isoform 1)	-	pY182
ERK1 (MAPK3 isoform 2)	-	pT202; pY204; pT202/pY204
Myelin protein zero-like 1 isoform a	pY263	pY263
Paxillin	-	pY118
PI3K p85 β (regulatory subunit 2)	-	pY464
PLC γ 1 isoform b	pY771	-
PECAM-1/CD31	pY713	pY713
Polymerase I and transcript release factor	-	pY308
Pragmin	-	pY411
PTPN11/SHP2	pT59	-
Fyn isoform a	pY420; pT421	pY420; pT421
PTK2 isoform a/FAK1	pT575; pY576	pY576
SATB homeobox 2	pS5/pS7	-
Serine/threonine-protein kinase PRP4K	pT847	pY849
SH2 domain containing 3C isoform 1	-	pS492
SHC transforming protein 1 isoform p52Shc	pS180; pY181	pY181
Solute carrier family 15, member 3	-	pY177
Src homology 2 domain containing adaptor protein B	-	pY423
Talin 1	-	pY26
TYK2	-	pY292
Vinculin isoform VCL	-	pY822
Wiskott-Aldrich syndrome gene-like protein	-	pY256
Lyn isoform A	-	pY397; pT398

Table 3-2. Significant targets identified by phospho-tyrosine enriched mass spectrometry increases with surface lysis technique. HDMVEC were dosed with 20 ng/mL VEGF with and without the addition of 500 ng/mL PF-4 at either 15 or 30 minutes of treatment. MS runs were performed on HDMVEC and gels directly lysed with urea (using 4-plex iTRAQ) versus gels which were surface lysed first (using 8-plex iTRAQ). Samples were consolidated after labeling with iTRAQ reporter group. Reported samples values were identified by MASCOT and thresholded above background noise signal before normalization to their supernatant values. Only phosphosite peptide scores above 20 were considered true significant hits with quantifiable values. The different phosphosites that were identified from direct urea lysis covered 15 unique proteins while using direct surface lysis increased coverage to 36 unique proteins, with an overlap of 9 proteins across all signaling and time conditions used. Coverage changes between MS runs vary slightly and explain the differences observed between the two lysis techniques. *Notes that different iTRAQ labeling procedures can affect phosphosite detection; however, surface lysing provides a greater number of initial sites by MASCOT and overall significant proteins that have quantifiable values.

3.3.4. Luminex normalization and subsequent time course analysis reveal difficulty in phosphoproteomic data from typical analytic procedures.

Samples for optimizing Luminex bead kits were generated from the treatment conditions being considered along with a stress condition to have maximal coverage at 15 minutes. From the previous expectation of inaccurate protein concentrations, sample loading curves were tested for each xMAP bead kit considered (Figure 3-6). Instead of using inaccurate total protein values obtained from BCA (inflated due to collagen contribution), sample loading curves were based on serial dilutions of the total lysate (from 100% down to 10%). Generally, samples appeared to have maximal signaling across different treatment conditions and control within the 75% and 45% dilutions (25%, 55% lysate loaded respectively) with highest peak signaling trends for phospho-Akt, phospho-Hsp27, and phospho-P70S6K for conditions that included VEGF. Saturating lysate concentrations in phospho-ERK1/2, Akt, and P70S6k experienced a drop in signal past 60% lysate loading (Figure 3-6A,B,C) which was not observed for the other bead kits. No signal was captured for phospho-JNK or phospho-P38 using the HDMVEC cell system and dosing conditions, despite previous literature reports (27, 28) though may be due to short incubation times or insufficient protein concentration.

A different normalization parameter was required for the use of Luminex assays, as the total protein value obtained via BCA for normalizing signaling data was compromised by the presence of collagen. Since there existed such a large discrepancy between samples and empty collagen gels from both comparisons as well as plate-to-plate variation, internal normalization

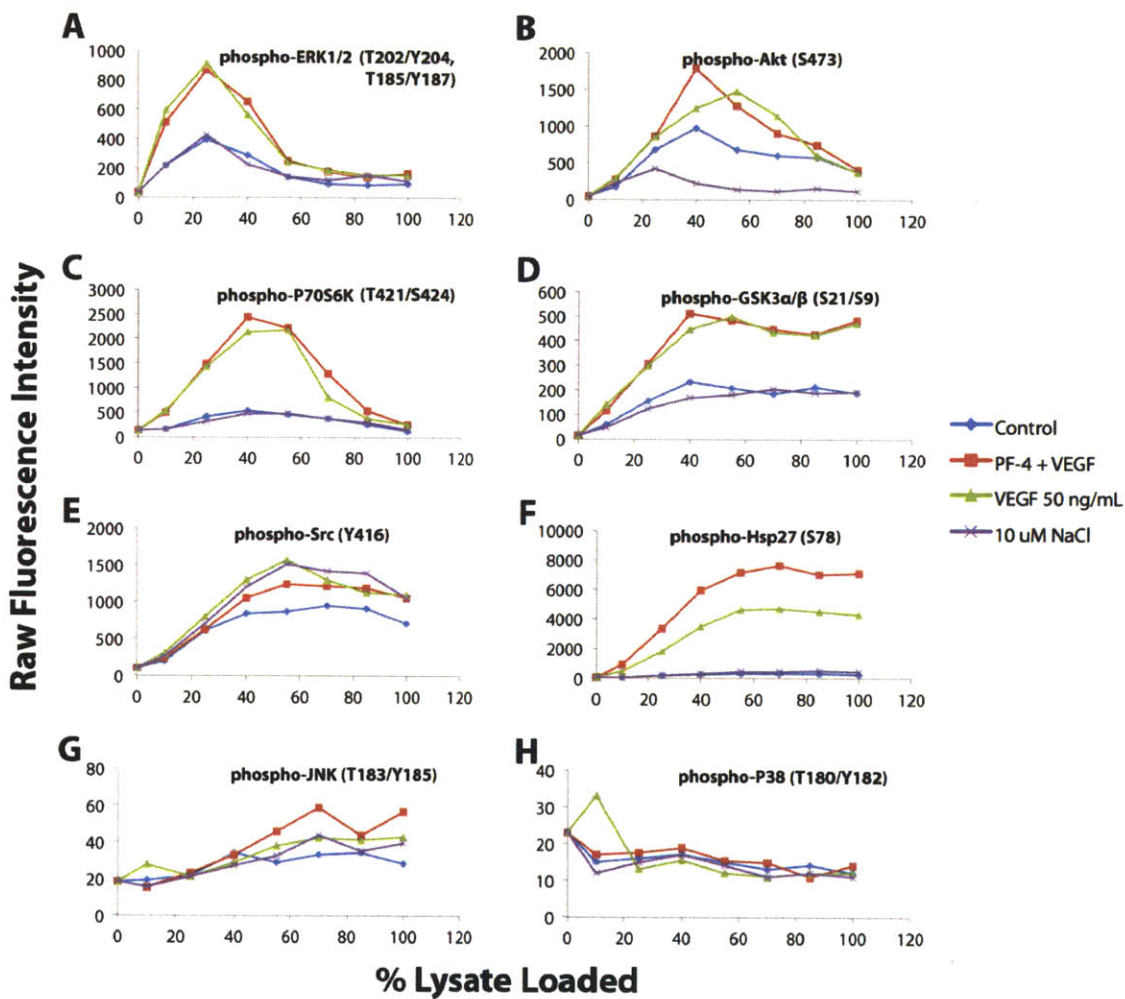


Figure 3-6. Luminex xMAP bead kit optimization curves. Different percentages of lysates were loaded to assess optimal detection by bead kits. Four treatments were used in order to cover a broad range of expected signaling pathways, both expected for the conditions of interest (PF-4 and VEGF), and broad coverage including stress pathways JNK and P38 (27). Samples were collected following 15 minutes after dosing. Phospho-ERK1/2, phospho-Akt, and phospho-P70S6K had optimal signal peaks between 25% and 55% lysate loading (A, B, C). Phospho-GSK3 α/β , phospho-Src, and phospho-Hsp27 had linear ranges for signaling between approximately 25% and 55%, where optimal signals were observed around 40% to 55% (D, E, F). Phospho-JNK and phospho-P38 were not detectable in the sample treatment conditions (G, H). A noticeable occurrence of attenuated fluorescence occurred in Phospho-ERK1/2, phospho-Akt, and phospho-P70S6k loading curves at lysate loading above 70%.

was required beyond that of a master lysate. A housekeeping protein, GAPDH, was also measured in each sample condition for normalization purposes. Sample loading curves were

tested in order to assess the linear range of the GAPDH sample, and whether it could be used at multiple dilutions for the different bead kits and their loading requirements (Figure 3-7). The linear range for the GAPDH kit went from 5% up to 55% lysate loaded, compatible with the ranges for a majority of the proteins examined using Luminex.

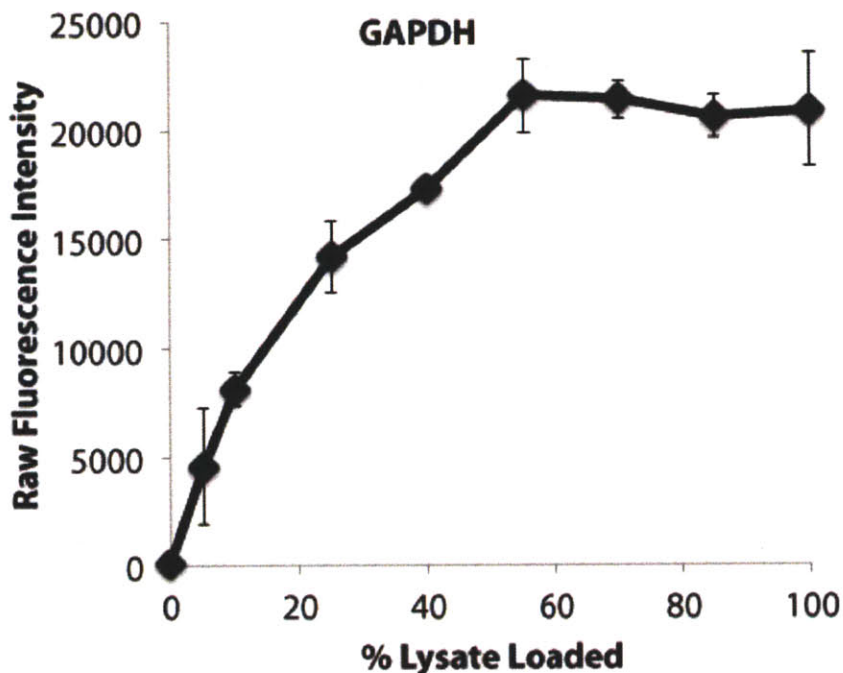


Figure 3-7. GAPDH curves for loading surface lysed samples. Detergent based surface lysates were run using the xMAP Luminex kit from Millipore. Samples were loaded at 100% or diluted down to 5% ($n=6$). Signal intensity for samples loaded saturated at approximately 60% lysate, and linear range was observed for signals between 10% and 55%.

Following optimization of sample loading for both phosphoprotein and GAPDH detection, identical treatment and time courses were collected for 500 ng/mL PF-4, 20 ng/mL VEGF, and 500 ng/mL and 20 ng/mL VEGF using Luminex bead kits (Figure 3-8) as for MS analysis (see Chapter IV for more detail about MS data). Signals were observed at 15 and 30 minutes for phospho-Akt, and P70S6K (Figure 3-8A, B, C). In conditions that were treated with VEGF, a late signaling trend was observed at 48 hours of dosing for phospho-Akt. Almost no signaling

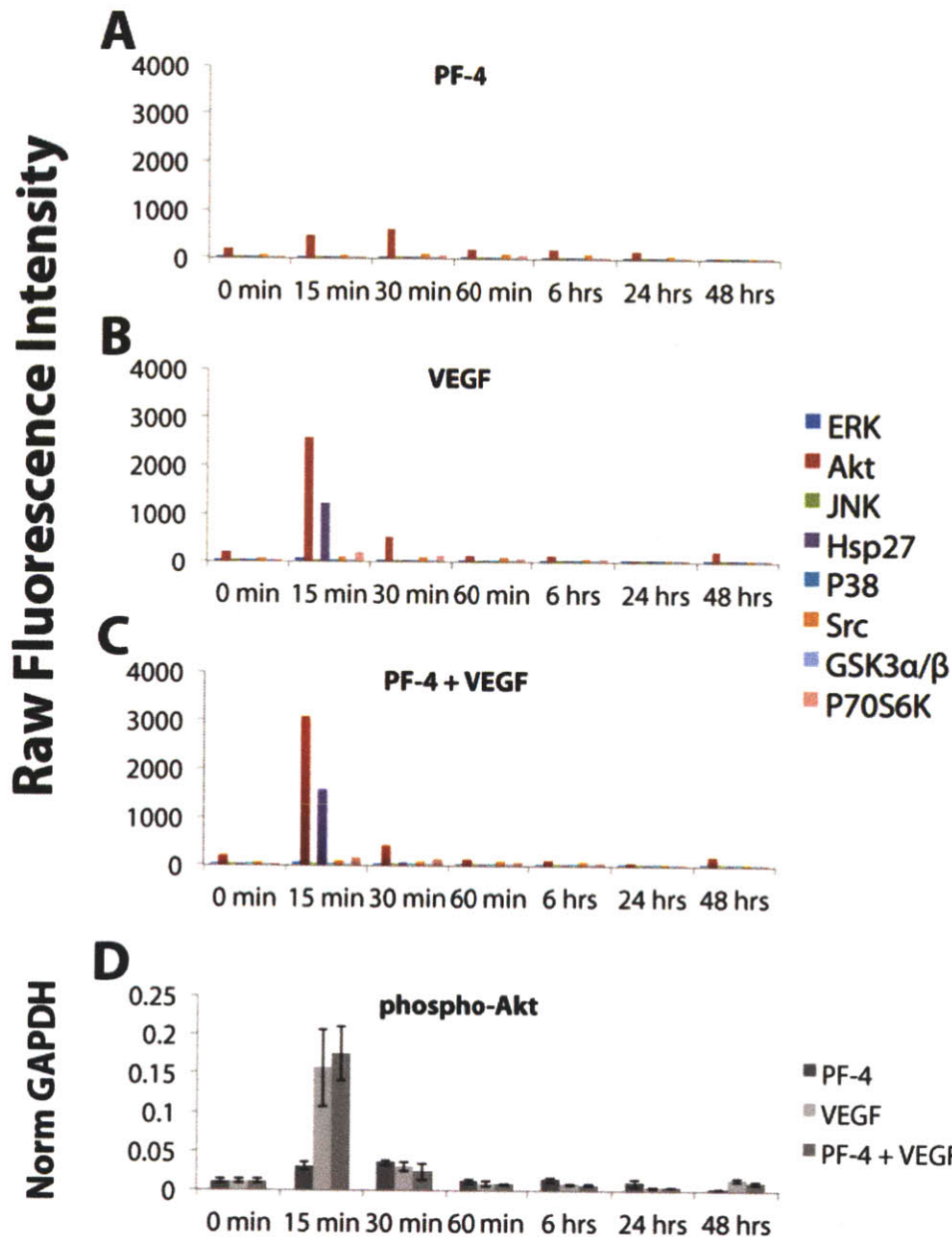


Figure 3-8. Phospho-protein signal is mainly captured at early time points for Luminex xMAP bead kits. Low detection of phosphoprotein activity was observed for all conditions (500 ng/mL PF-4, 20 ng/mL VEGF, 500 ng/mL PF-4 + 20 ng/mL VEGF) after 60 min (A,B,C respectively). Maximal signal detection occurred at around 15-30 min, with Akt, Hsp27, and P70S6K phosphoproteins having significantly higher values. Other phosphoprotein levels for ERK1/2 and Src were only slightly above background; JNK, P38, and GSK3 α/β were consistently below background signal for all time points measured. Initial time point at 0 minutes was control condition. Trends observed among raw fluorescence were conserved following normalization to GAPDH. Representative phospho-Akt time course is shown to indicate phospho-signaling drops off rapidly after 30 minutes, with a small spike in activity towards 48 hours (D).

was detected at any of the other time points. Following GAPDH normalization, most signals were still below background thresholds, and observed signaling trends for proteins such as Akt were conserved (Figure 3-8D). Additional Luminex data regarding phospho-VEGFR2 activity are included in Appendix G.

3.4 DISCUSSION

3.4.1. PF-4 influences endothelial signaling pathways.

Our Western blots indicated that there were discernible differences in signaling following treatment with PF-4. Since not much data exist on PF-4 signaling pathways in endothelial cells, our focus was to try and elucidate the potential signaling crosstalk and landscape of PF-4 and VEGF. We found that CXCR3 binding chemokines could reduce phospho-ERK1/2 levels of HDMVEC seeded on tissue culture plastic, including PF-4 treatment. This agrees with previous work with human umbilical vein endothelial cells that PF-4 can block MAP kinase signaling, albeit the mechanism is uncertain (38). Western blotting of PKA catalytic subunit phosphorylation did not show changes when dosed with PF-4 or VEGF. Previous research has indicated that PKA phosphorylation can inhibit downstream signaling of chemokines and our results do not disagree with previous findings (32). VEGF stimulation does not induce PKA phosphorylation either, as VEGF has not been previously reported to activate the adenylyl cyclase/cyclic AMP signaling pathway. Our initial Western blotting also demonstrated that it was possible to collect signaling data from HDMVEC seeded on collagen gels following VEGF treatment and could move forward with optimizing MS sample lysis methods. We were also able to conclude that PF-4 most likely does not prevent VEGF and VEGFR2 binding to inhibit angiogenesis signaling pathways (Appendix Figure G-1).

3.4.2. Lysate collection from 3D collagen gels is nontrivial

Despite the large data set yields that MS provides, MS requires significantly more sample than other assays such as Western blots or Luminex bead assays. Generally, MS samples are collected from 15 cm² dishes which can provide enough cellular lysate for two technical replicates. Collagen gels formed on 10 or 15 cm² would have very sharp menisci that would affect the overall spreading of collagen on the plastic surface. We observed that sprouting does not occur

on collagen gels less than 0.5 mm thick, as the rigidity of the polystyrene is transferred to the gel and more so than 1 mm thick gels (data not shown). To reduce the potential effect of meniscuses and reduce collagen gel consumption, technical and biological replicates were collected as whole 6 well plates where all the wells were pooled and consolidated into one sample.

Initial attempts at cell lysate preparation for MS analysis involved directly adding 8M urea buffer to the cell cultures on collagen gels. However, this proved inefficient as BCA analysis indicated that more than 95% total contribution of protein came from collagen rather than HDMVECs. To reduce collagen contamination, samples were spun down using a high speed elutriation centrifuge at 25,000 *g* for 3 minutes. Unlike typical detergent lysis protocols where centrifugation of samples allowed the sedimentation of collagen, we observed that the collagen did not separate very easily from the solution when urea was used instead. We speculate that since urea buffer is a very strong denaturing agent, the collagen gels were denatured by the disruption of noncovalent hydrogen bonds and could not be separated from the lysate solution as the proteins had dissolved into the buffer. The collagen contamination in these samples proved to be too high for sufficient phosphoprotein coverage by MS.

Many efforts were invested in methods to reduce collagen contribution to samples being collected by directly harvesting both cells and gels. This included snap freezing and surface scraping gels lysed with urea, along with cell detachments and harvesting prior to urea lysis. However, these attempts also proved to be inefficient. Other methods utilized involved harvesting cells using the base collagenase protocol outlined by Cosgrove et al. using LiberaseTM (11). Despite being able to pellet out collagen gels, the amount of time required to treat with Liberase made its use less than desirable. HDMVECs would be lysed at least 10 minutes after removal of dosing conditions from the samples strictly from Liberase incubation and centrifugation. The amount of time that this process takes could contribute significant background to the samples and skew output measurements, especially for those within the range of early time points (e.g. 15, 30, 60 minutes), as the delay could range anywhere from 15% to 67% of desired dosing times. We also noticed that in a short amount of time, LiberaseTM lost its efficacy in detaching cells. Following thawing and preparation of LiberaseTM for use, Liberase was unable to efficiently detach cells from collagen gels as soon as use on the second plate.

The best method that compromised between expense, time, effort, and output that we were able to utilize was the use of a detergent-based lysis buffer for surface lysing. By lysing the surface of the gels, we were able to reduce collagen contribution, since most of the collagen remained behind following the lysis procedure. There were significant number of dark nucleated bodies remaining; we suspect that these may be nuclei or cell bodies that remained following the lysis buffer treatment.

In parallel to MS protocol development for this system, we explored Luminex bead kits as a means to assess signaling pathways complementary to phospho-tyrosine MS. The low phosphoprotein detection in our data reflect the difficulty in obtaining more physiologically relevant data; the use of primary cells on a three-dimensional gel substrate has very low signaling. Most data that are collected on tissue culture plastic are potentially artefactual to strain placed on the cells from a rigid substrate (i.e. strain increases tyrosine phosphorylation and migration behavior of cells) (16, 17). The difficulty in obtaining signaling data is also reflected in the MS outputs. Typical MS data from cell lines cultured on tissue culture plastic yield 100-200 unique proteins, with 200-300 significant phosphosites detected.

We observed most of our signaling to occur at early time points for only some bead kits; proteins such as phospho-JNK, phospho-P38 were not detectable at all, despite previously reported findings about phospho-P38 mediating PF-4 signaling in HDMVEC (28). We suspect that this may primarily be a result of different culturing methods, as we collected lysate from cultures on collagen gels rather than cells seeded on polystyrene. This difference results in a two-fold difference due to protein concentration as well as substrate rigidity. Furthermore, Petrai et al. enriched for P38 MAPK protein with an immunoprecipitation step, which likely enhanced capture of phosphorylated proteins.

3.4.3. Summary

Regardless of which protocol was implemented, it was acknowledged that collagen would be a considerable contributor to the total protein of collected lysates. The final decision made for the sample lysis protocol was made with the conscious effort to minimize collagen contamination

and overall sample volume to help expedite processing as well as making samples physically more manageable.

3.5. REFERENCES

1. **Adair TH, Montani J-P.** Angiogenesis [Online]. Morgan & Claypool Life Sciences. <http://www.ncbi.nlm.nih.gov/books/NBK53242/>.
2. **Aidoudi S, Bikfalvi A.** Interaction of PF4 (CXCL4) with the vasculature: a role in atherosclerosis and angiogenesis. *Thromb. Haemost.* 104: 941–948, 2010.
3. **Balestrieri ML, Balestrieri A, Mancini FP, Napoli C.** Understanding the immunoangiostatic CXC chemokine network. *Cardiovascular Research* 78: 250–256, 2008.
4. **Barrientos S, Stojadinovic O, Golinko MS, Brem H, Tomic-Canic M.** Growth factors and cytokines in wound healing. *Wound Repair Regen* 16: 585–601, 2008.
5. **Bernardini G, Ribatti D, Spinetti G, Morbidelli L, Ziche M, Santoni A, Capogrossi MC, Napolitano M.** Analysis of the role of chemokines in angiogenesis. *J. Immunol. Methods* 273: 83–101, 2003.
6. **Bodnar RJ, Yates CC, Rodgers ME, Du X, Wells A.** IP-10 induces dissociation of newly formed blood vessels. *Journal of Cell Science* 122: 2064–2077, 2009.
7. **Bodnar RJ, Yates CC, Wells A.** IP-10 blocks vascular endothelial growth factor-induced endothelial cell motility and tube formation via inhibition of calpain. *Circulation Research* 98: 617–625, 2006.
8. **Carmeliet P, Jain RK.** Molecular mechanisms and clinical applications of angiogenesis. *Nature* 473: 298–307, 2011.
9. **Chung S, Sudo R, Zervantonakis IK, Rimchala T, Kamm RD.** Surface-treatment-induced three-dimensional capillary morphogenesis in a microfluidic platform. *Adv. Mater. Weinheim* 21: 4863–4867, 2009.
10. **Cosgrove BD, Alexopoulos LG, Hang T-C, Hendriks BS, Sorger PK, Griffith LG, Lauffenburger DA.** Cytokine-associated drug toxicity in human hepatocytes is associated with signaling network dysregulation. *Mol Biosyst* 6: 1195–1206, 2010.

11. **Cosgrove BD, Cheng C, Pritchard JR, Stolz DB, Lauffenburger DA, Griffith LG.** An inducible autocrine cascade regulates rat hepatocyte proliferation and apoptosis responses to tumor necrosis factor- α . *Hepatology* 48: 276–288, 2008.
12. **De Val S, Black BL.** Transcriptional control of endothelial cell development. *Dev. Cell* 16: 180–195, 2009.
13. **Ferrara N, Gerber HP, LeCouter J.** The biology of VEGF and its receptors. *Nat Med* 9: 669–676, 2003.
14. **Fivenson DP, Faria DT, Nickoloff BJ, Poverini PJ, Kunkel S, Burdick M, Strieter RM.** Chemokine and inflammatory cytokine changes during chronic wound healing. *Wound Repair Regen* 5: 310–322, 1997.
15. **Gillitzer R, Goebeler M.** Chemokines in cutaneous wound healing. *J. Leukoc. Biol.* 69: 513–521, 2001.
16. **Harley BAC, Kim H-D, Zaman MH, Yannas IV, Lauffenburger DA, Gibson LJ.** Microarchitecture of three-dimensional scaffolds influences cell migration behavior via junction interactions. *Biophys. J.* 95: 4013–4024, 2008.
17. **Janmey PA, Miller RT.** Mechanisms of mechanical signaling in development and disease. *Journal of Cell Science* 124: 9–18, 2011.
18. **Jeong GS, Han S, Shin Y, Kwon GH, Kamm RD, Lee S-H, Chung S.** Sprouting angiogenesis under a chemical gradient regulated by interaction with endothelial monolayer in microfluidic platform. *Anal. Chem.* (October 10, 2011). doi: 10.1021/ac202170e.
19. **Keeley EC, Mehrad B, Strieter RM.** Chemokines as mediators of neovascularization. *Arteriosclerosis, Thrombosis, and Vascular Biology* 28: 1928–1936, 2008.
20. **Kobayashi T, Liu X, Kim HJ, Kohyama T, Wen F-Q, Abe S, Fang Q, Zhu YK, Spurzem JR, Bitterman P, Rennard SI.** TGF- β 1 and serum both stimulate contraction but differentially affect apoptosis in 3D collagen gels. *Respir. Res.* 6: 141, 2005.
21. **Lasagni L, Francalanci M, Annunziato F, Lazzeri E, Giannini S, Cosmi L, Sagrinati C, Mazzinghi B, Orlando C, Maggi E, Marra F, Romagnani S, Serio M, Romagnani P.** An alternatively spliced variant of CXCR3 mediates the inhibition of endothelial cell growth induced by IP-10, Mig, and I-TAC, and acts as functional receptor for platelet

- factor 4. *J. Exp. Med.* 197: 1537–1549, 2003.
22. **Mehrad B, Keane MP, Strieter RM.** Chemokines as mediators of angiogenesis. *Thromb. Haemost.* 97: 755–762, 2007.
 23. **Mortensen P, Gouw JW, Olsen JV, Ong S-E, Rigbolt KTG, Bunkenborg J, Cox J, Foster LJ, Heck AJR, Blagoev B, Andersen JS, Mann M.** MSQuant, an open source platform for mass spectrometry-based quantitative proteomics. *J. Proteome Res.* 9: 393–403, 2010.
 24. **Nichols AM, White FM.** Manual validation of peptide sequence and sites of tyrosine phosphorylation from MS/MS spectra. *Methods Mol. Biol.* 492: 143–160, 2009.
 25. **Olsson AK, Dimberg A, Kreuger J, Claesson-Welsh L.** VEGF receptor signalling - in control of vascular function. *Nat Rev Mol Cell Biol* 7: 359–371, 2006.
 26. **Onuffer JJ, Horuk R.** Chemokines, chemokine receptors and small-molecule antagonists: recent developments. *Trends Pharmacol. Sci.* 23: 459–467, 2002.
 27. **Pearson G, Robinson F, Beers Gibson T, Xu BE, Karandikar M, Berman K, Cobb MH.** Mitogen-activated protein (MAP) kinase pathways: regulation and physiological functions. *Endocr. Rev.* 22: 153–183, 2001.
 28. **Petrai I, Rombouts K, Lasagni L, Annunziato F, Cosmi L, Romanelli RG, Sagrinati C, Mazzinghi B, Pinzani M, Romagnani S, Romagnani P, Marra F.** Activation of p38(MAPK) mediates the angiostatic effect of the chemokine receptor CXCR3-B. *The International Journal of Biochemistry & Cell Biology* 40: 1764–1774, 2008.
 29. **Petrai I, Rombouts K, Lasagni L, Annunziato F, Cosmi L, Romanelli RG, Sagrinati C, Mazzinghi B, Pinzani M, Romagnani S, Romagnani P, Marra F.** Activation of p38(MAPK) mediates the angiostatic effect of the chemokine receptor CXCR3-B. *The International Journal of Biochemistry & Cell Biology* 40: 1764–1774, 2008.
 30. **Rosenkilde MM, Schwartz TW.** The chemokine system -- a major regulator of angiogenesis in health and disease. *APMIS* 112: 481–495, 2004.
 31. **Saharinen P, Eklund L, Miettinen J, Wirkkala R, Anisimov A, Winderlich M, Nottebaum A, Vestweber D, Deutsch U, Koh GY, Olsen BR, Alitalo K.** Angiopoietins assemble distinct Tie2 signalling complexes in endothelial cell-cell and cell-matrix contacts. *Nat Cell Biol* 10: 527–537, 2008.
 32. **Shiraha H, Glading A, Chou J, Jia Z, Wells A.** Activation of m-calpain (calpain II) by

- epidermal growth factor is limited by protein kinase A phosphorylation of m-calpain. *Mol. Cell. Biol.* 22: 2716–2727, 2002.
33. **Shults MD, Janes KA, Lauffenburger DA, Imperiali B.** A multiplexed homogeneous fluorescence-based assay for protein kinase activity in cell lysates. *Nat Methods* 2: 277–283, 2005.
 34. **Singh H, Milner CS, Aguilar Hernandez MM, Patel N, Brindle NPJ.** Vascular endothelial growth factor activates the Tie family of receptor tyrosine kinases. *Cellular Signalling* 21: 1346–1350, 2009.
 35. **Slungaard A.** Platelet factor 4: a chemokine enigma. *The International Journal of Biochemistry & Cell Biology* 37: 1162–1167, 2005.
 36. **Spangler JB, Neil JR, Abramovitch S, Yarden Y, White FM, Lauffenburger DA, Wittrup KD.** Combination antibody treatment down-regulates epidermal growth factor receptor by inhibiting endosomal recycling. *Proc. Natl. Acad. Sci. U.S.A.* 107: 13252–13257, 2010.
 37. **Struyf S, Salogni L, Burdick MD, Vandercappellen J, Gouwy M, Noppen S, Proost P, Opdenakker G, Parmentier M, Gerard C, Sozzani S, Strieter RM, Van Damme J.** Angiostatic and chemotactic activities of the CXC chemokine CXCL4L1 (platelet factor-4 variant) are mediated by CXCR3. *Blood* 117: 480–488, 2011.
 38. **Sulpice E, Contreres J-O, Lacour J, Bryckaert M, Tobelem G.** Platelet factor 4 disrupts the intracellular signalling cascade induced by vascular endothelial growth factor by both KDR dependent and independent mechanisms. *Eur. J. Biochem.* 271: 3310–3318, 2004.
 39. **Szekanecz Z, Pakozdi A, Szentpetery A, Besenyei T, Koch AE.** Chemokines and angiogenesis in rheumatoid arthritis. *Front Biosci (Elite Ed)* 1: 44–51, 2009.
 40. **Tabruyn SP, Griffioen AW.** Molecular pathways of angiogenesis inhibition. *Biochemical and Biophysical Research Communications* 355: 1–5, 2007.
 41. **Thelen M.** Dancing to the tune of chemokines. *Nat. Immunol.* 2: 129–134, 2001.
 42. **Vandercappellen J, Liekens S, Bronckaers A, Noppen S, Ronsse I, Dillen C, Belleri M, Mitola S, Proost P, Presta M, Struyf S, Van Damme J.** The COOH-terminal peptide of platelet factor-4 variant (CXCL4L1/PF-4var47-70) strongly inhibits angiogenesis and suppresses B16 melanoma growth in vivo. *Mol. Cancer Res.* 8: 322–334, 2010.

43. **Vandercappellen J, Van Damme J, Struyf S.** The role of the CXC chemokines platelet factor-4 (CXCL4/PF-4) and its variant (CXCL4L1/PF-4var) in inflammation, angiogenesis and cancer. *Cytokine Growth Factor Rev.* 22: 1–18, 2011.
44. **Werner S, Grose R.** Regulation of wound healing by growth factors and cytokines. *Physiol. Rev.* 83: 835–870, 2003.
45. **Wozniak MA, Keely PJ.** Use of three-dimensional collagen gels to study mechanotransduction in T47D breast epithelial cells. *Biol Proced Online* 7: 144–161, 2005.
46. **Yancopoulos GD, Davis S, Gale NW, Rudge JS, Wiegand SJ, Holash J.** Vascular-specific growth factors and blood vessel formation. *Nature* 407: 242–248, 2000.
47. **Zhang Y, Wolf-Yadlin A, White FM.** Quantitative proteomic analysis of phosphotyrosine-mediated cellular signaling networks. *Methods Mol. Biol.* 359: 203–212, 2007.

Chapter 4

Angiostatic Platelet Factor 4 cues modulate distinct phosphoprotein signaling pathways involved with migration and sprouting in endothelial cells

4.1. INTRODUCTION

4.1.1. Inflammation and angiogenesis in tissue engineering

Angiogenesis, the formation of blood vessels from pre-existing blood vessels, is a complex process essential for repairing injured tissue or supporting tissue growth (1, 12). As such, a great deal of work has been done to focus on understanding this phenomenon as it occurs *in vivo*, in particular its roles in embryonic angiogenesis and development (60, 65, 84). On the opposite spectrum to embryonic development, adult angiogenesis and inflammation are closely related phenomena that occur *in vivo* in a number of physiologically relevant processes. Inflammation lies at the crux of multiple physiological events in biological systems that precede the induction of angiogenesis: wound healing (6, 20, 81), chronic wounds (81), inflammatory disorders (32, 71), and the development of cancer (32, 33).

Tissue engineering of implantable three-dimensional constructs provides an innovative perspective on clinical treatments of various diseases and injuries (5, 17, 24, 61, 63). As complex tissues become developed for applications in clinical trials, tissue vascularization for constructs of considerable size and volume is required for their survival (28, 67). Once implanted, these constructs will also experience significant inflammatory responses within their host's local milieu (31, 39). These circumstances demonstrate the necessity for understanding the interactions between inflammation and angiogenesis. Elucidating specific intracellular mechanisms can provide insight for novel approaches in treatment of diseases as well as predicting responses to artificially engineered tissues.

4.1.2. Chemokines induce inflammatory, angiogenic, and angiostatic responses

Recently, studies have shown that chemokines, which play a central role in inflammation, can influence the outcomes of angiogenesis (7, 29, 38, 58) by promoting new blood vessel growth (e.g. CXCL1-3, CXCL5-8, CXCL12) or inhibiting its formation altogether (e.g. CXCL4, CXCL9-11, CXCL13) (58). In particular, a large body of information is available on platelet factor 4 (PF-4/CXCL4) and its ability to inhibit angiogenesis. PF-4 is found throughout the adult body, with roughly 0.25-1.25 nM (2-10 ng/mL) in blood plasma, but can be present as high as 25 μ M in localized areas during wound healing (2, 66). PF-4 half-life in circulation is 1-2 minutes (fast components) and 60-80 minutes (slow components) with clearance mediated by the liver and kidney (59). Its ubiquitous presence, implication in cancer and vascular diseases, and use as a potential drug therapy have made PF-4 a key point of interest in influencing angiogenesis *in vivo* (2, 66, 76, 77). In addition to inducing angiostasis, PF-4 can inhibit cell proliferation (halting S phase progression) and reduce endothelial cell migration (2, 21, 38, 62, 76). Despite the wealth of information on PF-4 and its mechanistic effects on immune cells, scarce literature exists on the nature of the molecular signaling that it exerts on endothelial cells to inhibit angiogenesis. The complexity of PF-4 and its potential to interact through multiple binding mechanisms makes it difficult to determine how PF-4 can interfere with angiogenesis (2, 70, 72, 77). It can interfere with angiogenic signal network induction by sequestering growth factors and proteoglycans, antagonize integrin-mediated signaling, or directly signal through its chemokine receptor CXCR3 (2). One study found that PF-4 can activate P38 MAPK via CXCR3 on human microvascular endothelial cells cultured on tissue culture plastic (52) and suggested this as a potential anti-angiogenic perturbation of cell signaling.

4.1.3. Chapter overview

In an effort to understand how pro-angiogenic and anti-angiogenic cues can simultaneously coordinate stable blood vessel growth in an inflammatory environment, we investigated the role that PF-4 may play in regulating angiogenesis. The objective of this work was to determine early signaling cues and mechanisms that are necessary to induce angiogenesis following inflammation in both acute and chronic states. The underlying premise is that angiostatic factors such as PF-4 may act in concert with pro-angiogenic growth factors to provide a balance of signals that mediate precision and coordinate stable blood vessel formation.

Obtaining physiologically relevant data for angiogenic signaling is a nontrivial matter; it is difficult to extract signaling data from primary endothelial cells grown on three dimensional collagen gels. However, studying cell signaling and phenotypic outcomes in these more challenging culture systems is highly important, in recapitulating relevant physiological complexity and coordinated cell behaviors that are not observed in traditional two-dimensional cell cultures on tissue culture plastic. In our work here, we successfully captured phosphoprotein signaling data from quantitative mass spectrometry-based analysis of HDMVECs grown on three-dimensional constructs. We found statistically significant differences in phosphoprotein signaling when HDMVECs were dosed with VEGF with PF-4 as opposed to only VEGF. Following data validation, we were able to detect 95 phosphosites across 64 proteins in our system. We were able to find statistically significant changes in phosphoprotein signaling time courses in 11 out of 13 proteins for which we were able to obtain full time course data. Our preliminary data show that PF-4 primarily exerts its inhibitory effect on angiogenesis by modulating pathways associated with cell migration such as P38 α MAPK, EphA2, FAK, and Src family kinases. From our correlation network models, we have found evidence that EphA2 activation serves to negatively regulate rather than promote angiogenesis as seen in previous studies. To our knowledge, this is the first successful attempt in developing protocols to capture protein signaling pathway dynamics from primary human endothelial cells cultured on collagen gels using mass spectrometry (MS).

4.2. EXPERIMENTAL PROCEDURES

4.2.1. Cell culture

Adult HDMVECs were cells commercially purchased at passage 4 (Lonza, Walkersville, MD). Cells were cultured in EGM-2MV (Lonza) media until near confluency. Once near confluency, cells were rinsed with 1X PBS (Invitrogen, Carlsbad, CA) and detached by incubating with 0.05% Trypsin-EDTA (Invitrogen) for 3-5 minutes at 37°C and 5% CO₂ followed by addition of EBM-2 (Lonza) with 5% FBS (Thermo Fisher Scientific/Hyclone, Logan, UT) and 50 μ g/mL gentamicin (Sigma-Aldrich, St. Louis, MO) and pelleting at 1600 rpm (~450 g) for 5 minutes. Cells were resuspended in EGM-2MV and seeded on 50 μ g/mL rat tail collagen I (BD

Biosciences, Bedford, MA) coated tissue culture flasks at a minimum of 5,000 cells/cm². Medium was changed 24 hours following seeding and replaced once every 48 hours until nearing confluency. Cells were expanded to passages 6 and 7 and frozen for cryogenic storage at -196°C in 80% EGM-2MV, 10% FBS, and 10% DMSO (Sigma-Aldrich). CXCR3 ligands IP-10, Mig, and PF-4 were evaluated on HDMVEC seeded on collagen coated tissue culture plastic (Peptotech, Rocky Hill, NJ).

4.2.2. Three-dimensional collagen gel cultures

Collagen gels cultures were used to study capillary sprouting. Collagen gel solutions were made using 10X PBS (10%), rat tail collagen I solution stock, and 1N NaOH (Sigma-Aldrich) added at 2.3% of the collagen stock solution volume used. 1 mL of collagen gel solution was added to each well in 6 well plates (9.6 cm² per well). Sterile MilliQ purified water was added to reach the desired total volume and kept on ice until use. Gels were formed at a density of 2.0 mg/mL at approximately a pH of 7.2, and allowed to set at 37 °C for 2 hours before being rinsed with 1X PBS. Gels were then preconditioned with EBM-2 with 5% FBS and 50 µg/mL gentamicin for two days to minimize background changes and nonspecific ligand binding when dosing conditions were introduced to cells seeded on the gels.

HDMVEC were thawed and grown on 50 µg/mL collagen I coated tissue culture flasks up to passage 9 collected as above and counted using Neubauer-improved disposable C-Chip hemocytometers (INCYTO, Seoul, Korea) and seeded onto collagen gels at 50,000 cells/cm². Cells were allowed to adhere for 4-6 hours at 37°C in 5% CO₂ prior to rinsing with PBS and replacing the media with EBM-2 + 5% FBS and gentamicin. HDMVEC were allowed to incubate overnight. 24 hours after seeding, plates of HDMVEC were dosed with 20 ng/mL vascular endothelial growth factor (VEGF) 165 and with or without 500 ng/mL platelet factor 4 (PF-4) across designated time intervals (0 minutes, 15 minutes, 30 minutes, 60 minutes, 6 hours, 24 hours, and 48 hours) (Peptotech).

4.2.3. Confocal microscopy

Collagen gels were formed on 24 well glass slide bottom MatTek plates (MatTek Corporation, Ashland, MA) and HDMVEC were seeded following the protocol described above. Four hours

after seeding, media were replaced with EGM-2MV and allowed to equilibrate for 24 hours before imaging. Samples were fixed with 4% paraformaldehyde (Electron Microscopy Sciences, Hatfield, PA) for 30 minutes and rinsed gently with PBS before being permeabilized with 0.1% Triton-X in PBS. The fixed samples were incubated with 1 μ M phalloidin conjugated with fluorescein isothiocyanate (Sigma-Aldrich) for 1 hour before being rinsed with PBS. Samples were then stained with 1:500 Hoechst (Invitrogen). Samples were then imaged on a confocal Zeiss Axio Observer.A1 microscope with Metamorph software (Molecular Devices, Sunnyvale, CA).

4.2.4. Detergent surface lysis with subsequent urea lysis

Detergent based lysis buffer was made following previously established protocols (64). Slight modifications were made to the base protocol in order to maintain compatibility with MS lysate preparation protocols. Cell lysis buffer consisted of 1% Triton X-100, 50mM β -glycerophosphate, 10 mM sodium pyrophosphate, 30 mM sodium fluoride (Sigma-Aldrich), 50 mM Tris (Roche Applied Science), 150 mM sodium chloride, 2 mM EGTA, 1% Protease Inhibitor Cocktail (Sigma-Aldrich) and 1% Phosphatase Inhibitor Cocktail Sets I and II (EMD Calbiochem, Gibbstown, NJ).

Following a rinse with cold PBS on ice, 200 μ L of cold lysis buffer were gently added to the top of each gel. Plates were then quickly transferred to a Model 1000 standard orbital shaker (VWR International) set at approximately 185 rpm for 15 minutes at 4°C. Following lysis, lysate from each well of a 6 well plate was consolidated into one biological sample replicate at approximately 1.2 mL volume and mixed with 3.6 mL of 8M urea with 1 mM activated sodium orthovanadate (Sigma-Aldrich) to a final urea concentration of 6M. Samples were then immediately snap frozen in liquid nitrogen before placing into storage at -80°C.

4.2.5. Phosphotyrosine mass spectrometry

Sample processing followed protocols for chemical reduction, alkylation, trypsin digestion, and fractionation as previously described (69, 86). Groups of eight samples were labeled with eight unique isobaric iTRAQ reagents (Applied Biosystems, Carlsbad, CA) for 2 hours at room temperature and then combined and concentrated before immunoprecipitation with a mixture of

anti-phosphotyrosine antibodies (4G10 (Millipore, Billerica, MA), pTyr100 (Cell Signaling), and PT-66 (Sigma)) immobilized onto protein G agarose beads (Calbiochem) in iTRAQ IP buffer [100 mM Tris, 100 mM NaCl, 1% NP-40, pH 7.4] (Sigma-Aldrich) overnight at 4°C. Beads were washed four times in rinse buffer (IP buffer without NP-40) and phosphotyrosine-containing peptides were eluted into glycine buffer (100 mM, pH=2) at room temperature for 30 minutes on a rotator. Phosphopeptides were further enriched by immobilized metal affinity chromatography. Analysis and quantification of eluted peptides were conducted on an LTQ-Orbitrap via nano-ESI LC/MS/MS (Thermo Fisher Scientific/Scherf Praezision Europa GmbH, Meiningen-Dreissigacker, Germany). Raw files were processed with MSQuant software and DTASupercharge (42), followed by peptide sequence and protein identification with Mascot (Matrix Science, Boston, MA) (50). For details on MS, please see Appendix C.

4.2.6. Manual validation of mass spectra fragments

Phosphopeptide scores and signals were thresholded for significant hits and values were normalized to a master lysate (50 ng/mL VEGF treatment for 15 minutes) and normalized to total protein values obtained from an LC/MS/MS analysis of iTRAQ channel intensities of the IP supernatant. Each nonzero normalized mass spectra output was manually validated by hand following previously described guidelines to ensure correct sequence identification and phosphosite assignment (44). Peaks were compared with theoretical values for each of the peptides assigned by Mascot using the MS-Product component of Protein Prospector (Baker, P.R. and Clauser, K.R. <http://prospector.ucsf.edu>). For a detailed protocol, please refer to Appendix D.

4.2.7. Data processing and statistical analysis

After data were collected and processed, further analysis and biological hypothesis generation were performed using PTMScout (<http://ptmscout.mit.edu>) (43). Gene ontologies and phosphorylation predictions were queried through Gene Ontology and Scansite 2.0 (4, 48). Data from two biological replicates (with two technical replicates) were consolidated into one data set for assessing phosphoprotein levels. Statistical analysis of time course data was performed using Student's t test (Microsoft Excel).

4.2.8. Correlation network modeling

Methods to quantify signaling node relatedness follow those previously described (30). At every time point, geometric means of the phosphorylation fold change relative to a master lysate were calculated for each protein that had at least two nonzero measurements across two biological replicates (two technical replicates each). For time points and proteins where only one measurable replicate was collected, the single replicate value was used as a measure of best estimate of phosphorylation. Geometric means were then normalized to the control ($t < 0$) to provide a fold change in phosphorylation. Of the resulting MS data, 21 phosphosites fulfilled these the full time course criterion for initial modeling setup. Pearson correlation coefficients were calculated between each pair of phosphosites using the 21x6 data matrix. Statistical significance of pairwise correlation coefficients was assessed using the permutation test by shuffling time course data ($n=100,000$). This provided $21 \times 20/2 = 210$ unique pairwise correlation coefficients and p values (self-correlations ignored). The Benjamini method for multiple hypothesis correction was used to account for multiple hypothesis testing and assigning statistical significance. Please refer to Appendix F for scripts and functions used to implement correlation network modeling and statistical analysis.

4.3. RESULTS

4.3.1. Optimization of collagen gel culture system for collection of cue, signal, and response data

The signaling effects of a selection of chemokines that could bind to the CXCR3 receptor were initially observed to see whether there were distinguishable changes in phosphoprotein levels (see Figure 3-3). Cells plated on collagen-coated tissue culture plastic were serum starved for 12 hours before being dosed with 50 nM of PF-4/CXCL4, Mig/CXCL9, or IP-10/CXCL10 for 30 minutes in the absence of VEGF. Phospho-ERK1/2 levels were assessed from these samples, with an observable decrease of phospho-protein levels in PF-4 treatments (Figure 3-3A).

HDMVEC seeded on collagen gels had the capability to undergo sprouting (Figure 4-1). Although the occurrence of sprouting events are generally uncommon (as only a few cells

eventually break away from the bulk), the collagen gel culture system provided us with both a system that could provide quantitative intracellular signaling analysis and the future potential to capture extracellular endothelial response behaviors associated with angiogenesis. Lysis procedures of samples grown on collagen gels were assessed by visualizing phospho- and total ERK1/2 levels of lysates collected via surface lysis protocols (see Figure 3-3C), validating the use of the system in conjunction with surface lysing protocols. A decrease of sprouting occurrence was observed with increasing concentrations of PF-4 (data not shown).

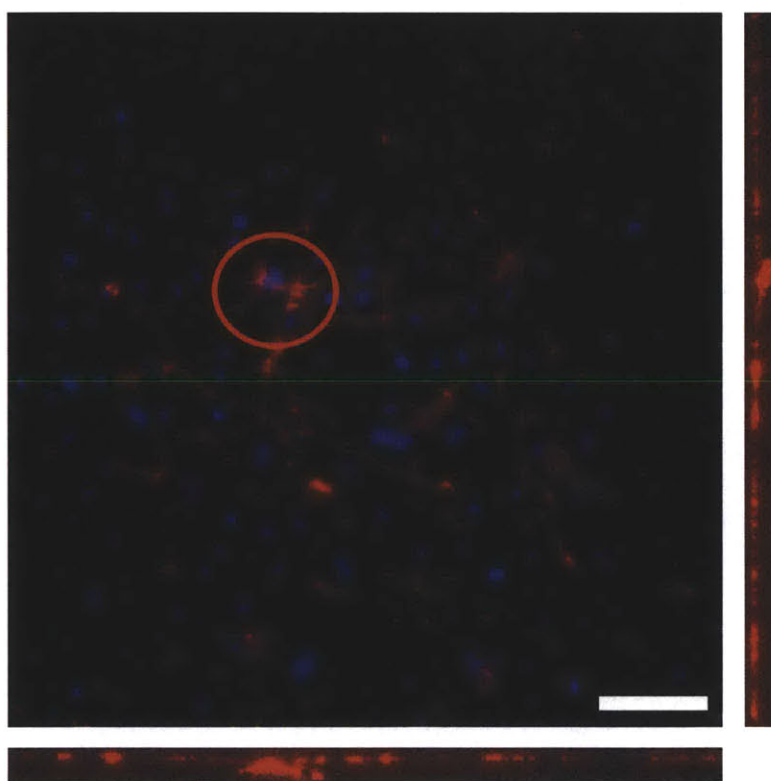


Figure 4-1. 3D collagen gel culture enables endothelial sprout initiation. Sprouting events could be observed 24 hours after HDMVEC seeding on collagen gels. Actin filaments were stained with phalloidin (red) and cell nuclei were stained with Hoechst (blue). The orthogonal Z projections of the initiated sprout (red circle) into the collagen gel are shown to the right and bottom of the main image. The collagen gel cultures are more physiologically representative of the environment that endothelial cells observe *in vivo*, as opposed to strictly culturing on tissue culture plastic which do not allow angiogenic behavior to be simulated or observed. Scale bar = 100 μm .

4.3.2. PTMScout Outputs and Predictions

Following manual validation of spectra outputs, 95 phosphorylation sites across 64 proteins were observed in our data set. The biological processes, molecular functions, and compartmentalization of the signaling proteins from Gene Ontology were procured by PTMScout. Since signaling proteins are not mutually exclusive of their roles and location, only the top 10 of each category were listed (Figure 4-2). Biological processes involved in the VEGF ± PF-4 treatment systems agree with those that are generally found in association with endothelial cell phenotype and inflammatory response (e.g., blood coagulation, platelet activation, leukocyte migration) (Figure 4-2A). Molecular functions reflect kinase activity occurring in our system (Figure 4-2B), confirming the relevance of measuring signaling and inferring crosstalk pathways. The localization of these signaling proteins are spread throughout the cell, and include those that are mostly expected, such as membrane-restricted signaling and cytosolic/cytoplasmic signaling (Figure 4-2C). The top listings do not necessarily cover all the processes and functions that these signaling proteins are involved; the top 10 biological processes represent only 15% of the total (106/683 reported biological processes), molecular functions represent only 40% of the total identified (92/233) (Figure 4-2B), and region compartmentalization is covered by 50% of the total (117/244 cellular regions) (Figure 4-2C). The full list of procured ontologies are available online through PTMScout.

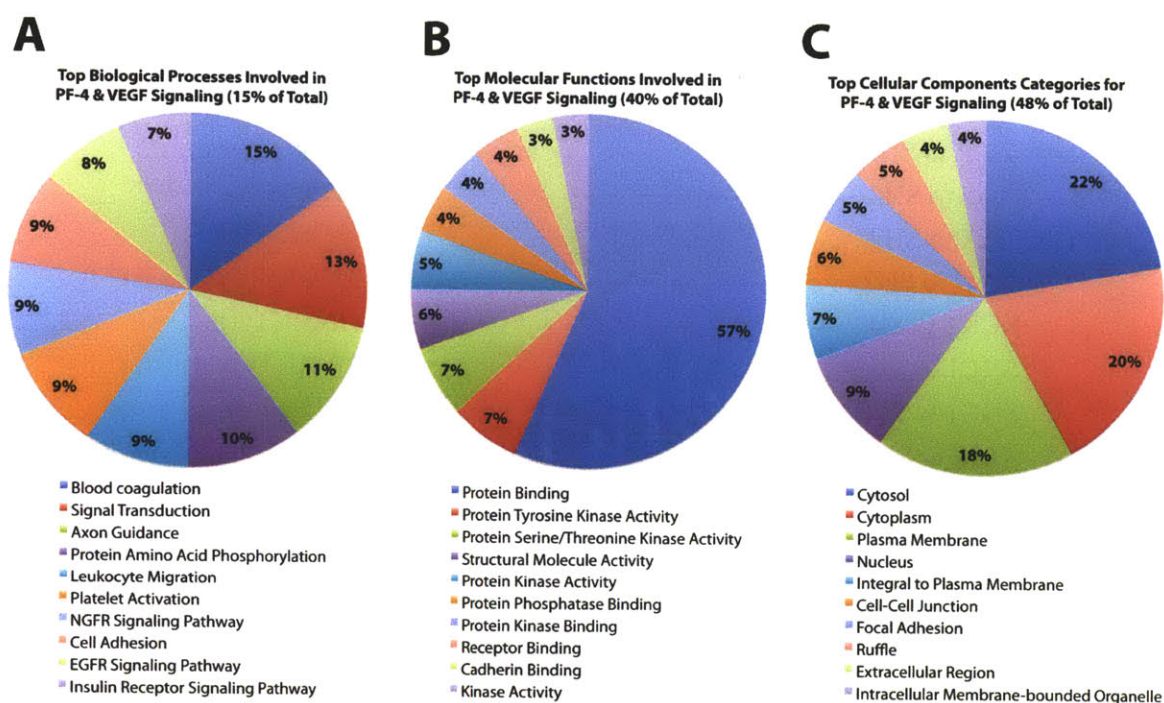


Figure 4-2. PTMScout gene ontology outputs of processes, functions, and compartmentalization of phosphoprotein signal measurements. The top 10 contributors to each of the different categories were selected and plotted to provide an overall sense of signaling dynamics and behavior. Biological processes involved included blood coagulation and inflammatory response (A) in agreement with our system. Molecular functions that were reported to be involved include kinase activity, especially that of tyrosine kinases, agreeing with our method of tyrosine enriched quantitative MS (B). Finally, the distribution of the signaling pathways through the cell indicate most to occur in the cytosol/cytoplasm and the membrane, again as what we would expect from the PF-4 and VEGF dosing treatments combined (C).

Predicted binding sites and potential kinase activity data were pulled from Scansite through PTMScout (Table 4-1). The procured list of predicting binding sites largely reflect interactions with SH2 domains, which are modulators of nonreceptor tyrosine kinase activity (18). Predicted kinase activity includes many receptor tyrosine kinases (RTKs) (e.g. EGFR, PDGFRB, INSR), as well as non-RTKs (Lck, Src, ITK, and Abl1). Caution must be exercised in the use of these predicted sites and activities; as the culture system requires the presence of serum for endothelial cell sprouting, these events may potentially be attributed to background signaling and thus may not be relevant to the differences in treatment conditions. Nonetheless, acute stimulations with VEGF and PF-4 should sufficiently perturb the system and contribute to these predictions.

<u>Predicted Binding Sites</u>	<u>Predicted Kinase Activity</u>
ITK to SH2	Src(Tyr)
FGR to SH2	Lck(Tyr)
Fyn to SH2	FGR(Tyr)
Lck to SH2	EGFR(Tyr)
Abl1 to SH2	PDGFRB(Tyr)
NCK1 to SH2	INSR(Tyr)
SHC1 to SH2	Abl1(Tyr)
SHC1 to PTB	ITK(Tyr)
Grb2 to SH2	PRKDC DNA Damage Kinase
Crk to SH2	PKC α (Ser/Thr)
Src to SH2	
PLC γ to SH2	
INPP5D to SH2	
p85 α (PI3KR1) to SH2	

Table 4-1. Predicted binding sites and kinase activity. The majority of predicted binding sites were to that of SH2 (Src homology 2) binding domains, with the exception of SHC1 having a binding prediction to PTB (phosphotyrosine-binding) domains. These predictions reflect mostly signal transduction pathway interactions and provide verification of some reported binding interactions in previous literature. The list of potential kinase activity is also suggestive of the various signaling pathways that are involved. However, a precautionary note should be considered that these predictions are based in a system supplemented with 5% serum, and therefore the data itself must be quantified for potential differences.

4.3.3. Time-resolved tyrosine phosphorylation measure by quantitative mass spectrometry indicate statistically significant differences over the course of stimulation

Out of the 64 unique proteins identified by PTMScout, only 13 had a minimum of two replicate measurements for each phosphosite at each time point, due to the unbiased, discovery-mode MS data acquisition across the different 8-plex iTRAQ sample sets in each individual MS run (Table 4-2). Of the 13 proteins, only 11 had statistically significant differences ($p < 0.05$) in signaling between VEGF and VEGF with PF-4 at any of the times compared (Figure 4-3). Comparisons of signaling data to PF-4 were excluded from these analyses due to physiological relevance and reduced quantitative signaling detection (due to lower levels of signaling). Their measurements and are included in Appendix E.

Protein	Phosphosite	Reported roles
Annexin I	Tyr21	EGFR binding, mitogenic response (54)
cdc2/cdk1	Thr14/Tyr15	Inhibition of cell cycle progression (46)
DYRK1B	Tyr273	MAPK substrate; autophosphorylation activation (35)
EphA2	Tyr772	No obvious phenotype; cell-cell interactions (16)
GSK3 β	Tyr216	Wnt signaling; Kinase activity (14)
P38 α MAPK	Tyr182	Inflammatory, stress response (55)
MPZL1	Tyr263	Scaffold protein, Shp2 docking (15)
Shp2	Tyr62	Uncharacterized (26)
PTPRA	Tyr798	Src dephosphorylation (activation) (73)
Fyn	Tyr420	Activation, kinase activity (47)
FAK	Tyr576	Kinase activity (9)
SHC1	Tyr318	Adaptor protein, ras activation (49)
Lyn	Tyr397	Autophosphorylation, activation (68)

Table 4-2. Full time course phosphoproteomic coverage, respective phosphosite, and functions reported in literature. Of the 64 proteins and their 95 phosphosites detected, we found 13 proteins to have complete coverage across the 6 time points of interest with at least 2 replicate measurements found for each time point. The proteins and the location of the phosphorylated residue were provided as an output from PTMScout.

Statistical significance was not found for all time points between VEGF and VEGF with PF-4, although different dynamics were observed for each of the 11 proteins. Annexin I experienced an early attenuation of signal intensity at 15 minutes when PF-4 was present, although signaling became indistinct from conditions where PF-4 was absent (Figure 4-3A). In PF-4 conditions, cell division control protein 2 (cdc2, or cyclin dependent kinase 1 (cdk1)) and ephrin receptor A2 (EphA2) appeared to have an initial decrease in signal followed by a delayed response in activation levels (Figure 4-3B, D). Focal adhesion kinase (FAK) decreased in the presence of PF-4 at the mid signaling time interval (60 minutes), however, increased above that of VEGF levels at 24 and 48 hours (Figure 4-3E). Src family tyrosine kinases Fyn and Lyn also increased in signal at early times before becoming similar to signaling observed in the VEGF only conditions, although Lyn experienced a decline during mid signaling (Figure 4-3F, H). P38 α MAPK increased in early and late time points when PF-4 was introduced (Figure 4-3J). DYRK1B, GSK3 β , MPZL1, and SHC1 were observed to be significant at a single time point, at either mid (GSK3 β) or late (DYRK1B, MPZL1, SHC1) signaling. With the exception of GSK3 β and SHC1, PF-4 introduction attenuated the signaling intensity (Figure 4-3C, G, I, K). Error from the pooled

data is higher in the culture system used due lower signaling intensities, collagen contamination, and inclusion of 5% serum to enable sprouting response.

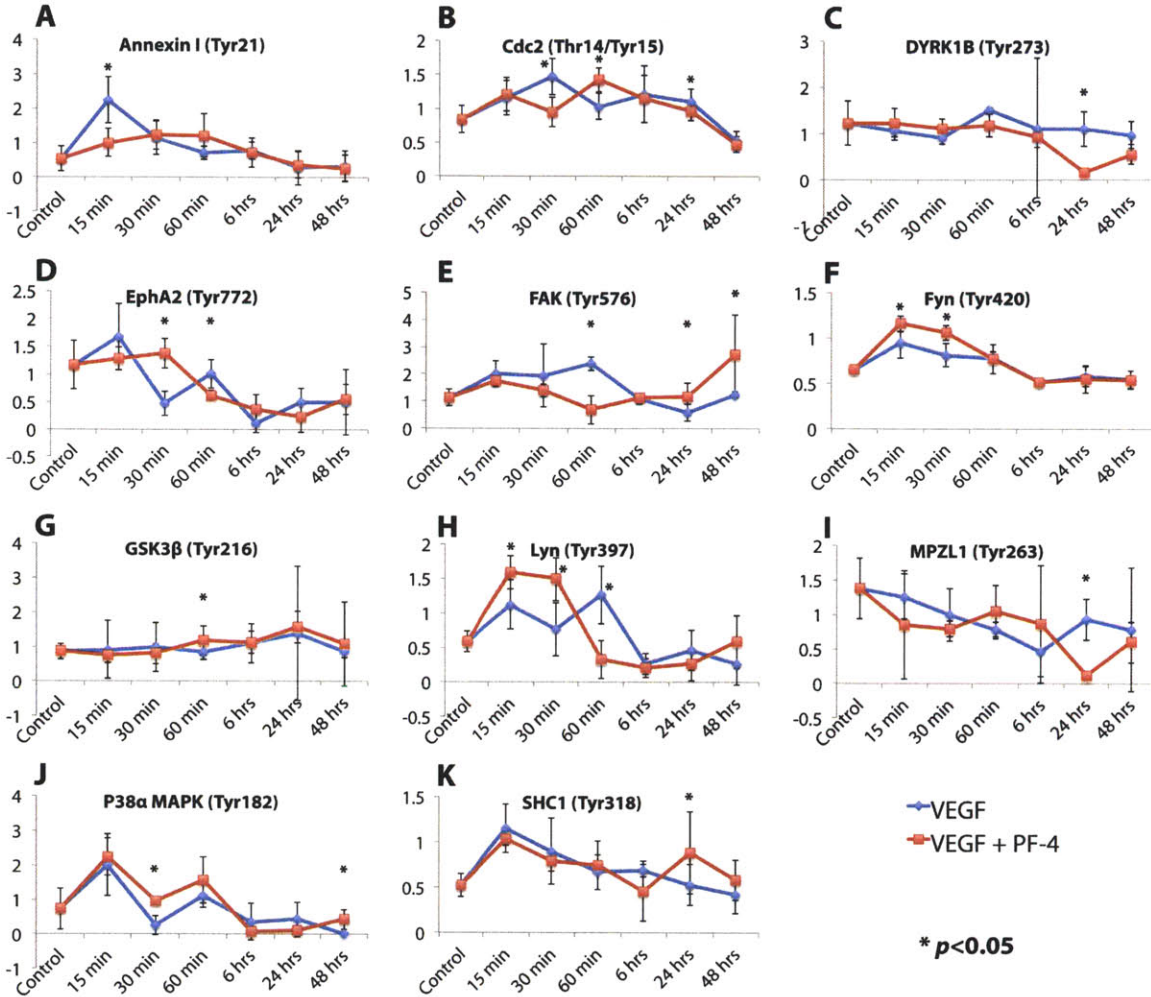


Figure 4-3. Graphs of statistically significant time course data from time resolved tyrosine phosphorylation measurements by quantitative mass spectrometry. Of 96 phosphorylation sites deemed significant, 11 different sites on unique proteins were found to have a full time course with statistics. Raw signal measurements were normalized to total protein from supernatants and a master lysate. Of these different proteins, several had statistical significance ($p < 0.05$) at one or more time points between 20 ng/mL VEGF (VEGF) treatment and 20 ng/mL VEGF with 500 ng/mL PF-4 (VEGF+PF-4) treatment. Notable temporal increases in signaling dynamics following PF-4 co-treatment were observed for Fyn/Tyr420 (F), GSK3 β /Tyr216 (G), Lyn/Tyr397 (H), P38 α MAPK/Tyr182 (J), and SHC1/Tyr318 (K). Attenuations in signaling were noticed for Annexin I/Tyr21 (A), dual specificity tyrosine-phosphorylation-regulated kinase 1B (DYRK1B/Tyr273) (C), and focal adhesion kinase (FAK/Tyr576) (E). In addition to these changes in dynamics, more complex signaling patterns were observed for some of these proteins as well, where both increases and decreases in phosphoprotein levels were observed at different time points (cdc2/Thr14/Tyr15 (B), Lyn/Tyr397 (H), and MPZL1/Tyr263 (I)). These complex patterns also included delayed activation (EphA2/Tyr772 (D)).

4.3.4. Correlation network modeling reveals significant changes in protein interactions involved in cell migration mechanisms.

With a relatively large data set, it is difficult to infer the exact mechanisms in how the introduction PF-4 changes the overall signaling landscape in HDMVEC angiogenesis. In order to make sense of the time course data, a network correlation model was employed to evaluate the topology changes in signaling pathways between the two treatment conditions. Pearson's pairwise linear correlation coefficients were evaluated and compared for differences between the two conditions (Figure 4-4). We included some proteins even though they did not possess a minimum of two replicates at each time point. In these cases, we used the single replicate as a representation of what signaling intensities were expected in order to provide an initial breadth of coverage when generating correlations in the signaling network.

We saw that the addition of PF-4 inverted many of the protein correlations. While ERBB2IP was positively correlated with all but GSK3 β , pragmin, and BCAR-1 in VEGF treatments, these positive correlations all became inversely correlated or reduced in strength. Shp2, PLC γ , MPZL1, and P38 α had very strong negative correlations with ERBB2IP. These similar trends were observed for most of EphA2 and FAK interactions (Figure 4-4A,B, inset). DYRK1B had the opposite correlations with BCAR-1; while they are negatively correlated in VEGF conditions, they become positively correlated in the presence of PF-4. These trends are also emphasized by examining the magnitude of the difference in value between correlation coefficients of the two conditions (Figure 4-4C).

The correlation values obtained for the full data sets were compared to a distribution of expected values generated from randomizing the original data set. These returned our p values, of which we considered those that appeared with $p < 0.05$ as significant (Figure 4-4, Figure 4-5). Although there were relatively fewer overlaps of correlational changes, the most interesting observation of the changes in correlation coefficients were those following PF-4 treatment. While many correlations were expected to be lost following PF-4 treatment (inhibition of angiogenesis), the increase in number of positive correlations was surprising (Figure 4-4).

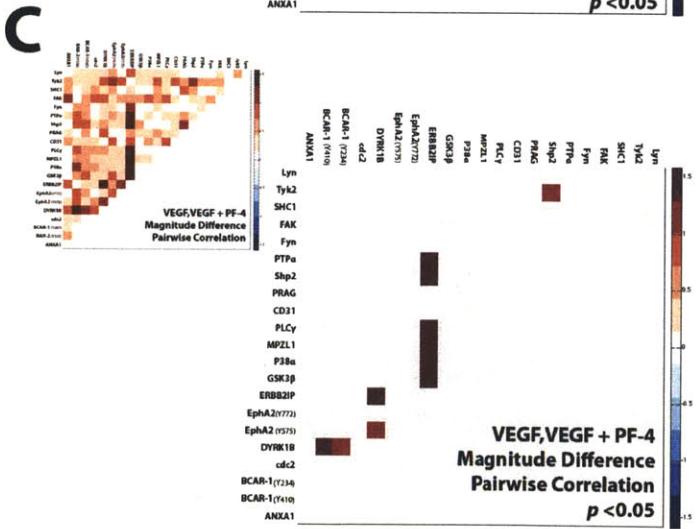
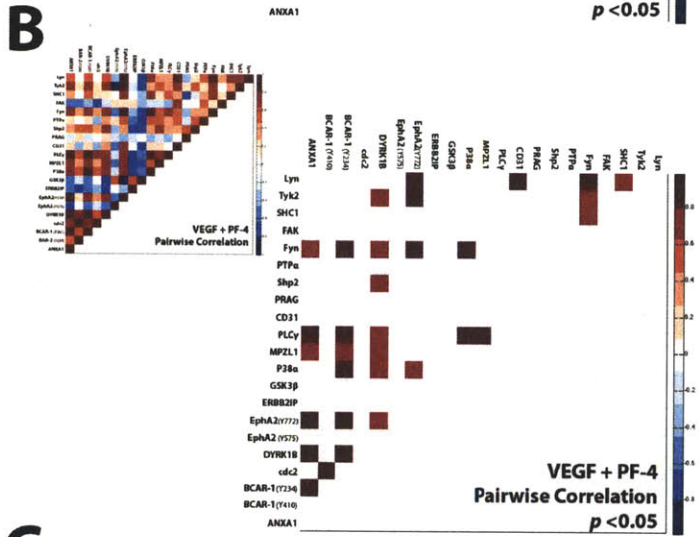
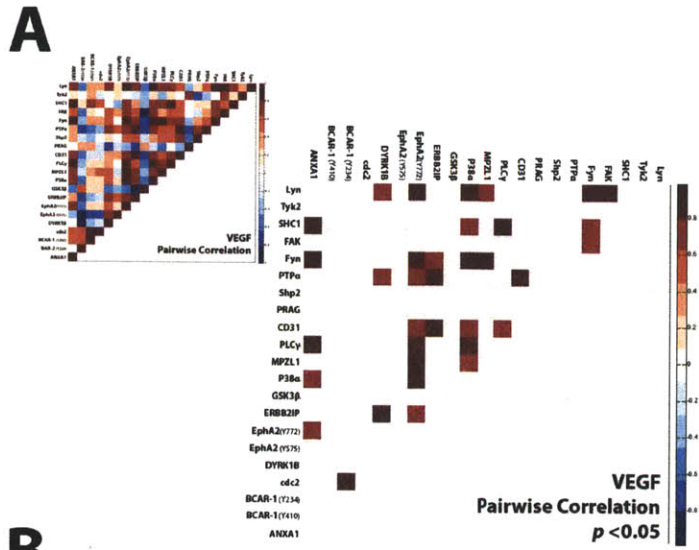


Figure 4-4. Heatmaps of statistically significant pairwise correlation in both VEGF with and without PF-4 treatments. Pairwise correlations for VEGF with and without PF-4 were calculated through phosphorylation fold changes measured for each time course (A,B, insets) and the magnitude of the differences in correlation coefficients were evaluated between the two treatments (C, inset). Although general trends in pairwise correlations were similar, there were noticeable differences that occur between the two treatments. Generally, correlation value trends appeared to become more strongly negative following the introduction of PF-4. Following significance evaluation with permutation tests, the majority of the pairwise correlations with statistically significant p values ($p < 0.05$) varied between VEGF and VEGF with PF-4. These pairwise correlations between proteins were almost always strongly positive in both conditions; from correlations centered though EphA2 and P38 α MAPK in VEGF treatments, with more statistically significant correlations appearing more focused around BCAR-1, cdc2, and DYRK1B when PF-4 was included (A,B). Correlational changes between proteins were largely different for ERBB2IP followed by DYRK1B and FAK (C) Statistically significant shifts in correlations were observed for ERBB2IP and DYRK1B interactions.

For a more intuitive understanding of the correlations $p < 0.05$, signaling diagrams were plotted to assist in data interpretation, where non-directional edges were representative of pairwise correlations (Figure 4-5). P38 α MAPK, Fyn, Lyn, PLC γ , EphA2, MPZL1 and Annexin were consistently correlated with a large number of other proteins (>4 edges) in both conditions (Figure 4-5A,B). Notably, ERBB2IP lost all of its edges with PF-4 treatment while TYK2 gained 2 correlation edges (Figure 4-5B). In comparing edges of when observing the magnitude in correlation coefficient differences ($p < 0.05$), DYRK1B and ERBB2IP were at the center of correlative changes (Figure 4-5C).

While modeling and conceptualizing the general trends occurring in our VEGF \pm PF-4 treatments, statistical significance threshold needs to be corrected to reduce the rate of finding false positives and increase confidence in our observations. Following the application of Benjamini correction, only 3 correlation coefficients for each of the treatments were found to meet the criterion. With the $q < 0.3$ ($p < 0.004$) and the expected discovery rate of one false edge, the correlations were mapped out onto flow charts (Figure 4-6).

All of the statistically significant correlations were strong positive correlations, as was observed with the broader set of correlation coefficients with $p < 0.05$ they were selected from (Figure 4-4A,B). While the correlations are positive, the overall signaling dynamics are not. While Annexin I and SHC1 are positively correlated with VEGF treatment, their statistical significance changes between PF-4 and VEGF occur at different stages of time (Annexin I is higher at early

times, SHC1 is lower at late times), although the signaling trends across all 6 time points remained relatively consistent (Figure 4-6A). Both EphA2 and P38 α are positively correlated; in the VEGF condition they both decrease over time following an initial activation (Figure 4-3D,J). ERBB2IP and PTPRA dropped well below initial signaling at 6 hours ($t < 0$) before gradually increasing again.

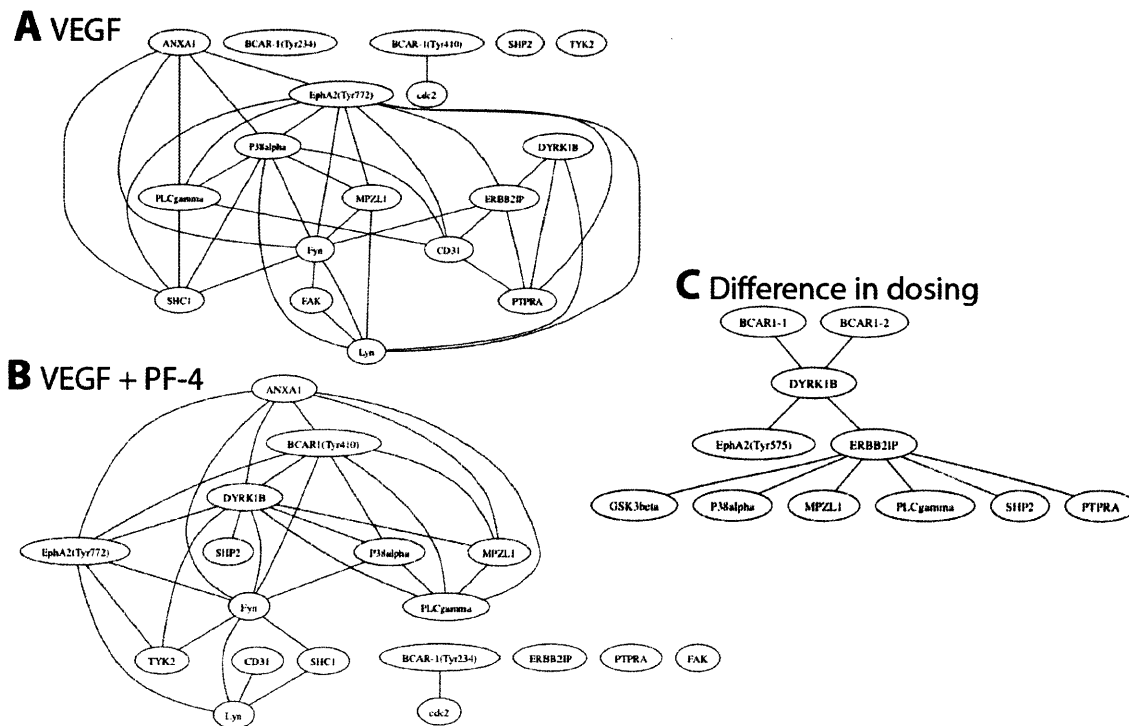


Figure 4-5. Diagrams of signaling pathways involved and changes in crosstalk when PF-4 is introduced. The topology of the signaling pathways from the proteins measured are displayed for VEGF dosing alone (A) and VEGF with the introduction of PF-4 (B). While several interactions are maintained, a majority of interactions, particular those with P38 α MAPK appear to have lost statistically significant correlations when PF-4 is present. Additionally, correlation between Lyn and FAK are lost with the addition of PF-4 indicating potential changes in migratory capacity. No changes were observed with *cdc2*; PF-4 most likely does not exert its effects on proliferative mechanisms in endothelial cells. Shp2 and PTPRA had at most one correlative edge, agreeing with findings of no statistical significance in the time course data.

While the significant edges in the VEGF + PF-4 model portray PLC γ as downstream of BCAR-1 correlation, we observed that all 3 follow an early increase (15-60 minutes) in signal, all of these signals decline in later signaling (6 - 48 hours) (Figure 4-6B). The significant edge between

EphA and P38 α MAPK disappeared following with PF-4, although a correlation arose between EphA and Fyn, where both appear to increase in levels following dosing with PF-4. While these correlations accounted for the false discovery rate, edges radiating from ERBB2IP, PTPRA, BCAR-1 and PLC γ were more cautiously considered over the EphA2 edges since these proteins did not possess either statistical significance or full time course coverage.

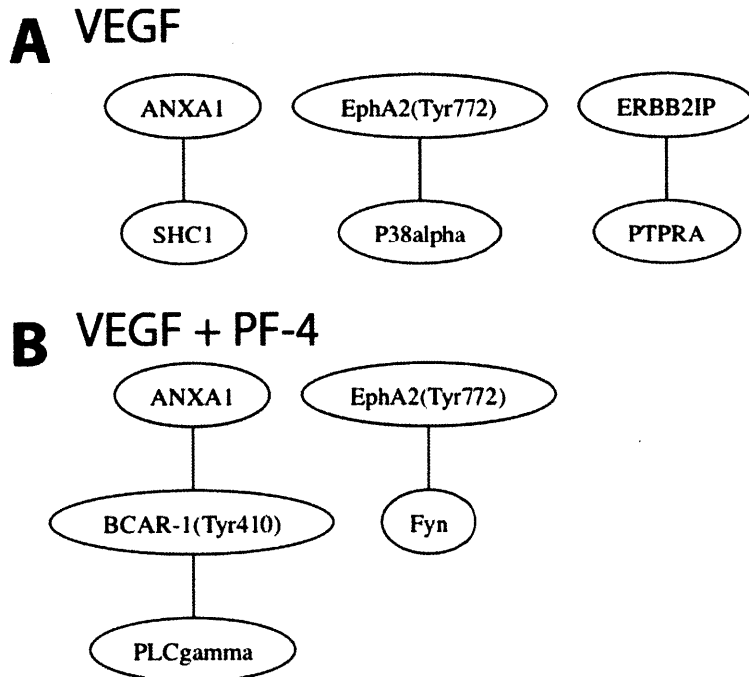


Figure 4-6. Multiple hypothesis testing correction of statistically significant correlations returns a smaller subset with some overlap. With FDR set to 0.3 ($p < .005$), only three edges in each of the conditions were statistically significant. Annexin and SHC1, EphA2 and P38 α , ERBB2IP and PTPRA (PTP α) possessed strong positive correlations in the presence of VEGF (A). In the additional presence of PF-4 the previous correlations in VEGF only treatments did not pass statistical significance and Benjamini correction. Annexin and BCAR-1, BCAR-1 and PLC γ , EphA2 and Fyn possessed strong positive correlations when PF-4 was also included in the treatment. Annexin I and EphA2 were the two proteins to retain statistically significant correlative connections of all the proteins analyzed. No edges in the difference magnitude correlations were statistically significant.

4.4. DISCUSSION

We have shown that we could successfully extract information about how PF-4 alters angiogenic signaling pathways utilized by HDMVECs, particularly those involved with cell migration and

subsequent sprout formation. Relatively few studies have been performed in the past on how this chemokine specifically affects intracellular signaling in endothelial cells. To our knowledge, this is the first large phosphoproteomic signaling data set collected from primary microvascular endothelial cells cultured in a three-dimensional gel system. These signaling data are more reflective of the physiological responses that are observed *in vivo* as opposed to the standard two-dimensional cultures performed in the past. In all, development of these protocols provides foundation for future studies of the molecular interplay involved in inflammation and angiogenesis.

4.4.1. Increased P38 α MAPK activity agrees with previously reported results

Similar to previous findings, we found that P38 α MAPK activity increased following PF-4 dosing (52). P38 α MAPK activity has been found to suppress endothelial cell migration capacity and may have similar anti-migratory effects in our system (27). This potentially agrees with previous data on PF-4 signaling through P38 α to exert its angiostatic activity (52). However, consideration of the different experimental approaches should be emphasized in comparison between the two studies; we used HDMVEC cultured on 3D gels (providing sprouting potential) while previous studies cultured microvascular endothelial cells directly on tissue culture plastic. We can conclude that our results do not disagree in the potential importance of P38 α MAPK signaling in mediating response effects of PF-4 on endothelial cells.

4.4.2. PF-4 modulates phosphorylations of proteins involved with cell migration

In addition, we observed an initial decrease followed by an increase in later times for FAK signaling. These phosphoprotein level changes and protein interactions may reflect PF-4's regulatory influence on reducing endothelial migration (38, 76). The modulations in Fyn and Lyn also lend credence to PF-4 influencing VEGF mediated signaling. While Fyn has been found to inhibit cell migration following VEGF stimulation, Lyn promotes it as a positive regulator (80). Both are increased when PF-4 is introduced, albeit Lyn has decreased signaling at 60 minutes, possibly contributing to PF-4's ability to inhibit cell migration. FAK promotes angiogenesis and cell migration in a Src dependent manner in which PF-4 may interfere (87). This is also supported by the phosphorylation levels we observe for Tyr576 on FAK, as it is a result of being in proximity to Src family kinases, such as Fyn and Lyn (9).

4.4.3. Other observed protein phosphorylation are delayed or attenuated

Ephrin and its class of RTK receptors have been recognized as important regulators of embryonic vascular development (class B) and vascular remodeling of mature tissues (class A) (8, 11). Deficient ephrin signaling has led to embryonic lethality due to cardiovascular defects and prevented endothelial tube assembly. Following PF-4 treatment, it appears that EphA2 phosphorylation dynamics were delayed behind those of VEGF treatment. However, phosphorylation levels dipped below that of VEGF at 60 minutes. These changes in signaling dynamics occur at similar times to those observed for FAK, Fyn, Lyn, and P38 α . PF-4 may also exert its angiostatic effects by delaying and decreasing EphA2 phosphorylation; decrease of EphA2 leads to reduced cell migration and vascular remodeling.

As Annexin I has anti-inflammatory effects, it would be logical inflammatory chemokine would decrease its phosphorylation (51). Annexin I has also been positively linked upstream to the MAPK pathway, with its phosphorylations associated with cell proliferation and survival (36). The observed downregulation of phospho-activity at 15 minutes relative to VEGF stimulation may explain the decreases in phosphoERK1/2 levels measured in our initial Western blots (Figure 3-3), and may contribute to the halt of cell proliferation in presence of PF-4 (21). Annexin I has also been found to be pro-angiogenic in its ability to rescue angiogenic sprouts, although its definitive role is still unclear (85). While we found statistical significance in *cdc2/cdk1* dynamics, there appeared to be no correlation with the other proteins in our data set. The differences in phosphorylation are most likely cyclic and may be due to asynchronous phases of HDMVECs between treatments (3, 25).

4.4.4. Implications from late time point data and integration with full time course signaling dynamics

It is difficult to assess the implications involved with the late time point increase in adaptor protein SHC1 phosphorylation, as this family of proteins is implicated in many mechanisms including MAPK/ERK activation (56, 78). While a slight but statistically significant increase was observed for GSK3 β at 60 minutes following PF-4 treatment, it is uncertain what particular role this may have, as GSK3 β is a near ubiquitous protein that has been implicated in many

processes including inflammation (14, 82). Other proteins that appeared to have decreased phosphorylation levels include DYRK1B (Mirk), a dual specificity tyrosine kinase that is associated with cell survival (40). MPZL1 has statistical significance at late time points, and may be associated with Shp2 activity. In our preliminary findings, we did not find any statistical significance in Shp2 activity between PF-4 and VEGF. Further characterization of the phospho-Tyr62 on Shp2 has yet to be reported in literature, although Shp2 appears to play important roles in activating substrates which are negatively regulated by phosphorylation (37). Our data indicate that MPZL1 may reduce docking sites with Shp2 and hence reduce certain kinase activities.

4.4.5. Correlation network models predict positive role of Annexin I but potentially negative regulatory role of EphA2 in angiogenesis

With a small subset of proteins such as ours, it is difficult to generate a relevant model of pathways as these proteins may not have any true correlation to each other in the cell. The use of a computational model such can provide some insight about how these proteins might interact they do exist. Our correlation network model demonstrated P38 α , Fyn, and EphA2 to be central nodes in both signaling environments to the changes in protein interactions following PF-4 treatment. While PF-4 attenuated many of the signals observed following VEGF treatment, the signals that increased in correlation strength were of particular interest. In fact, our significant correlations with $p < 0.05$ indicate positive correlations of multiple signaling; no negative correlations were found. Coupling the presence of P38 α , Fyn, and EphA2 as central nodes with the time course data collected in Figure 4-3, this seems to suggest that VEGF with PF-4 tends to generally increase phosphorylation levels while they decrease over time in VEGF only conditions. ERBB2IP and DYRK1B had a large number of associations and edges in the change of correlation and edges. Not much literature currently exists on their roles in endothelial cells and angiogenesis. As such, these proteins may be of interest to investigate further in PF-4 signaling mechanisms.

In order to the gain confidence in the correlations we obtained, we applied multiple hypothesis testing to our system of 210 unique correlations and their p-values. However, using the step-down false discovery rate (FDR) method proposed by Benjamini et al., the restrictions on p

values for significance tests here were perhaps too conservative. This is due to the theory of false discovery rate, and the threshold values being for accepting p values in our system are very small due to the number of unique pairwise correlations ($n=210$ p values and respective hypotheses tests). Permutation tests are exact values rather than estimated statistics, and do not fare well using methods for estimated FDR (10, 45, 83). The incorporation of resampling methods like Westfall and Young procedures for permutation adjusted FDR may be less stringent and provide more confidence in our results (45, 57, 75). These methods would allow us to gate out interactions we have strong confidence in as true positives, and perform the step-down FDR method (adjusted for permutations) on the remaining data to identify the false positive rate and family wise error (FWE).

An alternative interpretation for these data (from that of threshold stringency) is that the low level of statistical significance following adjustments for multiple hypothesis testing may also be reflective of the proteins we are evaluating in this network. Simply, there may be little to no correlation between the set of proteins in our data. The lack of correlation does not necessitate a lack of connections or importance in signaling; their dynamics may very well be intimately linked. Thus, the type of model to optimally represent signaling crosstalk must be considered carefully. Some cases may even require hybrid or multiple models to fully capture significance in signaling events. With more in-depth analysis and application of data processing methods, we will be able to extract additional information about the signaling topology changes by PF-4.

We can infer some critical information from the remaining correlative edges after applying the Benjamini method, particularly for Annexin I and EphA2 nodes that remained relevant in both conditions treatment conditions. Annexin I has been found to be involved in many cellular mechanisms responses, making it difficult to speculate on its specific function here in this system. Annexin I has been indicated in anti-inflammatory roles and is pro-angiogenic for endothelial cells (85). However, scarce data exist on Annexin I's interaction with BCAR-1 or SHC1. The indirect positive correlation of Annexin I and PLC γ may agree with previous findings. In our data, Annexin signaling is attenuated and dampened with the introduction of PF-4. Downregulation of annexin can lead to down regulation of PLC group signaling and is recapitulated here in our data (19). Phospho Tyr771 levels we observed here on PLC γ have not

been reported to affect PLC γ activity, although a nearby Tyr783 residue is implicated in integrin-mediated adhesion (74). Thus, the decrease in Annexin signaling, might be indicative of a decrease in PLC γ . However, this needs to be validated with more information on the role of Tyr771. In General PLC γ activation is required for endothelial cell migration mechanisms and this could be inferred to provide the same role in our data (79).

EphA2 is associated with mediating vascular remodeling promoting cell migration and sprouting (53). From the significant correlations provided by Benjamini testing, both Fyn and EphA2 have statistically significant increases in activity when PF-4 is introduced, while both EphA2 and P38 α MAPK are attenuated in its absence (e.g., only treated with VEGF). EphA2 Tyr772 phosphorylation is implicated in mediating cell-cell interactions, and from initial analysis of the time course data in context of previous studies, is required for progression of angiogenesis (8, 13).

When considering the positive correlation of EphA2 with Fyn and P38 α inhibiting cell migration, we speculate that PF-4 stimulates EphA2's regulatory role on cell-cell interactions to reduce the sprouting capacity of endothelial cells, or even implicate its role in ensuring only the most robust sprouts form by preventing bulk cell invasion. This behavior has been speculated previously for initiation of tumor metastasis and that EphA2 expression in tumor cells inhibits their propensity to migrate (34). Tumor malignancy occurs when these cells overcome this ligand inhibition. EphA2 has also been implicated in inhibiting integrin-mediated adhesion, migration, and signaling, thereby contributing to a potential role in negative regulation following PF-4 treatment (41). This would also agree with what we observe for signaling involved in migration; FAK decreases over time in the presence of PF-4 and is negatively regulated by EphA2. VE-cadherin and EphA2 crosstalk has been found in melanoma vasculogenic mimicry where EphA2 colocalizes with VE-cadherin (22, 23). This previous study found absence or downregulation of VE-cadherin caused dephosphorylation of EphA2. While we did not have a full time course data for VE-cadherin, we were able to detect a significant decrease in VE-cadherin levels following PF-4 treatment. In corresponding confocal microscopy PF-4 caused more diffuse localization of VE-cadherin at the membranes between adjacent HDMVECs, which may suggest an additional interaction with EphA2 may be involved (data not shown). Thus, the analysis of the EphA2 time

course data in the context of our correlation network model warrants re-evaluation of EphA2 as a positive signal requirement in angiogenesis.

4.4.6. Caveats to signaling data

We also collected signaling data on culture treatments dosed only with 500 ng/mL PF-4. Although we observed statistically significant changes due solely to the presence of PF-4 across dosing times, the measurements were not considered here for a number of reasons. Despite the interesting effects of PF-4 signaling, we deemed that it was physiologically irrelevant in the case of angiogenesis, as we are interested in the dynamic changes of HDMVEC signaling in the presence of simultaneous pro- and anti-angiogenic cues. Furthermore, PF-4 signaling was much lower in intensity than treatment conditions that included VEGF; it was difficult to resolve much of the quantify differences of PF-4 signaling for most phosphoproteins detected. For most data observed, PF-4 only dosed conditions were not statistically significant from control. Those that had statistically significant differences from the control were not statistically significant from treatment conditions that had VEGF and PF-4 together. From this statistical analysis observation, the effect of PF-4 may be additive to that of VEGF when the two are present together. This does not necessarily rule out the importance of independent signaling by PF-4; signaling cascades utilized by endothelial cells during inflammatory angiogenesis may become primed for certain responses due to the presence of this inflammatory cytokine (e.g., PF-4 is present at high concentrations during wound healing). Again, for the reader's reference, PF-4 data have been included in Appendix E.

Despite our success, we realize that a majority of signaling data was lost due to the inherent difficulties working with our system; a low signaling primary cell type in conjunction with a highly concentrated matrix scaffold can drown out low level signaling. This was apparent in our original captured list of phosphoproteomic data; we observed over 400 different phosphorylation sites across 350 unique proteins that were significant hits and matches via Mascot. However, there was insufficient quantitation in many of these measurements due to very low level signaling. The presence of a high concentration of serum (5%) also introduces a high proportion of background noise into our measurements (as is observed in some of the measurements shown in Figure 4-3). To recover some of the lost quantitation, we attempted to pool time points into

early, mid, and late signaling increases our phosphoprotein coverage from 13 proteins to 26 at the expense of statistical power. Although total coverage expanded from 13 to 26 proteins, we were only able to obtain statistical significance of time course data for 13 of the 26 proteins versus 11 of the 13 nonpooled time courses (data not shown). We believe that some of our signaling measurements may also be lost due to the preparation of samples for MS; we randomized loading and combination of samples across both conditions and all time points so that one iTRAQ run contained both early and late signaling. We expect to rescue more signaling dynamics by separate evaluation and capture of earlier (15 min, 30 min, 60 min) and later (6 hrs, 24 hrs, 48 hrs) signaling events via MS, as earlier time point signaling may drown out our quantitation of late signaling.

Obtaining signaling data from three-dimensional collagen gels is a nontrivial matter. The presence of the collagen gel substrate introduces multiple challenges to collecting signaling data; the first is the dilution of cell lysate collected while the second is the enormous contribution of the substrate protein to the overall protein concentration in the collected lysate. Collagen contamination invalidates most total protein assays used to determine sample-loading volumes for assays such as Westerns and ELISAs making normalization of some data difficult or implausible. We also investigated the use of the Luminex xMAP bead platform for assessing phosphoprotein signaling dynamics. Unfortunately, due to the nature of the collagen gel system we were unable to obtain significant signaling data for most assays. For the most abundant phosphoproteins we were unable to obtain signal above background past 30-60 minutes (data not shown).

Another caveat of our signaling data is the representation of unique signaling events in individual cells through the overall population. Relative to the number of cells present, sprouting is an uncommon event that occurs in our system. As such, the signaling data collected does not accurately represent the signaling that is observed when endothelial cells decide to initiate invasion into the extracellular matrix. However, this is encountered with almost all standard protocols. The importance of late time point signaling within these data may not be representative of the true sprouting population. For the most part, our consideration has focused on early signaling time points around 30-60 minutes as this appears to be where most of the

angiostatic influence of PF-4 has been exerted in our data and would likely be less affected by the separation into subpopulation of sprouting cells.

Thus, with additional data collection from quantitative MS we will be able to expand the time course set of data and increase coverage of the signaling network, including many that were not (but should be) considered in the correlational network model. Our predictions and observations of differential signaling dynamics with PF-4 will improve and flesh out the intracellular mechanisms involved in its ability to inhibit angiogenesis. The larger data set will also improve PTMScout predictions and outputs, and will its full utility in assessing differences in VEGF \pm PF-4 conditions and with the potential to discover new signal dynamics. Future work can be applied to creating a more complete picture by incorporating cue-response data.

4.4.7. Summary

We have developed new methods to explore pro- and anti-angiogenic. Our preliminary data indicate that PF-4 primarily induces its angiostatic effects on microvascular endothelial cells via pathways that control cell migration which precede sprouting/invasion phenotype. Thus, by modulating these protein interactions of P38, FAK, EphA2, and Src family kinases Fyn and Lyn, we can potentially increase how we can affect angiogenesis in the adult body, both in promoting tissue and graft vascularization, to inhibiting the progression of tumor growth. From both assessment of the time course data and correlation network modeling, we have found substantial implications of EphA2 signaling dynamics in negatively regulating cell migration and angiogenesis following stimulation, contrary to previous reports of its role in promoting cell migration and sprouting. Our work indicates EphA2 signaling as an area of interest and future focus for understanding angiostatic mechanisms.

4.5. References

1. **Adair TH, Montani J-P.** Angiogenesis [Online]. Morgan & Claypool Life Sciences. <http://www.ncbi.nlm.nih.gov/books/NBK53242/>.
2. **Aidoudi S, Bikfalvi A.** Interaction of PF4 (CXCL4) with the vasculature: a role in atherosclerosis and angiogenesis. *Thromb. Haemost.* 104: 941–948, 2010.
3. **Alberts B, Johnson A, Lewis J, Raff M, Roberts K, Walter P.** Molecular Biology of the Cell [Online]. 4th ed. Garland Science. <http://www.ncbi.nlm.nih.gov/books/NBK21054/>.
4. **Ashburner M, Ball CA, Blake JA, Botstein D, Butler H, Cherry JM, Davis AP, Dolinski K, Dwight SS, Eppig JT, Harris MA, Hill DP, Issel-Tarver L, Kasarskis A, Lewis S, Matese JC, Richardson JE, Ringwald M, Rubin GM, Sherlock G.** Gene ontology: tool for the unification of biology. The Gene Ontology Consortium. *Nat. Genet.* 25: 25–29, 2000.
5. **Ban D-X, Kong X-H, Feng S-Q, Ning G-Z, Chen J-T, Guo S-F.** Intraspinal cord graft of autologous activated Schwann cells efficiently promotes axonal regeneration and functional recovery after rat's spinal cord injury. *Brain Res.* 1256: 149–161, 2009.
6. **Barrientos S, Stojadinovic O, Golinko MS, Brem H, Tomic-Canic M.** Growth factors and cytokines in wound healing. *Wound Repair Regen* 16: 585–601, 2008.
7. **Bernardini G, Ribatti D, Spinetti G, Morbidelli L, Ziche M, Santoni A, Capogrossi MC, Napolitano M.** Analysis of the role of chemokines in angiogenesis. *J. Immunol. Methods* 273: 83–101, 2003.
8. **Brantley-Sieders DM, Caughron J, Hicks D, Pozzi A, Ruiz JC, Chen J.** EphA2 receptor tyrosine kinase regulates endothelial cell migration and vascular assembly through phosphoinositide 3-kinase-mediated Rac1 GTPase activation. *Journal of Cell Science* 117: 2037–2049, 2004.
9. **Calalb MB, Polte TR, Hanks SK.** Tyrosine phosphorylation of focal adhesion kinase at sites in the catalytic domain regulates kinase activity: a role for Src family kinases. *Mol. Cell. Biol.* 15: 954–963, 1995.
10. **Camargo A, Azuaje F, Wang H, Zheng H.** Permutation - based statistical tests for multiple hypotheses. *Source Code Biol Med* 3: 15, 2008.

11. **Campbell TN, Robbins SM.** The Eph receptor/ephrin system: an emerging player in the invasion game. *Curr Issues Mol Biol* 10: 61–66, 2008.
12. **Carmeliet P, Jain RK.** Molecular mechanisms and clinical applications of angiogenesis. *Nature* 473: 298–307, 2011.
13. **Cheng N, Brantley DM, Liu H, Lin Q, Enriquez M, Gale N, Yancopoulos G, Cerretti DP, Daniel TO, Chen J.** Blockade of EphA receptor tyrosine kinase activation inhibits vascular endothelial cell growth factor-induced angiogenesis. *Mol. Cancer Res.* 1: 2–11, 2002.
14. **Cole AR, Sutherland C.** Measuring GSK3 expression and activity in cells. *Methods Mol. Biol.* 468: 45–65, 2008.
15. **Eminaga S, Bennett AM.** Noonan syndrome-associated SHP-2/Ptpn11 mutants enhance SIRPalpha and PZR tyrosyl phosphorylation and promote adhesion-mediated ERK activation. *J. Biol. Chem.* 283: 15328–15338, 2008.
16. **Fang WB, Brantley-Sieders DM, Hwang Y, Ham A-JL, Chen J.** Identification and functional analysis of phosphorylated tyrosine residues within EphA2 receptor tyrosine kinase. *J. Biol. Chem.* 283: 16017–16026, 2008.
17. **Feil G, Daum L, Amend B, Maurer S, Renninger M, Vaegler M, Seibold J, Stenzl A, Sievert K-D.** From tissue engineering to regenerative medicine in urology--the potential and the pitfalls. *Adv. Drug Deliv. Rev.* 63: 375–378, 2011.
18. **Filippakopoulos P, Müller S, Knapp S.** SH2 domains: modulators of nonreceptor tyrosine kinase activity. *Curr. Opin. Struct. Biol.* 19: 643–649, 2009.
19. **Frey BM, Reber BF, Vishwanath BS, Escher G, Frey FJ.** Annexin I modulates cell functions by controlling intracellular calcium release. *FASEB J.* 13: 2235–2245, 1999.
20. **Gillitzer R, Goebeler M.** Chemokines in cutaneous wound healing. *J. Leukoc. Biol.* 69: 513–521, 2001.
21. **Gupta SK, Singh JP.** Inhibition of endothelial cell proliferation by platelet factor-4 involves a unique action on S phase progression. *The Journal of Cell Biology* 127: 1121–1127, 1994.
22. **Hendrix MJC, Seftor EA, Hess AR, Seftor REB.** Vasculogenic mimicry and tumour-cell plasticity: lessons from melanoma. *Nat Rev Cancer* 3: 411–421, 2003.
23. **Hess AR, Seftor EA, Gruman LM, Kinch MS, Seftor REB, Hendrix MJC.** VE-

- cadherin regulates EphA2 in aggressive melanoma cells through a novel signaling pathway: implications for vasculogenic mimicry. *Cancer Biol. Ther.* 5: 228–233, 2006.
24. **Hu X, Huang J, Ye Z, Xia L, Li M, Lv B, Shen X, Luo Z.** A novel scaffold with longitudinally oriented microchannels promotes peripheral nerve regeneration. *Tissue Eng Part A* 15: 3297–3308, 2009.
 25. **Hu X, Moscinski LC.** Cdc2: a monopotent or pluripotent CDK? *Cell Prolif.* 44: 205–211, 2011.
 26. **Huang PH, Mukasa A, Bonavia R, Flynn RA, Brewer ZE, Cavenee WK, Furnari FB, White FM.** Quantitative analysis of EGFRvIII cellular signaling networks reveals a combinatorial therapeutic strategy for glioblastoma. *Proc. Natl. Acad. Sci. U.S.A.* 104: 12867–12872, 2007.
 27. **Kanaji N, Nelson A, Allen-Gipson DS, Sato T, Nakanishi M, Wang X, Li Y, Basma H, Michalski J, Farid M, Rennard SI, Liu X.** The p38 mitogen-activated protein kinases modulate endothelial cell survival and tissue repair. *Inflamm. Res.* (December 3, 2011). doi: 10.1007/s00011-011-0405-7.
 28. **Kaully T, Kaufman-Francis K, Lesman A, Levenberg S.** Vascularization--the conduit to viable engineered tissues. *Tissue Eng Part B Rev* 15: 159–169, 2009.
 29. **Keeley EC, Mehrad B, Strieter RM.** Chemokines as mediators of neovascularization. *Arteriosclerosis, Thrombosis, and Vascular Biology* 28: 1928–1936, 2008.
 30. **Kim H-D, Meyer AS, Wagner JP, Alford SK, Wells A, Gertler FB, Lauffenburger DA.** Signaling network state predicts twist-mediated effects on breast cell migration across diverse growth factor contexts. *Mol. Cell Proteomics* 10: M111.008433, 2011.
 31. **Kirkpatrick CJ, Otto M, Van Kooten T, Krump V, Kriegsmann J, Bittinger F.** Endothelial cell cultures as a tool in biomaterial research. *J Mater Sci Mater Med* 10: 589–594, 1999.
 32. **Kobayashi H, Lin PC.** Angiogenesis links chronic inflammation with cancer. *Methods Mol. Biol.* 511: 185–191, 2009.
 33. **Kundu JK, Surh Y-J.** Inflammation: gearing the journey to cancer. *Mutat. Res.* 659: 15–30, 2008.
 34. **Larsen AB, Pedersen MW, Stockhausen M-T, Grandal MV, van Deurs B, Poulsen HS.** Activation of the EGFR gene target EphA2 inhibits epidermal growth factor-induced

- cancer cell motility. *Mol. Cancer Res.* 5: 283–293, 2007.
35. **Lee K, Deng X, Friedman E.** Mirk protein kinase is a mitogen-activated protein kinase substrate that mediates survival of colon cancer cells. *Cancer Research* 60: 3631–3637, 2000.
 36. **Lim LHK, Pervaiz S.** Annexin 1: the new face of an old molecule. *FASEB J.* 21: 968–975, 2007.
 37. **Matozaki T, Murata Y, Saito Y, Okazawa H, Ohnishi H.** Protein tyrosine phosphatase SHP-2: a proto-oncogene product that promotes Ras activation. *Cancer Sci.* 100: 1786–1793, 2009.
 38. **Mehrad B, Keane MP, Strieter RM.** Chemokines as mediators of angiogenesis. *Thromb. Haemost.* 97: 755–762, 2007.
 39. **Mendes JB, Campos PP, Ferreira MAND, Bakhle YS, Andrade SP.** Host response to sponge implants differs between subcutaneous and intraperitoneal sites in mice. *J. Biomed. Mater. Res. Part B Appl. Biomater.* 83: 408–415, 2007.
 40. **Mercer SE, Friedman E.** Mirk/Dyrk1B: a multifunctional dual-specificity kinase involved in growth arrest, differentiation, and cell survival. *Cell Biochem. Biophys.* 45: 303–315, 2006.
 41. **Miao H, Burnett E, Kinch M, Simon E, Wang B.** Activation of EphA2 kinase suppresses integrin function and causes focal-adhesion-kinase dephosphorylation. *Nat Cell Biol* 2: 62–69, 2000.
 42. **Mortensen P, Gouw JW, Olsen JV, Ong S-E, Rigbolt KTG, Bunkenborg J, Cox J, Foster LJ, Heck AJR, Blagoev B, Andersen JS, Mann M.** MSQuant, an open source platform for mass spectrometry-based quantitative proteomics. *J. Proteome Res.* 9: 393–403, 2010.
 43. **Naegle KM, Gymrek M, Joughin BA, Wagner JP, Welsch RE, Yaffe MB, Lauffenburger DA, White FM.** PTMScout, a Web resource for analysis of high throughput post-translational proteomics studies. *Mol. Cell Proteomics* 9: 2558–2570, 2010.
 44. **Nichols AM, White FM.** Manual validation of peptide sequence and sites of tyrosine phosphorylation from MS/MS spectra. *Methods Mol. Biol.* 492: 143–160, 2009.
 45. **Nichols TE, Holmes AP.** Nonparametric permutation tests for functional neuroimaging: a

- primer with examples. *Hum Brain Mapp* 15: 1–25, 2002.
46. **Norbury C, Blow J, Nurse P.** Regulatory phosphorylation of the p34cdc2 protein kinase in vertebrates. *EMBO J.* 10: 3321–3329, 1991.
 47. **O'Meara RW, Michalski J-P, Kothary R.** Integrin signaling in oligodendrocytes and its importance in CNS myelination. *J Signal Transduct* 2011: 354091, 2011.
 48. **Obenauer JC, Cantley LC, Yaffe MB.** Scansite 2.0: Proteome-wide prediction of cell signaling interactions using short sequence motifs. *Nucleic Acids Res.* 31: 3635–3641, 2003.
 49. **Patrussi L, Ulivieri C, Lucherini OM, Paccani SR, Gamberucci A, Lanfrancone L, Pelicci PG, Baldari CT.** p52Shc is required for CXCR4-dependent signaling and chemotaxis in T cells. *Blood* 110: 1730–1738, 2007.
 50. **Perkins DN, Pappin DJ, Creasy DM, Cottrell JS.** Probability-based protein identification by searching sequence databases using mass spectrometry data. *Electrophoresis* 20: 3551–3567, 1999.
 51. **Perretti M, Dalli J.** Exploiting the Annexin A1 pathway for the development of novel anti-inflammatory therapeutics. *Br. J. Pharmacol.* 158: 936–946, 2009.
 52. **Petrai I, Rombouts K, Lasagni L, Annunziato F, Cosmi L, Romanelli RG, Sagrinati C, Mazzinghi B, Pinzani M, Romagnani S, Romagnani P, Marra F.** Activation of p38(MAPK) mediates the angiostatic effect of the chemokine receptor CXCR3-B. *The International Journal of Biochemistry & Cell Biology* 40: 1764–1774, 2008.
 53. **Poliakov A, Cotrina M, Wilkinson DG.** Diverse roles of eph receptors and ephrins in the regulation of cell migration and tissue assembly. *Dev. Cell* 7: 465–480, 2004.
 54. **Radke S, Austermann J, Russo-Marie F, Gerke V, Rescher U.** Specific association of annexin 1 with plasma membrane-resident and internalized EGF receptors mediated through the protein core domain. *FEBS Lett.* 578: 95–98, 2004.
 55. **Raingeaud J, Gupta S, Rogers JS, Dickens M, Han J, Ulevitch RJ, Davis RJ.** Pro-inflammatory cytokines and environmental stress cause p38 mitogen-activated protein kinase activation by dual phosphorylation on tyrosine and threonine. *J. Biol. Chem.* 270: 7420–7426, 1995.
 56. **Ravichandran KS.** Signaling via Shc family adapter proteins. *Oncogene* 20: 6322–6330, 2001.

57. **Reiner A, Yekutieli D, Benjamini Y.** Identifying differentially expressed genes using false discovery rate controlling procedures. *Bioinformatics* 19: 368–375, 2003.
58. **Rosenkilde MM, Schwartz TW.** The chemokine system -- a major regulator of angiogenesis in health and disease. *APMIS* 112: 481–495, 2004.
59. **Rucinski B, Knight LC, Niewiarowski S.** Clearance of human platelet factor 4 by liver and kidney: its alteration by heparin. *Am. J. Physiol.* 251: H800–7, 1986.
60. **Saharinen P, Eklund L, Miettinen J, Wirkkala R, Anisimov A, Winderlich M, Nottebaum A, Vestweber D, Deutsch U, Koh GY, Olsen BR, Alitalo K.** Angiopoietins assemble distinct Tie2 signalling complexes in endothelial cell-cell and cell-matrix contacts. *Nat Cell Biol* 10: 527–537, 2008.
61. **Sahota PS, Burn JL, Brown NJ, MacNeil S.** Approaches to improve angiogenesis in tissue-engineered skin. *Wound Repair Regen* 12: 635–642, 2004.
62. **Shao XJ, Xie FM.** Influence of angiogenesis inhibitors, endostatin and PF-4, on lymphangiogenesis. *Lymphology* 38: 1–8, 2005.
63. **Sherwood JK, Riley SL, Palazzolo R, Brown SC, Monkhouse DC, Coates M, Griffith LG, Landeen LK, Ratcliffe A.** A three-dimensional osteochondral composite scaffold for articular cartilage repair. *Biomaterials* 23: 4739–4751, 2002.
64. **Shults MD, Janes KA, Lauffenburger DA, Imperiali B.** A multiplexed homogeneous fluorescence-based assay for protein kinase activity in cell lysates. *Nat. Methods* 2: 277–283, 2005.
65. **Singh H, Milner CS, Aguilar Hernandez MM, Patel N, Brindle NPJ.** Vascular endothelial growth factor activates the Tie family of receptor tyrosine kinases. *Cellular Signalling* 21: 1346–1350, 2009.
66. **Slungaard A.** Platelet factor 4: a chemokine enigma. *The International Journal of Biochemistry & Cell Biology* 37: 1162–1167, 2005.
67. **Soker S, Machado M, Atala A.** Systems for therapeutic angiogenesis in tissue engineering. *World J Urol* 18: 10–18, 2000.
68. **Sotirellis N, Johnson TM, Hibbs ML, Stanley IJ, Stanley E, Dunn AR, Cheng HC.** Autophosphorylation induces autoactivation and a decrease in the Src homology 2 domain accessibility of the Lyn protein kinase. *J. Biol. Chem.* 270: 29773–29780, 1995.
69. **Spangler JB, Neil JR, Abramovitch S, Yarden Y, White FM, Lauffenburger DA,**

- Wittrup KD.** Combination antibody treatment down-regulates epidermal growth factor receptor by inhibiting endosomal recycling. *Proc. Natl. Acad. Sci. U.S.A.* 107: 13252–13257, 2010.
70. **Sulpice E, Contreres J-O, Lacour J, Bryckaert M, Tobelem G.** Platelet factor 4 disrupts the intracellular signalling cascade induced by vascular endothelial growth factor by both KDR dependent and independent mechanisms. *Eur. J. Biochem.* 271: 3310–3318, 2004.
71. **Szekanecz Z, Koch AE.** Vascular endothelium and immune responses: implications for inflammation and angiogenesis. *Rheum. Dis. Clin. North Am.* 30: 97–114, 2004.
72. **Tabruyn SP, Griffioen AW.** Molecular pathways of angiogenesis inhibition. *Biochemical and Biophysical Research Communications* 355: 1–5, 2007.
73. **Tremper-Wells B, Resnick RJ, Zheng X, Holsinger LJ, Shalloway D.** Extracellular domain dependence of PTPalpha transforming activity. *Genes Cells* 15: 711–724, 2010.
74. **Tvorogov D, Wang X-J, Zent R, Carpenter G.** Integrin-dependent PLC-gamma1 phosphorylation mediates fibronectin-dependent adhesion. *Journal of Cell Science* 118: 601–610, 2005.
75. **van der Laan MJ, Hubbard AE.** Quantile-function based null distribution in resampling based multiple testing. *Stat Appl Genet Mol Biol* 5: Article14, 2006.
76. **Vandercappellen J, Van Damme J, Struyf S.** The role of CXC chemokines and their receptors in cancer. *Cancer Letters* 267: 226–244, 2008.
77. **Vandercappellen J, Van Damme J, Struyf S.** The role of the CXC chemokines platelet factor-4 (CXCL4/PF-4) and its variant (CXCL4L1/PF-4var) in inflammation, angiogenesis and cancer. *Cytokine Growth Factor Rev.* 22: 1–18, 2011.
78. **Vindis C, Cerretti DP, Daniel TO, Huynh-Do U.** EphB1 recruits c-Src and p52Shc to activate MAPK/ERK and promote chemotaxis. *The Journal of Cell Biology* 162: 661–671, 2003.
79. **Wang J, Taba Y, Pang J, Yin G, Yan C, Berk BC.** GIT1 mediates VEGF-induced podosome formation in endothelial cells: critical role for PLCgamma. *Arteriosclerosis, Thrombosis, and Vascular Biology* 29: 202–208, 2009.
80. **Werdich XQ, Penn JS.** Src, Fyn and Yes play differential roles in VEGF-mediated endothelial cell events. *Angiogenesis* 8: 315–326, 2005.

81. **Werner S, Grose R.** Regulation of wound healing by growth factors and cytokines. *Physiol. Rev.* 83: 835–870, 2003.
82. **Wu D, Pan W.** GSK3: a multifaceted kinase in Wnt signaling. *Trends Biochem. Sci.* 35: 161–168, 2010.
83. **Xie Y, Pan W, Khodursky AB.** A note on using permutation-based false discovery rate estimates to compare different analysis methods for microarray data. *Bioinformatics* 21: 4280–4288, 2005.
84. **Yancopoulos GD, Davis S, Gale NW, Rudge JS, Wiegand SJ, Holash J.** Vascular-specific growth factors and blood vessel formation. *Nature* 407: 242–248, 2000.
85. **Yi M, Schnitzer JE.** Impaired tumor growth, metastasis, angiogenesis and wound healing in annexin A1-null mice. *Proc. Natl. Acad. Sci. U.S.A.* 106: 17886–17891, 2009.
86. **Zhang Y, Wolf-Yadlin A, White FM.** Quantitative proteomic analysis of phosphotyrosine-mediated cellular signaling networks. *Methods Mol. Biol.* 359: 203–212, 2007.
87. **Zhao X, Guan J-L.** Focal adhesion kinase and its signaling pathways in cell migration and angiogenesis. *Adv. Drug Deliv. Rev.* 63: 610–615, 2011.

Chapter 5

Concluding Remarks

5.1.1. Microvascular physiology and the future of tissue engineering

The fundamental need to integrate microvascular research into artificial tissue development is increasingly apparent as tissue engineering itself advances. Tissue engineering is currently limited by the ability to emulate complex processes present in highly metabolic organs such as the liver (3). Thus, establishing the microvascular architecture as the foundation of these tissues will help maintain their survival and function. Already, recent studies have found that lung tissue regeneration requires endothelial cells for initiating signaling pathways for reconstructing alveolar tissue (2). By understanding endothelial cell roles in aiding regeneration of complex organs by vascular remodeling or eliciting start cues, we can advance the field of tissue engineering and perhaps eventually recapitulate full functions of other metabolically demanding organs.

5.1.2. Applications, limitations, and future work with primary differentiated LSEC cultures *in vitro*

In Chapter 2, our work with liver SEC investigates methods to meet these goals. The use of differentiated endothelial cell types inherent in organs versus generic vascular endothelial cells must be emphasized here; the use of endothelial cells not indigenous to the organs being constructed can be detrimental by issuing the wrong cues and interactions with the parenchymal cells. Serum-free culture medium for LSEC maintenance is an important finding, particular in applications towards tissue engineering. Serum itself present many unknown and uncontrollable variables such as levels of growth factors and molecules that could elicit negative responses or tissue rejection if it is not completely cleared from a tissue prior to grafting or implantation. The discovery that FFAs can support LSEC biology simplifies some of the potential clinical pitfalls that many engineered tissues encounter with biocompatibility.

The lipid supplementation to LSEC cultures however, is not without its limitations. For example, although lipids help sustain LSEC, we have found that the same concentrations are toxic to hepatocytes. This may limit the integration of LSEC monocultures *in vitro* into a structured vasculature for hepatocytes, as the survival of LSEC impinge on that of hepatocytes (4). The issue of lipotoxicity (or metabolic syndrome) can be encountered in tissues other than liver, such as the heart or pancreas (6-8). These limitations themselves are an interesting area of study, and can these culture techniques can be applied to studying the pathological phenomena as it occurs *in vivo*, such as fatty liver disease and steatosis (1, 5).

5.1.3. Applications, limitations, and future work of molecular pathways for inflammatory angiogenesis

In Chapter 3, we explored different methods to obtain physiologically relevant signaling data regarding angiogenesis. Previous work and literature have explored intracellular mechanisms of angiogenesis with a small sampling and focus of proteins. Those that have attempted to survey the signaling topology have utilized two-dimensional cultures on very stiff substrates. To our knowledge, no previous literature exists on exploring broad coverage of signaling pathways in collagen gel cell cultures. We have successfully developed protocols to obtain measurable lysates from three-dimensional culture systems.

In Chapter 4, optimization of lysate collection from collagen gels enabled us to capture a glimpse of how a large number of proteins in intracellular signaling pathways are modulated in angiogenesis and its inhibition by PF-4. The data that we have collected can be instrumental in decoding how angiogenesis occurs in inflammatory environments, as no *in vivo* vascular remodeling system occurs with strictly pro-angiogenic cues. Our conclusions on how PF-4 affect angiogenesis by modulating cell migration pathways can be applied to deriving a detailed mechanistic understanding of inflammatory angiogenesis in wound healing. These data and conclusions can also be applied to predictions on how vascularized, artificial tissues will respond once they are implanted into a host.

We have acquired expansive coverage of signaling cascades and crosstalks involved with angiogenesis using mass spectrometry. We have only analyzed a small subset of the data that we

obtained; further analysis and modeling will unquestionably provide more understanding to the intracellular pathways and crosstalk involved in angiogenesis. Even though signaling data is missing from certain time points, computation models and simulations have the ability to help fill in gaps and provide more in-depth analyses and predictions. Linking these cue-signal data with appropriate cue-response data in the endothelial sprouting assay will also help flesh out PF-4 and VEGF interactions. In broader perspectives, the protocols that we generated can be applied to study intracellular mechanisms in other systems where three-dimensional scaffolds are crucial for phenotypic behaviors, such as *in vitro* invasion assays to study tumor metastasis in a controlled environment.

While we overcame obstacles dealt with using more physiologically relevant culturing conditions in mass spectrometry, we did so at the expense of signal quality and resolution. With the breadth of coverage that mass spectrometry provides when sampling the phosphoprotein signaling landscape, our initial cellular protein concentrations available for assaying are much lower than typical samples. Most of the signaling data we acquired for protein identification and validation were only one or two orders of magnitude higher than background signal.

Thresholding of real signals was exacerbated by the process of lysate collection from collagen gels, as both dilution and collagen contamination contribute to this loss. The presence of serum in our cultures also increases the background signal, decreasing our signal resolution when validating peaks in our samples. We do not obtain the same volume of data that is collected from samples grown on tissue culture plastic; indeed, we observe almost a three-fold reduction in phosphoprotein coverage to keep our level of physiological relevance.

5.1.4. Conclusion

In the end, the work here explores and reveals more of the foundations for incorporating microvasculature into tissue engineering. We first enable the culture of differentiated endothelial cells inherent to the liver, a complex metabolic organ. Second, we developed protocols for examining signal transduction pathways necessary for angiogenesis as well as potential proteins of interest to modulate their behavior. These studies help elucidate mechanisms for maintaining and promoting endothelial cells phenotypes *in vitro*, and its applications can propel the field of tissue engineering further.

5.2. References

1. **Canbay A, Bechmann L, Gerken G.** Lipid metabolism in the liver. *Z Gastroenterol* 45: 35–41, 2007.
2. **Ding B-S, Nolan DJ, Guo P, Babazadeh AO, Cao Z, Rosenwaks Z, Crystal RG, Simons M, Sato TN, Worgall S, Shido K, Rabbany SY, Rafii S.** Endothelial-Derived Angiocrine Signals Induce and Sustain Regenerative Lung Alveolarization. *Cell* 147: 539–553, 2011.
3. **Kaullly T, Kaufman-Francis K, Lesman A, Levenberg S.** Vascularization--the conduit to viable engineered tissues. *Tissue Eng Part B Rev* 15: 159–169, 2009.
4. **Malhi H, Bronk SF, Werneburg NW, Gores GJ.** Free fatty acids induce JNK-dependent hepatocyte lipoapoptosis. *J. Biol. Chem.* 281: 12093–12101, 2006.
5. **Malhi H, Gores GJ, Lemasters JJ.** Apoptosis and necrosis in the liver: a tale of two deaths? *Hepatology* 43: S31–44, 2006.
6. **Navina S, Acharya C, Delany JP, Orlichenko LS, Baty CJ, Shiva SS, Durgampudi C, Karlsson JM, Lee K, Bae KT, Furlan A, Behari J, Liu S, McHale T, Nichols L, Papachristou GI, Yadav D, Singh VP.** Lipotoxicity causes multisystem organ failure and exacerbates acute pancreatitis in obesity. *Sci Transl Med* 3: 107ra110, 2011.
7. **Unger RH, Clark GO, Scherer PE, Orci L.** Lipid homeostasis, lipotoxicity and the metabolic syndrome. *Biochim. Biophys. Acta* 1801: 209–214, 2010.
8. **Wende AR, Abel ED.** Lipotoxicity in the heart. *Biochim. Biophys. Acta* 1801: 311–319, 2010.

Appendix A

Abbreviations

AA	amino acid
Abl1	v-abl Abelson murine leukemia viral oncogene homolog 1
AMP	adenosine monophosphate
ANOVA	analysis of variance
ANXA1	annexin I
BCA	bicinchoninic acid
BCAR-1	breast cancer anti estrogen resistance 1
BrdU	5-bromo-2'-deoxyuridine
BSA	bovine serum albumin
cdc2/cdk1	cell division cycle 2 protein/cyclin dependent kinase 1
CID	collision induced dissociation
Crk	proto-oncogene c-Crk
CXCL4L1	platelet factor 4 variant 1
CXCR3	CXC Receptor 3
Dex	dexamethasone
Di-I-Ac-LDL	dioctadecyl 3,3,3',3' tetramethylindo carbocyanine perchlorate labeled acetylated LDL
DMEM	Dulbecoo's modified essential medium
DMSO	dimethyl sulfoxide
DNA	deoxyribonucleic acid
DTT	dithiothrietol
DYRK1B/Mirk	dual-specificity tyrosine-(Y)-phosphorylation regulated kinase
EBM-2	endothelial basal medium 2
ECL	enhanced chemiluminescence
ECM	extracellular Matrix
EDTA	ethylenediaminetetraacetic acid
EdU	5-ethynyl-2'-deoxyuridine
EGFR	epidermal growth factor receptor
EGM-2MV	endothelial growth medium 2 (microvascular)
EGTA	ethylene glycol tetraacetic acid
EphA2	ephrin receptor A2
ERBB2IP	ERBB2 interacting protein
ERK	extracellular-signal-regulated kinase
ESI	electrospray ionization
FABP	fatty acid binding protein
FAK	focal adhesion kinase

FBS	fetal bovine serum
FDA	Food and Drug Administration
FDR	false discovery rate
FFA	free fatty acids
FGF	fibroblast growth factor
FGR	Gardner-Rasheed felinse viral oncogene homolog
FWE	family wise error
Fyn	protein-tyrosine kinase fyn
GAPDH	glyceraldehyde 3-phosphate dehydrogenase
GPCR	G-protein coupled receptors
Grb2	growth factor receptor-bound protein 2
GSK	glycogen synthase kinase
HCD	higher-energy collisional dissociation
HDMVEC	human dermal microvascular endothelial cell
HEPES	4-(2-hydroxyethyl)-1-piperazineethanesulfonic acid
HGM	hepatocyte growth medium
Hsp	heat shock protein
Hyd	hydrocortisone
I-TAC	CXCL11
INPP5D	phosphatidylinositol-3,4,5-triphosphate 5 phosphatase 1
INSR	insulin receptor
IP	immunoprecipitation
IP-10	interferon- γ inducible protein 10
ITK	IL2-inducible T-cell kinase
JNK	c-Jun N-terminal kinase
LC/MS/MS	liquid chromatography tandem mass spectrometry
Lck	lymphocyte-specific protein tyrosine kinase
LDL	low density lipoprotein
LPC	lysophosphatidylcholine
LSEC	liver sinusoidal endothelial cell
Lyn	Yamaguchi sarcomal viral oncogene homolog (v-yes-1)
m/z	mass to charge ratio
MEK1/2	mitogen-activated protein kinase kinase
Mig	CXCL9
MPZL1	myelin protein zero-like 1 isoform a
MS	mass spectrometry
MTT	3-(4,5-Dimethylthiazol-2-yl)-2,5-diphenyltetrazolium bromide
MW	molecular weight
NaOH	sodium hydroxide
NCK1	non-catalytic region of tyrosine kinase adaptor protein 1
OA	oleic acid
OPTN/SRTR	Organ Procurement and Transplantation Network/ Scientific Registry of Transplant Recipients

PBS	phosphate buffered saline
PBS-T	0.1% Tween-20 in PBS
PC	phosphatidylcholine
PCNA	proliferating cell nuclear antigen
PDGF	platelet derived growth factor
PDGFRB	PDGF receptor, beta-type
PECAM-1/CD31	platelet endothelial cell adhesion molecule 1/Cluster of Differentiation 31
PF-4	platelet Factor 4
PHx	partial hepatectomy
PI3K	phosphatidylinositol 3-kinase
PKA	protein kinase A
PKB/Akt	protein kinase B
PKC	protein kinase C
PLC γ	phospholipase C γ
PMA	phorbol myristate acetate
PMSF	phenylmethanesulfonylfluoride
PRAG	pragmin
PRKDC	protein kinase, DNA-activated, catalytic polypeptide
PTB	phosphotyrosine-binding domain
PTEN	phosphatase and tensin homolog
PTPRA	protein tyrosine phosphatase, receptor type A (PTP α)
SE-1	sinusoidal endothelial 1 antigen
SEM	scanning electron microscopy
SH2	Src homology 2
SHC1	SHC transforming protein 1
SHP2	tyrosine phosphatase non-receptor type 11
TGF- β	transforming growth factor β
Thr	threonine
TYK2	tyrosine kinase 2
Tyr	tyrosine
VEGF	vascular endothelial growth factor
VEGFR	VEGF receptor

Store aliquots at -20°C

Sodium selenite

Sigma # S-9133

Purchase 1.0 mg

Reconstitute in 50 ml sterile MilliQ water to 20 ug/ml

Make 200 ul aliquots

Store aliquots at -20°C

Insulin, human

Sigma # I-9278

Purchase 10 ml 10 mg/ml solution

Make 300 ul aliquots

Store aliquots at -20°C

Dexamethasone

(Dex MW = 392.47)

Sigma # D-8893

Purchase 1.0 mg

Reconstitute in 1 ml EtOH using sterile syringe and needle to fully dissolve powder, add 19 ml sterile PBS to 50 ug/ml (127 uM)

Make 450 ul aliquots

Store aliquots at -20°C

Hydrocortisone

(Hyd MW = 362.46 g/mol)

Sigma # H-0135

Purchase 1.0 mg

Reconstitute in 1 ml EtOH using sterile syringe and needle to fully dissolve powder, add 19 ml sterile PBS to 50 ug/mL (138 uM)

Make 450 uL aliquots

Store aliquots at -20°C

Gentamicin

Sigma # G-1397

Purchase 100 ml 50 mg/ml solution

	<p>Make 550 ul aliquots Store aliquots at 4°C</p>
Transferrin, from human serum	<p>Roche # 10652202001 Purchase 20ml 30 mg/ml solution Dilute 20 ml in 100 ml sterile MilliQ water to 5 mg/ml Make 550 ul aliquots Store aliquots at -20°C</p>
VEGF-165, recombinant human	<p>R&D Systems #293-VE/CF Purchase 10 or 50 ug (293-VE-10 or 293-VE-50) Dilute 10 ug in 200 uL of 0.1% BSA 1x PBS or 50 ug in 1000 uL of 0.1% BSA 1x PBS to 50 ug/mL stock Make 28 uL aliquots Store aliquots at -20°C</p>
L-Ascorbic Acid	<p>Dilute 50 mg in 1 mL milliQ water to 50 mg/mL Sterile filter and make into 12 uL aliquots (250 mM stock concentration) Take 1 aliquot – add 10 uL to 10 mL sterile PBS Make 200 uL aliquots (250 uM stock concentration) Store aliquots at -20°C</p>
Lipid Concentrate	<p>Gibco # 11905 100 mL Make 1.5 mL aliquots Store aliquots at 4°C under head of nitrogen gas</p>
Fetal Bovine Serum	<p>Hyclone #SV-30014.03 Make 1 mL aliquots Store aliquots at -20°C</p>

Protocol

Add dry, weighed supplements to 500 ml DMEM.

L-Proline	0.015 g	0.030 mg/ml final
L-Ornithine	0.050 g	0.100 mg/ml final
Niacinamide	0.153 g	0.305 mg/ml final
D-(+)-Glucose	0.500 g	2.250 mg/ml final (base DMEM has 1.0 mg/ml)
D-(+)-Galactose	1.000 g	2.000 mg/ml final
BSA	1.000 g	2.000 mg/ml final
Phosphoethanolamine	0.0141 g	0.2 mM final
Heparin	0.010 g	20 ug/mL final

Add non-sterile liquid supplements

Ethanolamine	6 ul	0.2 mM final
--------------	------	--------------

Allow supplements to fully dissolve into media for 10-30 min. Use 4 degrees C nutator to help expedite the process.

Sterile filter media in tissue culture hood. Thaw and add sterile aliquots to sterile-filtered media.

L-glutamine	2.5 ml	1.0 mM final	1:200 dilution
Sodium selenite	125 ul	5.0 ng/ml final	1:4000 dilution
Insulin	250 ul	5.0 ug/ml final	1:2000 dilution
Dexamethasone	400 ul	0.1 uM final	1:1250 dilution or
Hydrocortisone	400 ul	~0.110 uM final	1:1250 dilution
Gentamicin	500 ul	50 ug/mL final	1:1000 dilution
Transferrin	500 ul	5.0 ug/ml final	1:1000 dilution

Centrifugation media (Percoll isolation) (40 mL)

EDTA	40 ul	1 µM final
------	-------	------------

L-Ascorbic Acid	16 uL	100 nM final	1:2500 dilution
-----------------	-------	--------------	-----------------

Seeding media (10 mL)

rhVEGF-165	5 uL	25 ng/mL final	1:1000 dilution
L-Ascorbic Acid	4 uL	100 nM final	1:2500 dilution
FBS	200 uL	2% final	1:100 dilution

Right before use of culture media, to smaller media aliquots of 10 mL add:

rhVEGF-165	10 uL	50 ng/mL final	1:1000 dilution
CD Lipid Concentrate	10 uL	0.1% solution	1:1000 dilution
L-Ascorbic Acid	4 uL	100 nM final	1:2500 dilution

Storage:

Base media can be kept for up to 4 weeks.

Following addition of lipids and ascorbic acid, best to use media within 3-4 days, as half-life of ascorbic acid is 7 days at 4°C.

B.2. Primary Liver Sinusoidal Endothelial Cell Isolation

Adapted from protocols by Albert Hwa (2005), Ajit Dash (2007), and Braet et al. *Lab Inv.* 70(6): 944-952 (1994).

Materials: Calcium and magnesium free PBS (Gibco 10010-031); 2X PBS (diluted from 10X); Percoll (Sigma-Aldrich P-4937); modified HGM; EGM-2 (Lonza CC-3162); Hoechst 33342 (Molecular Probes / Invitrogen H-3570); Sytox Orange (Molecular Probes / Invitrogen S11368); EDTA (Sigma E6758) cell culture tested; Fetal Bovine Serum (Hyclone #SV-30014.03)

*Perfusion can be performed with Blendzyme flow at 15 mL/min or at 25 mL/min; the lower flow rate can potentially give higher yields (25 to 60E6 cells) than the faster flow rate (15 to

40E6 cells).

**Addition of 1 μ M EDTA to PBS and base medium may increase potential yields, however do note that pH change can drastically affect cell numbers and viability.

1. While the perfusion occurs, create 30 mL of 25% and 50% Percoll solutions. The 25% Percoll solution is made by using 7.5 mL Percoll + 7.5 mL 2X PBS + 15 mL 1X PBS with EDTA. The 30% Percoll solution is made with 15 mL Percoll + 15 mL 2X PBS with EDTA.

2. Following the perfusion, spin down the cells for 3 minutes at 50 x g at 4 degrees Celsius. Repeat twice. Save the supernatant from both spins. If being assisted, Percoll layering can be initiated at this time (or at the time the liver is removed during the perfusion). This will allow reduction in waiting times between steps.

3. Equally split the 25% Percoll solution into two 50 mL centrifuge tubes. Use a 10mL pipette and draw up to the red line with 50% Percoll solution. This should be approximately 14.5 mL. Do not wet the cotton inside the pipette tip. Taking the 10 mL pipette, lower the tip slowly to the bottom of the centrifuge tube. Raise the tip a bit from the bottom so that flow will not be blocked. [Lay the tip of the pipette a little above the v-rise at the bottom of the tube]

4. Slowly load the 50% Percoll underneath the 25% Percoll to obtain two distinct layers. Approximate unloading of the pipette should be about 1 mL every 10-15 seconds.

5. Spin the supernatant following the two 50 x g spins again at 50 x g for 3 minutes, but at room temperature. Take the supernatant and discard the pellet.

6. Spin the supernatants at 100 x g for 5 minutes to remove the rest of the parenchymal cells. All centrifugation from here on should be performed at room temperature to optimize cell viability (reduce thermal shock). Reserve the supernatant and discard the pellets.

6. Spin the remaining supernatant at 350 x g for 10 minutes. The supernatant is discarded. Resuspend the pellet of enriched endothelial cells in 20 mL of modified HGM or EGM-2 with 1

μ M EDTA.

7. Slowly load the 10 mL of cell suspension into both Percoll layered tubes, on top of the 25% Percoll. This can be done by wetting the wall and moving the pipette alongside the wall to release the liquid so that it slowly trickles down the wall from different points, reducing the interruption and break to the surface tension. Rate can be done at about 1 mL every 10-15 seconds.

8. Gently load the tubes into the centrifuge without disturbing the Percoll layers. Set brake to 0 and acceleration to 1. Spin at 900 x g for 20 minutes (can range from 18-22 minutes; note that the longer it spins, the more likely endothelial cells will move into the 50% Percoll layer).

9. The intermediate zone should be collected (5 ml above and below the layer line), which should be rich in LECs. Aspirate off the layers until liquid measures at 20 mL in the tube. Collect the cell layer and liquid until 10 mL is left.

10. Add equal amount of base modified HGM (or EGM-2) to the tube (20 mL to 20 mL). Set brake to 6 and acceleration to 9 (as we do not need to worry about disturbing Percoll layers anymore). Spin the suspensions at 950 x g for 15 minutes.

11. Aspirate the supernatant, break-up the pellet and resuspend in 10 mL of modified HGM (or EGM-2) with 2% FBS. If higher cell density is desired, resuspend in 5 mL of media.

12. Take 900 uL of modified HGM (or EGM-2), 2 uL Hoechst, 2 uL Sytox Orange, and 100 uL of cell suspension and count in Hemacytometer using DAPI filter (Hoechst 33342) and rhodamine filter (Sytox Orange). Nucleic acids of dead cells fluoresce bright orange while Hoechst nuclei show up as blue. Sytox Orange/Nuclei complexes have absorption and fluorescence emission maxima of 547 nm and 570 nm respectively.

OPTIONAL:

13. *Pipette the suspension into a 6 well plate (~1.75 mL each well) or into a large Petri dish and*

let cells sit for 10-20 minutes inside an incubator to allow selective attachment of Kupffer cells.

14. Remove the supernatant from the wells and mix thoroughly. Repeat cell count if desired.

15. Cells are ready for use.

Appendix C

Phosphotyrosine enriched mass spectrometry protocol

Adapted from White Lab protocols.

C.1. Buffer solutions

Ammonium acetate buffer: 100 mM ammonium acetate (pH to 8.9 with ammonium hydroxide)

Elution buffer: 250 mM monosodium phosphate (NaH_2PO_4) buffer (pH to 8.0)

EDTA solution: 100 mM EDTA (pH to 8.9)

Acetonitrile solutions: 100%, 80% acetonitrile/20% isopropanol

Iron(III) Chloride: 100 mM (162.2 g/mol) in milliQ H_2O

Organic rinse: 100 mM sodium chloride, 25% acetonitrile, 1% acetic acid

IP buffer: 100 mM Tris (pH 7.4), 0.3% NP-40

iTRAQ IP buffer: 100 mM Tris (pH 7.4), 1% NP-40

IP Rinse buffer: 100 mM Tris (pH 7.4)

IP Elution buffer: 100 mM glycine (pH 2-2.5)

C.2. Chemical modification and digestion

1. Make a fresh solution of 1M DTT (Sigma D0632) in 100 mM ammonium acetate buffer (pH = 8.9). Use at 1:100 to get final concentration of 10 mM DTT.
2. Vortex samples and incubate in 56°C water bath for 1 hour.
3. Prepare a fresh solution of 800 mM iodoacetamide (Sigma I1144) in ammonium acetate buffer (pH = 8.9). Use at 1:14.5 to get final concentration of 55 mM iodoacetamide.
4. Incubate at room temperature, with tubes wrapped in foil (to protect from light) on a nutator for 1 hour.
5. Add sequence grade trypsin (Promega V5113) at 1:50 to 100 mM ammonium acetate buffer (pH = 8.9). Buffer volume should be around two times the sample volume when at step 4 (e.g. 5 mL, add 10 mL).
6. Incubate at room temperature on the nutator overnight, making sure to protect from light.

7. End digestion by adding 1 mL of glacial acetic acid.
8. Samples are frozen at -80°C.

C.3. Sep-Pak, Speed-Vac, and lyophilization

1. Thaw out samples from above steps. Centrifuge samples for 5 minutes to pellet particulates which might clog Sep-Pak columns.
2. Precondition the Sep-Pak columns with solutions in the following order:
 - 10 mL 0.1% acetic acid at a rate of 2 mL/min
 - 10 mL of 90% acetonitrile and 0.1% acetic acid at a rate of 2 mL/min
 - 10 mL of 0.1% acetic acid at a rate of 2 mL/min

*Wet the Sep-paks before placing back on the syringe (reduces introduction of air bubbles)
3. Load sample on Sep-Pak columns at a flow rate of 1 mL/min
4. Rinse column with 10 mL acetic acid at a flow rate of 2 mL/min
5. Elute and collect peptides with acetonitrile. Do not wet before this step; wetting will change solvent concentration and loss of sample may occur.
 - a. Elute the first fraction with 25% acetonitrile in 0.1% acetic acid at a flow rate of 0.1 mL/min.
 - b. Elute the second fraction with 40% acetonitrile in 0.1% acetic acid at a flow rate of 0.1 mL/min.
6. Speed-Vac samples to reduce volume. This will take roughly 4 or 5 hours until volume is about 3-4 mL.
7. Split samples into two aliquots. Speed-Vac for 1 hour.
8. Snap freeze samples in liquid nitrogen or freeze the samples at -80°C for at least two hours. It does not matter as long as samples are solidly frozen.
9. Make sure sample tubes are opened slightly and place into lyophilizing chamber. Leave sample to lyophilize overnight.
10. Store lyophilized samples at -80°C.

C.4. 8-plex iTRAQ labeling

1. Dissolve lyophilized samples in 60 μL dissolution buffer (iTRAQ kit, also known as 0.5 M triethylammonium bicarbonate (TEAB, $\text{N}(\text{Et})_3\text{HCO}_3$). Samples should turn light pink.
2. Vortex each sample for 1 minute and spin at 13,400 rpm for 1 minute.
3. Add 70 μL isopropanol to each iTRAQ vial. Vortex each vial for 1 minute and spin at 13,400 rpm for 1 minute. Since there is high collagen content in samples, use two iTRAQ vials for each sample.
4. Transfer iTRAQ reagents to appropriate sample tubes. Vortex each sample for 1 minute and spin at 13,400 rpm for 1 minute.
5. Incubate samples at room temperature for 2 hours.
6. Speed-Vac samples to 30 μL . This should take roughly 20-30 minutes.
7. Aliquot 560 μL of 25% acetonitrile with 0.1% acetic acid solution into an eppendorf tube.
8. Combine all samples into a single tube. Use a single pipette tip to avoid sample loss.
9. Add 40 μL 25% acetonitrile with 0.1% acetic acid solution to each empty tube, vortex for 1 minute and spin at 13,400 rpm for 1 minute. Add the rinses to each sample. Again, use a single pipette tip to avoid sample loss.
10. Repeat rinse step.
11. Speed-Vac the samples until they are dry (6-8 hours or overnight). Samples can be stored at -80°C , or immediately processed for phosphotyrosine IP.

C.5. Phosphotyrosine peptide IP

1. Use 20 μL protein G agarose beads per 12 μg antibody
2. Wash 60 μL protein G agarose (calbiochem IP08) with 300 μL IP buffer (100 mM Tris-HCl, 0.3% NP-40, pH 7.4)
3. Combine in an eppendorf tube and centrifuge for 5 minutes at 6500 rpm.
4. Remove supernatant and add 300 μL IP buffer.
5. Add 12 μL 4G10 (Millipore), 12 μL PY100 (CST), and 12 μL PT66 (Sigma-Aldrich) to protein G agarose.
6. Allow mixture to incubate at 4°C on a rotor for 6-8 hours.
7. Spin down the mixture at 6500 rpm for 5 minutes at 4°C .
8. Remove and discard the supernatant.

9. Wash the beads with 400 μ L IP buffer. Let them sit in buffer for 5 minutes on rotor.
10. Spin down the beads at 6500 rpm for 5 minutes.
11. Resuspend Speed-Vac pellets in 150 μ L iTRAQ IP buffer (100 mM Tris-HCL, 1% NP-40, pH 7.4) and 400 μ L iTRAQ IP buffer. Vortex until all of the sample is dissolved.
12. Spin down the sample to ensure all are in the solution
13. Check to pH to see if it is close to 7.4 and compare with IP buffer. If pH is slightly lower, add \sim 5 μ L of Tris buffer (pH 8.5, 500 mM). iTRAQ labeled samples tend to be lower in pH.
14. Remove supernatant from beads and add samples.
15. Incubate the sample with beads overnight on the rotor at 4°C.
16. Centrifuge at 6500 rpm for 5 minutes at 4°C.
17. Save supernatant for total protein normalization and store at -80°C.
18. Wash the beads with 400 μ L iTRAQ IP buffer and then 400 μ L rinse buffer (100 mM Tris HCl, pH 7.4) for 5 minutes on the rotor.
19. Centrifuge at 6500 rpm for 5 minutes at 4°C.
20. Discard supernatant.
21. Repeat 2 more times (total of 4 times with 1st time using iTRAQ IP buffer).
22. Add 70 μ L IP elution buffer (100 mM glycine, pH 2-2.5) with 10 μ L acetonitrile and incubate on a rotor for 30 minutes at room temperature.
23. Prepare eluate for loading onto IMAC column.

C.6. IMAC enrichment of phosphotyrosine peptides using Ni-NTA agarose conjugates

1. Rinse 100 μ L Ni-NTA slurry (50 μ L resin) (Qiagen 30410) with 800 μ L MilliQ H₂O. 25 μ L of NTA resin enriches a total of 200 μ g cell lysate.
2. Centrifuge at 6500 rpm for 1 minute.
3. Remove supernatant.
4. Repeat two more times.
5. Strip nickel from the resin with 800 μ L 100 mM EDTA (pH 8.0). Incubate for 30 minutes at room temperature on a nutator.
6. Rinse residual nickel away with 800 μ L milliQ H₂O.
7. Repeat two more times.
8. Apply 800 μ L of 100 mM iron chloride solution and incubate for 30-45 minutes.

9. Wash beads with 800 μ L MilliQ H₂O three times.
10. Wash beads with 800 μ L 0.1% trifluoroacetic acid (TFA).
11. Resuspend beads in 50 μ L 0.1% TFA
12. Acidify the phosphotyrosine eluate (70 μ L) with 10 μ L 10% TFA before adding to the iron chelated resin. Incubate for 30-60 minutes at room temperature on a nutator.
13. Wash twice with 400 μ L 0.1% TFA
14. Wash twice with 400 μ L 0.1% acetic acid. This will remove TFA before MS analysis.
15. Elute into 40 μ L 250 mM sodium phosphate buffer (pH 8.0)
16. Incubate at room temperature for 30 minutes prior to directly loading eluate onto acidified precolumn.

Appendix D

LTQ Orbitrap MS Spectra Validation Protocol

These protocols require Xcalibur and Mascot software.

D.1. Spectra Validation Set-Up

- 1) Pull up Xcalibur and Qual Browser
- 2) Make sure the green tack is on the bottom window, jump to the scan number of interest.
- 3) Print out the spectra, write the name and sequence on the spectra printout.
 - a. Check to see if the spectra was collected in CID or HCD.
 - i. CID will have more background/lower resolution as it is collected via quadrupole MS away from the C-trap while HCD is collected on the Orbitrap magnet near the C-trap and will have higher resolution but more background in higher m/z. Make note of CID or HCD
 - b. Check the NL value: if it is E2 or higher, proceed. If below E2, discard due to high background.
 - c. You can also print out the peaks that are above 10% for that spectra. On the toolbar, there is a button to “View Spectrum List.” Click that and then go to Display options and set for viewing between 10 and 100% of highest peak.
- 4) Go to corresponding Mascot search. Match Query to Scan number. Scan number will be listed in the Query as “Finnegan Scan Number”
 - a. Take note of the Molecular Weight and reported molecular weight and charge (m/z, z) next to the full MW.
 - b. In the Select Summary Report tab, place the mouse cursor over the specific query that matches the Finnegan Scan number. Observe **all** significant underlined amino acids – these should also be underlined (use notation to dictate rank) in the sequence written on the spectra printout.
 - i. There may be more than one phospho-site present on that peptide sequence.

- ii. Neutral loss of a phosphate group may be important in matching y and b ions, as values will be shifted as a result, especially if MS-Product is used to find theoretical peaks.
- 5) Go back to Qual Browser
 - 6) Check preceding survey scan of full MS at the specific m/z point. Make sure that there are clean peaks and that only one peak lies within ± 0.5 Da (m/z) of that point.
 - a. If there are other peaks, they are only acceptable if they are 1/z distance away. These are part of the isotope series. For example, if z is +3, then the peaks will be 0.33 separated, +4 will be 0.25, etc. If peaks are exactly 1 away, they are junk, as are most likely charge from amino acids (like Arg, Lys).
 - b. If this is a peptide that has been assigned a pY, check the full MS scan for a peak at ~ 216.04 m/z. This is a pY ammonium ion and is present if you truly have phospho-tyrosine in samples.
 - c. In the case that there are other peaks within the 0.5 Da range, they can be ignored if they are $\ll 10\%$ of the peak that is being taken for analysis.
 - 7) Start assigning y and b ions (use MASCOT query to do initial assignments).
 - a. The MASCOT query will give a good assessment of whether the assignment is real or not; if the y and b ions are consistently in bold red (not too many gaps in the sequence), then it is highly likely that the peptide is correctly assigned.

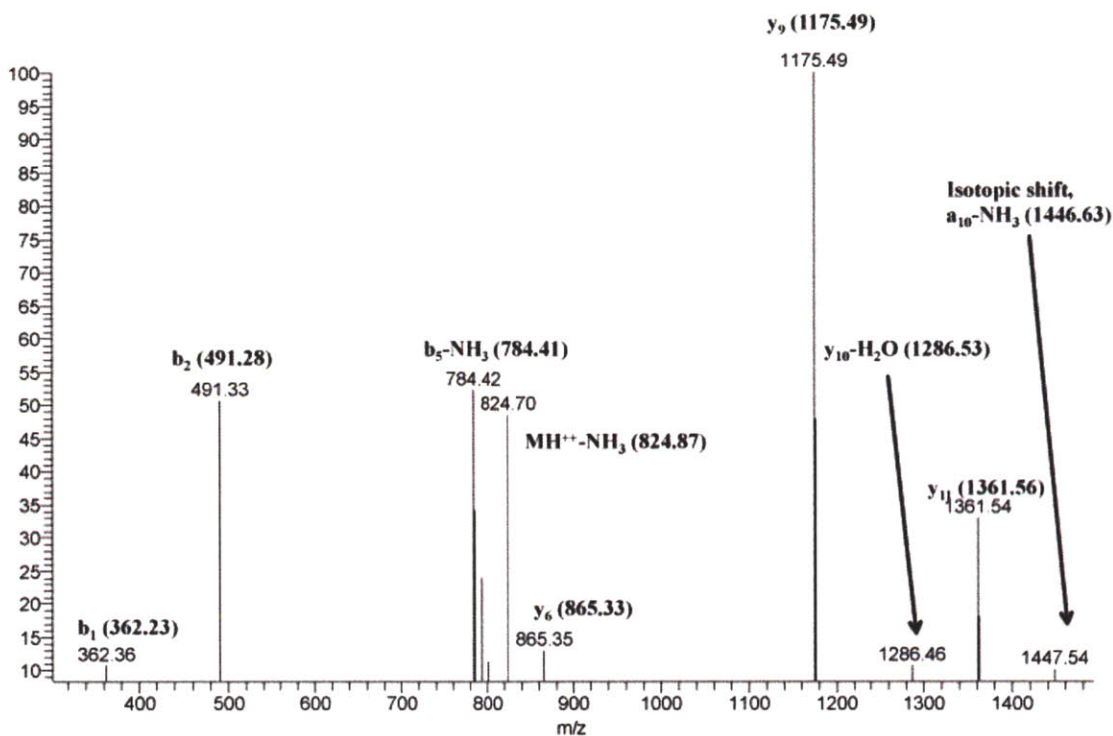


Figure D-1. Sample spectra of GSK3 β . Peak values in spectra are normalized to most abundant ion (here, the y₉ ion). b, y, and a ions are assigned to peaks that have above 10% of the intensity of the largest peak. An isotopic shift of 1 m/z is observed for the a₁₀ ion.

D.2. RULES FOR ASSIGNING PEAKS

- 1) **CARDINAL RULE: MUST ASSIGN ALL PEAKS THAT ARE ABOVE 10% OF THE MAXIMUM PEAK MEASURED.**
 - a. The cardinal rule can be relaxed for spectra that have a lower NL ($\leq E3$). If spectra around the 10% cutoff for these cannot be assigned, they can potentially be ignored (as long as the higher intensity peaks are all assigned). GSK3 β spectra is included as an example (Figure D-1).
- 2) Resolution of peaks may be off from reported peaks for y and b ions. Use personal judgement to assign peaks.
 - a. If collected on CID, the mass may not be as accurate, and can be off slightly.
 - b. If collected on HCD, the peaks must be accurate and easily assigned (above 121 m/z). If the m/z values are not, toss this spectra immediately.

- c. If the peak on the spectra being evaluated is low and close to the 10% cutoff, there will potentially be increased error and less resolution (up to 1 Da)
 - d. Spectra error should be within 10 ppm. However, due to the lower resolution of CID, as well as lower signal from these samples (primary HDMVEC on collagen gels), some samples may be off by more than 10 ppm (Sometimes up to 100-200 ppm).
 - e. The peaks may also be up to 1 Da off from the reported table of values. This may be a result if you observed some of the isotope series being within the 0.5 Da range on the full MS precursor survey scan (step 6a of the validation set-up).
 - i. The reasoning is that although we see peaks in QualBrowser, they are actually Gaussian curves with the average represented by the peak. Thus, there may be error due to centroid smearing of the peaks.
 - f. MASCOT searches have been set up with an error tolerance of 0.8 Da. If, combined with everything else mentioned above, the peak lies within 1 Da of the reported value, then it can generally be assigned to that y or b (or a) ion. Again, use personal judgement in assigning peaks.
- 3) If y and b ion values are not present in the MASCOT query output, can be attributed to neutral loss.
- a. Loss of Y: - 80 Da
 - b. Loss of S/T: -98 Da
 - c. Loss of water: -18 Da (y^0)
 - d. Loss of ammonia: -17 Da (y^*)
 - e. Loss of carboxyl (CO): -28 Da
- 4) Some peptide sequences will have more than one phosphosite reported in the MASCOT query. The presence of these phosphates may shift peak values for y and b ions and should not be omitted (see set-up step 4b).
- 5) Also note, sometimes y and b ions are doubly charged (b^{++} , y^{++}). In these cases, the actual neutral loss is HALF of the values listed in 2) (e.g., loss of S/T is -49 Da, loss of CO is -14 Da). In some cases, there can be triple and quadruple charge. Divide the neutral loss values in similar fashion.

- 6) Do not use more than 3 distinct losses per peptide. If these are needed, the value assignment is not real and should not be considered.
- 7) IF there are multiple neutral losses that are the same (e.g., 3H₂O), these are potentially real observations, particularly for larger peptides, as may be inherent in the equipment/machinery. Make note of the intensities of the peaks for mid to low NL = E3 to see if there is a pattern.
- 8) If not assignable to y and b ions, peaks **can** be assigned to a ions. Use judgement and discretion for this.
 - a. If none of these work, the parent ion (MH) can be considered, especially if the spectra was picked up in the CID. These values can be found using Protein Prospector. Further neutral losses can be applied to the parent ion than are listed in Protein Prospector.
- 9) If a proline (P) is present in the peptide sequence, there may be internal fragments present in the spectra. This is due to proline's resistance to electron transfers and will create internal fragments rather than the typical y and b ions. For more information on assigning internal fragment peaks, see http://www.matrixscience.com/help/fragmentation_help.html
- 10) For other non-matching y and b ions, they may be due to oxidation during the preparation process, and the presence of a methionine may change the m/z.
- 11) If you are at a loss of potential peaks and fragmentations and have unassigned peaks, you can use Protein Prospector to provide all the potential fragmentations and peaks that would be encountered with a specific peptide sequence. Use MS-Product to find all possible assignments. <http://prospector.ucsf.edu/prospector/cgi-bin/msform.cgi?form=msproduct>
 - a. Be aware of the potential peaks that are being assigned and use personal judgement on what seems plausible.
 - b. For the blanks in the form, fill out the following
 - i. N term: iTRAQ8plex
 - ii. Sequence: peptide sequence of interest
 1. If Lysine or Arginine present (K or R), can be modified by iTRAQ8plex. Simply adjust MW by placing K(iTRAQ8plex) or R(iTRAQ8plex)

2. For phosphorylation or oxidation, use lower case (e.g. phospho-Y is y, phospho-S/T is s/t, oxidation of M is m)
3. Since samples were reduced and alkylated, the cysteines (C) are heavier. Adjust MW by using C(57.03), or C(carbamidomethyl)
- iii. AA sequence: checkmark i and m
- iv. N-term sequence: checkmark a and b
- v. C-term sequence: checkmark y
- vi. Internal fragment: checkmark if you suspect internal fragmentation
- vii. Satellite sequence: checkmark d,v,w
- viii. Neutral loss sequence: checkmark all
- ix. Max charge: Whatever charge was listed in the MASCOT query and ignore basic AA
- x. Max losses: 3
- xi. Masses are: monoisotopic
- xii. Frag tol: 10 ppm
- xiii. Instrument: ESI-FT-ICR-CID
- xiv. Data format: PP M/Z Charge

12) In the MASCOT query, if there are additional S,T, or Y's in the sequence, there is a potential for more 'noise' to occur. Add these additional sequences to MS-Product (under the reported main sequence) to get potential values.

13) *Sometimes there may be unexplained mass shifts due to amino acid mutations. For a full list, see: <http://prospector.ucsf.edu/prospector/html/misc/mutation.htm>.*

14) *Since trypsin was used to cleave peptides, there is a potential for it to appear in the sample. If there are more unexplained peaks, refer to the list of masses and autolysis products here: <http://prospector.ucsf.edu/prospector/html/misc/trypsin.htm>*

15) There appears to be a potential issue with 8-plex and mass shifts in the spectra, primarily on the b ions on the largest N Terminal. There is a shift in mass that is not exactly the mass of the balance group (~300 for 8 plex); the shift may be lower because of internal fragmentation of the balance group. Flag this offset for now and place aside for later evaluation.

- a. Example: the y_{14} of a 14-mer peptide has loss of terminal Y ion in precursor. If charge = +1, loss of 86; +2, loss of 43
- 16) Finally, take note of the iTRAQ quantitation. Even if the protein assignment for the peptide is correct, the scan will be thrown out pending iTRAQ intensity. If the iTRAQ peak for the value that everything is being normalized to (e.g., the master) is missing, it will skew the overall values and increase the error in the output.

D.3. BRIEF OUTLINE OF STEPS

1. Identify scan number. Pull up scan in Qual Browser.
2. Find equivalent query in MASCOT. May be easier to search for ion score following selection by gi accession number if there are multiple queries listed.
3. Print peak list and scan from Qual Browser. Label properly.
4. Check preceding HCD – make sure iTRAQ for normalization is present
5. Check full MS scan to make sure no precursor contamination
6. Check MASCOT list
7. Use Protein Prospector list

Appendix E

Platelet Factor 4 Time Course Data

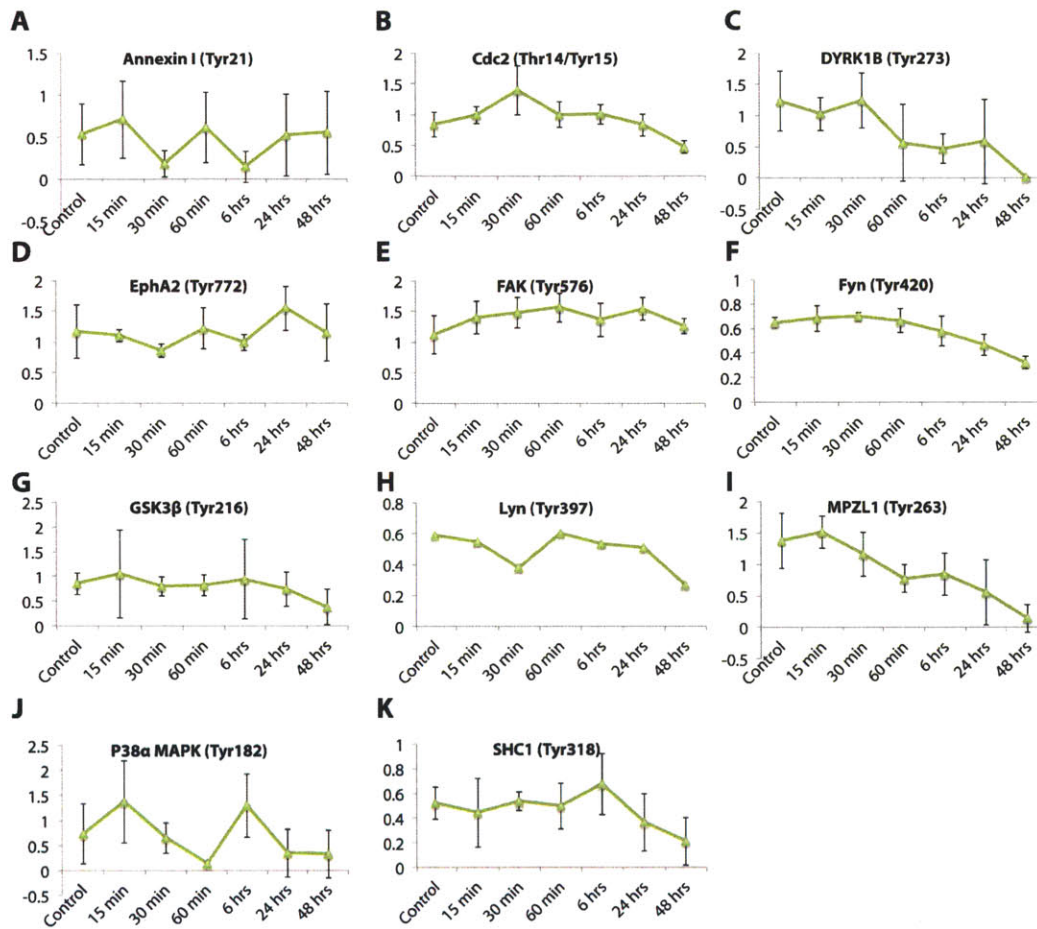


Figure E-1. Time course of PF-4 dosing. Sample treatment conditions were run in parallel with the VEGF ± PF-4 dosing treatments and were normalized to the same master lysate. Most PF-4 only dosing were not statistically significant from the control ($p > 0.05$). In cases where PF-4 was statistically significant ($p < 0.05$), these phosphoprotein measurements were not statistically significant from the VEGF with PF-4 condition ($p > 0.05$).

Appendix F

Correlation network model code and script

importmatrix.m

```
clear all; close all;
clc;

%% Call file and place into array

VEGFfilename = 'Vindnorm.txt';
PF4VEGFfilename = 'PVindnorm.txt';
Labelfilename = 'labelsind.txt';
% PF4filename = input('Input filename #3 of interest (PF-4 matrix) ','s')
%these matrice have the phosphosites as rows, and time course as columns
%V is VEGF, PV is PF-4 + VEGF, and P is PF-4 only
Vdata = dlmread(VEGFfilename);
PVdata = dlmread(PF4VEGFfilename);
% Pgeo = dlmread(PF4filename);

%% Create axes labels (for phosphoproteins)
fid=fopen(Labelfilename);
C=textscan(fid,'%q');
ProteinLabel = C{1};

% %% Generate heat map of differences
% % This is different than the others because what I'm comparing is the
% % correlation of Annexin I time course in VEGF to Annexin I time course in
% % PF-4 + VEGF. This is most likely not to mean anything, as I want to see
% % how things are changing within the system between proteins and this
% % doesn't do that; more like an incorrect comparison.
% [corrcompare, pval] = corr(Vgeo',PVgeo');
% difference = HeatMap(corrcompare, 'colormap', redbluecmap, 'RowLabels',
ProteinLabel, 'ColumnLabels', ProteinLabel);

%% Generate correlation heatmap for V and PV data difference
corrV= corr(Vdata');
corrPV = corr(PVdata');

absdifference = abs(corrV - corrPV);
absdifferencel = tril(absdifference);

% visualize = HeatMap(absdifference, 'colormap', redbluecmap, 'RowLabels',
ProteinLabel, 'ColumnLabels', ProteinLabel, 'Annotate', true, 'AnnotColor',
'k');
% addTitle(visualize, 'Absolute difference of pairwise correlation between
```

```

VEGF and PF-4 + VEGF treatments');

visualize = HeatMap(absdifference1, 'colormap', redbluecmap, 'RowLabels',
ProteinLabel, 'ColumnLabels', ProteinLabel, 'AnnotColor', 'k');
addTitle(visualize, 'Absolute difference of pairwise correlation between VEGF
and PF-4 + VEGF treatments');

% %% Generates correlation heatmap for pairwise correlation of each treatment
condition
%
% mapVgeo = HeatMap(corrVgeo, 'colormap', redbluecmap, 'RowLabels',
ProteinLabel, 'ColumnLabels', ProteinLabel);
% addTitle(mapVgeo, 'Pairwise correlation of VEGF treatment');
%
% mapPVgeo = HeatMap(corrPVgeo, 'colormap', redbluecmap, 'RowLabels',
ProteinLabel, 'ColumnLabels', ProteinLabel);

corrV1 = tril(corrV);
corrPV1 = tril(corrPV);

mapV = HeatMap(corrV1, 'colormap', redbluecmap, 'RowLabels', ProteinLabel,
'ColumnLabels', ProteinLabel);
addTitle(mapV, 'Pairwise correlation of VEGF treatment');

mapPV = HeatMap(corrPV1, 'colormap', redbluecmap, 'RowLabels', ProteinLabel,
'ColumnLabels', ProteinLabel);
addTitle(mapPV, 'Pairwise correlation of PF-4 + VEGF treatment');

```

shufflematrix.m

```

%%%generate random data files from shuffled data
rng('shuffle'); %run this once at the beginning
%%% Call file and place into array
% VEGFfilename = input('Input filename #1 of interest (VEGF matrix) ','s');
% PF4VEGFfilename = input('Input filename #2 of interest (VEGF + PF-4 matrix)
','s');
% Labelfilename = input('Input filename for phosphoprotein list ','s');
% Timefilename = input('Input filename for time course ','s');
% PF4filename = input('Input filename #3 of interest (PF-4 matrix) ','s')
%these matrice have the phosphosites as rows, and time course as columns
%V is VEGF, PV is PF-4 + VEGF, and P is PF-4 only

numiter = 50000; %number of iterations to collect data from

% Vdata = dlmread('Vind.txt');% Vgeo = dlmread(VEGFfilename);
% PVdata = dlmread('PVind.txt');% PVgeo = dlmread(PF4VEGFfilename);
% Pgeo = dlmread(PF4filename);
clear TotalMshuffle Vdatashuffle PVdatashuffle corrVpermute corrPVpermute
rowcol = size(Vdata,1);
timepts = size(Vdata,2);

%% Create structure array to store all permutation values

```

```

storageV = zeros(rowcol,rowcol,numiter);
storagePV = zeros(rowcol,rowcol,numiter);
storageVpval = storageV;
storagePVpval = storagePV;
% storage_diff = storageV;
% storage_diffpval = storageV;

%% Randomly shuffle
for i = 1:numiter
    %Randomly shuffles each of the matrices by the columns (by time)
    %This is done by *first* horizontally concatenating the two data sets
    %This is because the permutation/exact test pools observations of
    %BOTH groups being compared. Since correlation is being compared
    %between VEGF and PF-4+VEGF, time points are pooled together from
    %the two treatments, and randomized, while keeping the data
    %conserved for each protein measured
    TotalM = horzcat(Vdata,PVdata);
    %Then the matrices are shuffled
    TotalMshuffle = shake(TotalM,2);
    %Then the matrices are separated
    Vdatashuffle = TotalMshuffle(1:end,1:timepts);
    PVdatashuffle = TotalMshuffle(1:end,(timepts+1):(2*timepts));

%% Find pairwise correlations and permuted p values
[corrVpermute,pvalVpermute] = corr(Vdatashuffle');
[corrPVpermute, pvalPVpermute] = corr(PVdatashuffle');
[corr_diff_permute, pval_diff_permute] = corr( abs(Vdatashuffle-
PVdatashuffle)');
storageV(:,:,i) = corrVpermute;
storagePV(:,:,i) = corrPVpermute;
storageVpval(:,:,i) = pvalVpermute;
storagePVpval(:,:,i) = pvalPVpermute;
% storage_diff(:,:,i) = corr_diff_permute;
% storage_diffpval(:,:,i) = pval_diff_permute;
end

%% test statistic difference - absolute value - this does the two tailed test
instead of one tailed
storage_diffstat = abs(storageV-storagePV);

%These three matrix are stored in the 'ind permutation distribution.mat' or
%'eml permutation distribution.mat'

```

pvaldiscmatrix.m

```

%generate p values in matrix format corresponding to the correlation
%coefficient matrix (absolute differences)

% %%Phosphoprotein label
%
% fid1=fopen('labelsind.txt');% fid1=fopen(Labelfilename);
% C=textscan(fid1,'%q');
% ProteinLabel = C{1};
% fclose all;
% clear C;

```



```

% syssize = size(storage,1); %size of correlation matrix, 26 for EML
% pval = zeros(syssize,syssize);
% for j = 1:syssize
%     for k = 1:syssize
%         corrval = absdifference(j,k);
%         vector1 = storage(j,k,:);
%         vector1 = squeeze(vector1);
%         clear output
%         output = ge(vector1,corrval);
%         numeratorpval = sum(output);
%         pval(j,k) = numeratorpval/size(vector1,1);
%     end
% end

syssize = size(storage_diffstat,1); %size of correlation matrix
%storageV and storagePV and storage_diff
pvalV = zeros(syssize,syssize);
pvalPV = zeros(syssize,syssize);
pval_diff = zeros(syssize,syssize);
%test the distribution at each position in the matrix
for j = 1:syssize
    for k = 1:syssize
        corrvalV = corrV(j,k);
        corrvalPV = corrPV(j,k);
        corrval_diff = absdifference(j,k);

        %obtaining all possible distributed values from storage at position
        %(j,k) for testing
        vectorV = storageV(j,k,:);
        vectorV = squeeze(vectorV);
        vectorPV = storagePV(j,k,:);
        vectorPV = squeeze(vectorPV);
        vector_diff = storage_diffstat(j,k,:);
        vector_diff = squeeze(vector_diff);

        %Testing where the corrvalues lies, how many in the distribution
        %are greater than that correlation value?
        clear outputV outputPV output_diff
        outputV = ge(vectorV,corrvalV);
        outputPV = ge(vectorPV,corrvalPV);
        output_diff = ge(vector_diff,corrval_diff);

        numeratorpvalV = sum(outputV);
        numeratorpvalPV = sum(outputPV);
        numeratorpval_diff = sum(output_diff);

        %getting the probability out of the total discrete points in the
        %distribution
        pvalV(j,k) = numeratorpvalV/size(vectorV,1);
        pvalPV(j,k) = numeratorpvalPV/size(vectorPV,1);
        pval_diff(j,k) = numeratorpval_diff/size(vector_diff,1);
    end
end
end

```

significantmatrix.m

```
%%Run this after running importing matrix and pvaldiscovery matrix
%%Such that we have corrVgeo, corrPVgeo, pvalV, and pvalPV

%%%%%%%%%%%%%%%%%%%%%%%%%%%%%%%%%%%%%%%%%%%%%%%%%%%%%%%%%%%%%%%%%%%%%%%%
%%Make sure that these corrVgeo, corrPVgeo, pvalV, and pvalPV are from the
%%original matrices and NOT from the random ones generated from
%%genshuffleVPV.
%%%%%%%%%%%%%%%%%%%%%%%%%%%%%%%%%%%%%%%%%%%%%%%%%%%%%%%%%%%%%%%%%%%%%%%%

%Find the most significant edges, say pvalue <0.05

pvalue = 0.05;

%returns matrix with 1's where the pvalue is less than or equal to 0.05 -
%these are our significant edges
% nonzeroV = le(pvalV,pvalue);
% nonzeroPV = le(pvalPV,pvalue);
%try with pvalues returned from corr function
nonzeroV = le(pvalV,pvalue);
nonzeroPV = le(pvalPV,pvalue);
nonzero_diff = le(pval_diff,pvalue);

%pull out only half the matrix - since these are symmetric matrices
nonzeroV = tril(nonzeroV);
nonzeroPV = tril(nonzeroPV);
nonzero_diff = tril(nonzero_diff);

Vsend = nonzeroV.*corrV;
PVsend = nonzeroPV.*corrPV;
diff_send = nonzero_diff.*absdifference;

graph_to_dot(Vsend,'filename','corrV.dot','node_label',ProteinLabel,
'directed',0);
graph_to_dot(PVsend,'filename','corrPV.dot','node_label',ProteinLabel,
'directed',0);
graph_to_dot(diff_send,'filename','corr_diff.dot','node_label',ProteinLabel,
'directed',0);

Vsig = HeatMap(Vsend, 'Colormap', redbluecmap, 'RowLabels', ProteinLabel,
'ColumnLabels', ProteinLabel)
addTitle(Vsig, 'Statistically Significant Pairwise Correlation Coefficients
for VEGF treatment (p<0.05)');
PVsig = HeatMap(PVsend, 'Colormap', redbluecmap, 'RowLabels', ProteinLabel,
'ColumnLabels', ProteinLabel)
addTitle(PVsig, 'Statistically Significant Pairwise Correlation Coefficients
for PF-4 + VEGF treatment (p<0.05)');
diff_sig =
HeatMap(diff_send,'Colormap',redbluecmap,'RowLabels',ProteinLabel,'ColumnLabels',ProteinLabel);
addTitle(diff_sig,'Statistically significant absdifferences');
```

falsediscover.m

```

%%Run this after running importing matrix and pvaldiscovery matrix
%%Such that we have corrVgeo, corrPVgeo, pvalV, and pvalPV

%% Determine false discovery rate of the pvalues output by corr function

%Convert symmetrix matrix into a vector of p values to be sorted
%Determine size of matrix.
matrixedge = size(pvalV,1); %doesn't matter which, they're symmetric
vectorpvalueV = [];%initialize pvalue vector
vectorpvaluePV = [];%initialize pvalue vector
vectorpvaluediff = [];

indexcount = zeros(matrixedge,matrixedge); %initialize vector with index
numbers to find position of pvalues
numbering = 1:matrixedge;
clear i
for i = 1:(matrixedge-1)
    vectorpvalueV = horzcat(vectorpvalueV,pvalV(i,(i+1):end));
    vectorpvaluePV = horzcat(vectorpvaluePV,pvalPV(i,(i+1):end));
    vectorpvaluediff = horzcat(vectorpvaluediff,pval_diff(i,(i+1):end));
    indexcount(i,(i+1):end) = numbering(1:matrixedge-i);
    if ne(i,1);
        indexcount(i,(i+1):end) = indexcount(i,(i+1):end) + indexcount(i-
1,end);
    end
end

alphaV= .33; % our q value
alphaPV = .3;
alpha_diff = .5;

[sortedV, indexV] = sort(vectorpvalueV,'ascend');
[sortedPV, indexPV] = sort(vectorpvaluePV,'ascend');
[sorteddiff, indexdiff] = sort(vectorpvaluediff,'ascend');

%%Check to see how many p values can be accepted
checkV = le(sortedV,(1:length(sortedV)).*alphaV./length(sortedV));
checkPV = le(sortedPV,(1:length(sortedPV)).*alphaPV./length(sortedPV));
checkdiff =
le(sorteddiff,(1:length(sorteddiff)).*alpha_diff./length(sorteddiff));

sigV = sum(sum(checkV));
sigPV = sum(sum(checkPV));
sigdiff = sum(sum(checkdiff));

```

Appendix G

pVEGFR2 Luminex data

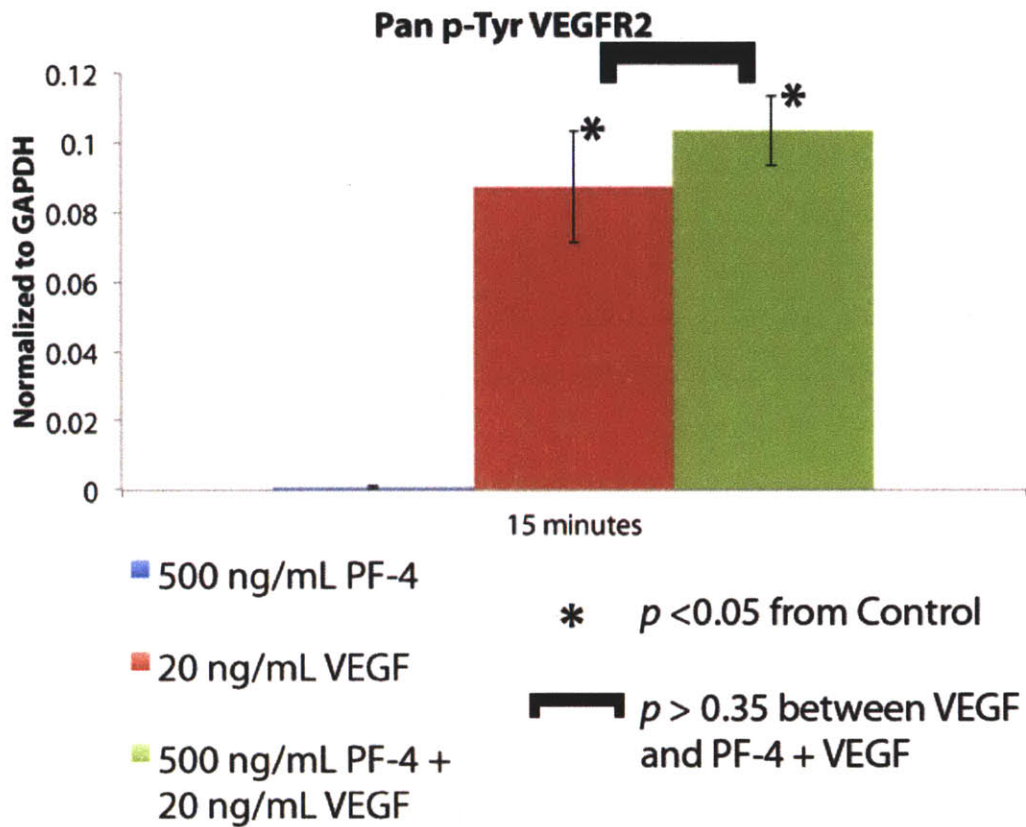


Figure G-1. pVEGFR2 activation levels do not change significantly when stimulated in presence of PF-4. PF-4 is speculated to induce angiostasis in vascular endothelial cells through several complex pathways, of which one includes interfering with the VEGF/VEGFR2 pathway. It is speculated to either sequester VEGF or bind heparin sulfates to reduce receptor binding, consequently decreasing phosphotyrosine activity of VEGFR2. Phospho-Tyr levels following stimulation with VEGF in both conditions were statistically significant ($p < 0.025$ for VEGF, $p < 0.005$ for VEGF+PF-4), the addition of PF-4 to VEGF did not deviate from significantly from that of VEGF dosing only. PF-4 dosing by itself did not induce any phosphorylation of VEGFR2. Thus, the influence of PF-4 on angiogenesis must utilize other mechanisms in our system.